UNIVERSITEIT VAN PRETORIA
UNIVERSITY OF PRETORIA
YUNIBESITHI YA PRETORIA

Petrography, mineralogy and geochemistry of rocks in the ZA-borehole, onshore Zululand Basin: Rock evaluation for CO_2 sequestration

by

Fillsmith Luzolo Ndongani

Submitted in partial fulfillment of the requirements for the degree

Masters of Science (MSc) Geology

to the Faculty of Natural and Agricultural Sciences

University of Pretoria,

Pretoria

Supervisor: Prof. W. Altermann

December 2017

DECLARATION

I, Fillsmith Luzolo Ndongani, student number 13356225, the undersigned, declare that:

1. I understand what plagiarism is and am aware of the University's policy in this regard.
2. This thesis is my own original work and where other people's work has been used (either from a printed source, Internet or from any other source), this has been properly acknowledged and referenced in accordance with University's requirements.
3. I have not used work previously produced by another student or any other person to hand in as my own.
4. I have not allowed, and will not allow, anyone to copy my work with the intention of passing it off as his or her own work.

Student's signature.....

Date.....

DEDICATION

First and far most, I would like to express my gratitude to my parents, Stanislas Ndongani Vola and Helene Kibunu Maloka. Papa and Mama, you were always supportive throughout my academic years; not only financially, but also emotionally. Secondly, I thank you for your constant supporting prayers. It is for this reasons that I dedicate this piece of my research work to you. You are the most well defined, articulate and dedicated people I ever knew in my life. I thank you Mom.

This thesis is also dedicated to my aunties and brothers Rose Bakongo Veyitondolua, Eugenie Ngamikwe, Philo Nzomina, Christian Matondo, Camille, Fernand, and Clovis Milandu for their moral and financial supports.

ACKNOWLEDGEMENTS

Acknowledgement is extended to the following parties:

1. The South African Centre for Carbon Capture and Storage for the financial support
2. Prof Wladyslaw Altermann for guidance and mentorship as supervisor of this dissertation
3. Mr Lowanika Victor Tibane for the logistical support and advises as co-supervisor of this project
4. The Council for Geosciences for the allowance to access the borehole ZA at the National Core Library
5. The University of Pretoria Carbon Capture and Storage Working Group (Brandon, Niel and Thifelimbilu, Mbonalo) for their collaboration.

ABSTRACT

The Cretaceous Zululand Basin is one of proposed areas for geological CO_2 storage in South Africa. The knowledge of the basin is however very limited. This thesis aims to describe the sedimentary facies of the ZA core, drilled onshore Zululand Basin, in KwaZulu-Natal, South Africa, and to assess their depositional environment as well as possible lateral correlation. Further aim is to investigate the suitability of these rocksfor a permanent sequestration of CO_2, based on their geochemical and petrographic characteristics.

The ZA drilling penetrated the Zululand Basin strata to a depth of 1779.9 m. The lowermost part of the ZA core from the recorded bottom at 1779.9 to 1602 m containing the Makatini Formation is however missing. Most of the core nevertheless is well preserved. The preserved ZA core from 1602 to 1041 m depth is characterised by dark grey coloured, bioturbated calcareous siltstone beds, rich in foraminifera, echinoderm and algae fossils and a dark grey coloured laminated glauconitic siltstone, overlain by a succession of siltstone strata with some interbeds of bioclastic packstones, calcareous and glauconitic siltstones (Lower Mzinene Formation). The Upper part of the Mzinene Formation starts from 1041 to 675 m depth, displaying a bioclastic packstone layer followed by bioturbated and wavy bedded arkosic wacke beds interbedded with calcareous sandstone layers rich in fossils and parallel bedded subarkose strata. The boundary between the Mzinene and St Lucia Formation is defined by the presence of a laminated siltstone bed at 675 m. The St Lucia Formation closing-up the Zululand Group, is comparable to the Mzinene Formation, except that the St Lucia Formation contains more fossil rich beds and glauconite. Above 675 m depth, the core displays siltstone layers intercalated by a bioturbated arkosic wacke bed, followed by 245 m thick calcareous siltstone beds. These 245 m

thick calcareous siltstone strata are overlain by cross-bedded arkose and glauconitic arkosic wacke layers, followed by calcareous and bioturbated siltstone units and bioclastic grainstone bed.

Only the sandstone strata between 1035 to 678 m, meet the criteria of a suitable reservoir for a permanent sequestration of CO_2. The sandstone strata are bound on top by a 42 m thick siltstone layers as potential cap rocks, covered by 242 m thick calcareous siltstone and sandstone. These depths however are by far too shallow for CO_2 sequestration. Nevertheless, petrographically, these sandstones are characterised as arkosic wackes, calcareous sandstone and subarkose and they contain mainly quartz, calcite and plagioclase minerals with a respective average of 47, 21 and 15% vol. Smectite, glauconite, mica, zeolite, hematite, and lithic fragments are present. The geochemical results of these sandstones supporting their mineralogical contents shows the predominance of SiO_2 (55 wt%), CaO (11 wt%), Al_2O_3 (10 wt%) and Fe_2O_3 (7 wt%) followed by other oxides such as MgO, Na_2O, K_2O, H_2O, MnO, TiO_2, P_2O_5 and Cr_2O_3 summing up to c. 17 wt%. The permeability and porosity of the middle sandstone rocks are respectively 8% and 10mD. The mineralogy of the possible cap rock layer is similar to the afore-mentioned sandstone units, dominated by quartz, calcite and plagioclase minerals. However, the clay mineral contents (mostly smectites) in the caprock bed are higher than in the possible sandstone reservoir. This higher clay content of the possible caprock is in accordance with the mineral spectral results showing the abundance of smectites and clay minerals in different depths.

The rock samples were treated with CO_2 under supercritical conditions of 100 bars and 100^0C for the duration of four weeks. The treatment results show a dissolution on the surface of quartz grains. The calcite cement was dissolved, created

secondary porosity and increasing the porosity and permeability of the rock. Therefore, the possible sandstone reservoir and the overlying siltstone rocks are probably unsuitable for injecting carbon dioxide because of the significant amount of calcite and authigenic minerals which may be dissolved during the $scCO_2$ - mineral reaction, creating secondary porosity and can lead to the disintegration of entire layers.

TABLE OF CONTENTS

LIST OF FIGURES

LIST OF TABLES

1. INTRODUCTION

In recent decades, the global warming phenomenon causes profound climate changes, due to emissions of greenhouse gases like carbon dioxide (CO_2). The CO_2 is effective in trapping heat. Generally, anthropogenic actions like deforestation or burning of fossil fuels CO_2 into the atmosphere (EASAC, 2013) lead to a rise of the mean atmospheric temperature. Even at remote places like the Mauna Loa summit, an infrared analyser reports daily concentration of CO_2 in the atmosphere of more than 400 parts per million (ppm), a value not reached for the last few million years. Emissions of CO_2 is also increasing, pushing its total equivalent concentration in the atmosphere to around 478 ppm, in April 2013 (Monastersky, 2013).

According to projections of energy use worldwide, global CO_2 emissions are expected to increase by 55% until 2030, or 1.7% per year (Gasda, 2007). Approximately $30x10^9$ tons of CO_2 per year are produced by burning of fossil fuel methods (Holloway, 2001). The estimation of the International Energy Agency (IEA) shows that by 2050 this rate will rise to $60x10^9$ tons/year under a “business-as-usual” scenario. This value is considered acceptable by the Intergovernmental Panel on Climate Change (IPCC) only if the atmospheric CO_2 amounts are to stay below 500 ppm. Then by 2050, emissions must be mitigated to $14x10^9$ tons/year, a four-fold decrease from the “business-as-usual” scenario. In the next 40 years, the largest rises in CO_2 emissions will come from developing countries notably Russia, China, Brazil, South Africa and India (BRICS), particularly in India and China (Verdon, 2010).

The storage of CO_2 is a major contribution to climate change mitigation and it is not an untested or new science. This CO_2 storage technique has been used for decades to improve the hydrocarbons’ production from oil and gas fields. During this method, other substances including gas were stored in geological reservoirs (Cloete

et al., 2010), at similar geological conditions that have trapped economically viable oil and gas accumulations underground. Carbon Capture and Storage (CCS) technique consists of capturing, transporting, injecting and storing CO_2 into deep subsurface geological formations (Gasda, 2013). The CO_2 is anticipated to react with minerals making up the reservoir and thereafter expected to remain in the rocks for geologically long periods.

South Africa is an important contributor to CO_2 emissions on a worldwide scale (Cloete et al., 2010) as it depends heavily on fossil fuels to meet its energy needs. According to the United Nation Framework Convention on Climate Change (UNFCCC), almost 400 Mt CO_2 is emitted annually by South Africa. This is mainly from synthetic-fuel and electricity industry. Both, government and industry realised the importance of finding suitable storage reservoirs locally as the CO_2 - capture technique is already available.

The president of South Africa, Mr Jacob Zuma has announced a target to mitigate CO_2 emission by 34% in 2020 and 42% in 2025 during the Conference of Parties (COP 15) in Copenhagen, subjected to financial, technical and capacity support from developed countries (Mining Weekly, 2010).

The Research and Development Agreement between the South African National Energy Development Institute (SANEDI) under the South African Centre for Carbon Capture and Storage (SACCCS), the contracted Council for Geoscience (CGS), and the Petroleum Agency SA (PASA) or the South African Agency for Promotion of Petroleum Exploration and Exploitation (Pty) Ltd, initiated a research project relating to “the effective CO_2 storage capacity assessment in South Africa”. The project was managed by Project Leader, Dr M. Cloete of the Council for Geoscience whereby he compiled an Atlas on Geological Storage of Carbon Dioxide

in South Africa. The CCS Atlas highlights at theoretical level, clarifies and assesses the existing South African potential for CO_2 storage (Cloete et al., 2011).

1.1. Aim and Objectives of the Project

The onshore Mesozoic/Cretaceous Zululand Basin was chosen for this purpose and research is currently conducted by the SACCCS to understand the geological properties of the Zululand Basin and the suitability for a safe test of CO_2 injection and storage, which is planned for 2017. As part of the SACCCS project, this thesis contributes new geological data for detailed understanding of the geology of the Zululand Basin and asserting of the possibility of injecting CO_2 therein. This thesis uses a drill core drilled in 1960's by SOEKOR (now PetroSA).

This project aims to characterise sedimentary facies of the onshore Zululand Basin in KwaZulu-Natal, by describing its lithostratigraphy, petrography, porosity, permeability, mineralogy and geochemistry based on the ZA core, in order to understand the sedimentary depositional environments and the rock CO_2 storage suitability. The core was recovered in 1965, by SOEKOR (now PetroSA) for oil and gas exploration.

The project objectives were as follows:

1. To determine the lithofacies, deposition and stratigraphic sequences of the borehole ZA.
2. To determine the mineralogical and geochemical characteristics of the different ZA rocks.
3. To use the results of objectives (i) and (ii) to determine suitable layers of possible reservoir and cap rocks for storing CO_2.

1.2. Delimitations, Limitations and Assumptions

This research can only be achieved with an adequate knowledge of geological conditions of CO_2 storage relative to the geology of the onshore Zululand Basin. Borehole ZA (also recorded as or BHA) (Table 1), stored at the National Core Library managed by the Council for Geosciences in Donkerhoek, Pretoria was made available for this investigation by Dr Marthinus Cloete in collaboration with SACCCS.

Table 1. The detailed information of the borehole ZA

Borehole number	ZA or BHA
Field area	Coalfields 2273
District	Dundee
Registration date	4 January 1965
Magisterial District	Ingwavuma
Date started	23 September 1965
Date completed	25 September 1965
Depth From	291.9856 feet
Depth End	5147.016 feet
Borehole depth	1779.96 m (5839 feet and 9 inches)
Geode borehole number	4202987
Sample type	CR
Drilled by	Anglo Transvaal Consolidated Investment
Old company name	Zululand Oil Exploration
Farm and registration district	Reserve N°14 7638, Natal
Province	Kwazulu-Natal
Latitude	-26.98333
Longitude	32.65
Collar elevation	50.1
Inclination	Vertical, -90
Central Meridian	33
Comments	1972-0253
Additional work reference	Dr H.M.Beer
Core storage	National Core sheds/Council for Geosciences, Silverton Pretoria

The ZA core is part of the ten petroleum exploration boreholes drilled in the Zululand Basin (Fig. 1). The boreholes were drilled by SOEKOR (now PetroSA) in 1965 for oil and gas exploration. Because the drill cores were dry and barren, they were therefore abandoned and donated to the CGS.

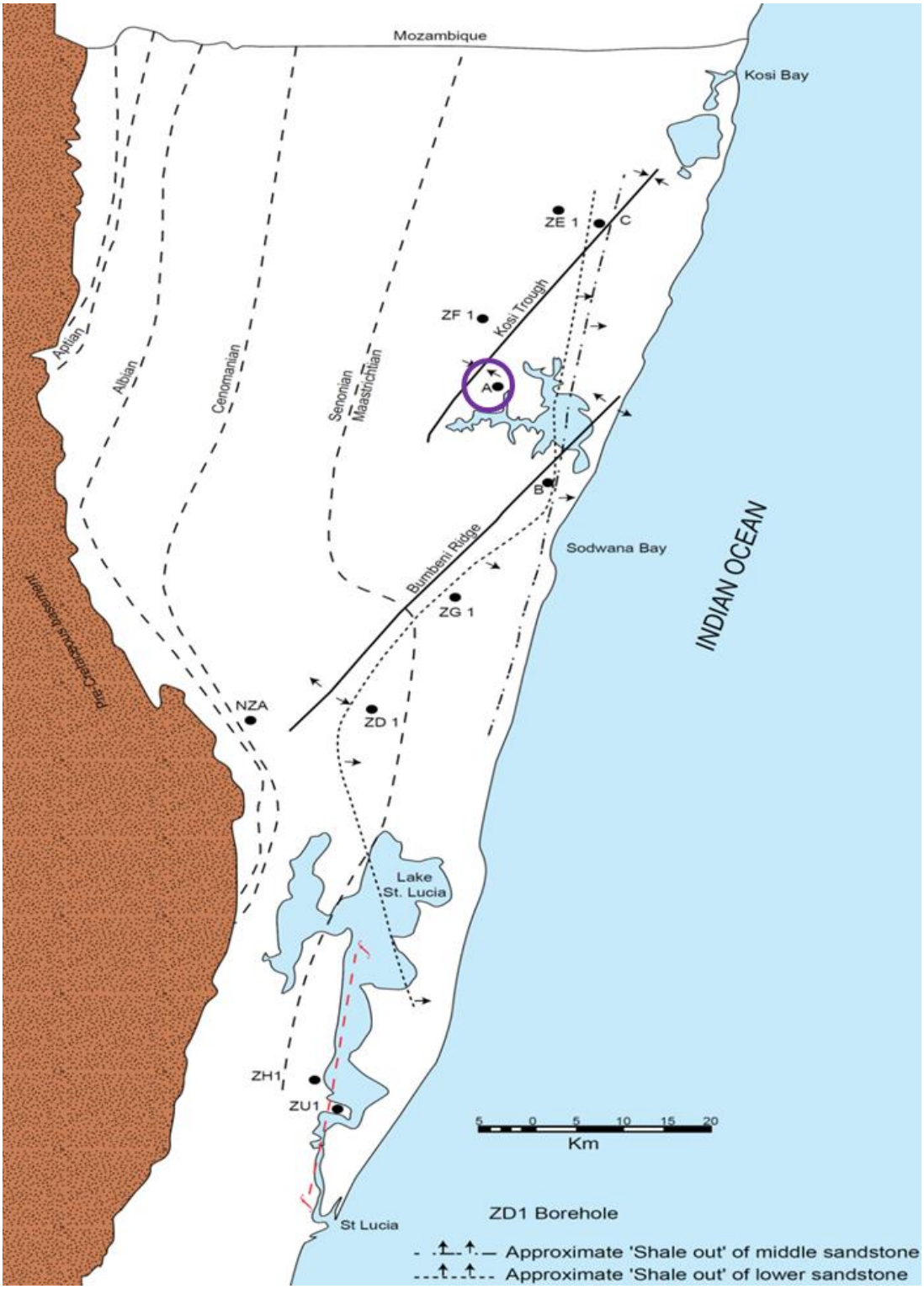

Figure 1. Location of borehole ZA and relation boreholes-faults within the onshore Zululand Basin (modified after Gerrard, 1972a in Cloete et al., 2010)

1.3. Carbon Dioxide and Geological Storage Conditions

Carbon dioxide is the main greenhouse gas emitted through human activities. It is a colorless and odorless gas at surface pressure and temperature, with about 1,98 kg/m^3 of density. In the environment, the carbon dioxide circulates through the carbon cycle process. Huge quantities of CO_2 are released into the atmosphere by the large-scale industrial processes, living systems and volcanoes. Conversely, oceans, rivers, lakes and plants collect CO_2. Although the concentration of CO_2 in the earth's atmosphere is low (~0.04% by volume), CO_2 is a very important component, because it absorbs infrared radiation and enhances the greenhouse effect (Hexiang, 2007).

Contrary to other greenhouse gases e.g. methane, CO_2 is very stable in the earth's atmosphere. The stability of CO_2 depends generally on temperature and pressure conditions. It condenses into a "dry ice" which is a white solid, at the temperatures below -78^{0}C. Liquid CO_2 can also be formed with enough added pressure. This liquid CO_2 is essentially immiscible with water. Only a small CO_2 content is soluble in formation waters (Ennis-King and Paterson, 2000) – creating a weak carbonic acid in the process. Carbon dioxide solubility increases with rising pressure and decreases with an initial increase in temperature and salinity. CO_2 solubility in water rises again at very high temperatures and particularly in a high-pressure condition, i.e. a deep pressurised basin (Cloete et al., 2010). The CO_2 thermodynamic critical point is at 7,38 MPa and 31,1^{0}C. CO_2 arises in the supercritical point and has typical characteristics of both a fluid and gas at pressures and temperatures in excess of this point. This CO_2 can diffuse over solids like a gas, and dissolve materials as a liquid. It can reach a density ranging from 150 to 1060 kg/m^3 (Fig. 2). However, above 850 kg/m^3 of density is only reached in over-pressurised basins (Bachu, 2003).

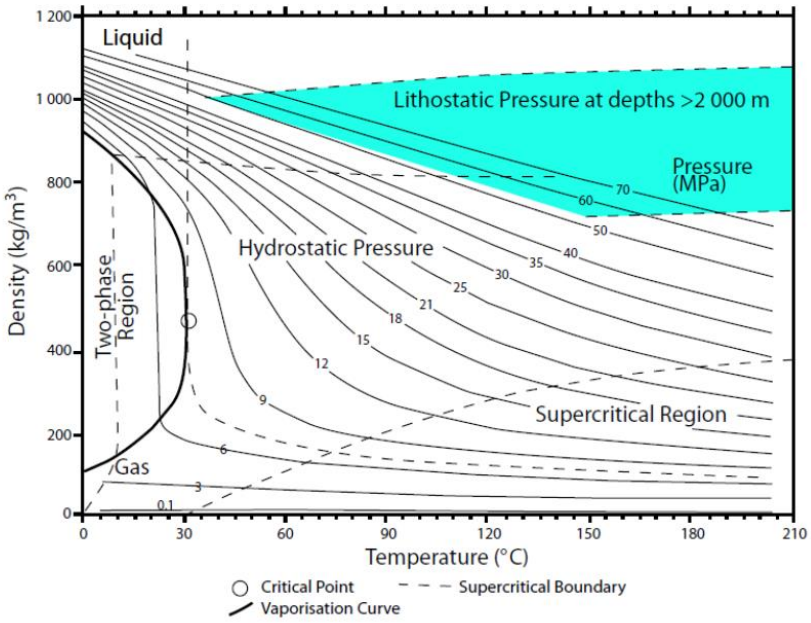

Figure 2. Variation of CO_2 density as function of pressure and temperature (from Bachu, 2003).

At least 800 m burial depth is needed to achieve a high enough pressure and temperature for CO_2 to occur in the supercritical phase considering hydrostatic pressure conditions and average geothermal gradients (IPCC, 2005).

1.4. Types of Geological Storage of CO2

Geological CO_2 storage (sequestration) involves injecting carbon dioxide directly into underground geological formations. It has been used for decade for pressure control and enhanced in most developed countries and presents a minimal risk as oil and gas extraction. Cloete et al. (2010) suggested that the anthropogenic CO_2 storage can target un-mineable coal seams, depleted hydrocarbon reservoirs and deep saline aquifers (Fig. 3). However, this project is only focusing on storing CO_2 in deep sedimentary basins.

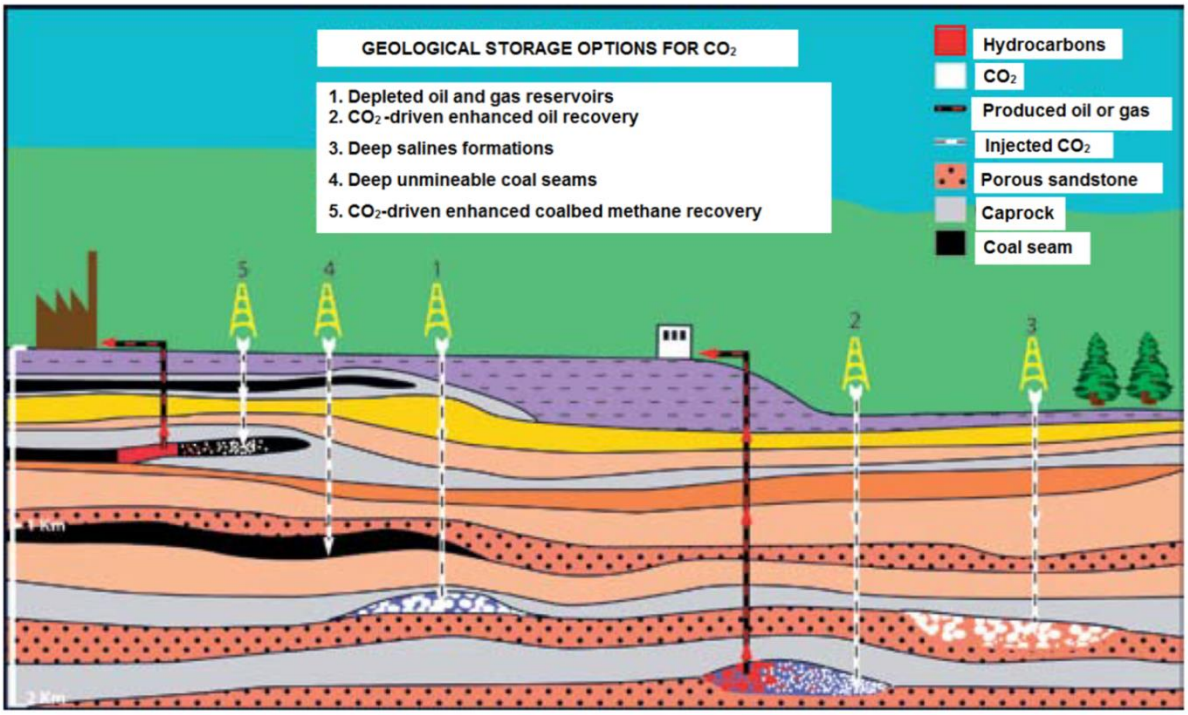

Figure 3. Geological storage options in depleted oil and gas fields with enhanced oil and gas recovery (1 and 2), in deep (>800 m) saline aquifers (3), in unmineable coal seams with enhanced coal bed methane (ECBM) production (4 and 5), after CO2CRC (2009).

1.4.1. Storage in Saline Aquifers and Deep Sedimentary Basin Layers

This storage type requires highly porous rock layers (mostly sandstone) in deep sedimentary basin that are overlain by impermeable layers (Table 2) and are saturated with formation waters unsuitable for agriculture or human consumption. Such rocks are very rarely filled with hydrocarbons. They remain filled usually with brine (Verdon, 2010). Saline aquifers have great capacity for CO_2 sequestration owing to long time CO_2 stability and large volume of these basins occurring at suitable depth for storage in supercritical point (Cloete et al., 2010). The CO_2 storage is controlled through hydrodynamic, structural/stratigraphic, solubility and mineral trapping mechanisms (Verdon, 2010).

Table 2. Parameters and properties of a geological formation suitable for the storage of CO2 (modified from Cloete et al., 2010)

Parameters	**Properties**
Reservoir depth	Between 800 m and 2500 m
Cap rock type	Impermeable (shale)
Cap rock thickness	>100 m
Reservoir type	Permeable and porous (sandstone)
Reservoir thickness	50 m
Reservoir porosity	>10%
Reservoir permeability	300 mD

In addition, there are other options for storage of CO_2 including mafic rocks or shales (containing little organic matter). Intense research is underway on these methods (Cloete et al., 2010).

1.5. Criteria for Assessing the Sedimentary Basins of South Africa for the CO_2 Geological Storage

According to Cloete et al. (2010) the potential basins for CO_2 storage can be broadly characterised by:

1. Basin characteristics, such as geology, tectonism, hydrodynamic and geothermal regimes (“hard” criteria because they do not change).
2. Basin resources (coal, hydrocarbons, other mineral resources), maturity and infrastructure “semi-hard” criteria.
3. Societal criteria, such as economy, level of development, political structures and stability, attitude and public education “soft criteria”.

Table 3 illustrates the criteria and criteria classes for evaluating South Africa’s sedimentary basins for the geological storage of CO_2 (modified after Bachu, 2003 in Cloete et al., 2010).

Table 3. Classification of criteria for assessing sedimentary basins of South Africa for the geological storage of CO_2 (modified after Bachu, 2003; Gibson-Poole et al., 2006).

	Criterion	Classes				
		1	2	3	4	5
1	Tectonic setting	Very unstable (e.g. subduction)	Unstable (e.g. syn-rift, intramontane, strike-slip)	Intermediate (e.g. foreland)	Mostly stable (e.g. passive margin)	Stable (e.g. cratonic)
2	Size of basin	Very small (<1000 km^2)	Small (1000-5000 km^2)	Medium (5000-25000 km^2)	Large (25000-50000 km^2)	Very lrge (>50000 km^2)
3	Depth of basin	Very shallow	Shallow (300-800m)		Deep (>3500m)	Intermediate (800-3500m)
4	Geology: reservoir seal pairs	Poor		Intermediate		Excellent
5	Faulting intensity	Extensive		Moderate		Limited
6	Dolerite dykes/ sheets	Extensive		Moderate		None
7	Geothermal gradient	Warm basin (>40°C/km)		Moderate (30--40°C/km)		Cold basin (<30°C/km)
8	Hydrocarbon potential	None	Small	Medium	Large	Giant
9	Maturity	Unexplored	Exploration	Developing	Mature	Over mature
10	Coal	None	Very shallow (<300 m)	Very deep (>1500 m)	Deep (800-1500 m)	Shallow (300-800 m)
11	Coal rank	Anthracite	Lignite		Sub-bituminous	Bituminous
12	On-/offshore	Deep offshore		Shallow offshore		Onshore
13	Other economic commodities	Large-scale mining	Active mining	Confirmed (No mining)	Potential	None
14	Infrastructure	None	Minor		Moderate	Extensive
15	Major CO_2 sources	>1000 km	500-1000 km		300-500 km	<100 km

Table 4 summarizes all possible South African CO_2 storage basins varieties and gives the comparison of the country-scale screening criteria for each basin/region.

Table 4. Comparison of country-scale screening criteria for each basin/region, Bachu, 2003.

		Southern Karoo	Northern Karoo	Katberg/ Molteno–Indwe	Durban–Lebombo Belt	Springbok Flats	Tuli	Tshipise	Lephalale	Onshore Algoa Basin	Onshore Zululand Basin	Durban/ Zululand Basin	Outeniqua Basin	Orange Basin
1	Tectonic setting	Stable (e.g. cratonic)	Stable (e.g. cratonic)	Stable (e.g. cratonic)	Stable (e.g. cratonic)	Stable (e.g. cratonic)	Stable (e.g. cratonic)	Mostly stable	Stable (e.g. cratonic)	Mostly stable	Mostly stable	Mostly stable	Mostly stable	Mostly stable
2	Size	Very large (>50 000 km²)	Large (25 000–50 000 km²)	Medium (5 000–25 000 km²)	Small (1 000–5 000 km²)	Medium (5 000–25 000 km²)	Very small (< 1 000 km²)	Medium (5 000–25 000 km²)	Small (1 000–5 000 km²)	Small (1 000–5 000 km²)	Small (1 000–5 000 km²)	Very large	Very large	Very large
3	Depth	Interme-diate (800–3 500 m)	Interme-diate (800 –3 500 m)	Interme-diate (800–3 500 m)	Interme-diate (800–3 500 m)	Shallow (300–800 m)	Shallow (300–800 m)	Interme-diate (800–3 500 m)	Shallow (300–800)	Interme-diate (800–3 500 m)	Interme-diate (800–3 500 m)	Interme-diate (800–3 500 m)	Interme-diate (800–3 500 m)	Interme-diate (800–3 500 m)
4	Geology: reservoir seal	Poor	Poor to in-termediate	Poor to in-termediate	Poor to in-termediate	Poor to in-termediate	Poor to in-termediate	Poor to in-termediate	Poor	Interme-diate	Poor to in-termediate	Interme-diate	Excellent	Interme-diate
5	Faulting intensity	Limited	Limited	Limited	Moderate	Moderate	Moderate	Extensive	Extensive	Moderate	Limited	Moderate	Moderate	Moderate
6	Dolerite dykes/ sheets	Extensive	Extensive	Extensive	Extensive	Moderate	Extensive	Moderate	None	None	None	None	None	None
7	Geothermal gradient	Cold basin	Cold basin	Cold basin	Cold basin	Cold basin	Cold basin	Cold basin	Cold basin	Cold basin	Cold basin	Cold basin	Cold basin	Cold basin
8	Hydrocarbon potential	None	Small	None	None	None	None	None	None	Small	Small	Medium	Large	Large
9	Maturity	Exploration	Exploration	Exploration	Exploration	Exploration	Exploration	Exploration	Developing	Exploration	Exploration	Exploration	Mature	Exploration
10	Coal	None	Shallow	Shallow	Shallow	Shallow	Shallow	Shallow	Shallow	None	None	None	None	None
11	Coal rank	N/A	Bituminous	Anthracite	Anthracite	Bituminous	Anthracite	Bituminous	Bituminous	N/A	N/A	N/A	N/A	N/A
12	On-/Off-shore	Onshore	Onshore	Onshore	Onshore	Onshore	Onshore	Onshore	Onshore	Onshore	Onshore	Deep to shallow offshore	Deep to shallow offshore	Deep to shallow offshore
13	Other eco-nomic com-modities	Confirmed	Confirmed	None	None	Confirmed	None	None	None	None	None	None	None	None
14	Infrastruc-ture	Minor	Minor	Minor	Minor	Minor	None	Minor	Moderate	Minor	Minor	None	Moderate	None
15	Major CO_2 sources	500–1 000 km	<300 km	300–500 km	<300 km	<300 km	300–500 km	300–500 km	300–500 km	500–1000 km	300–500 km	300–500 km	500–1000 km	>1 000 km

2. GEOLOGICAL SETTING OF THE ONSHORE ZULULAND BASIN

The onshore Zululand Basin is located along the east coast of South Africa, in the province of KwaZulu-Natal, bounded northwards by the Republic of Mozambique and to the east by the offshore Zululand Basin (Indian Ocean). Situated between 32° to 36° longitudes East and 26° to 30° latitudes South (Fig. 4) and covers an area of 7500 km^2. It is one of the largest onshore Mesozoic basins, likely to contain viable deep geological formations and being onshore, this basin is accessible to do geological investigations and monitoring (Cloete et al., 2010). The offshore part of the basin totals 13 500 km^2 down to the 1500 m isobaths (Shone et al., 2006). According to Cloete et al. (2010), the Zululand Basin is unlikely to ever be used for gas/or oil production because of the low carbon and hydrogen content. Although cap rocks are present in the basin, they do not form a sufficient regional lateral seal to avoid the migration of the CO_2 towards the surface.

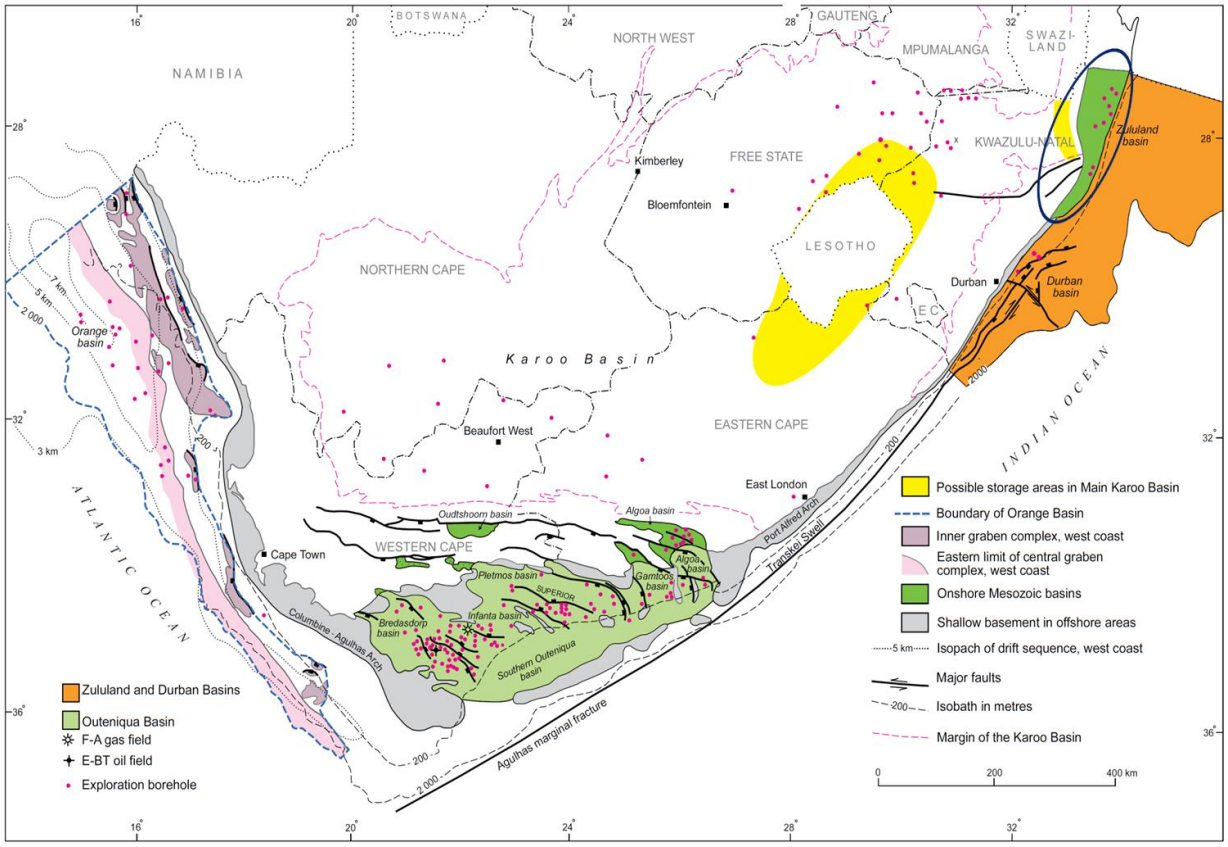

Figure 4. Location of the onshore Zululand (after Van Vuuren et al., 1998 in Cloete et al., 2010).

The onshore Mesozoic Zululand Basin continues into the southern Mozambique Basin and represents the southernmost portion of the 7 000 km long taphrogenic zone known as the East African Rift that reaches from the Red Sea along eastern Africa into South Africa (Dingle et al., 1983). The Mesozoic Zululand Basin is mostly buried beneath Cenozoic sediments in the northern KwaZulu-Natal (Maputaland) coastal plain. The western limit of the Basin is defined by the 180-140 Ma Lebombo Group volcanics in the Lebombo monocline (Watkeys, 2002), which dip eastwards underneath the basin at 10-25°. The basin is subdivided into two structural units, the northern Kosi Trough and the southern St Lucia Trough, by a northeast-trending basement ridge, known as the Bumbeni Ridge, which extends offshore. The

Cretaceous succession in the Kosi Trough is ~2 000 m thick, whilst the succession in the southern St Lucia Trough thins to ~1 000 m (Broad et al., 2006).

The Zululand Basin originated during the break-up of west Gondwana into the African and South American plates: ref. Fig. 5 below (Jungslager, 1999: in Cloete et al., 2010). This event started in the lower Jurassic, at the time of Karoo volcanism approximately between 190 Ma and 160 Ma (Dietz and Holden, 1970).

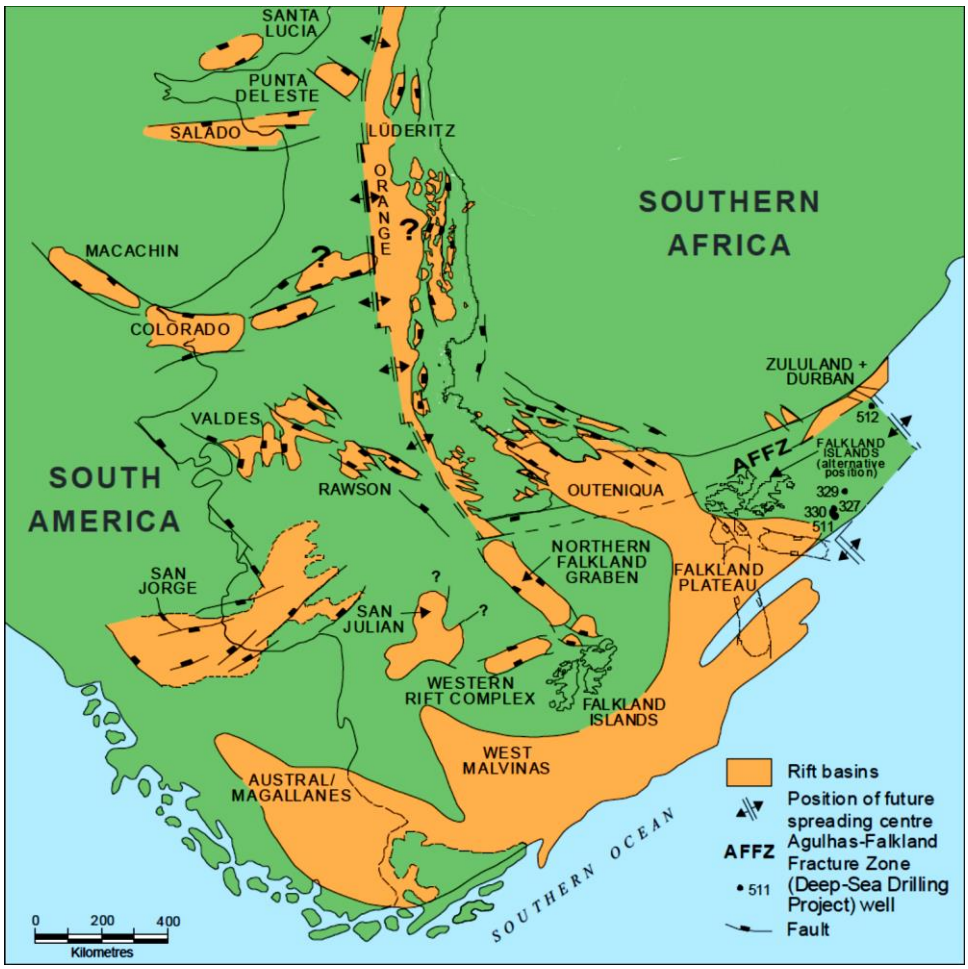

Figure 5. Location of the Zululand Basin during the pre-break-up distribution of rift basins within southwest Gondwana (after Jungslager, 1999: in Cloete et al., 2010).

The end of this process may be regarded as detachment of the Falkland Plateau from the Agulhas Bank in the Late Cretaceous, between 135 Ma and 130 Ma (Siedner and Mitchell, 1976). At this period, the continental crusts of South America and Africa finally lost contact with each other (Shone, 2006). Figure 6 below, shows a summary of the

principal geological events that impacted the development of the Durban and Zululand Basins.

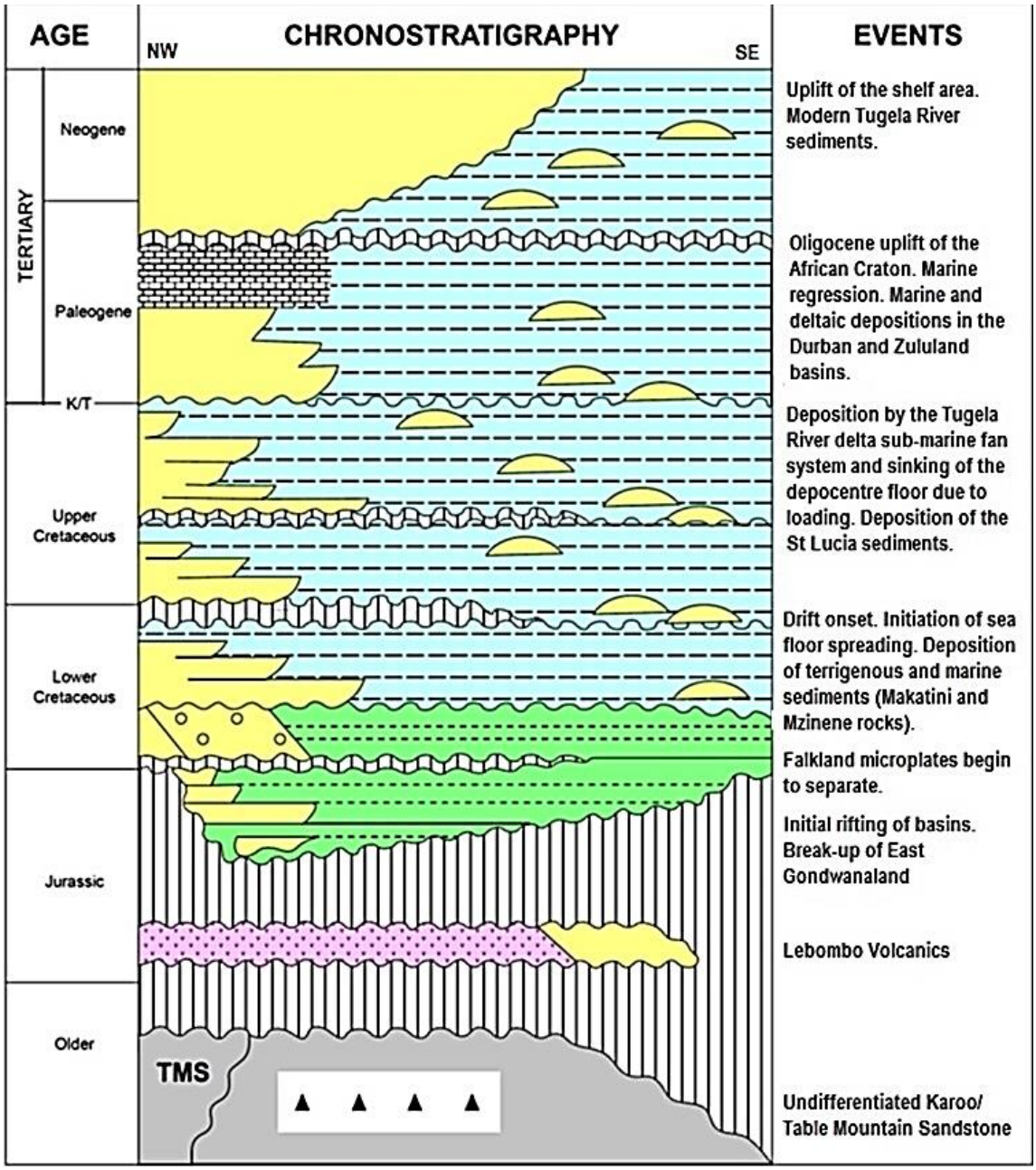

Figure 6. Chronostratigraphy of the Durban and Zululand Basins (after Petroleum Agency SA, 2008).

The Mesozoic and Cenozoic history of southeastern Africa reflects the continental uplift, transtensional tectonic regime and rifting associated with the fragmentation of the Gondwana supercontinent. Superimposed on this faulted

continental margin are influences of episodic epirogenic uplift events and glacio-eustaic sea-level change in response to cyclical climatic change (Dingle et al., 1983).

The Zululand Group comprises of three stratigraphic formations. The lower Cretaceous Makatini and the overlying Mzinene Formation, together, thicken towards the northeast, reaching a maximum thickness of 722 m whilst the Upper Cretaceous St Lucia Formation covering the Mzinene Formation attains a maximum thickness of 876 m (Kennedy and Klinger, 1975). The Zululand Group thus defines the Late Barremian to Late Masstrichtian sedimentary fill. The Makatini Formation is of Barremian to Aptian, ca. 125-115 Ma age and reposes unconformably above the Jurassic Lebombo Group volcanic rocks (Dingle and Scruttton, 1974). This formation is characterized by small-pebble conglomerates, sandstone, siltstones including the thin bed shale. These sedimentary rocks represent shallow marine deposition which was controlled by progradating of braided fluvial deposits (Tankard et al., 1982). A limestone bed is found in the uppermost part of the formation and was deposited during a regressive stage (McMillian, 2003). According to Dingle and Scrutton, 1974, the entire Makatini Formation lithofacies was deposited during the Barremian transgression linked to drifting of East Gondwana from West Gondwana.

The Mzinene Formation, Early Albian to Late Cenomanian (ca. 120 – 95 Ma), rests unconformably in some areas on the Makatini Formation and elsewhere it is found overlying directly the Lebombo Group (Kennedy and Klinger, 1972). The Mzinene Formation is rich in fossils and its lithofacies consist of glauconitic siltstones and fossil rich sandstones deposited in a shallow marine environment (Kennedy and Klinger, 1975; Shone, 2006).

The St Lucia Formation, Conacian to Masstrichtian (ca. 90-65 Ma) is lithologically very similar to the Mzinene Formation, except, that the former is richer in

fossils and in glauconite (Kennedy and Klinger, 1972). A shallow angular unconformity separates the St Lucia Formation from the Mzinene Formation in proximal areas like the onshore Zululand Basin. The rocks of the Lucia Formation were deposited during a renewed transgression across the Zululand Basin (Kennedy and Klinger, 1975; McLachlan and McMillian, 1979).

3. METHODOLOGY

Various techniques of investigation were applied to the ZA core in this research. Starting with core logging, spectral logging, sampling, petrography (visual observation and thin section), X-Ray diffraction (XRD) and X-Ray fluorescence (XRF) were performed in order to characterise the onshore Zululand lithofacies and understand its CO_2 storage suitability. Fluid-rock interaction laboratory experiments, porosity and permeability measurements were also performed to investigate the suitability of the Zululand Basin rocks for CO_2 storage.

3.1. Hyperspectral Imaging and Logging

The GeoSpectral Imaging technology is a passive, non-destructive technique with the ability of measuring and logging the reflectance of different energy wave lengths from rocks and cores, both objectively and consistently, but only reflecting the surface composition. This technique was applied at the National Core Library of the Council for Geosciences using the sisuRock Mobile GeoSpectral Imaging instrument (sisuMobi) provided by the Geospectral Imaging Company. The sisuMobi instrument (Fig. 7) was used for rapid and accurate scanning of the entire drill cores.

Figure 7. The sisuMobi GeoSpectral Imaging System in operation at the National Core Library at Donkerhoek.

The spectral Imaging method was utilized for *in situ* measurements to determine the mineralogy and geochemistry of the core. The core was poorly preserved, dirty and covered with dust. The dust particle on the surface of the core masks the minerals and geochemistry. Thus, it was necessary to wash the core and allow it to dry overnight as water also influence the results.

SisuMobi Hyperspectral Imager uses two imaging sensors operating across the visible and infrared region of the electromagnetic spectrum and provides a wide range of mineral detection capabilities (Fig. 8).

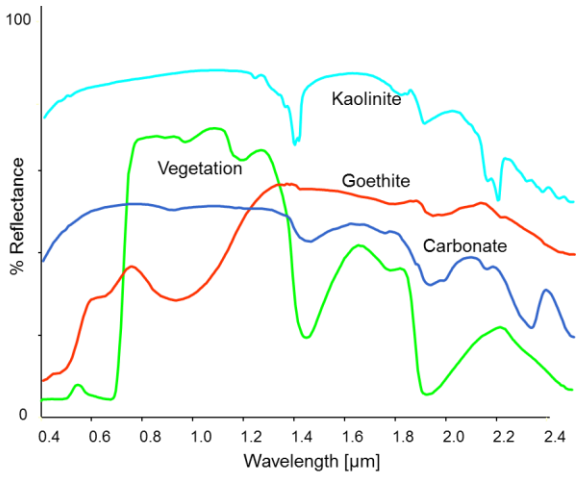

Figure 8. Range of mineral detection capabilities provided by the hyperspectral technique and characteristic reflectance examples of different materials.

Measurements are recorded from the surface of the sample between the range of 0.4 and 14 µm wavelengths (Table 5). However, for this investigation, the Short-Wave Infrared (SWIR) was utilised for clay mineral detection (section 3.1.1).

Table 5. Approximate ranges of the different Infrared Wavelengths in microns.

Region	**Code**	**Approximate range (microns)**
Visible Near Infrared	VNIR	0.4 – 1.0
Short-Wave Infrared	SWIR	1.0 – 2.5
Mid-Wave Infrared	MWIR	3.0 -6.0
Long-Wave Infrared	LWIR	6.0 -14.0

The SWIR is an important range for mineral detection (Fig. 8). The hyperspectral imaging results in a continuous log of the spectral characteristics of the surface of the entire core and allows further identification of the mineralogy/geochemistry of the core.

3.1.1. Mineral detection

Mineral detection is based on the Short-Wave Infrared (SWIR) and the Long-Wave Infrared (LWIR) of the hyperspectral core logging. However, only the SWIR was used in this project. The spectral information can be illustrated via colour images, feature extraction images (distribution images) that can be transferred to mineral presence and abundance maps using special image analysis software. The geochemical and mineralogical data of the core together with the hyperspectral information are used for evaluation, validation, and interpretation of the lithology of the cores. The images are significant as they show the spectral variations, which indicate the areal extent of mineral assemblages, distributions, abundances, and alterations, which reflect major lithological changes.

The typical spectral signatures are characteristic features of energy adsorption for the minerals that allow mineral identification and determination of mineral variations. The hyperspectral data contain mineral indices, mineral count, statistical data, graphical areal representations which can further be used for interpretation and statistical comparison of the lithology of the drill core ZA. The VNIR is very important for the detection of minerals containing iron (e.g. hematite, goethite). The spectral characteristics of hydroxyl groups and carbonates are typically measured in the SWIR. Phyllosilicates such as clay minerals, micas and chlorites are identified between 2.0 and 2.5 µm (SWIR). These spectral characteristics in the SWIR are related to the different bonding forces of the molecules of calcite, dolomite etc. (Ca-CO_3; Mg-CO_3; Al-OH^-; Mg-OH^-). The Long-Wave Infrared (LWIR) region can detect and identify silicate minerals such as quartz and feldspar can be detected and identified. This region is often also referred as the Thermal Infrared (TIR). The combination of SWIR, MWIR and LWIR provides a powerful mineral detection tool.

3.2. Core Logging

Geological (lithological, conventional) core logging was performed at the National Core Library of the Council for Geosciences (Fig. 9) on the entire borehole to determine the lithofacies, mineralogy and sedimentary structures and the depth and thicknesses of the individual beds of the various formations. After thorough washing and cleaning of the core, the core logging of the 1779.96 m long drill core ZA, stored in 171 boxes, was performed on wet core material to ensure better visibility of the sedimentary structures and minerals.

Figure 9. Zululand Cores laid out on the floor at the core shed, National Core Library – Council for Geosciences.

A pen, marker, note book, measuring tape, and hand lens, core logging sheet, 5% hydrochloric acid, and a camera were utilised for recording of the lithological features of the entire borehole. Induration, colour, grain size, texture, presence of

organic matter and carbonate materials, sedimentary structures and rock types were recorded. From the hand written description, a lithostratigraphic log was constructed using Strater software package.

3.3. Sample collection

Fourty rock samples were collected from the bottom to the top of the ZA core. The sample selection was based on the lithological changes. Emphasis was put on samples below 800 m depth which is required for CO_2 storage. Photographs were taken before and after numbering and cutting the samples in half, longitudinally at the core shed. Thereafter, all the samples were stored and labeled in sample bags for further analyses.

3.4. Petrographic analysis

3.4.1. Visual observation

A visual description was performed at the Department of Geology of the University of Pretoria to identify detailed petrographic characters of all samples. The petrographic description included rock colour, induration, and grain size, presence of organic matter, fossils, carbonate matter, clasts, sedimentary structures and rock types. Unfortunately, the induration of the deteriorating shale and clay rich rocks could only be assessed after the long storage and weathering of the core in the core shed and is thus not significant.

3.4.2. Thin section analysis

The descriptions of uncovered thin sections were performed using a transmitted light petrographic microscope (Leitz) to determine the microfacies features of the samples. The identified criteria include the mineralogy and the compositional and structural sorting of the grains, fossils, grain size, grain shape, texture and matrix, to

understand the type of the rocks, depositional and diagenetic conditions and environments, provenance of the sediments; and to recognise suitable lithofacies for CO_2 storage.

3.5. X-Ray analyses

X-Ray Diffraction (XRD) is one of the primary techniques used to identify minerals in the samples while the X-Ray fluorescence (XRF) technique was used to measure quantitatively the elemental composition of samples. The initial sample preparation for both XRD and XRF analyses was performed at the Stoneman building, Department of Geology, University of Pretoria. Fourty samples were crushed and thereafter milled to powder materials in micrometer size. Later the XRD and XRF analyses of the milled samples were carried out in the laboratory of the Council for Geosciences in Pretoria. These analyses were undertaken to support the Microscopic and hyperspectral interpretation of the core.

3.5.1. X-Ray Fluorescence (XRF)

For major elements analysis, the sample preparation followed a standard procedure: the milled sample (<75 µm fraction) was roasted at 1000 °C for at least 3 hours to oxidise Fe^{2+} and S and to determine the weight loss on ignition (L.O.I.). Followed by a preparation of the glass discs by fusing 1g roasted sample and 9.5 g flux consisting of 70.689% $Li_2B_4O_7$ and 19.786% $LiBO_2$. Eleven major oxide elements were measured among others SiO_2, TiO_2, Al_2O_3, Fe_2O_3, MnO, MgO, CaO, Na_2O, K_2O, P_2O_5 and Cr_2O_3. For trace element analysis, mixing of 12 g milled sample and 3 g of Hoechst wax and then pressed into a powder briquette by a hydraulic press with the applied pressure of 25 tons. Analysing of the glass disks and wax pellets by using a PANalyticalAxios X-ray fluorescence spectrometer equipped with a 4 kW Rh tube.

3.5.2. X-Ray Diffraction (XRD)

The XRD technique is concerned with testing polycrystalline and amorphous materials present in the sample. This method is adapted from British Standard: BS EN 13925-2003 and implemented to suit the specifics of CGS XRD Laboratory.

Instrumentation and Measurement Conditions: The measurements of X-Ray Diffraction were performed using a BRUKER D8ADVANCE instrument with 2.2kW Cu, long fine focus tube (Cu Kα, λ=1.54060) and 90 position sample changer. This system is furnished with LynxEye detector with 3.7º active area. Scanning of the samples was done from 2 to 70° 2θ at a speed of 0.02° 2θ steps size/3 sec, and generator settings of 40 kV and 40mA. Sample Processing: The treatment of the samples using X-ray examination depends on the objectives of the work and the materials to be studied. For bulk (whole rock) analysis a representative rock sample was crushed, milled and homogenized. The milling procedure using the McCrone micronizing mill was performed to reduce the particle size to approximately 5-10 μm in size. To ensure random orientation, a sub-sample was pressed into a shallow plastic sample holder against a rough filter paper. Data processing and analysis: phase identification was based on BRUKER DIFFRAC^{Plus}- EVA evaluation program. The ICDD (JCPDS) Inorganic/Organic Data base was used for phase search, of which the PDF- 2, Release 2006 was available. Quantitative XRD analyses by Rietveld method were performed using DIFFRAC^{Plus}– TOPAS software with accuracy in the region of ±1%. The structures of the components were generated from structure databases such as the Cambridge Structure Database (CSD) or TOPAS Structure Database and the Inorganic Crystal Structure Database (ICSD) provided by the instrument/software supplier. The quantification of the amorphous phase was completed by adding ZnO as an internal standard.

3.6. Laboratory experiments with CO2 and porosity and permeability measurements

The laboratory experiments on the ZA samples were done in Germany, at the Martin-Luther University of Halle by my team members, Mr Victor Tibane and Mr Brandon Landman to investigate the CO_2-H_2O-rock interaction, strength, porosity and permeability of the rock samples. Various rock samples were utilised before and after the contact with $scCO_2$, to evaluate the suitability of the deep Zululand formations for CO_2 injection.

The main purpose of mineralogical characterisation was to assess whether and how the different types of sandstone and the various types of the overlying siltstone change their mineralogical, physical and geochemical properties as a result of chemical reactions with $scCO_2$. The mineralogy of rocks in general, can react with CO_2. The porosity and permeability of the rocks can be altered due to such geochemical interactions (Andre et al., 2007) and the changes can affect the rock strength and the CO_2 injectivity (Gaus et al., 2008).

3.6.1. Geomechanical and Petrophysical Investigation

The point-load test (PLT) was conducted on silicic sandstone, calcareous sandstone, silicic siltstone and calcareous siltstone using simple portable Enerpac equipment (Fig. 10). The point-load test in this study was primarily used to provide a reliable and quick measurement of the strength of untreated samples in the laboratory. The laboratory results were utilised to assess the strength of the geological units considered for CO_2 sequestration. This test consists of compressing an irregular shaped piece of rock sample between two points, as illustrated in Fig. 11. The Enerpac apparatus comprises of a small loading frame which is activated by a hydraulic hand pump and rams (Fig. 10). Rock cores were placed between pointed platens of

standard dimensions and loaded until failure occurs. The point-load index (Is) was calculated as $I_s = P/D^2$, which is the ratio of the applied load (P) to the square of the distance (D) between the loading points. The measurements are given in Table 6. The dimensions of the loading "points" are standardised and given in Fig. 11. The relationship between the uniaxial compressive strength (UCS) and point-load index was determined using normalising core diameter of 50 mm.

Figure 10. Simple Enerpac point-load tester.

The tests were carried out along two axes with shortest axis of the lump being the one parallel to the bedding planes representing the diameter of the sample less than 50 mm. Broch and Franklin (1972) have shown that the value of diametral point load strength is dependent on the core size. The larger diameter cores produced smaller values of point load index. The standard classification is adopted by correcting all values to a reference diameter of 50 mm. The figure 12 shows the correction chart for this purpose.

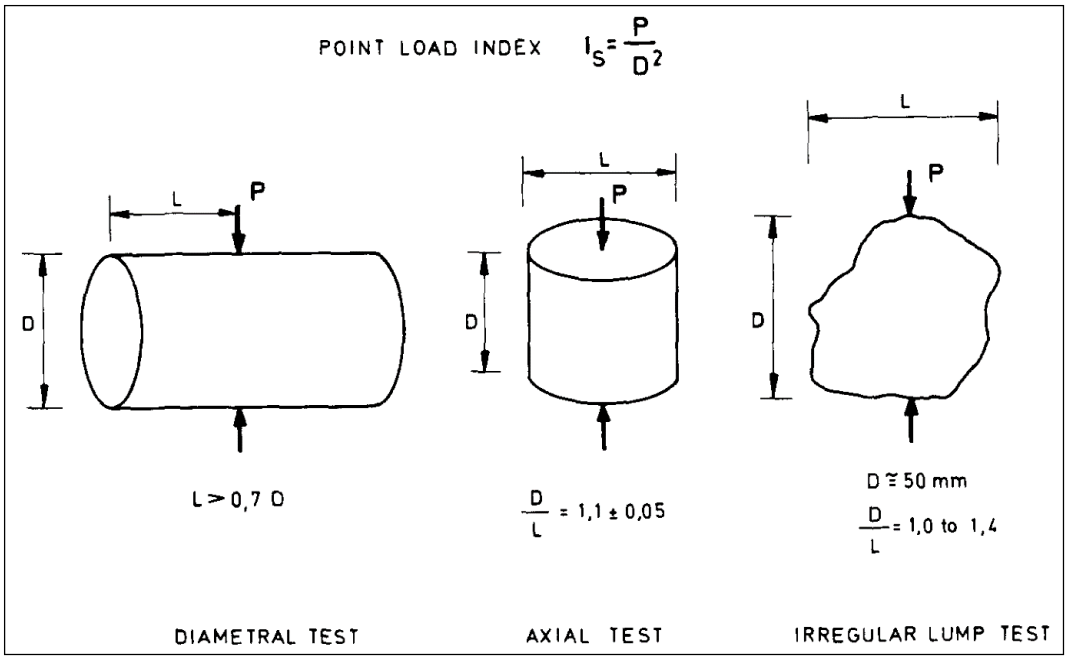

Figure 11. Geometrical specifications for the diametrical, axial and irregular lump test.

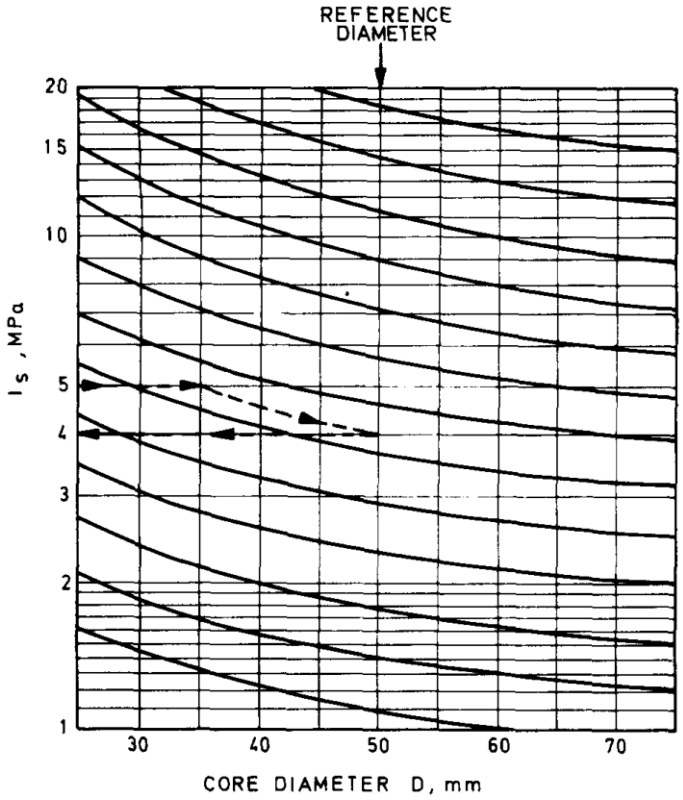

Figure 12. Size correlation chart for point-load index proposed by Broch and Franklin (1972).

The rock samples were classified for strength based on their uniaxial compressive strength rather than the point-load index itself as this point-load tests were utilised for strength classification purposes. The uniaxial compressive strength was calculated from the point-load test and then used to classify the rock material for strength (see Table 6).

Table 6. Size correlation chart for point-load index proposed by Broch and Franklin (1972).

Description (MPa)	Uniaxial compressive strength (MPa)	Point-load index (MPa)
Very high strength	>200	>8
High strength	100 – 200	4 – 8
Medium strength	50 – 100	2 – 4
Low strength	25 – 50	1 – 2
Very low strength	< 25	< 1

3.6.2. Porosity and Permeability tests

The porosity and permeability measurements have not been completed because the standard size requirement for such tests is 100 mm core length and 50 mm diameter. Thus, even though the samples of ZA met length requirement, they were only half the core and about 30 mm diameter. Therefore, the porosity was estimated with the help of the petrographic microscope using blue dyed epoxy, and by using the petrographic and mineralogical composition of the samples and their textures. Thereafter, the samples were plotted in the Porosity and Permeability *vs*. Depth diagram in relationship with the sandstone composition (North, 1985) (Fig. 13).

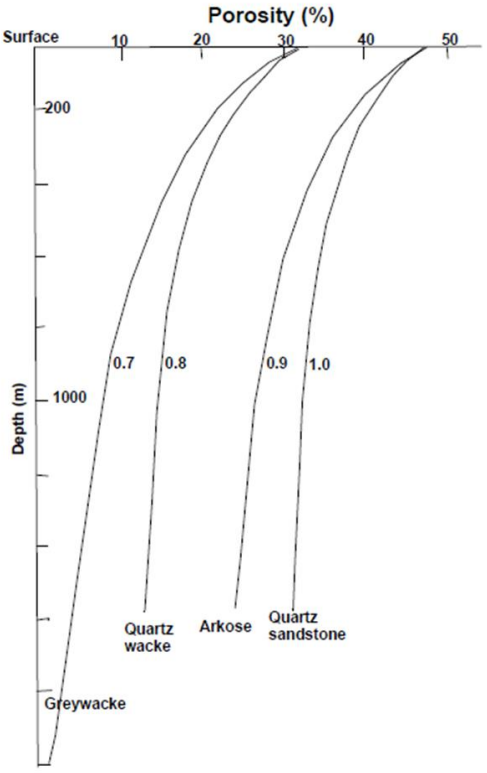

Figure 13. Porosity and permeability vs depth diagram in relationship with the sandstone composition (North, 1985). For instance, a greywacke occurring at 1000 m depth will have the porosity 8% and the permeability of 0.7 milliDarci.

3.6.3. Geochemical Modelling

Rock samples of the sandstones and siltstones were placed in autoclaves before exposing to simulated *in situ* reservoir conditions of 100°C temperature and 100 bars pressure in pure water and $scCO_2$ for a period of four weeks. The study aimed at modeling long-term storage to assess the ultimate fate of the CO_2 injection and its impacts on physical and mineralogical properties of the rocks. The conditions for samples immersed in $scCO_2$ were kept constant for a period of four weeks for sandstone and siltstone rocks. The purpose of treating the rocks with $scCO_2$ was to experimentally evaluate the changes of the mineralogy, geochemistry, and grain shape of the rocks, which may affect the porosity and permeability of the sandstone and cap rock materials.

4. RESULTS

The results of the present study are presented in the sequence of work from visual and spectral core analysis to geochemical investigations and petrography in an attempt to address the project objectives.

4.1. Core logging results

4.1.1. Location and lithological characterisation of the ZA rocks

The lowermost part of the ZA core from the recorded bottom at 1779.9 to 1602 m is missing. The preserved part starting at 1602 m depth of the ZA drill core is characterised by heterogeneous lithology dominated by siltstones followed by sandstones associated with abundant fossils such as algae, echinoderm fragments, foraminifera, bivalves, gastropods, specules and plant debris, and minor carbonate rocks.

The main siltstone intervals are encountered at 1595.63 - 1445.00 m; 1386.84 - 1041.25 m; 675.31 - 649.30 m; 635.43 - 625.09 m; 612.80 - 482.14 m; 426.72 - 415.00 m; and 240.61 - 129.84 m depth. The sandstone intervals occur at the following ranges of depth: 1035.66-965 m; 866.14 - 795.76 m; 787.60 - 675.31 m; 649.30 - 635.43 m; and 360 - 240.61 m. Both siltstone and sandstone layers occur in varying colours ranging from dark brown, brown, light brown, dark green to brown grey and grey. They are all weakly to moderately indurated and some of them effervesce with 5% HCl indicating carbonate content (calcareous). These calcareous siltstones and calcareous sandstones are greyish in colour. They occur at 1602.69 - 1577.34 m; 1445.23 - 1386.84 m; 482.14 - 426.72 m and 415-360 m for calcareous siltstones; and 965-866.14 m and 795.76-787.60 m, for calcareous sandstones. The alternation of siltstone and sandstone beds is evident throughout the ZA sequence (Fig. 14).

The other beds of rocks of the ZA core, namely the bioclastic limestones are light grey to grey coloured. They are rich in algae, foraminifera, gastropods, bivalve and plant remains, and strongly effervesces with 5% HCl. These limestone layers occur respectively at 1340 – 1310 m, 1178, 87 - 1178.8 m, 1161.49 - 1161.39 m, 1148.98 - 1147.78 m, 1093.55 - 1093.55 m, 1084.78 - 1084.56 m, 1053.59 - 1053.44 m, 1041.3 - 1035.4 m and 129.84 to 89 m.

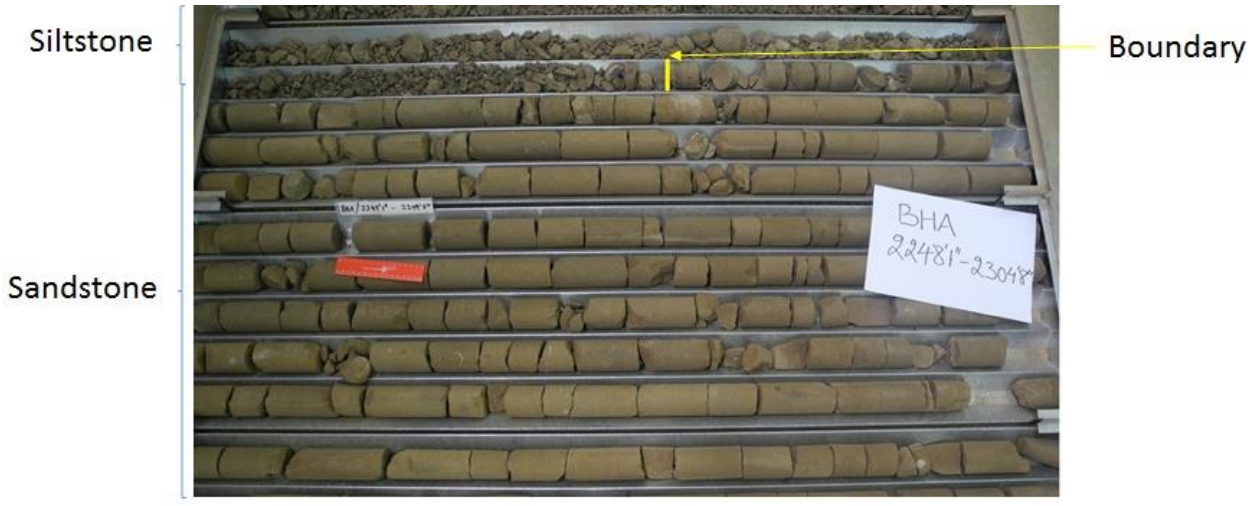

Figure 14. Illustration of the sharp boundary (marked in yellow) between siltstone (friable) and sandstone (intact) layers at 675 m depths in the ZA core. The longtime of core storage at the national core library allowed for weathering and alteration of clay minerals that resulted in increased friability of siltstones and mudstones of the core.

4.1.2. Description of the ZA Sequence

The missing part of the ZA core from 1779.9 to 1602 m has been probably taken after the boreholes were drilled by SOEKOR in the 1970's to assess their hydrocarbon potential. However, the missing core part was reported in the "Phase A Report" entitled "An effective CO_2 storage capacity assessment of the Zululand Basin, South Africa" prepared by Viljoen et al. (n.d.), and identified as arenites. They probably represent the entire Makatini Formation.

Thus, the herein described investigations start at 1602 m depth. Between 1602 and 1577 m, the layers are characterised by dark grey coloured calcareous siltstone,

rich in foraminifera and algae fossils and overlain by a greyish brown siltstone layer at the depth between 1577 m and 1512 m. This greyish brown siltstone bed contains dark spots of organic matter and hematite and it is overlain by the succession of siltstone layers from 1512 m to 1041.25 m. These siltstone layers contain some thin carbonate interbeds at the depths between 1445.23 to 1386.84 m and 1326.59 to 1323.54 m respectively (Fig. 15). The ZA core at the depth between 1041.25 to 1035.4m is characterised by the occurrence of c. 6 m thick bioclastic limestone bed. This carbonate layer is greyish-brown coloured, rich in fossils such as bivalves and gastropods and overlain by the alternation of calcareous sandstone and arkosic wacke strata at the depth between 1035.66 - 675.31 m. There is occurrence of subarkose beds intercalating the calcareous sandstone and arkosic wacke layers at 749.66-731.95m. These sandstone strata are bedded and bioturbated, contain also some bivalve and gastropod shells with plant remains.

At the depth between 675.31 to 612 m, the ZA core consists of a succession of siltstone and sandstone layers. The siltstone and the sandstone beds are brown coloured. The siltstone strata show in some part thin lamination whereas the sandstones are rather massively bedded without internal sedimentary structures. Dark brown to green coloured, bioturbated siltstone beds also occur overlying this siltstone and sandstone succession at 635.43 - 612.8 m depths. The siltstone beds contain dark spots of organic matter and bivalve and gastropod fossils. This succession of sedimentary rocks is followed by 245 m thick calcareous siltstone sequence ending at 360 m depth. The calcareous siltstone sequence is overlain by a brownish and massive sandstone followed by glauconitic sandstone at 256 m depth. Both contain plant remains and organic matter, and are covered by brown grey siltstone strata at the depth from 240 to 129 m. A bioclastic limestone terminates the core at 89 m depth

(Fig. 15). The top 89 m strata are missing, but probably represented mainly unconsolidated materials, soils and sands. Nonetheless, no information is available from the previous reports.

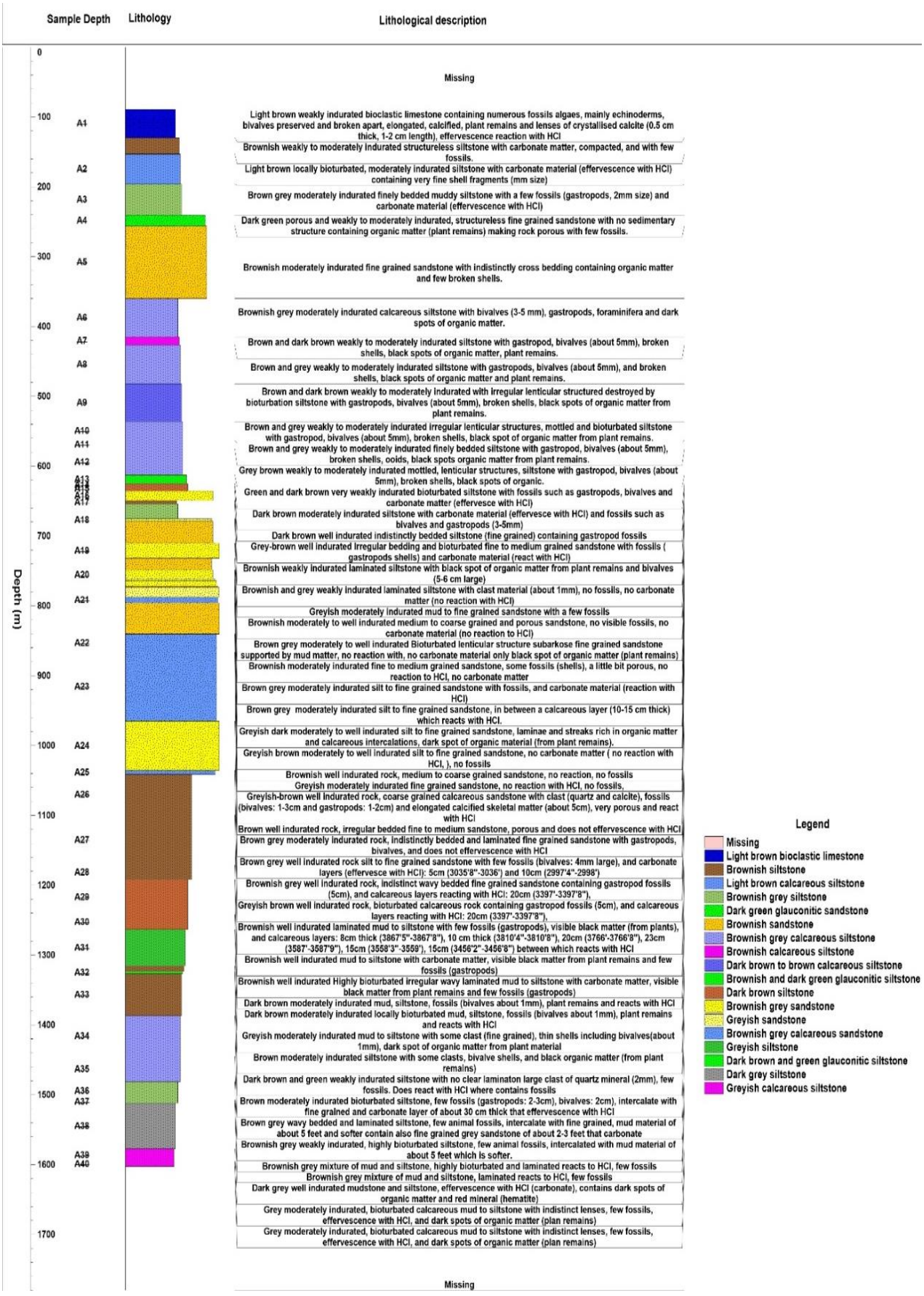

Figure 15. Lithological sequence and description of the ZA core.

4.2. Spectral logging results

In Figure 16, the distribution of the spectrally deduced carbonate, gypsum and clay minerals in depth of the ZA core is shown. The rocks are dominated by the occurrence of clay minerals such as Mg_smectite (0-100%), Al_smectite (0 – 60%), chlorite (0 – 20%), kaolinite (0-2%), nontronite (0 – 1.5%) and illite (0-1%). Gypsum mineral is also present. Gypsum occurs at the depth between 200 and 400 m. Minerals such quartz, plagioclase, hematite and micas were not detected because of the Short-Wave Infrared which does not detect such minerals.

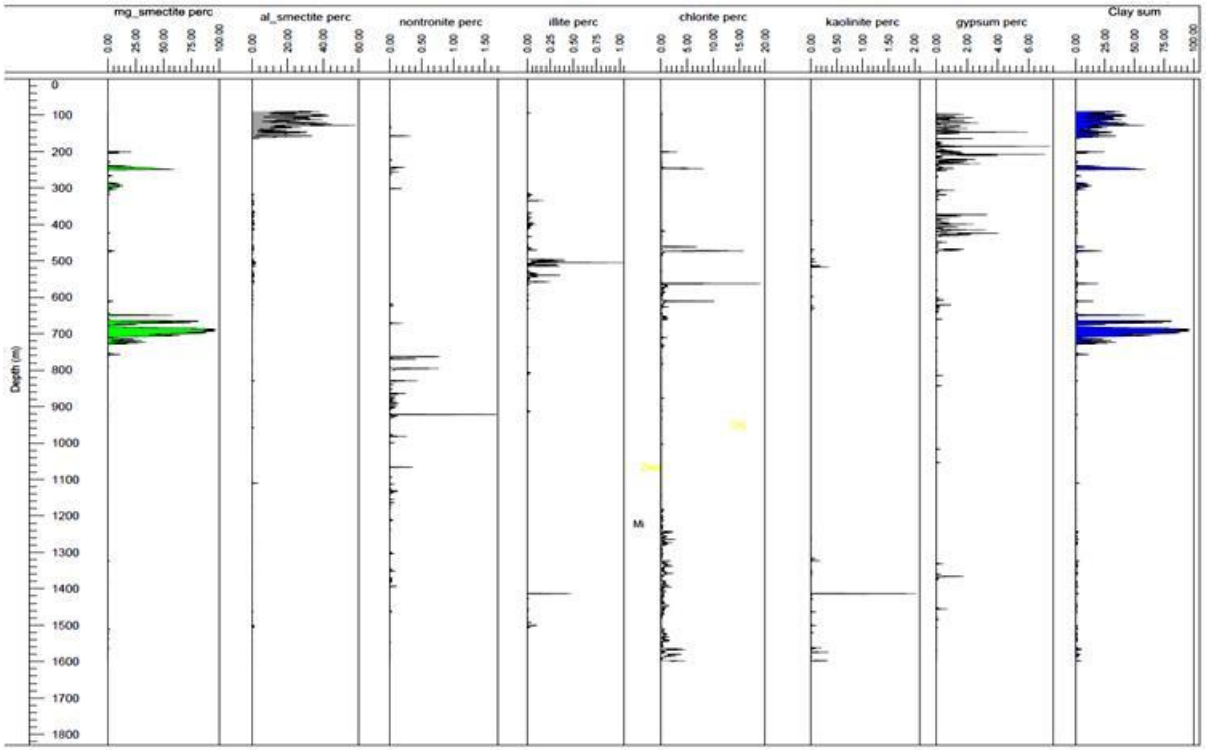

Figure 16. Mineral spectral results of the ZA core. The graphs show in depth measured minerals including clays and gypsum. The other 50% represents the empty spaces where there are not peaks in the spectral graphs, which indicate the minerals (quartz, plagioclase, hematite and micas that were detected using Short-Wave Infrared.

4.3. Petrography results

4.3.1. Siltstones

Based on the mineralogical descriptions of uncovered thin sections, three siltstone types were discriminated throughout the entire ZA core. There are calcareous siltstone, glauconitic siltstone and argillaceous siltstone. The calcareous siltstones are brown grey, dark grey and grey coloured, locally to commonly bioturbated. Sedimentary structures such as laminations and wavy lamination are visible. The calcareous siltstones are represented by the samples A6 (379.3 - 379.5 m), A8 (445.5 - 445.6 m), A10 (536.4 - 536.5 m), A11 (562.6 - 562.7 m), A12 (575.5 - 575.7 m), A34 (1415.6 - 1415.8 m), A39 (1592.6 - 1592.7 m) and A40 (1597.4 - 1597.5 m). These rocks have a strong effervescence in contact with 5% of HCl, indicating the presence of carbonate content visible as grains and in the matrix. The calcareous siltstones are compositionally immature and rich in shallow marine fossils such as foraminifera, echinoderms, bivalve, and algae, visible to the naked eye as well as in the thin sections, all constituting 32 to 60% of calcite. Sample A23 (911.3 - 911.4 m), A34 (1415.6 - 1415.8 m), A39 (1592.6 - 1592.7 m) and A40 (1597.4 - 1597.5 m) contain 57 to 60% of calcite. The calcite occurs as grains, matrix and cement in the calcareous siltstone rocks. The calcite grain size varies from micritic to silt size (10 to 60 µm). The calcite dominant matrix occurs in the samples A2 (188.1 - 189.98 m), A14 (625 – 625.1 m), A10 (536.4 - 536.5 m), A12 (575.5 - 575.7 m), A34 (1415.6 - 1415.8 m), A39 (1592.6 - 1592.7 m) and A40 (1597.4 - 1597.5 m). Clay minerals and limonite also occur within the matrix. The calcite cement shows a poikilotopic texture in some siltstones such as A10 (536.4 - 536.5 m) and A12 (575.5 - 575.7 m) (Appendices A and B). There are also grains of quartz, plagioclase, mica and light green glauconite present in the calcareous siltstone rocks. Idiomorphic plagioclase in the form of albite

was also encountered within a calcite matrix in the samples A10 (536.4 - 536.5 m) and A40 (1597.4 - 1597.5 m) (Fig. 17.1).

The glauconitic siltstones are laminated or structureless, dark brown to greenish coloured with dark spots of organic matter. These glauconitic siltstones are represented by sample A13 (612.8 – 613 m), A32 (1324 – 1324.1 m) and A38 (1529.4 - 1529.5 m) in their respective depths. These are compositionally immature rocks containing light green to green coloured, subrounded to rounded glauconite grains. These glauconite grains occur as part of the matrix associated with smectites (Fig. 17.2), chlorite and hematite, and are filling the interstitial part of fossils. The glauconite content is about 25 to 33% in the glauconitic siltstone rocks. These rocks contain also silt- sized (20-60 µm), angular grains of quartz, plagioclase and flakes of mica.

The argillaceous siltstones are laminated and structureless, light brown, brown to brown-grey coloured. These argillaceous siltstones occur in different depths throughout the ZA core: samples A2 (188.1 - 189.98 m), A3 (218.5 – 218.6 m), A9 (482.14 - 482.19 m), A14 (625 – 625.1 m), A15 (632.9 - 632.8 m), A17 (651.7 - 651.9 m), A26 (1076.8 - 1076.9 m), A30 (1242 – 1242.1 m), A31 (1294.1 - 1294.2 m), A33 (1369 – 1369.2 m), and A36 (1484.3 - 1484.4 m). They are as well compositionally immature rocks and contain 27 to 54% of clay minerals in the matrix (Fig. 18). This clayey matrix is made up of smectite displaying brown colours, chlorite (greenish colour) including minerals such as calcite, glauconite, hematite and zeolites. The matrix is supporting silt- sized (25-60 µm) grains of angular detrital quartz, feldspar and mica. The argillaceous siltstone rocks have an average of 27% of quartz, 23% calcite, and 14% of plagioclase. Hematite and mica have respectively 2 and 1% on average. Bivalves and broken shells are also encountered in all these argillaceous siltstones except sample A3.

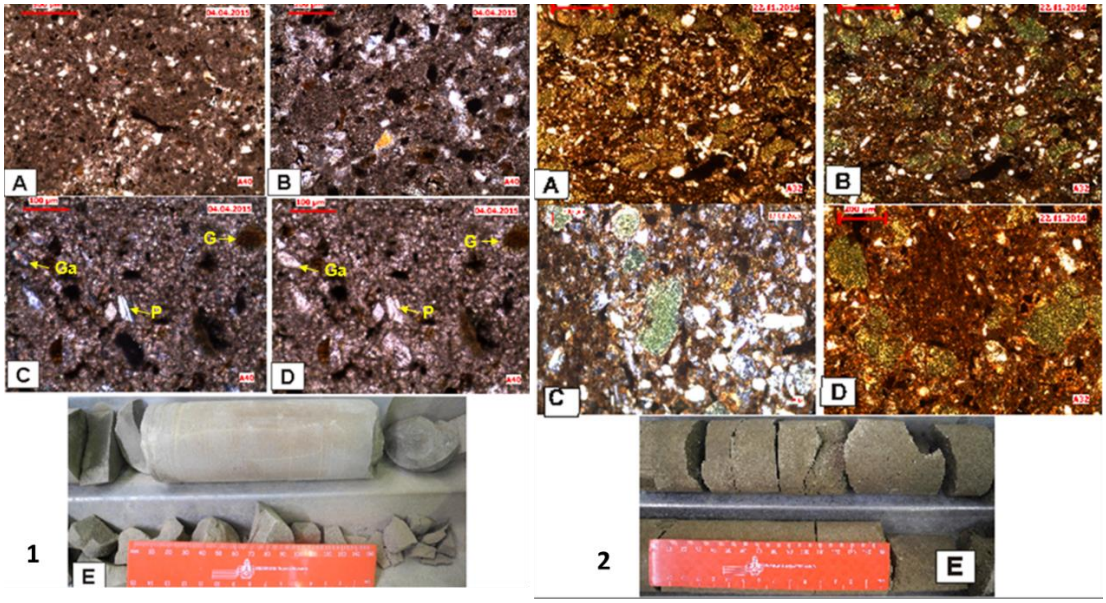

Figure 17. ***1.*** *Photomicrographs and photograph of a calcareous siltstone sample: A40 (depth of 1597.4 - 1597.5 m). A (PPL) and B (XPL): silt- sized quartz grains with glauconite, limonite and plant debris in a calcite matrix. C (XPL) and D (PPL) both show idiomorphic plagioclase (P), glauconite (G) and Gastropod (Ga) in a calcite matrix. E. Pale grey well indurated calcareous siltstone.* ***2.*** *Glauconitic siltstone (sample 32: 1324 – 1324.1 m): A, B, C and D: Microphotographs. A (PPL) and B (XPL): Siltstone rich in glauconite, quartz and plagioclase grains floating in clayey matrix. C (XPL): clast of quartz and plagioclase in the matrix with glauconite and clay minerals associated with organic matter. D (PPL): Glauconite grains associated with other clay minerals and organic matter as matrix supporting silt- sized clast of quartz and plagioclase. E: Dark green coloured siltstone not clear lamination.*

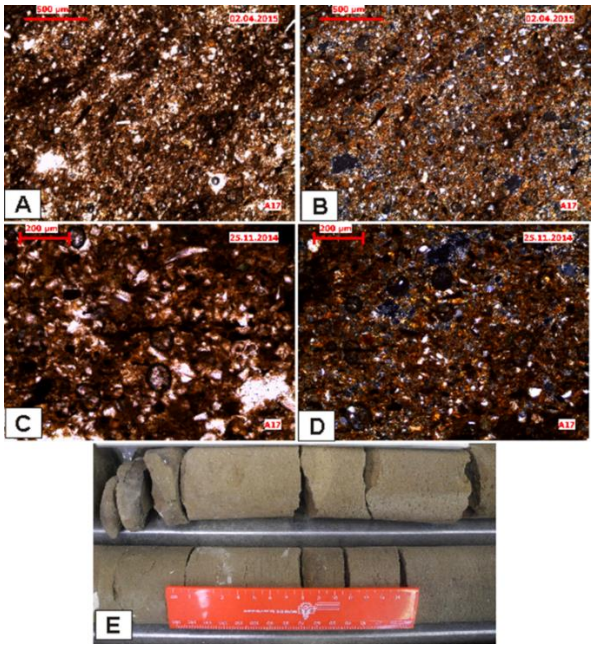

Figure 18. Photomicrographs and photograph of the siltstone sample: A17 at the depth of 651.7 - 651.9 m. A (PPL), B (XPL): argillaceous siltstone showing silt sized quartz

(the whitish subangular grains) and plagioclase (greyish elongated grains) in a clayey matrix with lamination structure. C (PPL), D (XPL): Clayey matrix associated with hematite (reddish colour).

4.3.2. Sandstones

The sandstones are represented by the samples A4 (246.5 - 246.6 m), A5 (311.2 - 311.3 m), A16 (648.8 - 648.9 m), A18 (685.4 - 685.5 m), A19 (710.4 - 710.5 m), A20 (760.7 - 760.9 m), A21 (788.1 - 788.2 m), A22 (855.5 - 855.6 m), A23 (911.3 - 911.4 m), A24 (965.8 - 965.9 m) (Appendices A and B). Macroscopically, the sandstones are dark brown to green, brown and grey coloured, moderately to well indurated, bioturbated, massive, laminated, cross-bedded and parallel bedded sedimentary rocks. Pore spaces are visible by unaided eyes in some samples, namely A16, A18 (Fig. 19.2), A19, and A20, which indicates that the porosity of these sandstone is good.

Microscopically, the sandstones are compositionally poorly to moderately sorted (immature to submature sedimentary rocks), and fine to medium grained. The size of grains ranges from 70 to 600 µm and these grains are composed mostly of subangular to angular quartz (80 to 600 µm), plagioclase (90 to 600 µm), and flakes of mica (100 to 200 µm). Sample A16 (Appendix B) shows evidence of polycrystalline quartz and altered plagioclase. The lithic fragments are encountered all the sandstones (see samples A16: 648.8 - 648.9 m, A18: 685.4 - 685.5 m, A19: 710.4 - 710.5 m, and A21: 788.1 - 788.2 m). Zircon also occurs, particularly in the sample A19 displaying euhedral shape, high relief and birefringence with parallel extinction.

All sandstone samples like A16 (648.8 - 648.9 m), A21 (788.1 - 788.2 m), A22 (855.5 - 855.6 m), A23 (911.3 - 911.4 m), A24 (965.8 - 965.9 m) and A25 (1035.4 – 1035.5 m) contain abundant of unbroken and broken fossils such as elongated

calcified algae, bivalves, echinoderms, foraminifera, gastropods, pellets and plant debris. The size of these fossils varies from 40 µm up to about 15 mm. The grains of these sandstones are supported by clayey matrix associated with glauconite, hematite and zeolite. Calcite is also present in the sandstone samples, notably A21, A22, A23 (Fig. 20) and A25. It occurs as grains, as part of the matrix with clay minerals and as cement. Glauconite grains are scattered in the matrix and occur as rounded and greenish grains in the sandstones, like in A4 (Fig. 19.1) and A23 (Fig. 20).

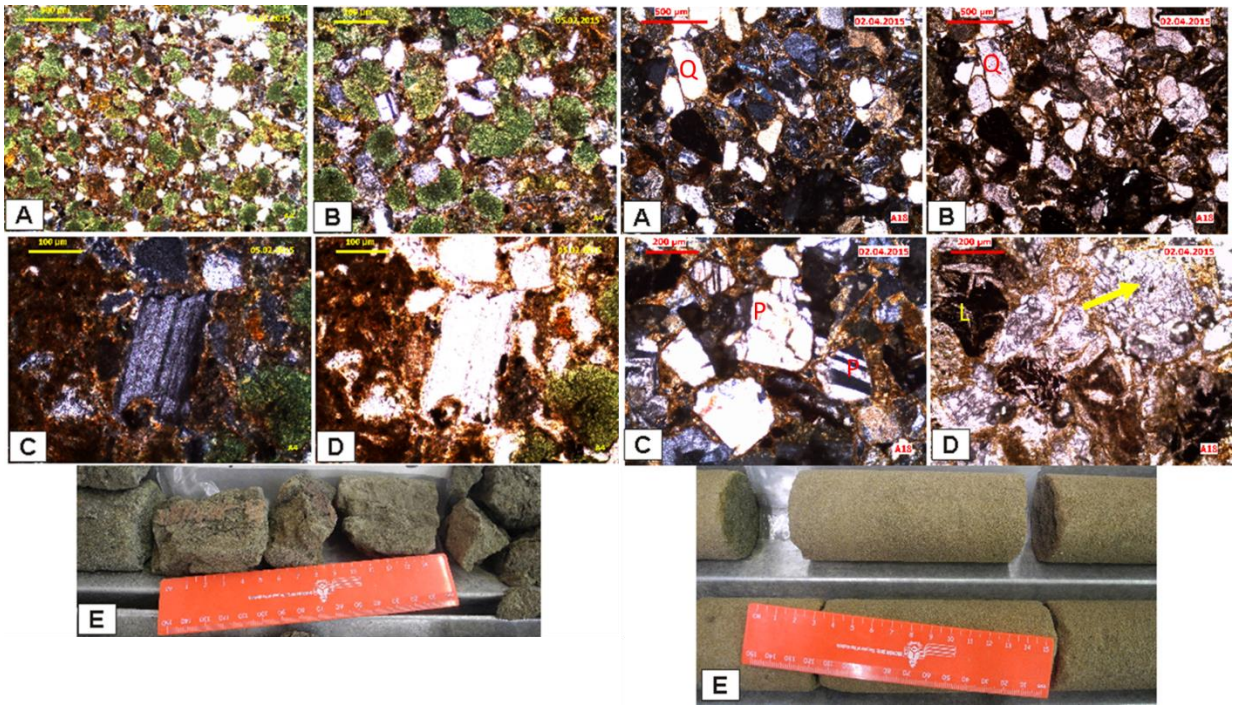

Figure 19. ***1.*** *Glauconitic sandstone photomicrographs: sample A4 (246.5 - 246.6 m). A and B show subrounded green glauconitic grains supporting subangular quartz. C (XPL) and D (PPL) angular plagioclase (P) grains in clayey matrix. E. Photograph shows green coloured structureless sandstone.* ***2.*** *Parallel bedded arkosic wacke photomicrographs and photograph of A18 (685.4 - 685.5 m): sandstone. A (XPL) and B (PPL) showing angular quartz (Q) and plagioclase (P) grains supported by clayey matrix. C. Angular plagioclase with twinning in clayey matrix (10x). D. Lithic fragments (L). E: brown coloured, medium to coarse grained, parallel bedded sandstone.*

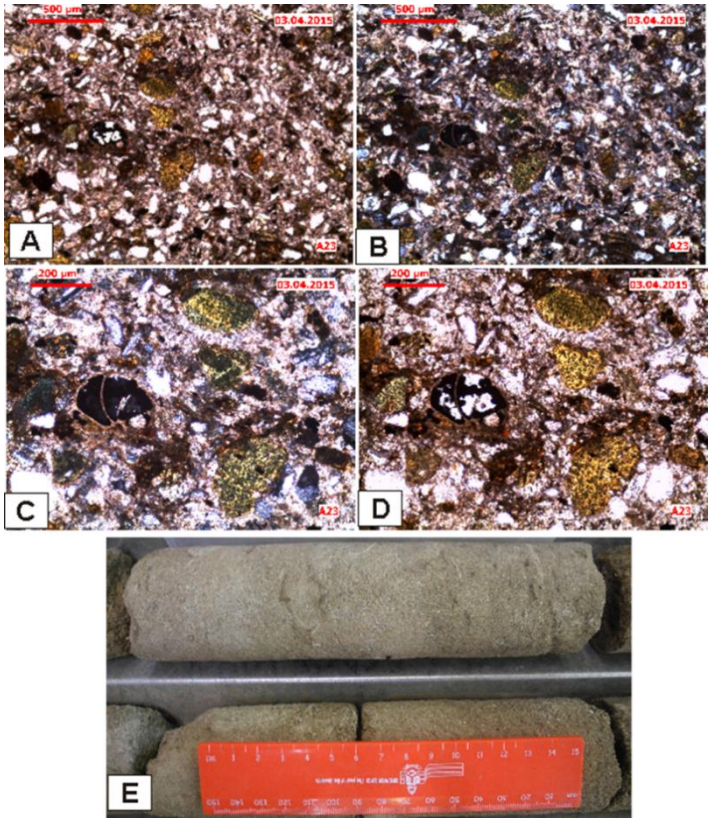

Figure 20. Photomicrographs and photograph of the calcareous sandstone sample A23 (911.3 - 911.4 m). A (PPL), B (XPL) green, rounded glauconite, plagioclase and quartz grains in mainly calcitic cement. C (XPL), D (PPL) Angular plagioclase, quartz, rounded greenish glauconite with moderately preserved foraminifera and calcite inclusion. E: Light brown fine grained sandstone, rich in broken and unbroken fossils, irregular lamination with streaks and lenses of broken shells.

Based on the mineralogical analysis, the ZA sandstones are classified as quartzofeldspathic sandstone and hybrid sandstones notably glauconitic and calcareous sandstone. The quartzofeldspathic sandstones have in sum more than 70% of quartz and plagioclase grains combined with clay minerals up to 15%. Samples A5 (311.2 - 311.3 m), A16 (648.8 - 648.9 m), A18 (685.4 - 685.5 m), A19 (710.4 - 710.5 m), A20 (760.7 - 760.9 m), and A24 (965.8 - 965.9 m) represent this type of sandstone. The calcareous sandstones have calcite content ranging from 28 to 79% which is inversely proportional to the sum of quartz and plagioclase in the same samples. The calcareous sandstones are rich in bivalve, gastropod, brachiopod,

echinoderm and foraminifera fossils which are indicatives of a shallow marine environment. The calcareous sandstone rocks are represented by samples A21 (788.1 - 788.2 m), A22 (855.5 - 855.6 m), A23 (911.3 - 911.4 m) and A25 (1035.4 – 1035.5 m). The glauconitic sandstone contains more than 10% of authigenic glauconite grains which indicate marine diagenetic conditions. This glauconitic sandstone rock is represented by the sample A4 and occurs at 240-256 m depth.

The glauconitic and arkosic sandstone samples (except A19) are discriminated based on the sand, silt, clay grades (Tucker, 1991) as clayey sandstones (Fig. 21A). Sample A19 (710.4 - 710.5 m) has more than 90% of sand grains, it is therefore classified as subarkose (Fig. 21B) according to the classification of sandstones adopted by Dott (1964), and modified by Pettijohn et al. (1973), in Greensmith (1978). Sample A5 (311.2 - 311.3 m) is an arkose (Fig. 21B) and others are categorised in the wacke group because of their matrix amount exceeding 15%. Sample A4 (240 – 256 m) is a glauconitic arkosic wacke; whereas A16 (648.8 - 648.9 m), A18 (685.4 - 685.5 m), 20 (760.7 - 760.9 m), and A24 (965.8 - 965.9 m) are arkosic wackes (Fig. 21C).

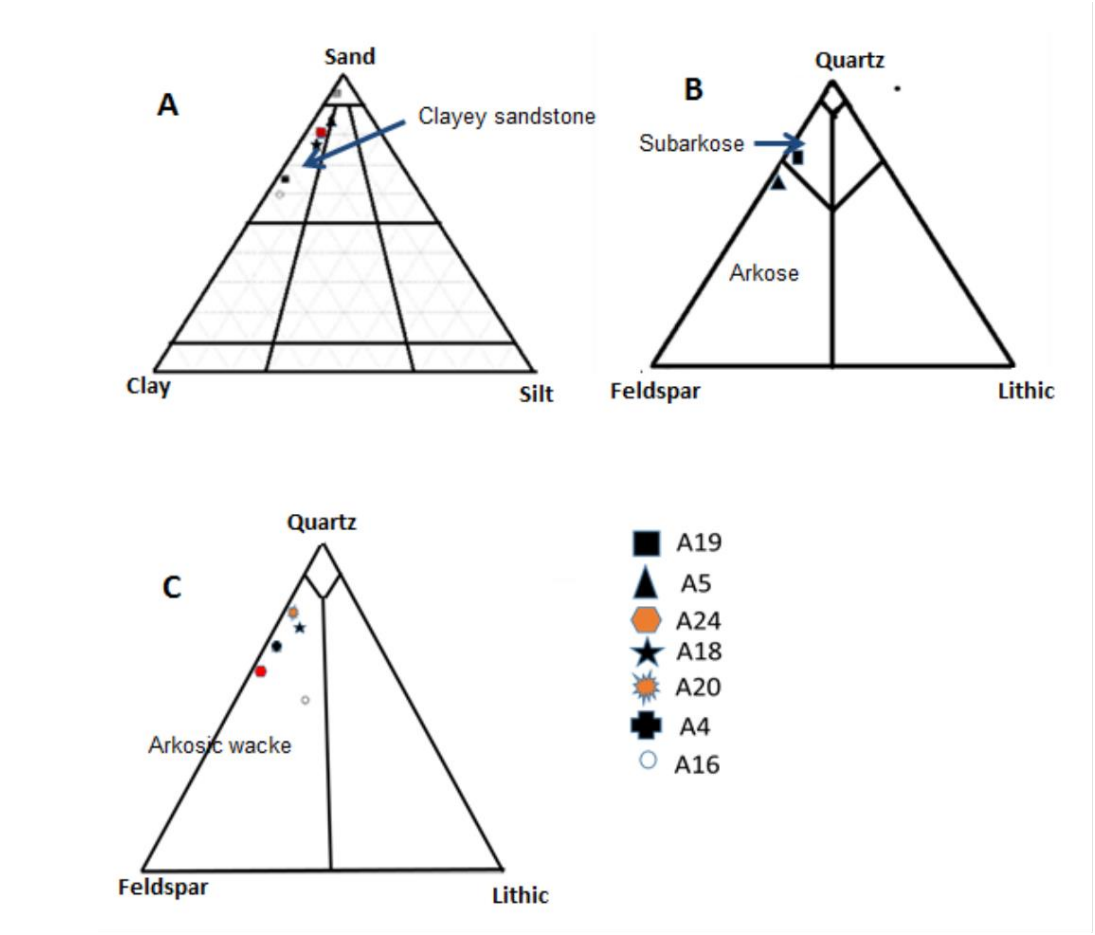

Figure 21. Ternary diagrams: A. Classification of ZA sandstones based on sand, silt and clay content, modified from Folk (1974) in Tucker (1991). B and C (wacke group): classification of ZA sandstones according to Dott (1964), Pettijohn et al. (1973), in Greensmith (1978). B only sandstones with less than 15% clay minerals and C only sandstones with more than 15% of clay minerals.

4.3.3. Carbonate rocks

The carbonate rocks are represented by the samples A1 (105.3 – 105.5m: see Fig. 22) and A25 (1035.4 – 1035.5 m) which are limestones. These limestones are light brown to grey coloured, fine grained, weakly indurated (sample A1) to well indurated (A25). They have massive texture without other clear sedimentary structures. The sample contains plenty of fossils, dominated by echinoderms including elongated, spherical, and platy shapes. There is also evidence of broken carapaces showing pentagonal and hexagonal shapes (Appendix B1). Other fossils such as

foraminifera, specules, bivalves, gastropods and algae also occur. The size of the fossil fragments varies from 30 µm to about 5 cm length.

The sample A1 (105.3 – 105.5m) (Fig. 22) shows mostly unbroken skeletal fragments (bioclasts). All the fossils are in contact with each other. Whereas the sample A25 shows plenty of unbroken fossils. Grains such as plagioclase and quartz are surrounding skeletal fragments. Clay and hematite minerals are present in the matrix, whereas calcite occurs as cement. These limestone samples comprise on average 86% calcite in the form of grains, matrix and skeletal fragments. The remaining 14% consists of 5% for each of plagioclase and clay minerals, 3% quartz and 1% hematite.

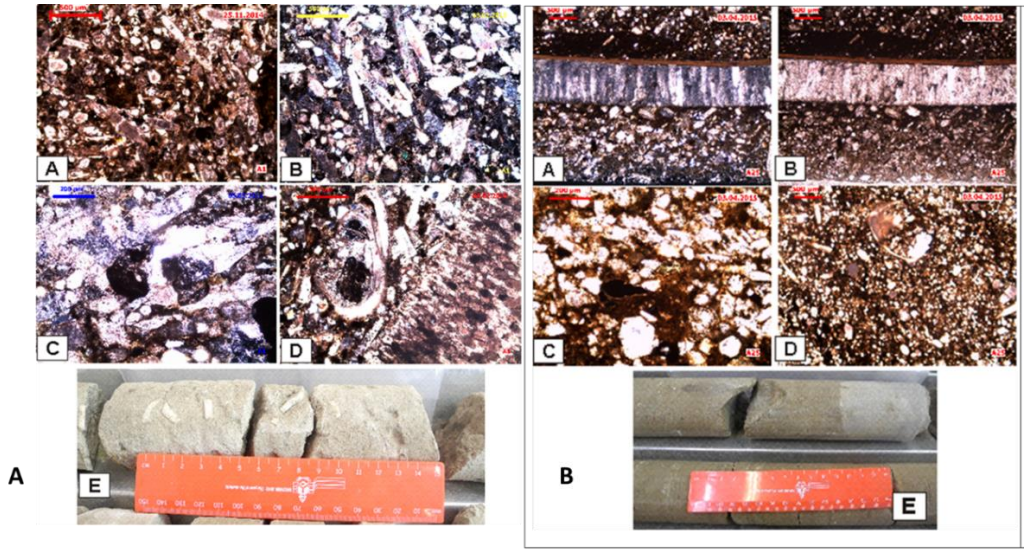

Figure 22. Bioclastic limestone photomicrographs and photographs: ***1.*** *Sample A1 (105.3 – 105.5 m): A (PPL), B (XPL) calcified elongated echinoderms embedded in calcite cement with some clay minerals. C (XPL) large calcite grains (sparite) associated with quartz and clay minerals. D (PPL) Large inoceramid bivalve showing prismatic structures, associated with much small skeletal fragments. E. Light brown to grey biosparite containing 5mm thick plate algae and broken fossils.* ***2****. Sample A25 (1035.4 – 1035.5 m): A, B, C and D: Microphotographs. A (XPL) and B (PPL): elongated shell fragment associated with grains of quartz, plagioclase and calcite in the clayey and micritic matrix. C (PPL) sparite grains supported by clay and micrite matrix. D. Brachiopods with shell fragments associated with quartz and plagioclase grains embedded in a clayey and micritic matrix. E. Bioclastic limestone showing two beds of different colour: grey bed is harder than the brown grey and rich in carbonate minerals than the brown grey bed (rich in broken shells).*

4.4. XRD results

Table 7. Mineralogical analysis of fourtyfourty samples in weight percentages.

Sample no (Depth)	Calcite	Hematite	Gypsum	Microcline	Plagioclase	Quartz	Mica	Chlorite	Zeolite	Smectite	Total
A1 (105.3 – 105.5 m)	73	Tc	-	2	10	9	Tc	Tc	-	4	98
A2 (188.1 - 189.98 m)	18	2	Tc	4	24	33	-	Tc	8	8	97
A3 (218.5 – 218.6 m)	14	4	0	-	14	47	-	-	12	9	100
A4 (246.5 - 246.6 m)	7	2	0	-	23	49	-	-	3	15	99
A5 (311.2 - 311.3 m)	7	2	Tc	-	29	61	-	-	-	-	99
A6 (379.3 - 379.5 m)	46	2	0	-	16	15	-	-	7	13	99
A7 (426.4 - 426.7 m)	19	3	0	-	19	35	2	2	7	13	100
A8 (445.5 - 445.6 m)	34	2	Tc	-	15	34	2	-	Tc	12	99
A9 (482.14 - 482.19 m)	16	3	Tc	-	22	29	3	-	3	25	101
A10 (536.4 - 536.5 m)	33	2	Tc	-	18	29	Tc	-	3	13	98
A11 (562.6 - 562.7 m)	32	2	Tc	-	19	27	-	Tc	2	16	98
A12 (575.5 - 575.7 m)	33	Tc	Tc	-	13	40	2	Tc	0	8	96
A13 (612.8 – 613 m)	6	4	Tc	-	17	46	5	-	Tc	21	99
A14 (625 – 625.1 m)	4	4	-	-	24	40	3	3	3	20	101
A15 (632.9 - 632.8 m)	3	4	Tc	-	21	41	3	2	3	23	100
A16 (648.8 - 648.9 m)	10	2	Tc	-	18	35	Tc	-	-	33	98
A17 (651.7 - 651.9 m)	10	4	Tc	-	28	13	2	3	4	35	99
A18 (685.4 - 685.5 m)	-	Tc	Tc	-	15	63	Tc	-	-	19	97
A19 (710.4 - 710.5 m)	-	12	-	-	18	63	2	-	-	4	99
A20 (760.7 - 760.9 m)	2	Tc	2	-	15	63	Tc	-	2	12	96

A21 (788.1 - 788.2 m)	48	Tc	Tc	-	8	41	Tc	-	-	Tc	97
A22 (855.5 - 855.6 m)	28	2	-	-	17	29	2	-	5	17	100
A23 (911.3 - 911.4 m)	60	Tc	-	-	6	23	2	2	Tc	5	98
A24 (965.8 - 965.9 m)	6	3	0	-	27	45	3	4	3	10	101
A25 (1035.4 – 1035.5 m)	79	Tc	Tc	-	5	9	Tc	Tc	3	-	96
A26 (1076.8 - 1076.9 m)	5	2	Tc	-	24	31	-	3	14	20	99
A27 (1129.8 - 1129.9 m)	8	3	-	-	18	36	-	-	3	32	100
A28 (1170.1 - 1171.1 m)	6	2	Tc	-	22	42	3	3	-	20	98
A29 (1194.1 - 1194.2 m)	4	2	Tc	-	30	30	3	2	2	25	98
A30 (1242 – 1242.1 m)	10	2	Tc	-	20	32	3	3	6	22	98
A31 (1294.1 - 1294.2 m)	6	2	Tc	-	14	35	Tc	3	4	35	99
A32 (1324 – 1324.1 m)	3	2	Tc	-	25	26	3	4	3	32	98
A33 (1369 – 1369.2 m)	8	4	-	-	19	23	-	4	8	35	101
A34 (1415.6 - 1415.8 m)	57	Tc	-	-	9	21	2	2	2	5	98
A35 (1445.2 - 1445.4 m)	Tc	2	Tc	-	15	27	2	3	2	47	98
A36 (1484.3 - 1484.4 m)	27	Tc	Tc	-	17	31	Tc	3	2	17	97
A37 (1507.8 - 1507.9 m)	Tc	Tc	0	-	15	44	Tc	3	2	33	97
A38 (1529.4 - 1529.5 m)	Tc	2	Tc	-	13	28	3	10	Tc	41	97
A39 (1592.6 - 1592.7 m)	57	Tc	-	-	4	29	Tc	Tc	3	5	98
A40 (1597.4 - 1597.5 m)	57	4	-	-	11	14	-	-	3	10	99

Note:

- (-) : Not detected
- (Tc) : Trace

The table 7 shows the XRD results of fourty samples. The lithology is dominated by minerals such as quartz (9 to 63 wt%), calcite (2 to 79%), plagioclase (4 to 30wt%) and smectite contents (4 to 47wt%), followed by chlorite (2 to 10wt%), zeolite (2 to wt%), hematite (2 to 12wt%), mica and microcline (2 to 4wt%).

The amount of gypsum detected using spectral imaging is roughly 2%, whereas X-ray powder diffraction method has measured mainly traces around the same depth between 200 m and 400 m. However, the XRD technique has detected about 2% gypsum at the depth of 700 m, while the spectral imaging revealed the occurrence of gypsum mostly above 700 m. This clearly shows that the gypsum is only concentrated on the surface of the core probably as a result of core alteration in the core shed.

4.5. XRF results

Table 8 illustrates major elements analysis of fourty samples in weight percentages. SiO_2 and CaO contents are abundant, their amounts range individually from 21.6 to 67.5 wt% and 2 to 36.5 wt%. They are followed by Al_2O_3 (5-14 wt%), Fe_2O_3 (2.7 to 14 wt%), MgO (1 to 4.6 wt%), Na_2O (0.54 to 2.71%wt%), K_2O (0.58 to 4 wt%) and TiO_2 contents (033 to 1.27% wt%). The XRF results show also the presence of MnO, P_2O5 and Cr_2O_3 contents, which their individual amounts are less than 1 wt%. LOI and H_2O contents vary respectively from 1.32 to 28.09 wt% and 0.97 to 4.88 wt%.

Table 8. XRF results of the fourty samples in weight percentages.

Sample ID (Depth)	SiO_2	TiO_2	Al_2O_3	Fe_2O_3	MnO	MgO	CaO	Na_2O	K_2O	P_2O_5	Cr_2O_3	LOI	H_2O-	Total

A1 (105.3 – 105.5m)	23,07	0,33	5,29	2,68	0,04	1,54	35,6	0,54	0,95	0,05	0,01	27,67	2,3	100,1
A2 (188.1 - 189.98m)	58,65	0,88	10,69	6,15	0,06	3,21	7,87	2,22	1,66	0,1	0,03	6,12	3,88	101,5
A3 (218.5 – 218.6m)	64,32	0,8	9,69	6,73	0,04	2,84	5,59	1,7	1,86	0,11	0,03	3,6	4,07	101,4
A4 (246.5 - 246.6m)	50,48	1,01	10,95	7,36	0,12	3,57	17,29	2,13	1,63	0,11	0,03	1,94	3,77	100,4
A5 (311.2 - 311.3m)	60,32	0,94	12,18	7,56	0,06	4,18	4,45	2,53	1,94	0,1	0,03	3,16	3,04	100,5
A6 (379.3 - 379.5m)	54,82	0,87	11,25	7,03	0,06	3,81	4,13	2,41	1,9	0,09	0,03	10	3,34	99,7
A7 (426.4 - 426.7m)	52,07	0,99	12,4	8,32	0,06	3,38	8	2,44	2,29	0,1	0,03	7,17	3,33	100,6
A8 (445.5 - 445.6m)	46,81	0,96	10,32	7,42	0,09	3,26	14,77	2,09	1,53	0,09	0,03	9,27	3,56	100,2
A9 (482.14-482.19m)	51,95	1,04	12,9	9,12	0,08	4,25	7,16	2,71	2,13	0,1	0,03	5	4,23	100,7
A10 (536.4 - 536.5m)	47,31	0,94	11,67	7,57	0,1	3,02	12,46	2,29	1,88	0,09	0,02	8,99	3,65	100
A11 (562.6 - 562.7m)	53,05	0,93	10,69	7,8	0,08	2,88	10,68	2,09	1,86	0,09	0,03	6,49	3,65	100,3
A12 (575.5 - 575.7m)	49,17	0,86	9,33	6,39	0,09	2,25	15,57	1,68	1,6	0,09	0,03	10,95	2,47	100,5
A13 (612.8 - 613m)	53,4	0,93	10,15	6,94	0,1	2,45	16,93	1,82	1,74	0,1	0,03	2,38	3,31	100,3
A14 (625 – 625.1m)	57,1	0,93	11,31	13,42	0,05	3,42	2,49	1,67	3,59	0,1	0,03	1,68	4,2	100
A15 (632.9 - 632.8m)	58,47	1,06	12,92	9,86	0,06	3,68	3,27	2,42	2,39	0,11	0,03	2,17	3,84	100,3
A16 (648.8 - 648.9m)	55,74	0,98	9,68	12,33	0,08	4,69	5,54	2,12	1,82	0,14	0,03	2,32	4,88	100,4
A17 (651.7 - 651.9m)	45,58	1,27	13,89	11,79	0,15	4,4	8,75	2,66	2,09	0,27	0,03	3,57	4,47	98,9
A18 (685.4 - 685.5m)	67,54	0,91	9,8	7,54	0,09	4,04	3,25	2,44	1,37	0,13	0,03	1,49	2,73	101,4
A19 (710.4- 710.5m)	60,45	0,78	9,05	8,84	0,05	1,43	2,92	2,67	1,62	0,09	0,02	10	1,77	99,7
A20 (760.7 - 760.9m)	62,51	0,82	12,25	7,23	0,08	3,02	3,35	3,67	1,6	0,08	0,02	2,67	3,05	100,4
A21 (788.1 - 788.2m)	55,05	0,35	5,89	3,01	0,06	1,04	18,15	1,85	0,91	0,07	0,01	12,77	1,82	101
A22 (855.5 - 855.6m)	49,38	0,95	11,02	7,84	0,1	3,55	12,66	2,38	1,35	0,1	0,02	7,1	3,88	100,3
A23 (911.3 - 911.4m)	27,89	0,65	5,75	5,1	0,73	1,81	31,38	0,9	1,03	0,14	0,02	24,08	1,42	100,9
A24 (965.8 - 965.9m)	58,64	1,08	13,44	9,28	0,06	3,66	4,24	2,27	1,97	0,12	0,03	1,49	4,3	100,6
A25(1035.4-1035.5m)	22,64	0,44	5,3	3,13	0,55	1,28	36,5	0,84	0,58	0,09	0,01	27,55	1,06	100
A26(1076.8-1076.9m)	59,58	1,03	12,53	9,06	0,07	3,77	4,45	2,33	2,06	0,11	0,03	1,93	4	100,9
A27(1129.8-1129.9m)	56,92	1,13	12,42	9,64	0,09	4,07	6,04	2,44	1,77	0,12	0,03	2,15	3,98	100,8
A28(1170.1-1171.1m)	58,83	1,11	12,55	9,62	0,08	4,02	4,93	2,29	1,85	0,11	0,03	1,77	3,71	100,9
A29(1194.1-1194.2m)	56,79	1,03	13,08	9,32	0,08	3,92	4,7	2,49	2,02	0,11	0,03	3,36	3,28	100,2
A30(1242 – 1242.1m)	57,24	0,98	12,57	8,98	0,09	3,75	6,31	2,43	1,61	0,13	0,03	3,01	3,37	100,5
A31(1294.1-1294.2m)	55,13	1,05	13,45	9,44	0,08	3,82	5,23	2,65	1,98	0,12	0,03	4,35	3,48	100,8
A32 (1324 – 1324.1m)	53,86	1	12,69	12,4	0,07	3,82	3,94	2,17	2,78	0,14	0,03	3,97	4,04	100,9
A33 (1369 – 1369.2m)	49,47	1,17	13,96	10,44	0,09	3,89	6,62	2,62	2,28	0,14	0,02	6,29	3,73	100,7
A34(1415.6-1415.8m)	34,98	0,64	8,27	5,04	0,21	1,74	25,42	1,48	1,49	0,09	0,01	19,68	1,28	100,3
A35(1445.2-1445.4m)	60,41	1,12	13,96	8,95	0,06	3,95	3,06	1,99	1,99	0,11	0,03	1,8	3,42	100,8
A36(1484.3-1484.4m)	46,69	0,86	10,92	6,58	0,18	2,71	15,25	1,69	1,46	0,19	0,02	11,4	2,16	100,1
A37(1507.8-1507.9m)	62,88	1,06	13,22	8,58	0,06	3,9	2,76	2,3	1,64	0,13	0,03	1,56	3,54	101,7
A38(1529.4-1529.5m)	58,07	1,05	11,55	13,84	0,1	4,56	2,85	1,99	1,93	0,16	0,04	1,32	3,17	100,6
A39(1592.6-1592.7m)	22,54	0,52	5,74	3,32	0,39	1,29	35,6	0,94	0,89	0,09	0,01	27,51	0,97	99,8
A40(1597.4-1597.5m)	21,59	0,48	5,79	4,03	0,8	1,42	35,95	0,77	0,87	0,13	0,01	28,09	1,07	101

5. INTERPRETATION OF THE PETROGRAPHY, MINERALOGY AND GEOCHEMISTRY THE ROCKS OF ZA CORE

5.1. Petrography of the ZA core

The petrographic interpretation of the ZA rocks provided an insight to the lithofacies characteristics and the depositional environment of each facies in the borehole ZA. The overall lithology of the borehole ZA is heterogenous resulting from the fluctuations of the sea level during the breakup of Gondwana, causing accumulation and deposition of vertically stacked facies (Tankard, 1982; Shone, 2006). These geological conditions and processes impact on the grain size, texture, mineralogy and chemistry of the sedimentary rocks. The ZA sedimentary rocks are grouped into three groups notably, siltstones, sandstones and limestones. The siltstones and sandstones are discussed together because they are compositionally similar.

5.1.1. Siltstones and Sandstones

The siltstones and sandstones show sedimentary structures such as parallel lamination, wavy beds, parallel beds and cross beds. The lamination structures are mostly found in the ZA siltstones, indicate a low rate of sedimentation in the basin, allowing the sediment to settle horizontally (Tucker, 2009). The wavy beds are caused by the agitation of water forming waves (Reineck and Singh, 1980). The cross-bed occurs typically in the ZA sandstones and indicate that the sediments were deposited as ripples due to the water flow (Tucker, 2009). The bioturbation structures were encountered in some of the siltstones and sandstones and are resulting from burrowing activities of organisms, which destroyed the original sedimentary structures (Gringras et al., 2013).

Both ZA siltstones and sandstones are dark coloured owing to mineralogy and the occurrence organic matter. The dark-grey coloured fine-grained siltstones possess a high content of organic matter, suggesting deposition in reducing environment (Reineck and Singh, 1980). The green colour is due to the presence of chlorite and glauconite minerals (Eichhoff and Reineck, 1953: in Reineck and Singh, 1980) and indicate deposition in a marine environment, whereas the brown colour generally indicates occurrence of hematite, deposited in the oxidising environment (Tucker, 1991; Reineck and Singh, 1980).

Thin section observation show that ZA sandstones are texturally immature to submature. It is evident from the thin section description that both ZA siltstones and sandstones are compositionally immature, dominated by the occurrence of quartz grain. The thin section results reveal that the plagioclase is the second abundant mineral. Both quartz and plagioclase are mostly angular shaped and detrital in origin. Therefore, they located close to their source area (Tucker, 1991).

The calcite minerals of the ZA siltstones and sandstones occur in the matrix. This calcite is mainly authigenic and occurs as poikilotopic cement, as fossils and grains. According to Leeder (1982) the calcite minerals mostly originate by marine predation of shell fragments during diagenesis process. The poikilotopic calcite cement is an consequence of authigenic diagenesis increasing the carbonate-bicarbonate ratio in the insterstial space whereby the calcite precipitation will produce large single crystal which envelop many clast grains (Greensmith, 1978; Tucker, 1991). The thin sections show the occurrence of flakes of mica in almost all the siltstones and sandstones. These micas are also detrital and indicate that could be derived from igneous or metamorphic sources (Tucker, 1991).

The most dominant minerals in the matrix of the ZA siltstones and sandstones are clay minerals. Amongst the clay minerals, smectite is the mostly dominated clay mineral phase of the ZA sediments, followed by chlorite. These clay minerals are formed from breakdown of unstable silicates such as calcic-plagioclase, mica, and pyroxenes (Chamley, 1980). The occurrence of quartz, plagioclase, microcline, mica flakes and rare pyroxene suggests that they are detrital in origin, related to a magmatic source rock (Leeder, 1982).

Glauconite displays light green colour and it is subrounded to rounded in shape. The glauconite is associated with clay minerals in the matrix. The grains of glauconite were derived from the diagenetic replacements of the sediment in a shallow marine environment, associated with the fluctuation of the sea level, allowing upwelling of iron cation and/ or replacement of clay minerals by glauconitisation (Greensmith, 1978; Tucker, 1991; Leeder, 1982). Notably, smectite and chlorite result from the alteration of unstable plagioclase and pyroxenes. Thereafter, the smectite forms well round grains with rims by the enrichment of iron content in the matrix. This glauconitisation process clearly shows the increase of iron content in a reduced environment (Berner, 1981). During this process, primary clay mineral grains experience successively dissolution of terrigeneous biogenic materials, a precipitation of Fe-smectite and therefore glauconite is precipitated with smectite in pores (Odin and Fullagar, 1988).

An oxidizing environment is suggested by the occurrence of hematite and limonite minerals in the matrix in shallow shelf whereby the iron is originated from the dissolution of iron rich detrital sediments like pyroxene and biotite (Ahmed, 2007). The limonite is particulary derived from a progressive dissolution of hematite and glauconite (Tucker, 1991). Alteration of volcanic rocks produces zeolites (Tucker, 1991).

The aforementioned descriptions of the ZA siltstones confirm a deposition in low energy shallow shelf marine environment (Tucker, 1991). Thus, siltstones of which the matrix is dominated by smectite associated with hematite, indicate an aerated or oxidised shelf environment (Bland et al., 2013; Reineck and Singh, 1980). Contrarily, the glauconitic siltstones suggest a reducing shelf environment associated with organic matter and lower sedimentation rates (Odin and Fullagar, 1988; Tucker, 1991). The calcareous siltstone is dominated by calcite from skeletal fragments and it contains idiomorphic diagenetic plagioclase. The foraminifera, bivalve and algae fossils are evidence of a marine environment (Flügel, 2004). Therefore, the calcareous siltstones are deposited in the shelf environment (Bland et al., 2013). These sediments were deposited due to sea level changes which reached the Zululand latitudes during the opening of the Indian Ocean, supplying large volume of sediments in the Barremian and the Late Cretaceous periods (Heirtzler et al., 1968; Klinger and Kennedy, 1977).

The ZA sandstones mark more proximal conditions from the source than the siltstones, but in a very similar environment. The sub-angular to angular grains indicate a relatively short distance of transportation by saltation and by rolling (Leeder, 1982; Reineck and Singh, 1980). The occurrence of primary detrital quartz, feldspar, mica and pyroxene indicates that the ZA sediments were originated from a magmatic source rock with a short transportation distance (Tucker, 1991; Leeder, 1982).

The above descriptions and interpretations indicate logically two different conditions notably oxic and anoxic conditions. The presence of hematite and calcite cement confirms a relatively shallower environment, wheras the glauconitization suggest relatively low sedimentation rates. The latter occurs under anoxic conditions during marine transgression. According to Berner (1981), this environment is also

named post-oxic diagenetic environment and requires a sufficient organic matter for the consumption of all dissolved oxygen through oxidation of organic matter and minerals. In addition, the occurrence of thin shelled bivalve and foraminifera fossils in the sandstone support deposition in shallow marine environment (Flügel, 2004).

Compared to siltstones depositional conditions, the ZA sandstones were deposited in relatively high energy shallow shelf environment (Aljinović, 1995; Bland et al., 2013). The detrital grains are probably originated from the Lebombo magmatic basement (Duncan and Marsh, 2006; Melluso et al., 2008). Diverse broken and intact, skeletal and non-skeletal fossils suggest that the sandstone as well as the siltstone were deposited in the shallow shelf of the Zululand basin (Tankard et al., 1982). The glauconitic sandstones are the results of continuous diagenetic processes in slightly reducing and low energetic conditions (Tucker, 1991). The calcareous sandstones are deposited in the shallow shelf environment, under marine regression controlled by warm water currents and soluble calcareous skeletal matter are multiplied. During lithification process, the sand bodies might have become rich in introduced calcareous cement (Greensmith, 1978).

5.1.2. Carbonate Rocks

Based on the petrographic descriptions, sample A1 (105.3 – 105.5 m) and A25 (1035.4 – 1035.5 m) are classified as limestone and are composed mainly of calcite and calcitic fossils. The rocks are light brown to grey, rich in bioclasts of echinoderms, algae, bivalves, specules, foraminifera, gastropods and pellets. The skeletal fragments display different shapes such as elongated and spherical. They have different sizes ranging from micrometres to centimetres.

The calcite abundance in thin sections is consistent with the XRF results which show high amount of CaO content about 36 wt% in the rock while the SiO_2 content is

about 22 wt% on average, as confirmed by XRD analyses. Whereas the remaining oxide percentages are 5 wt% Al_2O_3, 2 wt% Fe_2O_3, 2 wt% MgO, 2 wt% CaO, but the content of TiO_2, MnO, Na_2O, K_2O, P_2O_5, Cr_2O_3 all combined contribute about 4 wt%. The loss on ignition is high, around 27 wt% because of the high carbonate content. In the carbonate rocks, some terrigeneous and diagenetic grains together with monocrystalline quartz, plagioclase, hematite and clay minerals occur. Silica cements occupy the pore spaces. The plagioclase grains show a dissolution effect along cleavage and fracture planes. Mica flakes were observed in the carbonate rock. The XRD results revealed microcline with about 2 wt% in sample A1, which was missed in thin section examination.

Based on the calcite content and the abundance of fossils, the rocks are classified in terms of their textures as biosparite (Folk, 1959 in Greensmith, 1978). According to the idealised sequence of standard facies belts (from Wilson, 1975: in Flügel, 2004) and the fact that these rocks lack mud and are grain supported (Dunham, 1962: in Tucker, 1991), they are named respectively as bioclastic grainstone (A1: 1041 – 1035 m) and bioclastic packstone (A25: 1035.5 – 1035.4 m). Thus, the bioclastic grainstone is related to the reef to foreslope shelf environment whereas the bioclastic packstone is deposited in the foreslope shelf. In accordance with the transgressive and regressive (T/R) cycles (Fig. 29), both the bioclastic packstones and the bioclastic grainstone were deposited during marine regression in a shallow shelf, and were formed by debris from shallower carbonate deposits (Bland et al., 2013; Wilson, 1974: in Flügel, 2004).

The grey colour of this limestone is mainly a function of the abundance of calcite formed by the accumulation of skeletal and non-skeletal fragments during diagenesis (Leeder, 1982). The abundance of the above-mentioned fossils suggests a shallow

marine environment. They are mostly well preserved and not strongly fragmented, which signifies that they were deposited near their living place and in low energetic condition (Tucker, 1991). The silica cement is formed by the precipitation of silica gel within pore spaces. The silica gel results from the dissolution of the silica rich sediment like quartz and plagioclase. The quartz and plagioclase are mainly detrital while clay minerals and hematite were derived from the alteration of plagioclase, pyroxene and biotite phases.

5.2. Mineralogy of the ZA sedimentary rocks

This subchapter discusses the vertical variations of the mineralogy of ZA borehole and the nature of the source of the sediments.

5.2.1. Distribution of minerals with depth in ZA Borehole demonstrated using XRD results in comparison with thin section and spectral results

The mineralogy of the ZA sedimentary rocks is dominated by quartz ranging from 9 to 65%, based on thin section description and supported the XRD. Normally, the quartz content is higher in the sandstones than in siltstones or carbonate rocks. The vertical distribution of the minerals (Figs. 23A and B, Appendix E), shows in the continuous profile of the borehole recorded by the spectral logging, which showed that the lower part of the log (1580 to 1340 m) is characterised by a low quartz content, about 14%. This may be caused by the occurrence of a carbonate-rich siltstone at the same depth. A slight high quartz content with an average of 30% is encountered from the bottom to the middle part of the ZA log (1340 to 850 m). A higher quartz content with an average of 50% is observed from 850 to 680 m, indicating a sandstone occurrence. At 650 m depth, low quartz content (average of 13%) is encountered because of the occurrence of siltstone rich in clay minerals. From 650 to 350m, the

content of quartz is low, about 30% average, resulting from the occurrence of siltstone rich in clay, glauconite and carbonate minerals. From 350 to 240m, the content of quartz is on average 50%, resulting from the presence of sandstone layers. The top of the sequence (240 to 80 m depth) is characterised by low quartz content (roughly 29% on average) because of the presence of bioclastic limestone and calcareous siltstone beds.

Calcite content in the ZA core ranges from 3 to 79%. The highest amount of calcite content is found at 1041 – 1036 m in the middle of the sequence (bioclastic limestone: 79%), followed by 73% at the top (80 m) of the sequence which is also a bioclastic limestone (Fig. 23 A and B, and Appendix E). The lowest calcite content (2%) is found at about 760m depth where an arkosic wacke layer occurs.

Feldspars are the third abundant minerals in the ZA sedimentary rocks. Plagioclase is the main feldspar ranging from 4 to 30%. It is associated with quartz, therefore its high grade indicates the occurrence of siliciclastic sediment especially sandstone, whereas the lower grade points out the occurrence of carbonate sedimentary rocks or the high content of clay minerals in the clastic sedimentary rocks. Ca-Na-K diagram shows that the majority of the ZA samples plotted towards the Ca apex confirming the existence of plagioclase and calcite. According to the vertical mineral distribution (Fig. 23A and B, and Appendix E), the lowest plagioclase grade (4 to 11%) is observed at the bottom (1602 to 1577 m depth) because of the occurrence of calcareous siltstone (rich in calcite). The highest grade of plagioclase is encountered at about 1200 m depth indicating the presence siliciclastic sediment rich in plagioclase which should be an arkosic sandstone. Microcline occurs at the upper sequence (Fig. 23A and B) from 450 to 380 m depth with a grade of 1% and from 220

to 105 m with 2-4%. The microcline given by the XRD results is supported by the XRF analyses, which shows the content of K_2O ranging from 1 to 2% at the same depths.

Clay minerals are encountered in the sediment contribute up to 51%. The clay mineralogy is predominantly of smectites making up to 41%. The predominance of smectite is confirmed by the mineral spectral result indicating the presence of aluminum smectite and magnesium smectite. The later occurs as matrix generally associated with chlorite, glauconite and calcite in almost all the ZA sedimentary rocks. The higher smectite content (35 - 41%) is observed at the bottom of the sequence from 1100 to 1440 m (Fig. 23A and B, and Appendix E) and 30% at about 650 m depth, confirmed by the spectral results and characterised by low SiO_2/Al_2O_3 ratio of 3.28. This indicates a moderately degree of alteration of the sediment showing the presence of siltstone layers. The mineral spectral results reflect the above results, displaying the highest peak of 75% of Mg-smectite at the depth of 650 m. Furthermore, the mineral spectral results display Mg-smectite at the top (300-100 m) followed by Al-smectite (Fig. 17, Appendix E), with the highest peak of Al-smectite reaching 60%.

Nontronite was only detected by the mineral spectral scanning method and found sporadically in the sedimentary rocks resulting from Fe^{3+} replacement of Al^{3+} (Tucker, 1991). The mineral spectral results show 0.25 to 1% nontronite (Fig. 16) and can be observed from middle towards the top of the ZA sequence. Illite and kaolinite were also revealed by the mineral spectral analysis, they could be probably associated with smectites. The mineral spectral results show a small amount of the illite and kaolinite respectively 0.25-1% and 0.5-2% (Fig. 16). Both illite and kaolinite are mostly concentrated in the middle of the sequence at 350 - 550 m depth (illite), and at the bottom of the sequence around 1400-1600 m depth (kaolinite), see Fig. 16 and Appendix E.

Chlorite is associated with the smectite displaying greenish colour in the matrix. Its content ranges from 1 to 10%. The high chlorite content occurs at the depth between 1512 and 1577 m (Fig. 23 A and B) (Appendix E). The mineral spectral results show a variation from 5 to 20% chlorite, with higher contents at about 630 m, 560 m and 480 m depths (Fig. 16) while the spectra occur constant at the bottom of the sequence (from 1200-1600 m).

Glauconite is green, displaying subspheroidal patchy occurrence with the size of grain varying from 40 to 200 μm. It is a diagenetic, in situ formed mineral, sometimes associated with smectite as part of the matrix and forming mixed-layer clay minerals. In addition, it is found for example, filling the interstitial voids of foraminifera where it can be altered to limonite which indicates later oxidation and formation of hematite and goethite. Its content varies from 1 to 33%. The higher contents are observed at the depth of 1223-1227 m, 612-625 m, and 240-256 m comprising the glauconitic sandstone and glauconitic siltstone beds (Fig. 23A and B). Limonite is occasionally found in the sediment, displaying brown to yellow coloured and associated with clay minerals, hematite and glauconite in the matrix. Limonite is a mixture of goethite with hematite as a product of alteration (Prather, 1905).

Hematite occurs associated with clay minerals in the matrix and it is blood-red under transmitted light. The hematite content ranges from 1 to 12%. Its higher contents occur in the middle of the sequence (710-732 m depth), materialised by the presence of a brown sandstone layer (Fig. 23A and B, and Appendix E).

The XRD results identified the existence of possibly two types of zeolite such as clinoptilolite and heulandite. The zeolite content varies from 2 to 14%. The high zeolite content is encountered in the middle of the sequence, at 1041-1099 m depth,

and 206-223 m depth constituting respectively the sandstone and mudstone (Fig. 23A and B, and Appendix E).

Micas occur through almost all ZA sedimentary rocks together with detrital grains of quartz and feldspar (Tucker, 1991). Their contents range from 1 to 5% in all ZA sedimentary rocks. Biotite is predominant over muscovite; this confirms that the MgO content is higher than K_2O content.

Gypsum is identified by the XRD and the mineral spectral results. It occurs towards the top of the sequence (Fig. 23A and B) from 750-762 m with the content of 2% in the sandstone and constituting 1% at the depth of 153-196 m in the mudstone (Appendix E). The mineral spectral result supports the XRD analyses showing gypsum concentration from the middle towards the top of the sequence varying from 2-6% (Fig. 16). Nonetheless, the gypsum was invisible in thin sections which justifies that it has been detected on the surface of the core using spectral method than by XRD or thin sections. This speaks strongly for core weathering that produced the gypsum from alteration of sulfides and carbonates: $Fe_2(SO_4)_3 + 3CaCO_3+5H_2O+O_2 \rightarrow 2Fe(OH)_3 + 3CaSO_4.2H_2O+3CO_2$.

Single zircon grains occur in some sedimentary rocks such as A19 and A36 (Appendices B2 and B4). It is colourless under plan polarised light with high relief and high-order interference colours. The grain size ranges from 45 to 90 μm. The occurrence of the zircon grains indicate proximity to magmatic source rocks (Tucker, 1991).

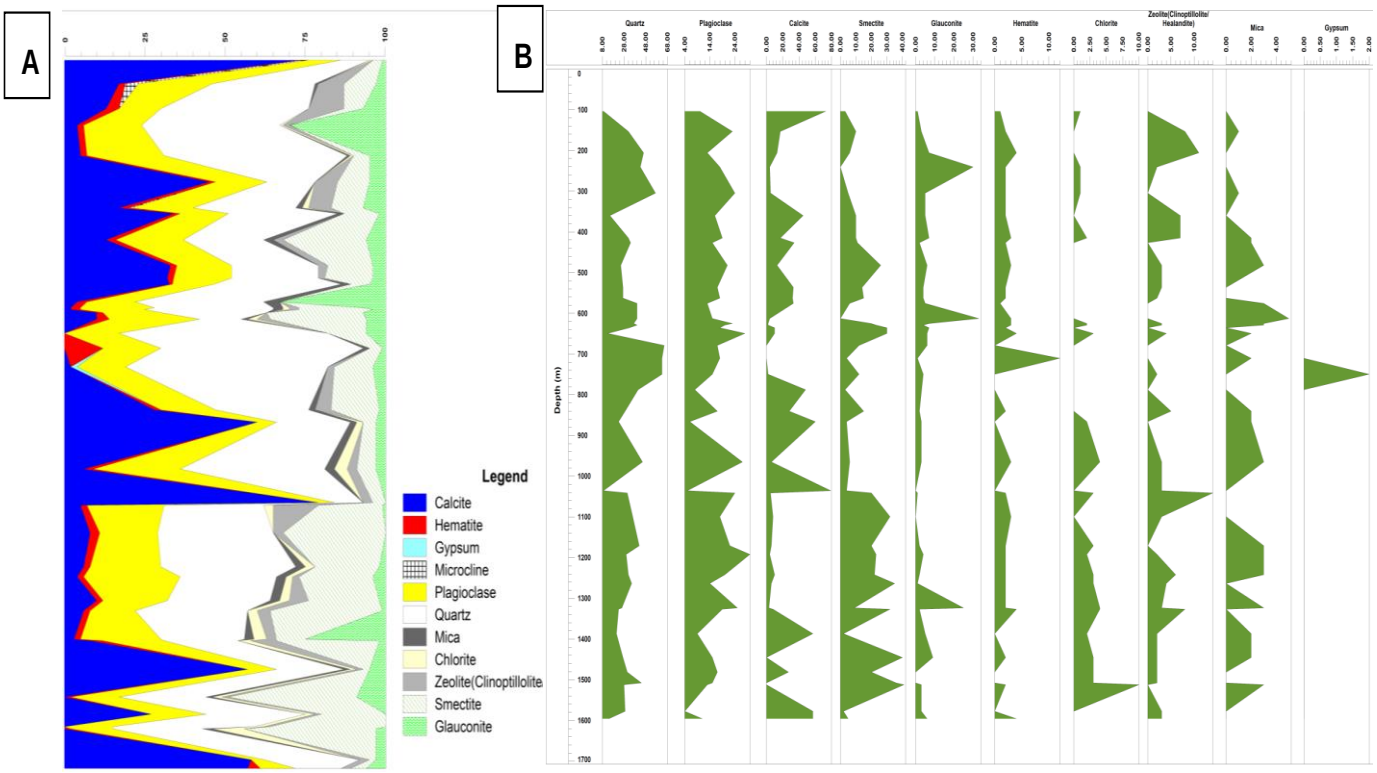

Figure 23. Illustration of vertical variations of the minerals in weight percentage of the ZA sequence measured by the XRD method (A: Combined variation of major elements and B: individual variation of major elements). The variations are indicating low content of quartz, plagioclase, hematite, mica and clay minerals at the depth of 1040 m. Comparably, the content of calcite and zeolite minerals is high at the same depth of 1040m. At the depth of 700 m, the content of quartz, plagioclase, hematite, mica and clays is high, whereas the content of calcite and zeolite is showing an opposite trend around the same depth of 700 m.

5.3. Geochemistry of the ZA rocks

5.3.1. Distribution of the major element in the ZA sequence based on XRF results

The XRF results showed that the major element content is dominated by SiO_2 ranging from 21.6 to 67.5 wt%. According to the ZA vertical sequence (Fig. 24A and B), the SiO_2 content is prominent in the siliciclastic layers like sandstones (59%), siltstones (56%), glauconitic siltstones (55%) and glauconitic sandstones (50%). This SiO_2 content is less in the calcareous siltstones (43%), calcareous sandstones (44%) and limestone (23%).

The CaO is the second abundant major element ranging from 2.49 to 36.5% in the ZA siliciclastic rocks. This CaO content indicates the presence of calcite and plagioclase minerals. However, this CaO content was recalculated to separate the CaO content from Calcite and CaO from plagioclase. The high CaO content is encountered at different ZA borehole depths (Fig. 24A and B); firstly, at the lowermost part of the borehole (32% from XRF) where a calcareous siltstone occurs at the depth of 1580 m (Fig. 24 and Appendix E); secondly, in the middle of the ZA core (25% from XRF) where a calcareous sandstone layer occurs at the depth of 1040 m, and lastly, at the top of the sequence (35% from XRF) where bioclastic limestone was encountered.

The Al_2O_3 is the third most abundant major oxide in the ZA sequence ranging from 5 to 14% according to XRF results. The Al_2O_3 is always incorporated in clay minerals, glauconite, zeolites, mica and feldspars. The Al_2O_3 plotted with depth (Fig. 24A) does not show a remarkable variation which means that the overall of ZA sedimentary rocks contain on average the same amount of Al_2O_3 content. The considerable Al_2O_3 content in the sandstone layers shows that none of the sandstones is compositionally matured. The low Al_2O_3 content (5 to 13%) in the middle part of the sequence (from 1040 to about 677 m) is caused by the high amount of SiO_2 and CaO due to the occurrence of sandstones and carbonate rocks (Fig. 24 and Appendix E).

Fe_2O_3 content is recorded in all samples, ranging between 2.7 and approximately 14% as illustrated by XRF analyses. The occurrence of Fe_2O_3 in all the studied samples of sedimentary rocks indicates the presence of iron minerals such as hematite, glauconite, limonite and some mafic minerals such as pyroxene and biotite. The variation of the Fe_2O_3 content is almost the same with the variation of Al_2O_3 with depth showing similar trend with less amount of Fe_2O_3 in middle of the sequence (from

1040 to about 677 m depth). Fe is thus most probably bound predominantly to clay minerals in all samples.

The MgO content is varying from 1 to 4.6% and most of the time associated with Fe_2O_3. Both MgO and Fe_2O_3 characterise the presence of magnesium and iron silicate minerals such as biotite, Mg-smectite, chlorite, and zeolite. The MgO is also present in all the lithological units of the ZA core, whereby the low value of MgO (1%) is encountered at 788m depth (Fig. 24A and B, and Appendix E). MgO content in the carbonate rich rocks is low (about 1.5%) which suggests the presence of limestone rocks as opposed to dolomite rocks.

The Na_2O and K_2O contents are very low ranging respectively from 0.54 to 2.71% and 0.58 to 4% with a drop at the depth of 1040 m, akin to the behavior of other elements. This is because of the higher amount of CaO and SiO_2. The K_2O content indicates probably the presence of mineral such as microcline, muscovite and kaolinite, whereas the Na_2O is incorporated in the plagioclase series.

The percentages of other major element oxides such as TiO_2, MnO, P_2O_5 and Cr_2O_3 are very low and varying individually from 033 to 1.27%, 0.04 to 0.80%, 0.05 to 0.27%, and 0.01 to 0.04%. These oxides are all incorporated in the sedimentary rocks, mostly in the clay minerals. Similarly, to the other oxides, these TiO_2, MnO, P_2O_5 and Cr_2O_3 have the lowest values at the same depth of 1040 m (Fig. 24).

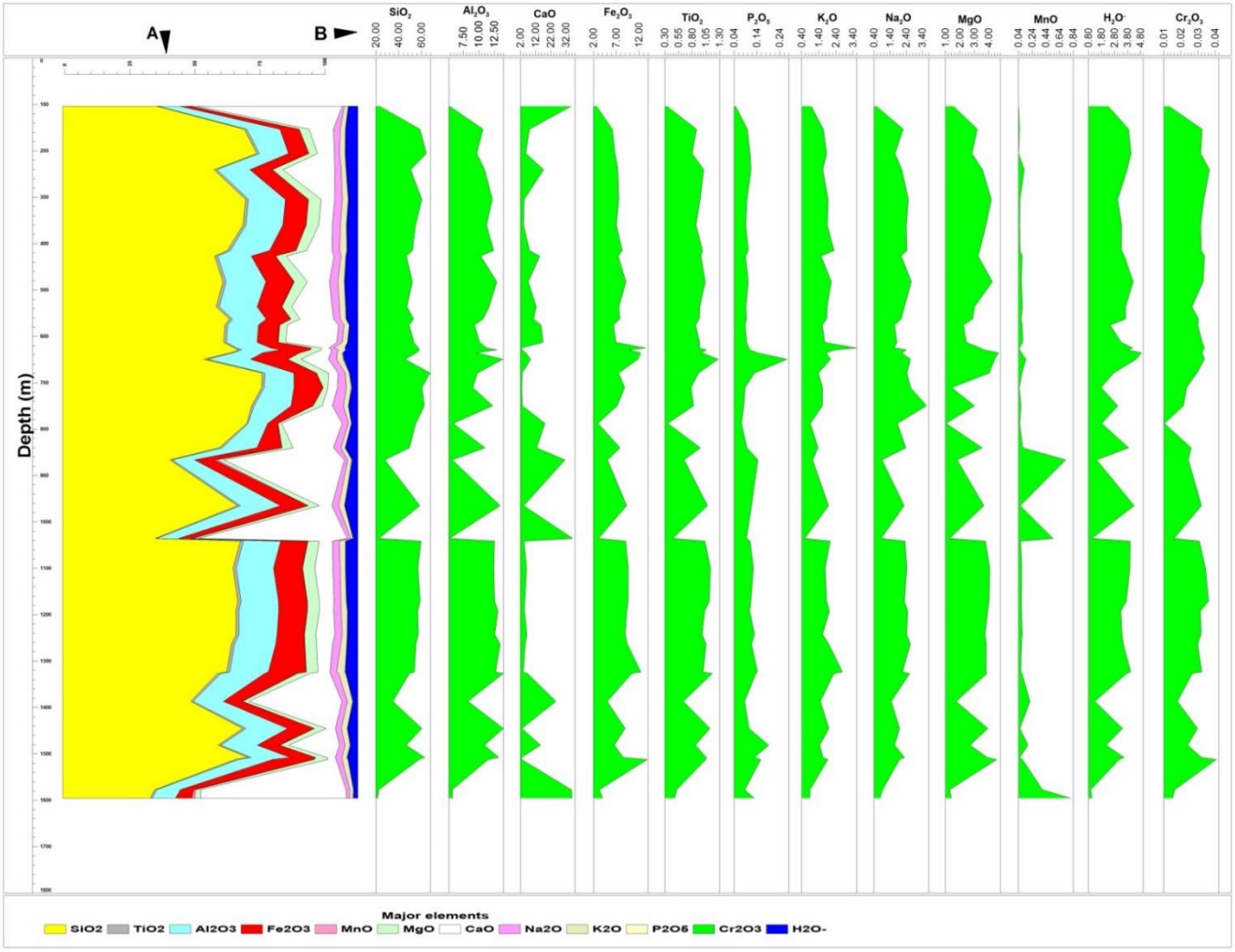

Figure 24. Vertical distribution in percentage of major elements in the ZA sequence as measured by the XRF method, showing high CaO content at 1580 m, 1040 m and at 100 m depth, whereas the SiO2 shows an opposite trend. B: Demonstrations of the vertical variations of the individual major element in the ZA sequence indicating high CaO and MnO contents at the depth of 1580 m, 1040 m and 100 m. Contrarily, SiO_2 content illustrates a low trend at the similar depths as those of CaO.

5.3.2. Nature, maturity and weathering of the sedimentary rocks

The chemistry of sedimentary rocks is very useful to determine the nature, provenance, weathering, and the maturity of the sediment (Bhatia, 1983). The Harker diagrams (Fig. 25) show positive correlations with the increase of SiO_2 in the ZA rocks being directly proportional to the increase of Al_2O_3, MgO, TiO_2, Na_2O, K_2O and Fe_2O_3. This implies that the amount of these elements increases in the ZA sedimentary rocks

with the increase of the SiO_2 content. The Harker diagrams show that the content of P_2O_5 remains constant while the content of SiO_2 is increasing. In contrast, the SiO_2 versus CaO and MnO show negative correlations meaning that CaO and MnO contents in the ZA sedimentary rocks are inversely proportional to the content of SiO_2. Comparably, the content of Ca and Mn is high in calcareous siltstone-sandstones and carbonate rocks whereas the SiO_2 content is low.

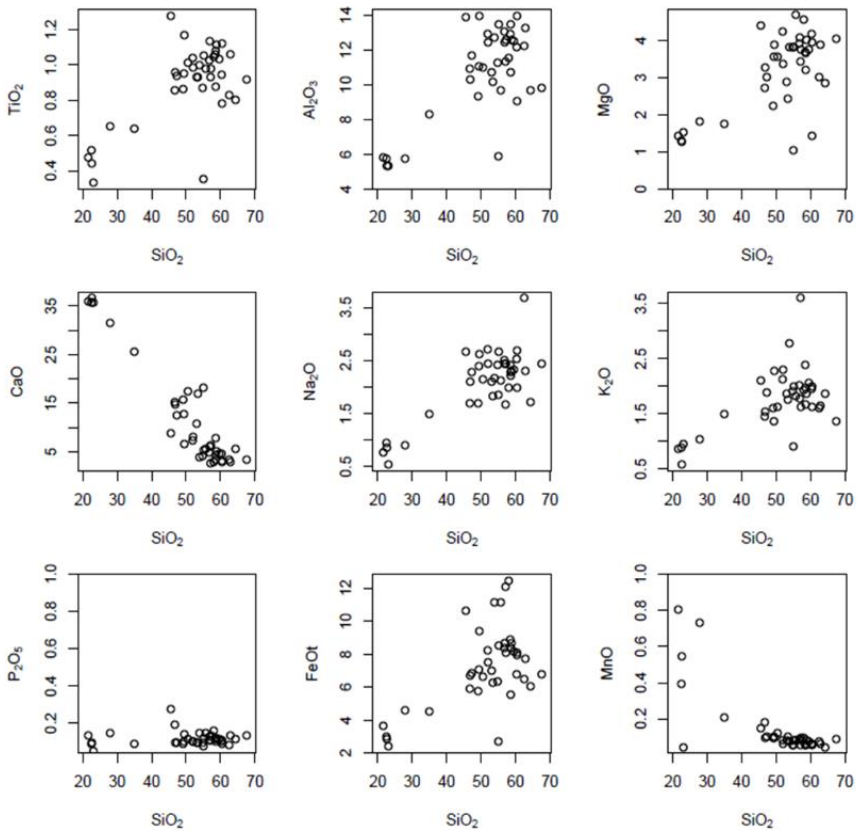

Figure 25. Harker diagrams of major oxides of the ZA sedimentary rocks, showing positive correlations of SiO_2 with Al_2O_3, MgO, TiO_2, Na_2O, K_2O and Fe_2O_3 except with CaO and MnO which show negative trends, whereas P_2O_5 remains constant while the content of SiO_2 is high.

According to McLennan et al. (1983), the SiO_2/Al_2O_3 ratio discriminate the textural maturity of the sedimentary rocks, whereby increasing this ratio, signifies positively increasing the maturity and the silica content. Nonetheless, the average

SiO_2/Al_2O_3 ratio of the ZA samples is 4.8. Therefore, the ZA sedimentary rocks are discriminated as immature to sub-mature, poorly to moderately sorted rocks (Table 9).

Table 9. Classification of textural maturity of the ZA samples based on the SiO_2/Al_2O_3 ratio using the discrimination diagram by McLennan et al. (1993).

SiO_2/Al_2O_3	Sorting	Maturity	Samples
High: >8	Well sorted	Mature	A21
Intermediate: 4.79-7.37	Poorly to moderately sorted	Immature to Sub-mature	A2, A3, A4, A5, A6, A7, A8, A9, A10, A11, A12, A13, A14, A15, A16, A18, A19, A20, A22, A23, A24, A25, A26, A27, A28, A29, A30, A31, A32, A34, A35, A36, A37, and A38
Low: <4.5	Poorly sorted	Immature	A1,A17, A39 and A40

Based on the McLennan et al. (1993), classification criteria for maturity the "Mature" class of the ZA sedimentary rocks is represented by sample A21 (788.1 - 788.2 m) with the SiO_2/Al_2O_3 ratio of 9.3 which is higher than the average ratio of 4.8 for the rest of the samples. The higher ratio of sample A21 results from Al_2O_3 content which is lower than that of the other samples. Thus, A21 is mature and contains lesser matrix.

Using the Bhuiyan et al. (2011) classification diagram to demonstrate the nature of the sedimentary rocks, the ratio of SiO_2/Al_2O_3 was plotted against CaO and shows a negative correlation for all the investigated samples of drill core ZA. Three different classes were discriminated as illustrated in the Table 10 below:

Table 10. Evaluation of the nature of the sedimentary rocks using the plots of the ratio of SiO_2/Al_2O_3 against CaO content for ZA sedimentary rocks, modified after Bhuiyan et al. (2011) classification diagram.

SiO_2/Al_2O_3 vs CaO	Type of sediment	Samples
1st class: High > 0.52	Rich in alumina-silica	A2, A3, A5, A6, A7, A9, A14, A15, A16, A18, 19, A20, A24, A26, A27, A28, A29, A30, A31, A32, A33, A35, A37 and A38
2nd class: Moderate 0.2-0.52	Calcium-alumina-silica	A21, A4, A17, A8, A10, A11, A12, A13, A21, A22, A36
3rd class: Low < 0.2	Calcium rich sediment	A1, A23, A25, A34, and A40

The first class in Table 10 shows the sedimentary rocks rich in alumina-silica which reflects their nature of siliciclastic rocks, i.e. sandstones and siltstones. The second class illustrates the sedimentary rocks rich in both calcium and aluminum-silicates, and reflecting the calcareous sandstones and calcareous siltstones. Whereas the third class shows calcium rich rocks such as limestone, calcareous sandstones and calcareous siltstones with more than 25% of calcium content.

The low K_2O/Na_2O ratio (Appendix C) indicates the dominance of plagioclase versus K-feldspar and mica (Roser and Korsch, 1986; Bhatia, 1983). It is supported by $CaO+NaO-Al_2O_3-K_2O$ and $CaO-Na_2O-K_2O$ diagrams (Fig. 26). The CaO content of ZA sedimentary rocks was recalculated to separate the CaO content from plagioclase and the one from calcite before applying the above-mentioned ternary diagram (Appendix C3). Thus, only the CaO content deducted from plagioclase was used. The ternary diagram $CaO-Na_2O-K_2O$ illustrates the predominance of CaO in the sediment which indicates the evidence of Ca-plagioclase than alkali feldspars, whereas the $CaO+Na_2O-Al_2O_3-K_2O$ diagram indicates the presence of plagioclase, smectite, and a small amount of mica, mostly biotite. The samples next to Al_2O_3 axis contain more smectite than the samples next to the Na_2O+CaO axis.

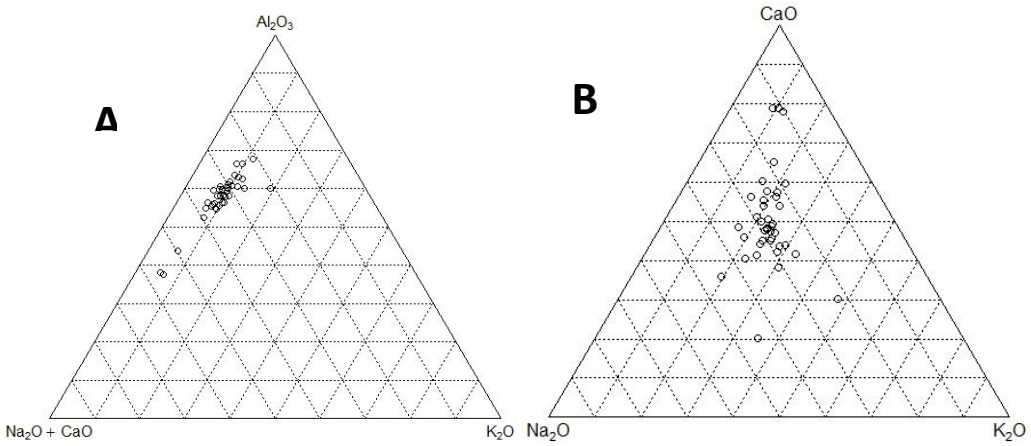

Figure 26. Ternary diagrams of ZA sedimentary rocks (A: $CaO+NaO-Al_2O_3-K_2O$ diagram and B: $Ca_2O-Na_2O-K_2O$ diagram). The $CaO+NaO-Al_2O_3-K_2O$ diagram illustrates besides

the Na_2O and CaO content, a relatively higher of Al_2O_3 content which reveals the presence of smectite. The small amount of K_2O reflects the occurrence of biotite and microcline in the ZA rocks. Ca_2O-Na_2O-K_2O diagram shows the predominance of CaO content, indicating the presence of Ca-plagioclase than alkali feldspars.

The relative high of Al_2O_3 content (Fig. 26) reflects the degree of the weathering of the ZA sedimentary rocks. According to the chemical index of alteration (CIA), see Table 11, which is used to quantify weathering intensity due to progressive alteration of plagioclase and potassium feldspars to clay minerals, show that all the samples are moderately weathered (Bhuiyan et al., 2011). Note that only the CaO content from plagioclase is used here. The CIA is calculated using molar proportions of oxides using the following equation CIA = (Al_2O_3/Al_2O_3 + CaO + Na_2O + K_2O) x 100.

Table 11. Illustrates the Chemical Index of Alteration (CIA) for the siliciclastic rock samples of drill core ZA (Nesbitt and Young, 1984).

CIA	**Degree of weathering in the source area**	**Samples**
High values (76-100)	Intensive chemical weathering in the source areas	None
Moderate values (51-75)	Moderately weathered in the source areas	A2, A3, A5, A6, A7, A8, A9, A10, A11, A12, A14, A15, A16, A17, A18, A19, A20, A21, A22, A23, A24, A26, A27, A28, A29, A30, A31, A32, A33, A34, A35, A36, A37, A38 and A39
Low values (50 or less)	Unweathered source areas	A4, A13 and A40

According to the CIA analysis, most of the ZA sedimentary rocks are derived from moderately weathered source areas. The CIA values of the ZA sedimentary rocks vary from low (42) to moderate (59). The occurrence of microcline and plagioclase suggests proximal deposition from the source rocks. Carbonate rocks such as bioclastic limestone illustrated by the samples A1 (105.3 – 105.5 m) and A25 (1035.4 – 1035.5 m) are not included under the CIA classification scheme because of the abundance of CaO content from calcite grains.

5.4. Tectonic settings of the ZA sedimentary rocks based on the geochemistry and mineralogy.

Different bivariate diagrams permitted the understanding of the tectonic provenance of the ZA sedimentary rocks. According to Bhatia, 1983, the oceanic island arc (OA) sandstones are most distinctive and characterised by high content of Fe_2O_3 + MgO (8 to 14%), high TiO_2 (0.8 to 1.4%), and high ratio of Al_2O_3/SiO_2 (0.24 to 0.33), low K_2O/Na_2O (0.2 to 0.4), and low Al_2O_3/ (CaO+Na_2O) (1 to 2). In comparison, the continental island arc (CA) sandstones are characterised by their lower contents of Fe_2O_3 + MgO (5 to 8%), lower TiO_2 (0.5 to 0.7%), and lower ratio of Al_2O_3/SiO_2 (0.15 to 0.2), higher K_2O/Na_2O (0.4 to 0.8) and higher Al_2O_3/ (CaO+Na_2O) (0.5 to 2.5). The sedimentary rocks of active continental margin type tectonic setting (ACM) are characterised by their lower Fe_2O_3 + MgO (2 to 5%), lower TiO_2 (0.25 to 0.45%), lower Al_2O_3/SiO_2 (0.1 to 0.2), and higher K_2O/Na_2O (1.05). In the passive margins (PCM) sands and sandstones exhibit a large variation in their compositions, especially in the SiO_2 content (> 65%), K_2O/Na_2O (> 1) and Al_2O_3/ (CaO + Na_2O) (values) ratios. Note that the CaO content used here, was recalculated (Appendix C3).

The Zululand Basin is clearly a rift basin developed on the dispersal graben margins of the opening oceans of Gondwana (Dingle, 1983; Jungslager, 1999: in Cloete et al., 2010; Klausen, 2009). It is thus expected to have a signature of rifting. However, the hinterland is of very varying character, including continental volcanics, basement rocks, greenstone belts and the entire variety of cratonic realms.

Based on the Bhatia (1983) and Roser & Korsch (1986) diagram (Fig. 27), the majority of ZA sedimentary rocks show low Al_2O_3/SiO_2 (0.1-0.25), moderate to high TiO_2 (0.78-1.27%), higher to very high Fe_2O_3+MgO (8.64-18.40%), and high to very high K_2O/Na_2O (0.4-2.15%). Therefore, the Zululand sedimentary rocks plot

overlapping between all the tectonic settings. This indicates that the tectonic setting of the Zululand Basin possesses higher values of Fe_2O_3+MgO contents (8.27% and low SiO_2 content (51.75 on average) and is therefore associated with the rifted continental margin. This is confirmed by the literature suggesting the affinities of the Lebombo basement rocks to the volcanic Rifted Margin (VRM), Klausen, (2009).

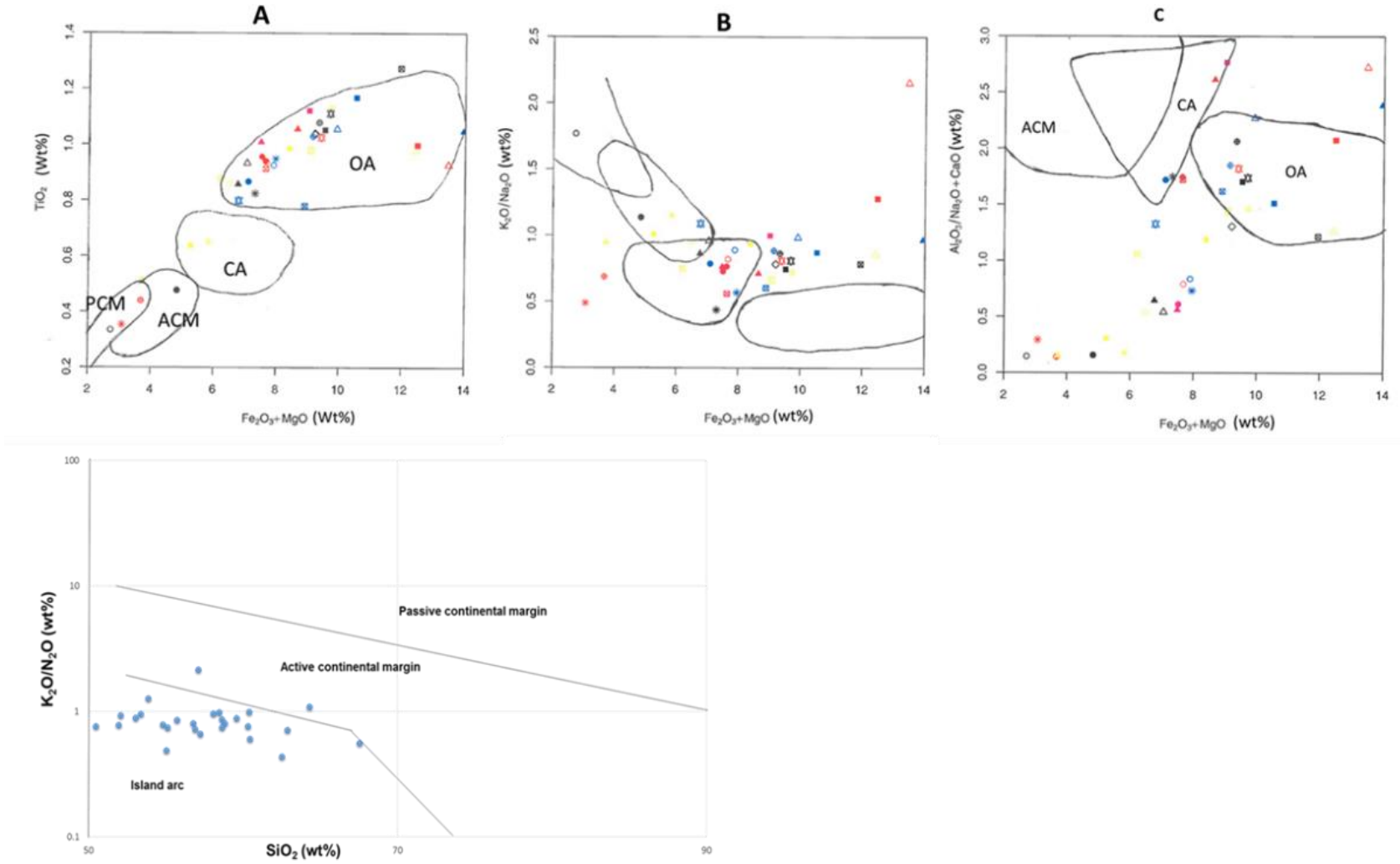

Figure 27. Bivariate chemical diagrams : A: Fe_2O_3+MgO vs Ti_2O; B: Fe_2O_3+MgO vs K_2O/Na_2O; C: Fe_2O_3+MgO vs $Al_2O_3/(Na_2O+CaO)$ after Bhatia, 1983; D: SiO_2 vs K_2O/Na_2O after Roser & Korsch (1986). These diagrams show how the ZA plots are overlapping between all the tectonic settings.

The total quartz-feldspar-lithic fragments (QFL) diagram (Fig. 28) classifies the tectonic setting and the provenance of the ZA sandstones. The QFL diagram indicates a Transitional Continental Arc provenance of sandstone (Dickinson, 1985: in Tucker, 1991) and confirms that the Zululand Basin is a Rifted Continental Margin (RCM) with the average of 48 percent quartz. According to Dickinson and Valloni (1980), sands derived from the rifted margin contain more quartz than those from orogenic continental margin. Maynard et al. (1982) supported this hypothesis and concluded that the sands derived from rifted margins typically have more than 40 % of quartz, whereas the sands from active margin settings have less than 40 %.

The occurrence of primary minerals like quartz, plagioclase, mica, microcline, rare pyroxene and lithic fragment confirms their magmatic provenance. Therefore, the source rocks of the Zululand sedimentary rocks should be basalts, andesites, and dacites, as can be found in different parts of the Lebombo Mountain (Duncan and Marsh, 2006). Possible examples are the Movene Basalt Formation and the andesites and dacites of the Jozini and Mbuluzi Formations (Duncan and Marsh, 2006; Melluso et al., 2008).

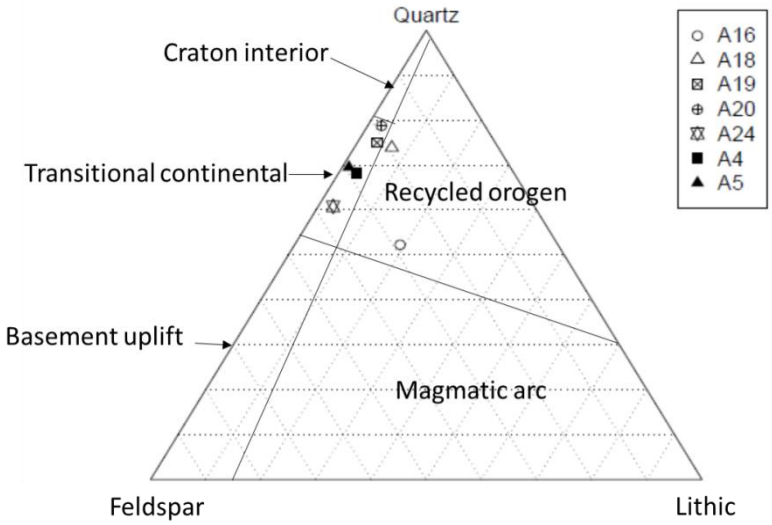

Figure 28. Tectonic setting showing that the ZA sandstones are associated with the transitional continental margin.

6. DISCUSSIONS

6.1. Sedimentary facies characterisation and depositional environments of the ZA rocks

The sedimentary facies of the ZA borehole were characterised based on the core logging and the above-mentioned petrographic results. These sedimentary facies were defined in comparison to the available data related to lithostratigraphy of the Zululand Basin, as described in the literature (Tankard et al., 1982; Shone, 2006; Cloete et al., 2010; 2011). According to literature descriptions, the Zululand Group sedimentary rocks start with small-pebble conglomerates, sandstones and siltstones capped by pink terrestrial limestone which constitute the Makatini Formation (Mc Millian, 2003; Kennedy and Klinger, 1975), however this part of the core is missing. The unconformities and the teredo-bored (marine bivalve) sediments described in the literature (Tankard et al., 1982; Shone, 2006; Cloete et al., 2010; 2011) were not

recognized during the logging of the borehole core because of the missing lowermost ca. 200 meters. The delimitation of the boundary between the formations was based on the T/R cycles and the change of the lithofacies in accordance with the literature (Tankard et al., 1982; Mc Millian, 2003; Kennedy and Klinger, 1975; Cloete et al., 2010; 2011; Van Vuuren et al., 2009).

Three upward coarsening sequences were recognized in the drill core ZA (Fig. 29). The first one starts from the lowermost part of the middle of the core (1577.34 to 675.31 m), followed by the second one from 675.31 to 240.61 m. The last upward coarsening sequence is located on the top of the drill core (240.61 to 89 m).

The lowermost upward coarsening sequence starts from the bioturbated calcareous siltstone layers at 1577.34 m depth, followed by different siltstone layers including laminated glauconitic siltstone (1577.3 – 1512.1 m), bioturbated siltstone (1512.1 – 1481.3 m), wavy laminated and bioturbated siltstone (1481.3 – 1386.8 m), bioturbated siltstone (1386.8 – 1326.6 m), laminated glauconitic siltstone (1326.6 – 1323.5 m), and a bioturbated and wavy laminated siltstone layer (1323.5 – 1041.3 m) intercalated with a laminated siltstone bed (1170.9 – 1099.4 m). Bioclastic limestone beds (packstones) occurs in different depths in this cycle until the depths between 1041.3 m to 1035.7 m and divide this regressive cycle into small cycles. This cycle terminates by the alternation of arkosic wacke and calcareous sandstone strata from 1041.3 to 675.31 m, with an intercalation of a bioturbated subarkose bed (731.95 – 710.41 m). The characteristics of the lithofacies of this first regressive sequence does not reflect the abovementioned descriptions of the Makatini Formation which is attributed to braided river, estuary to tidal flat environments (e.g., Tankard et al., 1982; Mc Millian, 2003; Kennedy and Klinger, 1975). However, this first regressive sequence reflects the lithofacies of the Mzinene Formation which was deposited in the inner shelf

environment (Tankard et al., 1982; Mc Millian, 2003; Kennedy and Klinger, 1975; Dingle et al., 1983). The occurrence the small cycles marked by the presence of the packstone beds indicates the alternation between foreslope and inner shelf environments.

The second coarsening upward sequence is observed from the depth of 675.31 m to 240.61 m (Figure 29, Appendix D and E). From the depths of 675.31 m to 612.8 m, this sequence is characterized by the presence of the laminated and glauconitic siltstone strata intercalated by bioturbated arkosic wacke and bioturbated siltstone beds. The bioturbated calcareous siltstone layer occurs at the depths from 612.8m to 360m and is overlain by a cross-bedded arkose and this sequence is terminated by a structureless glauconitic arkosic wacke at 240.61 m depth. According to the authors (Tankard et al., 1982; Mc Millian, 2003; Kennedy and Klinger, 1975; Dingle et al., 1983), after the depositions of the Mzinene Formation there was alternation of marine transgression and regression related to the St Lucia Formation. However, the transgressive sequences were not recognized from the Drill core ZA, only the regressive sequences.

The last regressive coarsening sequence of the St Lucia Formation commences from the depth of 240.61 m ending at the depth of 89 m. The sequence starts with a laminated siltstone layer (240.61 to 196.19m), followed a bioturbated calcareous siltstone (196.19 to 153.31 m) and capped at the top by bioclastic limestone (89 m). See Figure 26, and Appendix D and E for more details about the depths of the individual lithology.

The above mentioned coarsening upwards sequences are interpreted to be caused by the fluctuations of the sea level resulting from the breakup of the Gondwana (Tankard et al., 1982). The coarsening upward sequences can be interpreted as

regressive sequence, where the sediment are deposited in a fluctuating (shallowing), overall relatively upper shelf shallow marine environment.

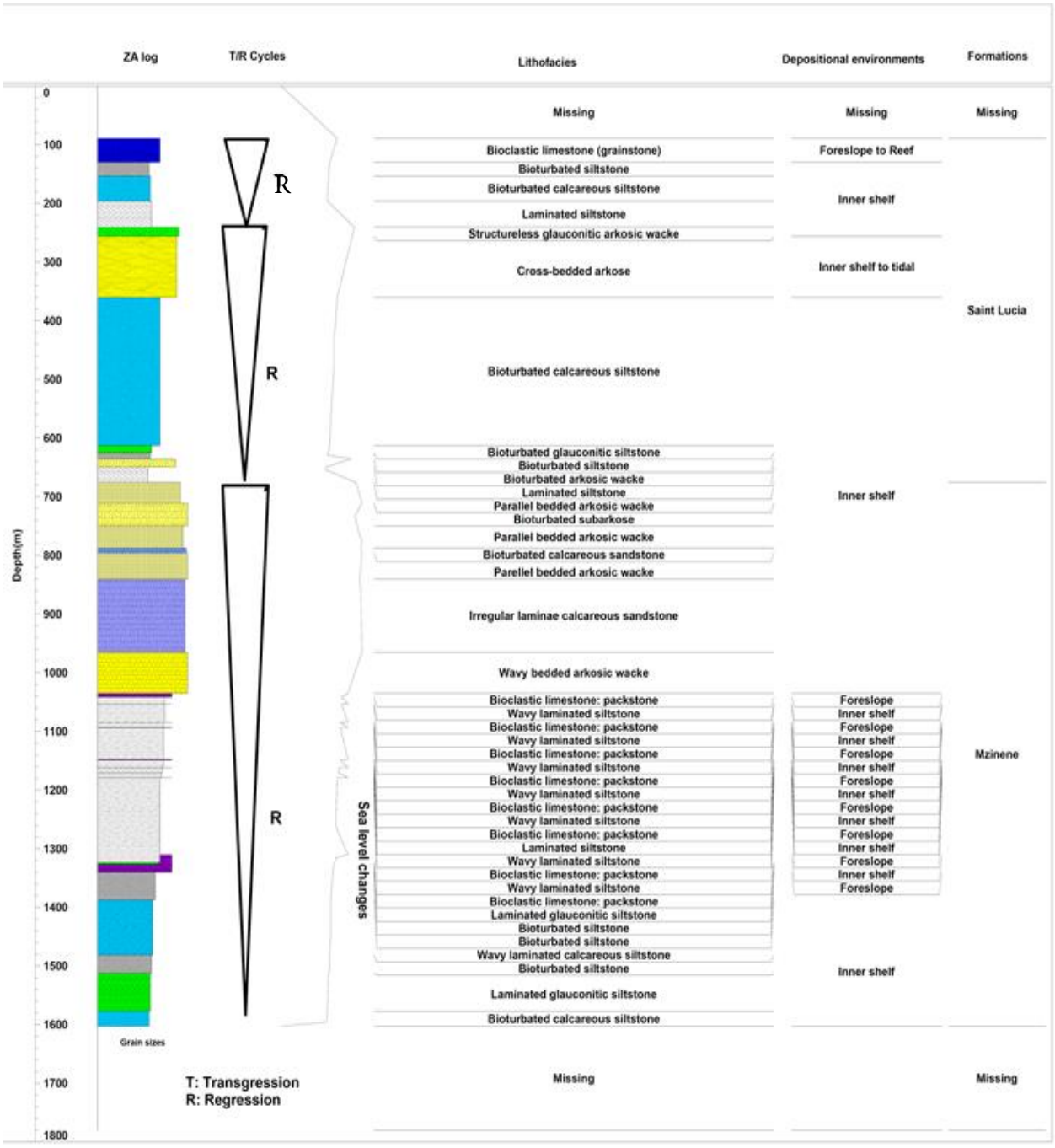

Figure 29. Sedimentary sequences model of the ZA drill core showing three shallowing upwards sequence.

Based on the preserved core, several sedimentary facies were identified from the bottom to the top of the ZA core and grouped into two formations (Fig. 29):

6.1.1. The Mzinene Formation

The Mzinene Formation stretches between 1602 and 675.31 m depth in the ZA borehole and consists of the following lithofacies:

- *Bioturbated calcareous siltstone facies (1602 – 1577.34 m)*

This facies is a dark grey coloured calcareous siltstone commonly bioturbated and rich in foraminifera and algal fossils. Quartz, detrital mica flakes, plagioclase and with glauconite occur in micritic matrix (samples A39: 1194.1 - 1194.2 m and A40: 1597.4 - 1597.5 m, Fig. 17). The above fossil fragments and glauconite sediments give the evidence of a shallow marine environment (Odin and Fullagar, 1988).

- *Laminated glauconitic siltstone facies (1577.4 – 1512.11 m)*

This facies occurs at the lower part of the Mzinene Formation in the ZA sequence (Fig. 29). It is dark grey coloured, laminated (clearly visible to the naked eyes), containing dark spots of organic matter, red hematite and carbonate materials (at its lower part). The facies consist of silt-sized monocrystalline quartz grains, detrital and shattered plagioclases and flakes of mica with some broken shells embedded in a glauconitic matrix of smectite, limonite and chlorite (sample A38: 1529.4 - 1529.5 m, see Appendix B4). The occurrence of glauconite and the fossils indicate a shallow marine shelf environment (Odin and Fullagar, 1988; Flügel, 2004).

- *Bioturbated and laminated siltstone facies (from 1512.11 to 1446 m)*

The colour of the facies changes from dark brown at the bottom to greyish brown in its upper part. This facies displays lamination structures with local

bioturbation. The occurrence of organic matter explains the dark colour at its lower part. The facies is made up of silt-sized grains of monocrystalline and angular quartz, plagioclases, mica flakes and rare heavy mineral (zircon) in clayey matrix dominated by smectite and chlorite associated with hematite (sample A37: 1507.8 - 1507.9 m and A36: 1484.3 - 1484.4 m, see Appendix B4). Calcite (micrite) is present in the matrix predominantly from the middle part of the facies and contributes to the grey colour. Foraminifera, sponges and broken shells also occur. The above characteristic including fossils, bioturbation associated with lamination structures suggest a shallow marine environment, of distal part of the inner shelf environment as suggested by Rutherford et al. (1999), Flügel (2004) and Gingras et al. (2014).

- *Wavy laminated and bioturbated calcareous siltstone facies (1446 – 1386.84m)*

The calcareous siltstone facies is brown-grey coloured, containing organic matters and with carbonate. The wavy lamination structure is mostly obliterated by bioturbation and the occurrence of fossils such as foraminifera and broken shells. Sample A35 (1445.2 - 1445.4 m) and A34 (1415.6 - 1415.8 m) (Appendix B4) are representing this facies and show under the microscope poikilotopic calcite cement embedding silt-sized monocrystalline subangular quartz, plagioclase, subrounded glauconite grains with shells and foraminifera fossils. The calcite cement is associated with clay minerals and hematite. The foraminifera and other broken shells indicate a shallow marine environment while the wavy lamination structure suggests the influence of currents in the marine shelf environment (Okoro and Igwe, 2014; Rutherford et al., 1999).

- *Bioturbated siltstone facies (1386.84 – 1326.59 m)*

This siltstone facies is brown coloured, commonly bioturbated with indistinctive sedimentary structures and intercalated with a carbonate bed of about 30 cm thicknesses, at depth of 1340m. Fossils such as gastropods and bivalves are present. The thin section of the sample A33 (1369 – 1369.2 m) (Appendix B4) shows a siltstone consisting of silt-sized monocrystalline angular quartz and plagioclase grains with few shell fragments in a clayey matrix. Calcite is also present in the matrix. The carbonate bed is macroscopically similar to the sample 25 (1035.4 - 1035.5 m) which is a bioclastic limestone consisting of plenty of broken shells with strong effervescence in contact with the HCl. Gastropod and bivalve fossils suggest a shallow marine environment (Flügel, 2004). Based on the above description and according to the carbonate facies model idealized sequence of standard facies belts (from Wilson, 1975: in Flügel, 2004), the carbonate bed suggests a foreslope shelf deposition.

- *Laminated glauconitic siltstone facies (1326.59 – 1323.54 m)*

The facies is dark brown and green coloured, silt sized grains with some clasts of quartz (2 mm diameter size). The lamination structures are indistinct due to the presence of broken shells. This glauconitic siltstone (sample A32: 1324 – 1324.1 m, Appendix B4) is composed mostly of subrounded glauconite grains, associated with chlorite and smectite in the matrix. Grains such as subangular monocrystalline quartz and detrital plagioclase also occur. The characteristics of this facies including glauconite mineral indicate a shallow marine shelf environment (Odin and Fullagar, 1988).

- *Bioturbated siltstone facies with wavy lamination (1323.54 – 1041.25 m)*

This facies is dark brown to brown grey coloured and contains bivalve, gastropods fossils, plant remains, organic matters (showing dark spots). The strata are highly bioturbated and the burrows mostly destroyed the wavy lamination

structure. A clear laminated siltstone layer is also visible at the depth between 1099.41 to 1170.89 m (see sample A26 (depth): Appendix B3). Texturally, this bioturbated siltstone facies represented by samples A31 (1294.1 - 1294.2 m), A30 (1242 – 1242.1 m), A29 (1194.1 - 1194.2 m), A28 (1170.1 - 1171.1m), A27 (1129.8 - 1129.9 m), and A26 (1076.8 - 1076.9 m) is compositionally immature and consisting of silt-sized, angular monocrystalline quartz, plagioclase, and flakes of mica with skeletal fragments (Appendices B3 and B4). The clayey matrix supporting these grains is rich in smectite and associated calcite, hematite and rare glauconite mineral. Foraminifera, algae and some broken shells suggest a shallow marine environment (Flügel, 2004; Reineck and Singh, 1980).

This bioturbated siltstone with wavy lamination strata is intercalated with several carbonate layers of different thicknesses like 10 cm thick (1161.39 – 1161.49 m), 8c m thick (1178.8 – 1178.87 m), 20 cm thick (1147.78 – 1148.98 m), 23 cm thick (1093.32-1093.55 m), 15 cm (1084.56 – 1084.78 m), 15 cm (1053.44 – 1053.59 m), see Appendices D and E. These carbonate beds are also macroscopically similar to the samples A25 (1041.25 - 1035.66 m) which is a bioclastic packstone. According to the T/R cycles (Fig. 29) and based on the carbonate facies belt, these sediments are deposited during marine regression in foreslope environments (Wilson, 1975: in Flügel, 2004).

- *Bioclastic limestone facies: Packstone (1041.25 - 1035.4 m)*

This facies displays distinctly two different colours. The grey colour is very rich in carbonate and with stronger effervescence in contact with HCl than the grey brown beds. The facies contains plenty of fossils such as algae, foraminifera, spicule, bivalve and some broken shells are visible macroscopically and microscopically with some grains. The presence of the above fossils indicates a shallow marine environment

(Flügel, 2004). Based on the carbonate facies model (Wilson, 1974: in Flügel, 2004), this packstone facies is associated with foreslope shelf environment.

- *Wavy bedded arkosic wacke facies (1035.4 – 965 m)*

The wavy bedded arkosic wacke facies is greyish brown coloured with indistinctive wavy bedding structures. It consists of fine sand-size grains and bioclasts of gastropod and bivalve. It is texturally immature (poorly sorted) and contains sand-sized grains of angular monocrystalline quartz, plagioclase and flakes of biotite. The chloritisation process is visible in some of biotite (sample A24: 965.8 - 965.9 m, Appendix B3). The grains are supported by clayey matrix dominated by smectite, followed by glauconite, chlorite associated with calcite and hematite. Besides fossils of bivalves and gastropods which are also visible in the microscope, plant debris is present. The sediments, fossils and wavy bedding structures in agreement with the T/R cycles (Fig. 29), indicate an upper shelf environment (Okoro and Igwe, 2014; Palma et al., 2007).

- *Alternation of calcareous sandstone and arkosic wacke facies (965 – 675.31 m)*

The calcareous sandstone facies occur at the depths between 965 – 840.33 m, 795.76 -787.60 m and are brown-grey coloured, fine grained to medium grained with clasts of quartz and calcite. They are rich in fossils like bivalves, foraminifera, algae, gastropods and broken shells (samples A23: 911.3 - 911.4m; A22: 855.5 - 855.6m; and A21: 788.1 - 788.2 m, see Fig. 20 and Appendix B3) displays irregular bedding and lamination structures. The upper part of the facies is highly bioturbated (A21: 788.1 - 788.2 m). Texturally, the rock is composionnally and rich in calcite in different forms, as grains, as cement and as matrix. The calcite matrix is associated with smectite, chlorite, and some glauconite minerals supporting angular grains. The

angular grains consist of monocrystalline quartz, plagioclase and flakes of mica. The occurrence of foraminifera, bivalve, and gastropod fossils, and the physical characteristics of the sediments and structures, indicate a shallow marine, such as a shelf environment (Sharief, 1986).

Arkosic wacke facies (840.33 m – 795.76 m; 787.60 – 749.66 m; and 710.41 – 675.31 m) are brown, greyish brown coloured, fine to medium grained with irregular wavy bedding, parallel bedding and lamination structures. Compositionally, it is a poorly to moderately sorted arkosic wacke consisting of angular monocrystalline quartz, plagioclase, flakes of mica, calcite grains (sparite) and lithic fragments embedded by a clayey matrix made up of smectite and chlorite associated with calcite and hematite (sample A20: 760.7 - 760.9 m; sample A18: 685.4 - 685.5 m, Appendix B2). These sediments were deposited during the marine regression and based on the position of the underlying bioclastic limestone, this sandstone was deposited in the upper shelf environment.

These interbedded calcareous sandstones and arkosic wacke facies are intercalated with a bioturbated subarkose facies at 749.66 – 710.41 m depth. The latter is of brown grey colour, fine to medium grained sandstone, containing shells, dark spots of organic matter and plant debris. Bedding planes are discernable. The subarkoses in this facies (sample A19: 710.4 - 710.5 m, Appendix B2) display submature composition which consists of angular grains of monocrystalline quartz, plagioclase and biotite associated with lithic fragments and euhedral zircon mineral supported by a matrix of smectite with some hematite. As the above sandstone facies, the sediments of the bioturbated subarkose facies are also the deposited in the upper shelf environment during a progressive regressive cycle (Aljinović, 1995).

Interpretation of the Mzinene Formation

The Mzinene Formation is characterised at the bottom by the alternation of bioturbated calcareous siltstone, laminated glauconitic siltstone, laminated siltstone and wavy laminated siltstone intercalated with thin carbonate beds. Based on their characteristics such as the occurrence of glauconite, bivalve, foraminifera and algae fossils and the carbonate beds (packstones) which are good facies indicators, the abovementioned lithologies were deposited in a shallow marine, inner shelf environment (Flügel, 2004; Odin and Fullagar, 1988; and Aljinović, 1995). The sedimentary structures are controlled by the fluctuation of water in the shelf environment while the bioturbation is caused by burrowing and grasing organism, which destroy the sedimentary structures (Okoro and Igwe, 2014; Reineck and Singh, 1980; Tucker, 2009). This change of the sea level took place during the dispersing of the Gondwana supercontinent (Tankard et al., 1982). According to the literature (Kennedy and Klinger, 1975; Tankard et al., 1982), these sediments were deposited during the Albian to Cenomanian time period.

The coarsening upward of this sequence from the depth of 1602 m to 675.31 m) is in accordance with the postulated marine regression defining the Mzinene Formation (Fig. 29 and Kennedy and Klinger, 1975; Tankard et al., 1982) (Fig. 29). The upper part of the Mzinene Formation is represented by the different sandstone facies named Middle Sandstone facies (MS) according to Cloete et al. (2010). This Middle Sandstone (MS) starts at 1041.25 m depth by the presence of coarse grained siliciclastic sediments signifying a change of the energetic conditions in the basin due to the decrease of the sea level.

In accordance with the T/R cycle and the Wilson carbonate facies model (Wilson, 1975: in Flügel, 2004), the bioclastic packstones are deposited during marine

regression in the foreslope environments. The overlying Middle Sandstone facies were deposited in the shallow shelf environment whereas the underlying siltstone facies were deposited under low sedimentation rate in a shallow shelf environment (Tucker, 2009; Odin and Fullagar, 1988; and Aljinović, 1995). These packstone facies divided this regressive sequence into small cycle confirming the alternation between foreslope and inner shelf facies.

6.1.2. The Saint Lucia Formation

The Saint Lucia Formation stretches between 675.31 and 89.0 m depth of the ZA Borehole. The strata above were either not recovered or the core was not preserved.

- *Laminated siltstone facies (675.31 – 649.30 m)*

The lower part of the St Lucia Formation is marked by the laminated siltstone facies (675.31 – 649.30 m) – this facies is brownish-grey coloured, laminated and contains silt quartz grains and abundant dark spots of organic matter. It is a compositionally immature rock (e.g., sample A18: 651.7 - 651.9 m) consisting of silt-sized monocrystalline quartz, plagioclase and flakes of muscovite, all embedded in clayey matrix of mainly smectite with chlorite. Bivalves, gastropods and broken shells also occur (Fig. 18, and Appendix B2). The sedimentary lamination and fossils suggest a shelf environment as suggested by Aljinović (1995).

- *Bioturbated arkosic wacke facies (649.30 – 635.43 m)*

This facies is grey-brown coloured, fine to medium grained containing gastropod fossils and calcite grains. This bioturbated arkosic wacke facies is texturally immature to submature (sample A16: 648.8 - 648.9 m, Appendix B2). It consists of angular monocrystalline and polycrystalline quartz grains with chert, shattered plagioclase and lithic clasts possibly indicating a volcanic origin. Shell fragments

associated with plant debris occur. These grains are supported by the smectitic clayey matrix associated with chlorite and hematite. The sediments of this facies including fossils and bioturbation designate a shallow shelf environment (Palma et al., 2007; Gingras et al., 2014).

- *Bioturbated siltstone facies (635.43 – 625.09 m)*

This facies is dark brown coloured moderately bioturbated. The facies is rich in carbonate matter and contains fossils such as bivalves, gastropods and broken shells. This bioturbated siltstone facies (samples A15: 632.8 - 632.9 m and A14: 625 – 625.1 m, Appendix B2) contains angular quartz, plagioclase and mica flakes and organic matter. The grains are supported by clayey matrix made up of smectite, chlorite, and limonite. Rounded glauconite grains are also present in the upper part of the facies. Based on the above descriptions, in accordance with the T/R cycle (Fig. 29), the sediments of this facies suggest a marine regression shelf deposition (Tucker, 1991; Aljinović, 1995).

- *Glauconitic siltstone facies (625.09 – 612.80 m)*

The greenish to dark brown coloured glauconitic and bioturbated siltstone contains gastropod and bivalve broken shells and rich in organic matters. The sediments of this facies contain subrounded glauconite grains. The matrix is also associated with smectite and hematite (sample A13: 612.8 – 613 m, Appendix B2). Subangular monocrystalline quartz and plagioclase also occur as silt grains. Calcite occurs in the matrix as micrite and as veinlets in the rock. The glauconite and fossils are evident of a shelf environment (Odin and Fullagar, 1988; Aljinović, 1995).

- *Calcareous mottled and bioturbated siltstone facies (612.80 – 360 m)*

The colour of this facies varies from dark brown to brown grey because of the presence of organic matter and the abundance of carbonate matter (33%). There is

occurrence of bivalves, foraminifera, gastropods, broken shells. Based on the description of thin sections of samples A12 (575.5 - 575.7 m), A11 (562.6 - 562.7 m), A10 (536.4 - 536.5 m), A8 (445.5 - 445.6 m) and A6 (379.3 - 379.5 m) in Appendices A, B1 and B2 this facies is characterized by silt-sized grains of subangular quartz, plagioclase, calcite (sparite) grains and flakes of mica embedded in the calcite cement. The calcite cement shows a poikilotopic texture, whereas the matrix consists of micrite, smectite, chlorite, limonite and rare glauconite. Calcite veinlets also occur. A remarkable decrease of calcite content is encountered at the depths between 536.05 to 482.14 m and 426.72 to 415 m represented respectively by the samples A9 (482.14 - 482.19 m) and A7 (426.4 - 426.7 m). Besides the above-mentioned grains, there is also occurrence of detrital microcline embedded in a clayey and micritic matrix. The clay minerals are associated with glauconite and limonite. In accordance with the regressive cycle (Fig. 29), the above descriptions these facies such us bivalve, foraminifera, gastropod fossils, calcite cement with poikilotopic texture and glauconite suggest a shelf environment (Bland et al., 2013; Aljinović, 1995).

- *Cross-bedded arkose facies (360 – 256.03 m)*

This is a brownish coloured silt to fine grained sandstone facies with cross bedding structures. Sample A5 at the depth between 311.2 m and 311.3 m (Appendix B1) contains organic matter and carbonate. Compositionally, this facies is a moderately sorted arkosic wacke, consisting of angular grains of monocrystalline quartz, plagioclase, with flakes of mica in the matrix of smectite forming mixed layer with chlorite and rare illite, and glauconite replacement. Hematite also occurs in the matrix. The sediments and cross-bedding structures of this facies indicate an upper shelf to tidal environment (Leeder, 1982; Bland et al., 2013; Aljinović, 1995).

- *Structureless glauconitic arkosic wacke (256.03 – 240.61 m)*

This facies is dark green coloured owing to the occurrence of green subrounded grains of glauconite. It is a fine grained sandstone with no apparent sedimentary structures. Compositionally, it is immatured glauconitic arkosic wacke, e.g., sample A4 (246.5 - 246.6 m). The subrounded glauconite occurs as grains and as part of matrix associated with smectite, micrite and hematite. The matrix is supporting subangular grains of monocrystalline quartz and plagioclase. The calcite cement occurs along the edges of glauconite grains and clasts of quartz. Rare foraminifera fossils are present (Fig. 19.1 and Appendix B1). The above descriptions of the sediments and the fossils indicate a shelf marine environment (Odin and Fullagar, 1988; Flügel, 2004).

- *Laminated siltstone (240.61 – 196.19 m)*

This siltstone facies is brown grey coloured and horizontal fine bedding structures are visible, but are not prominent due to bioturbation. It contains organic matter, plant debris, some clasts of quartz and carbonate. It is poorly sorted as shown by sample A3 (218.5 – 218.6 m) in Appendix B1. Sample A3 contains subrounded monocrystalline quartz, angular plagioclase, volcanic fragments, subrounded glauconite, calcite veins and gastropod fossils. The matrix is of smectite. According to Tucker (2009) and Aljinović (1995), in accordance with the T/R cycles (Fig. 29), the sediments of this facies are deposited during the beginning of the marine transgression in an upper shelf environment.

- *Calcareous weakly bioturbated siltstone and bioturbated siltstone facies (196.19 – 153.31 m)*

Encountered at the depth of 196.19 – 153.31 m a light brown coloured calcareous, weakly bioturbated siltstone, whilst brownish bioturbated siltstone beds

occur at 153.31 – 129,84 m. The calcareous siltstone layer is rich in bioclasts of echinoderm, algae, foraminifera, pellet and plant debris, whereas the bioturbated siltstone facies display only a few broken shells. Sample A2 (188.1 - 189.98 m) represents the calcareous siltstone, which is compositionally immature with angular monocrystalline quartz, plagioclase and flakes of micas embedded in the matrix made up with smectite, zeolite, hematite and glauconite (Appendix B1). According to the work by Aljinović (1995) on the mixed siliciclastic and carbonate succession near Knin (Southern Croatia and Western Bosnia and Herzegovina, including the work by Flügel (2004) on the carbonate lithofacies, the occurrence of the above sediments and fossils of these facies underlying the following bioclastic limestone facies suggest the evidence of a shelf environment.

- *Bioclastic limestone facies (129.84 – 89 m)*

Greyish brown limestone rich in bioclasts of echinoderms and algae associated with colonies of skeletal fragments of spicules, foraminifera, gastropods, bivalves and pellets. Certain fossils are well preserved and still intact, whereas others are broken apart. The intact fossils are displaying different shapes like elongated and spherical, polygonal body (Fig. 22). Detrital grains of angular monocrystalline quartz and altered feldspar are present as in sample A1 (105.3 – 105.5 m). Clay minerals including smectite with limonite also occur filling the pore space and the internal part of the skeletal fragments. Calcite and silica cement are also encountered (Appendix B1). Based on the Wilson facies model, Flügel (2004) suggested that the grain stone facies such as the one described here with occurrence of the bioclastic sediments reveals a reef to foreslope environment.

Interpretation of the St Lucia Formation

According to the Sedimentary sequences model of the ZA drill core (Fig. 29), the St Lucia Formation marked by two regressive sequences. The lowermost regressive sequence of the St Lucia starts with lamination siltstone (675.31m depth), followed by arkosic wacke, bioturbated siltstone, glauconitic siltstone, cross-bedded arkose and ends by glauconitic arkosic wacke (at 240.61 m depth). The occurrence of fossils such as bivalves, gastropods and foraminiferas and the above-mentioned sedimentary structures (from a laminated siltstone to cross-bedded arkose) indicate a shallowing upwards in a shallow marine environment from inner shelf to tidal environment. This argument was also suggested by Tankard et al. (1982) that the sediments of the lowermost part of the St Lucia were deposited in the upper shelf to tidal environment. Dingle and Scrutton (1974) suggested detrital input caused by the ancient Tugela and Limpopo Rivers during Campanian age. The uppermost regressive sequence of the St Lucia Formation is confirmed by the occurrence of the bioclastic limestone on top of the sequence (at 89 m depth). Based on the Wilson facies model which illustrates the depositional environments of different carbonate facies (Wilson, 1974: in Flügel, 2004), this uppermost bioclastic limestone facies (grainstone) is related to a reef to foreslope carbonate depositions. Therefore, the siltstone facies underlying the uppermost bioclastic limestone were deposited in the beginning of this marine regression in the upper shelf environment.

6.2. EVALUATION OF ZA ROCKS FOR CARBON DIOXIDE STORAGE

6.2.1. Reservoir rock

Based on the above criteria (Table 2), two sandstone assemblages of the ZA core referred as the middle and the upper sandstones were assessed. However, on the basis of the thickness and lithology, only the middle sandstone (MS) meets the requirements. The upper sandstone (US) assemblage is situated at the shallow depth between 360 to 240 m (Fig. 29, Appendix D and E). This precludes conditions that convert CO_2 into a supercritical state to make it dissolvable in the formation water, and does not provide secure storage because of proximity to the surface, which may lead to CO_2 leakage.

- *Lithostratigraphy and thickness of the Middle Sandstone (MS) assemblage*

The middle sandstone (MS) assemblage is about 382 m thick, located between 1034 to 654 m (Fig. 29, Appendix D and E). The MS is represented by samples A18 (685.4 - 685.5 m), A19 (710.4 - 710.5 m), A20 (760.7 - 760.9 m), A21 (788.1 - 788.2 m), A22 (855.5 - 855.6 m), A23 (911.3 - 911.4 m) and A24 (965.8 - 965.9 m), bounded at the bottom by a calcareous sandstone facies, rich in fossil at about 1035.66 m depth. Its lower part consists of an arkosic wacke interbedded with calcareous sandstone between 866-965 m and 788-866 m depths. The upper part of the MS is above the required depth for CO_2 storage and comprises arkosic wacke strata with the intercalation of a subarkose bed at the depth between 749.66 and 710.41 m. Its upper limit is bounded by a siltstone layer at 675.31 m depth.

- *Petrography and mineralogy of the Middle Sandstone (MS) assemblage*

More detail about the petrography and mineralogy of the Middle Sandstone (MS) is described and discussed the above chapters 4 (section 4.1 and 4.3) and 6.

However, texturally, the MS group is immature to submature, the lower part is poorly sorted, fine grained and rich in carbonate minerals while the upper part is moderately sorted. The average grain size varies from c. 100 µm to 600 µm, the mineralogy changes from calcite dominated (36% on average) at the bottom to a quartz dominated (up to 63% SiO_2) arkosic sandstone, subarkose and arkosic wacke in the upper part of the sequence. Quartz and calcite make individually an average of c. 47% and 21% of the MS composition followed by 15% plagioclase, 10% smectite, 2% of each of hematite and glauconite, 1% of each of mica, chlorite and zeolite.

- *Geochemistry of the Middle Sandstone assemblage*

The microscopic observations are supported by XRF results which show a relative upward increase in SiO_2 content (28 to 67%) and decrease in CaO content (31 to 3%) see Appendix E and D. The overall sandstone layer has on average 55% SiO_2, 11% CaO, 10% Al_2O_3, 7% Fe_2O_3, 4% Na_2O + K_2O, 3% of each MgO and H_2O, 2% Na_2O and minimal amount of TiO_2, MnO, P_2O_5 and Cr_2O_3 adding up to 1% combined.

- *The strength, porosity and permeability of the middle sandstone*

The samples of the middle sandstone are classified from low to medium strength (Table 12), with a low value of uniaxial compressive strength and point-load index ranging from <1 to 4 MPa.

Table 12. Strength results of samples 10 samples of borehole ZA.

Sample ID	Uniaxial compressive strength (MPa)	Point-load index (Mpa)	Description
A12 (575.5 - 575.7 m)	25 – 50	1 – 2	Low strength
A15 (632.9 - 632.8 m)	< 25	< 1	Very low strength
A16 (648.8 - 648.9 m)	< 25	< 1	Very low strength
A18 (685.4 - 685.5 m)	50 – 100	2 – 4	Medium strength
A19 (710.4 - 710.5 m)	50 – 100	2 – 4	Medium strength

A21 (788.1 - 788.2 m)	< 25	< 1	Very low strength
A22 (855.5 - 855.6 m)	< 25	< 1	Very low strength
A24 (965.8 - 965.9 m)	25 – 50	1 – 2	Low strength
A28 (1170.1 - 1171.1 m)	< 25	< 1	Very low strength
A31 (1294.1 - 1294.2 m)	< 25	< 1	Very low strength
A37 (1507.8 - 1507.9 m)	< 25	< 1	Very low strength
A39 (1592.6 - 1592.7 m)	< 25	< 1	Very low strength

The porosity and permeability of the samples A18 (685.4 - 685.5 m), A19 (710.4 - 710.5 m), A20 (760.7 - 760.9 m) and A24 (965.8 - 965.9 m) were analysed based on their petrographic thin section descriptions. Based on the Porosity-Depth Graph in relationship with the sandstone composition (North, 1985), the porosity of the samples A18 (710.4 - 710.5 m), A20 (760.7 - 760.9 m) and A24 (965.8 - 965.9 m) is approximately 6% whereas the one of A19 (710.4 - 710.5 m) is 8% (Fig. 30). The permeability of the samples A18, A20 and A24 is less than 0.7 milliDarci whereas the one for the sample A19 is approximately 1 milliDarci (Fig. 30).

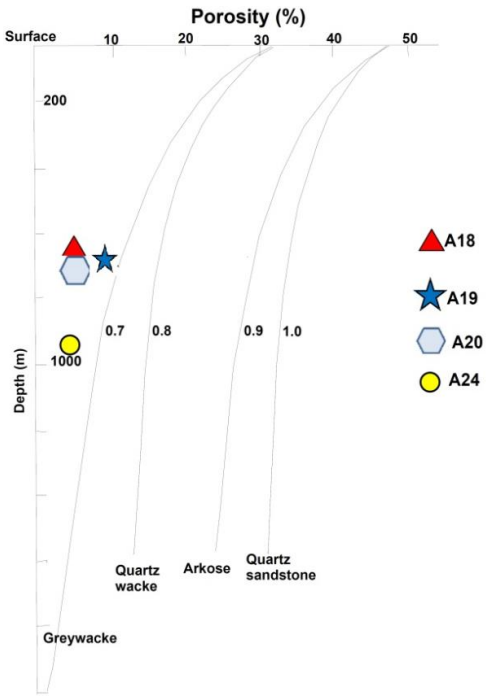

Figure 30. Diagram illustrating the relationship between the porosity-depth and permeability based on sandstone composition (North, 1985).

- *CO_2-rock experimentation*

The Scanning Electron Microscopy (SEM) (Figure. 31A, C, E and 32A and C) illustrates the texture of the rock samples A20 (760.7 - 760.9 m), A27 (1129.8 - 1129.9 m), A29 (1194.1 - 1194.2 m), A31 (1294.1 - 1294.2 m) and A38 (1529.4 - 1529.5 m) before the CO_2 treatment. These pictures show quartz (with sharp edges), plagioclase, mica, calcite and some K-feldspar embedded in the matrix composed of clay minerals with some calcite. The treatment of the rock samples with CO_2 was done under supercritical conditions of 100°C and pressure of 100 bars, during a period of four weeks. The SEM photomicrographs show dissolution of the cement/matrix around plagioclase (Figure 31B, D and F), reaction of clay minerals (Figure 32D), and rough texture on the surface of quartz grain (Figure 32B and D). The calcite cement has reacted creating secondary porosity (Figure 31B, D and F) and changing permeability of the rock. The CO_2-H_2O-$CaCO_3$ chemical process formulated below shows how the

dissolution takes place after forming the carbonic acid (H_2CO_3) in increasing the acidity of the reservoir (Gaus 2009 and Kjøller et al., 2011).

$$CO_2\ (aq) + CaCO_3 + H_2O \leftrightarrow Ca_2^{+} + 2HCO_3^{-} \quad (1)$$

$$CaCO_3 + H^{+} \rightarrow Ca_2^{+} + HCO_3^{-} \quad (2)$$

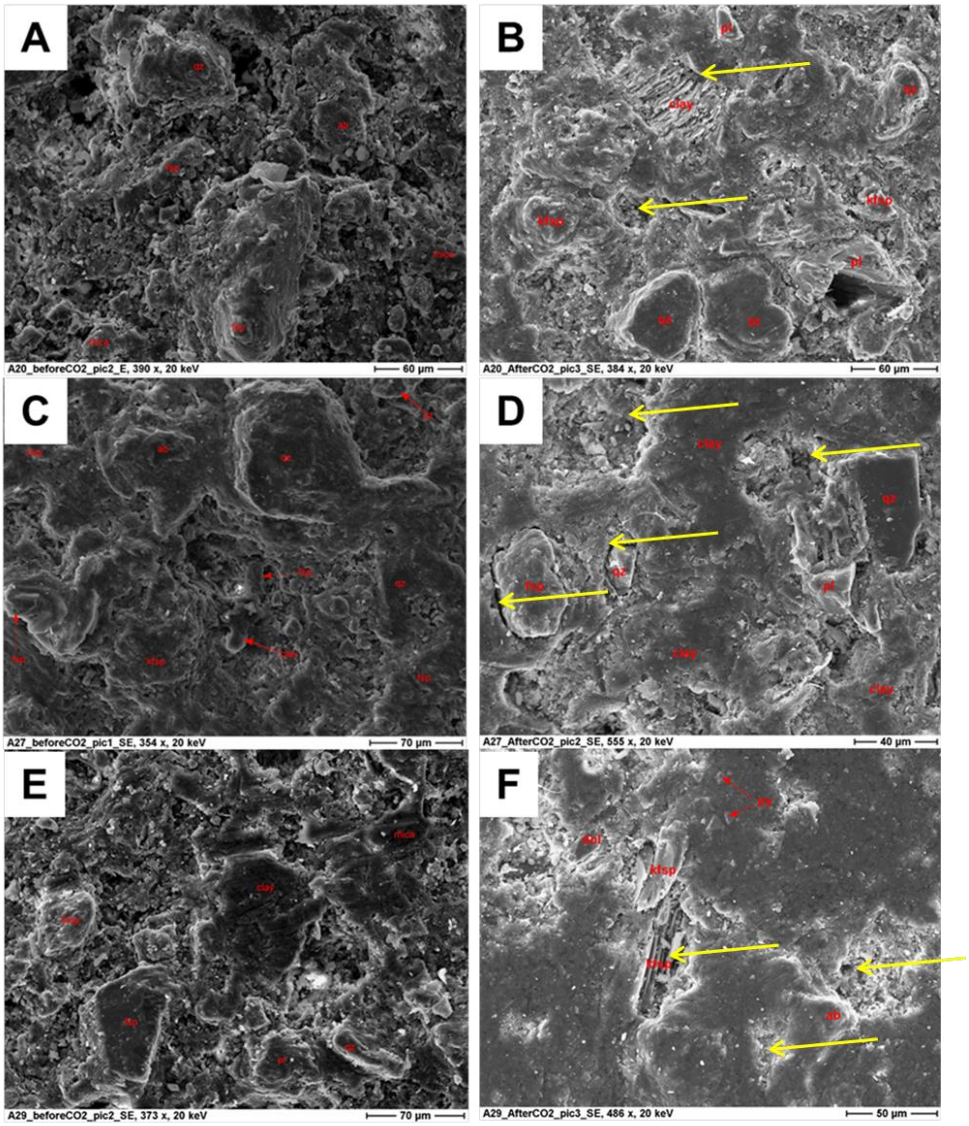

Figure 31. SEM photomicrographs of sample A20 (760.7 - 760.9 m), A27 (1129.8 - 1129.9 m) and A29 (1194.1 - 1194.2 m) showing the texture before (A, C and D) and after (B, D and F) treatment with CO2 at 100°C and 100 bars for four weeks. Textural and mineralogical changes after the sample reactions are illustrated by the dissolution of cement/matrix and the creation of secondary porosities as shown by the yellow arrows.

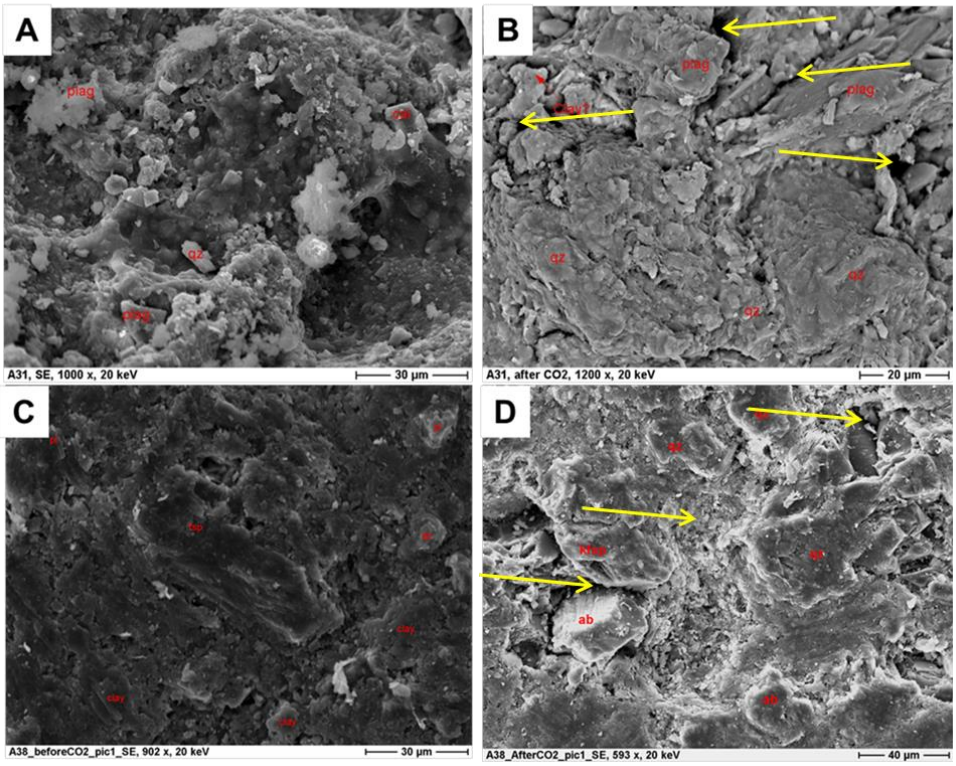

Figure 32. SEM pictures of the rock samples A31 (1294.1 - 1294.2 m) and A38 (1529.4 - 1529.5 m) show before and after CO_2-rock reaction, and dissolution of the cement/matrix and creation of secondary porosities (yellow arrows).

The experimental results on the ZA samples treated with supercritical CO_2 have shown modifications of the texture from smooth to rough surfaces of the grains of quartz. Dissolution of calcite cement around the quartz grains has resulted in creation of secondary porosity as illustrated by cavities (Figure 31B, D and F and 32 B and D). The dissolution process of the authigenic minerals may reduce the stability of the reservoir and lead to severe cracking due to the intense generation of secondary porosity, leading to a collapse in the layers as stipulated by Weibel et al. (2011). On the other hand, this dissolution of the authigenic minerals will increase the permeability and the injectivity in the reservoir.

6.2.2. Cap rock

A reservoir cap rock must be impermeable, thicker than 100 m, covering laterally and continuously the reservoir.

However, above the Middle Sandstone, different siltstone layers occur starting with a 26 m thick laminated siltstone (671.31 m depth) and represented by sample A17 (651.7 - 651.9 m), to a 252 m thick bioturbated calcareous siltstone (612.8 – 360 m depths). The petrography, mineralogy and geochemical descriptions of these sedimentary layers overlying the Middle Sandstone are enlightened in the chapters 4 (section 4.1 and 4.3) and 6 (section 6.2).

The samples of these siltstones representing the caprock are rich in calcite minerals occurring as both grains and cement. The calcite cement sometimes displays poikilotopic texture indicating that the siltstone layers cannot serve as a good quality cap rock. A suitable cap rock should be impermeable like laminated shale or mudstone and should have a thickness of more than 100 m. At interaction with supercritical CO_2 with these rocks may disintegrate and cause the destruction of the layers, and therefore leakage of the CO_2 towards the surface.

Sample A12 (575.5 - 575.7 m) representing calcareous siltstone was experimentally exposed to supercritical CO_2, performed under the temperature of 100°C and pressure of 100 bars for a period of four weeks. This resulted in a rough texture on the surface of quartz pointing at dissolution of calcite cement around grains of quartz, creating secondary porosity (Fig. 33).

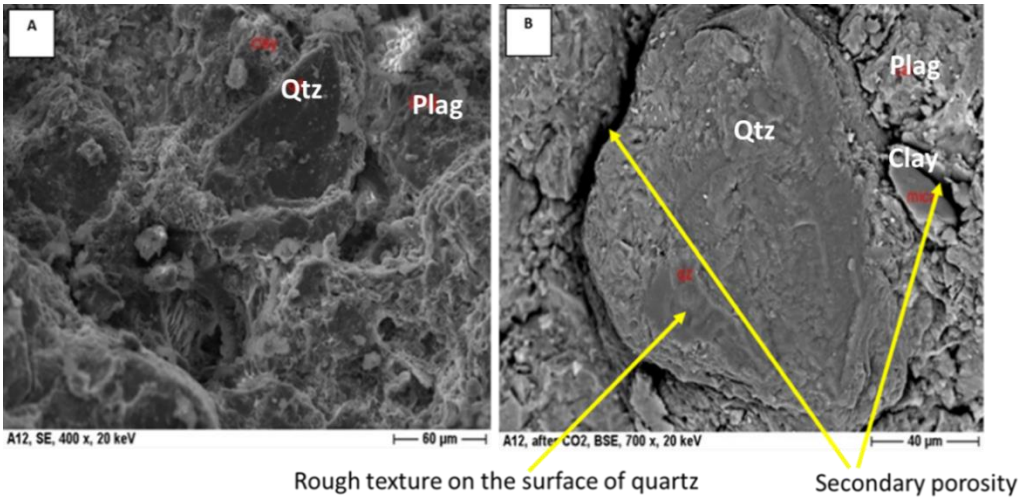

Figure 33. SEM photomicrographs showing mineral components of the sample A12 (575.5 - 575.7 m) before and after treatment with scCO2. (A) Shows untreated sample before the reaction whereas (B) demonstrates the treated sample after the reaction and showing the creation of secondary porosity due to the dissolution of the calcite cement.

Based on the petrography and mineralogy the siltstones consist of grains of calcite, plagioclase, quartz, glauconite and clays, which react with CO_2 under the supercritical conditions. Its overall thickness of 62 m. Thus, the siltstone bed cannot be considered a suitable cap rock. In addition, this siltstone package is overlain by a siltstone and sandstone alternation, with a combined thickness of 252 m. Both siltstone and sandstone units are rich in calcite which may react upon contact with $scCO_2$ and allow the leakage of CO_2 to the surface.

7. CONCLUSIONS

The detailed study of the sedimentary facies of the Zululand Basin in the borehole ZA showed notably siliciclastic and carbonate rocks distributed throughout two uppermost formations (Mzinene and St Lucia) of the Zululand Group. The lowermost part of the ZA core characterising the sedimentary facies of the Makatini

Formation is missing because of the core loss during storage. The preserved Mzinene Formation starts with marine regressive cycle at 1602.7 m, identified by the presence of a bioturbated calcareous siltstone facies, and ending at the depth 675.31 m marked by the arkosic wacke facies. The packstone beds divide this cycle into small cycles which indicate the intercalation between foreslope and inner shelf facies throughout the Mzinene Formation. The contact between the Mzinene and the St Lucia Formations is marked by the beginning of the second marine regression at 675.31 m depth with the presence of a laminated siltstone facies. This second regressive sequence terminates by the occurrence of a glauconitic arkosic wacke facies at 240.61 m depth. The uppermost marine regression is marked by the occurrence of the bioclastic grainstone facies and indicating a shallowing upwards from the underlying laminated siltstone facies at 240.31 m depth towards the top of the ZA sequence. Based on the occurrence of the carbonate beds throughout the ZA sequence in agreement with the carbonate facies model and the T/R cycle, the ZA sedimentary rocks are deposited in shallow shelf environments.

A possible 360 m thick reservoir rock was identified at the depth between 1035.66 m to 675.31 m, here named the Middle Sandstone. The petrographic, mineralogical, and geochemical analyses suggest that the chosen reservoir is texturally immature and compositionally rich in calcite grains and cements with clay matrix. Moreover, this identified reservoir rock consists mainly of calcareous sandstone and arkosic wacke beds with subarkose layer. The clay matrix reduces the porosity and permeability of the reservoir, and the capacity for storing CO_2. According to CO_2-H_2O-rock experiments conducted on the borehole ZA core, the encountered Middle Sandstone is not suitable for the CO_2 injection, because of the dissolution of calcite grains and calcite cement upon contact with the supercritical CO_2. Thus,

creating secondary porosity in the reservoir rock, which in *situ* may lead to the advanced destruction of the entire layers and the leakage of CO_2 towards the surface.

Comparably, the overlying siltstone layers were found unsuitable for acting as cap rock because they consist of only 62 m thickness whereas the required thickness should at least be 100 m and above. The entire siltstone sequence is overlain by 252 m thick calcareous siltstone strata, all at a depth that is too shallow for secure and effective capping of the reservoir. Similarly, the mineralogical composition of the siltstone demonstrated reaction with $scCO_2$ leading dissolution of authigenic minerals. Hence, leading to increased porosity, permeability and weakening the entire cap rock.

8. RECOMMENDATIONS

It must be taken into account that the ZA borehole rock sequence not only does not have a good quality reservoir rock to serve as a storage unit, but also lacks a suitable cap rock to serve as seal stopping the upward migration of the CO_2 fluids. This however, does not preclude a more suitable reservoir and cap rock qualities in lateral continuation of these rocks, in more distal or more proximal deposition directions, or parallel to the paleo coastline. Topographic and see level fluctuations of the geological past may have created much more favorable conditions for the deposition of CO_2 storage suitable rocks even in relative vicinity, within few or few tens of kilometres from the ZA borehole. A lateral correlation of ZA sequence with other boreholes such as NZA, ZB and ZC is presently carried out in a separate study at PhD (VL Tibane) level at UP to determine the size and the lateral continuity of the reservoir and the cap rocks.

Further laboratory experiments on CO_2-H_2O-rock reaction should help to better understand the possible physical changes of the reservoir and the cap rocks. Geochemical modeling experiments are necessary to study CO_2 migration within the storage and capping rocks during CO_2 injection. Interaction between minerals and $scCO_2$ should be monitored to avoid a possible collapse of both reservoir and cap rocks. Most importantly, the investigations performed in this thesis should be repeated on a fresh core to better assess the reservoir and cap rock quality and the possible CO_2-H_2O-rocks reactions. Such experiments should help to determine individual reaction rates and the dissolution and precipitation rates and to asses possible long - term changes in the reservoir rocks. Predictions should be modelled geochemically based on a large data sets and experimental experience.

9. REFERENCES

Ahmed, W., 2007. Comparison of authigenic minerals in sandstones and interbedded mudstones, siltstones and shales, East Berlin formation, Hartford Basin, USA. *Bulletin of the Chemical Society of Ethiopia*, *21*(1).

Aljinović, D., 1995. Storm influenced shelf sedimentation-an example from the Lower Triassic (Scythian) siliciclastic and carbonate succession near Knin (Southern Croatia and Western Bosnia and Herzegovina). *Geologia Croatica*, *48*(1), pp.17-32.

Andre, L., Audigane, P., Azaroual, M., Menjoz, A., 2007. Numerical modeling of fluid–rock chemical interactions at the supercritical CO2–liquid interface during supercritical CO2 injection into a carbonate reservoir, the Dogger aquifer (Paris Basin, France). Energy Conversion and Management 48, 1782–1797.

Bachu, S., 2003. Screening and ranking of sedimentary basins for sequestration of CO2 in geological media in response to climate change. Environmental Geology, 44, pp. 277−289. Bachu, S. (2007). Carbon dioxide storage capacity in uneconomic coalbeds in Alberta, Canada: Methodology, potential and site identification. International Journal of Greenhouse Gas Control, 1, pp. 374−385.

Bathia, M.R., 1983. Plate Tectonics and geochemical composition of sandstones. Department of Geology, Australian National University, Canberra A.C.T. 2600 Australia. Journal of Geology. Vol. 91, number 6. 611-627.

Berner, R.A., 1981. New geochemical classification of sedimentary environments. J. Sedim. Petrol. 51, 359-365.

Bhuiyan, M.A.H., Rahman, M.J.J., Dampare, S.B., Suzuki, S., 2011. Provenance, tectonics and source weathering of modern fluvial sediments of the

Brahmaputra-Jamuna River, Bangladesh: Inference from geochemistry. Journal of Geochemical Exploration. Elsevier. 113-137.

Bland, K.J., Hendy, A.J., Kamp, P.J. and Nelson, C.S., 2013. Macrofossil biofacies in the late Neogene of central Hawke's Bay: applications to palaeogeography. *New Zealand Journal of Geology and Geophysics*, *56*(4), pp.200-222.

Blatt, H., 1992. Sedimentary Petrology. University of Oklahoma. W.H. Freeman and Company. Second Edition. New York.United State of America. Pp 139-150.

Broad, D.S., Jungslager, E.H.A, McLachlan, I.R., Roux, J., 2006. Offshore Mesozoic Basins, In: M.R. Johnson, C.R. Anhaeusser, R.J. Thomas (eds.): The Geology of South Africa. The Geological Society of South Africa and Council for Geoscience, Pretoria, 553-571.

Broch, E. and Franklin, J.A., 1972. The point-load strength test. Int. J. Rock Mech.& Min. Sci. 9: 669-697.

Chamley, H., 1989. Clay sedimentology. Springer-Verlag Berlin Heidelberg. ISBN 3-540-50889-9. Germany. 4-366.

Cloete M., Viljoen J.H.A. and Stapelberg F.D.J., 2010. *Technical Report of the Geological Storage of Carbon Dioxide in South Africa*. Council for Geosciences.236pp.

Cloete, M., Viljoen, J.H.A., Hicks, N., Botha, G.A., Davids, S., Musekiwa, C., Singh, R.G., Stapelberg, F.D.J., 2011. Towards an effective CO2 storage capacity assessment of the Zululand Basin, South Africa. Council for Geosciences. Petroleum Agency of South Africa. 115pp.

CO_2CRC, 2009. http://www.co2crc.com.au/aboutgeo/storage. html. Web page visited on 2009.01.14.

Dickinson, W.R., 1985.*Interpreting provenance relations from detrital modes of sandstones*. In: Tucker, Maurice E. *Sedimentary petrology: an introduction to the origin of sedimentary rocks*, second edition, Blackwell Scientific, Oxford, 1991, 1992. 63-65.

Dickinson, W.R., Valloni, R., 1980. Plate settings and provenance of sands in modern ocean basins. The Geological Society of America. Geology, v. 8, p82-86.

Dingle, R.V., Scrutton, R.A., 1974. Continental break-up and the development of post-Paleozoic sedimentary basins around southern Africa. geol. Soc. Amer. Bull. 85: 1467-1474.

Dingle, R.V., Siesser, W.G. and Newton, A.R., 1983. Mesozoic and Tertiary geology of Southern Africa. A.A. Balkema Rotterdam, 375pp.

Dietz, R.S., Holden, J.C., 1970. Reconstruction of Pangaea: breakup and dispersion of continents, Permian to present. Jour. Geophys. Res. 75:4939-4956 in: Tankard, A.J., Jackson, M.P.A., Eriksson, K.A., Hobday, D.K., Hunter, D.R. and Minter, W.E.L. (1982). *Crustal Evolution of Southern Africa*. Springer-Verlag, New York. Pp 407-423.

Duncan, A.R. and Marsh, J.S. 2006. The Karoo igneous province. In: The geology of South Africa. Edited by M.R. Johnson, C.R. Anhaeusser and R.J. Thomas. Geological Society of South Africa, Johannesburg/Council for Geoscience, Pretoria.

Dunham, R.J., 1962. Classification of carbonate rocks according to depositional texture. In Classification of carbonate rocks, W.E. Ham (ed.), 108-121. Amer. Ass. Petrol. Geol. Mem. 1, in: Tucker, Maurice E. 1991. Sedimentary petrology: an introduction to the origin of sedimentary rocks, second edition, Blackwell Scientific, Oxford. Pp 127-128.

Dott, R.H., 1964. Wacke, greywacke and matrix – what approach to immature sandstone classification? J. Sed. Petrol. 34, 625-32 7.

European Academies Sciences Advisory Council (EASAC), 2013. Carbon Capture and Storage in Europe. Technical Report, ISBN 978-38047-3180-6, German National Academy of Sciences Leopoldina. 1-4.

Eichhoff, H.J., Reineck, H.E., 1953. Sekundäre Verfärbungen durch Herauslösen von Hämatit aus Gesteinen. Neues Jahrb. Mineral. Monatsh. 1952, 315-324, in: Reineck, H.E., Singh, I.B. 1980. Depositional Sedimentary Environments with Reference to Terrigenous Clastics. Springer-Verlag, second, revised and updated Edition. Berlin. 549pp.

Ennis-King, J. and Paterson, L., 2000. Reservoir engineering issues in the geological disposal of carbon dioxide. In: Proceedings of the 5th International Conference on Greenhouse Gas Control Technologies (GHGT-5), 13−16 August 2000, Cairns, Australia (D.J. Williams, R.A. Durie, P. McMullan, C.A.J. Paulson and A. Smith, eds). CSIRO Publishing, Collingwood, Victoria, Australia, 290−295. http://lib.kier.re.kr/balpyo/ghgt5/Papers/D6 percent205.pdf

Flügel, E. 2004. Microfacies of carbonate rocks. Analysis, interpretation and application. Institute of Paleontology. Springer, Berlin. Germany. 94-645.

Folk, R.L. 1959. *Practical petrographic classification of limestones*. Bull. Am. Ass. Petrol. Geol. 43, 1-38 in Greensmith, J.T. 1978. *Petrology of the sedimentary rocks*, London: Allen & Unwin, 6th ed. 124-152.

Folk, R.L. (1974). *Petrology of Sedimentary Rocks*. Hemphill, Austin, Texas, 159pp in Tucker, Maurice E. *Sedimentary petrology: an introduction to the origin of sedimentary rocks*, second edition, Blackwell Scientific, Oxford, 1991, 1992. P91-92.

Gasda S.E. (2008). Numerical Models for Evaluating CO_2 Storage in Deep, Saline Aquifers: Leaky Wells and Large-Scale Geological Features. Doc. Thesis, Princeton University, Department of Civil and Environmental Engineering. 1-18.

Gaus, I., Audigane, P., Andre´, L., Lions, J., Jacquemet, N., Durst, P., Czernichowski-Lauriol, L., and Azaroual, M., 2008. Geochemical and solute transport modeling for CO2 storage, what to expect from it? International journal of greenhouse gas control 2, 605 – 625.

Gerrard, I., 1972a. Report on progress on the evaluation of the Zululand Basin. Report, SOEKOR, PSV 1325 (unpubl.): in Cloete M., Viljoen J.H.A., and Stapelberg F.D.J. 2010. *Technical Report of the Geological Storage of Carbon Dioxide in South Africa*, p106, 107, 113. Council for Geosciences.

Gingras, M.K., Pemberton, S.G. and Smith, M., 2014. Bioturbation: Reworking Sediments for Better or Worse. *Oilfield Review*, *2015*(26), p.4.

Greensmith, J.T. 1978. Petrology of the sedimentary rocks. Sixth Edition. George Allen & Unwin Ltd/ Thomas Murby. Vol. 2. London. 16-190.

Heirtzler, J.R., Dickson, G. O., Herron, E. M., Pitman, W.C., Le Pichon, X. 1968. Marine magnetic anomalies, geomagnetic field reversals, and motions of the ocean floor and continents. Jour. Geophys. Res. 73: 2119-2136.

Hexiang, Z. 2007. Supramolecular chemistry on carbon dioxide. MSc thesis, Faculty of the Graduate School of the University of Texas at Arlington. USA. 25-26.

Okoro, A.U. and Igwe, E.O., 2014. Lithofacies and depositional environment of the Amasiri Sandstone, southern Benue Trough, Nigeria. *Journal of African Earth Sciences*, *100*, pp.179-190.

Holloway, S., 2001. Storage of fossil fuel-derived carbon dioxide beneath the surface of the earth. Annual Reviews of Energy and the Environment 26, 145-166.

IPCC (Intergovernmental Panel on Climate Change), 2005. IPCC Special Report on Carbon Dioxide Capture and Storage (B. Metz, O. Davidson, H.C. De Coninck, M. Loos and L.A. Mayer, eds). Cambridge University Press, Cambridge, U.K. and New York, NY, U.S.A., 442 pp.

Jungslager, E.H.A., 1999. Petroleum habitats of the Atlantic margin of South Africa. Special Publication, Oil and Gas Habitats of the South Atlantic, Geological Society of South Africa, 153–168.

Kennedy, W.J. and Klinger, H.C. 1972. Hiatus concretions and hardground horizons in the Cretaceous of Zululand. Paleontology 15: 539-549.

Kennedy, W.J. and Klinger, H.C. 1975. Cretaceous faunas from Zululand and Natal, South Africa. Introduction, Stratigraphy. Bulletin of the British Museum of Natural History (Geology), 25, 265-315.

Kjøller, C.; Weibel , R.; Bateman , K.; Laier, T.; Nielsen, L.H.; Frykman, P.; and Springer, N. 2011. Geochemical impacts of CO2 storage in saline aquifers with various mineralogy – results from laboratory experiments and reactive geochemical modelling. Energy Procedia 4 (2011) 4724-4731.

Klinger, H.C., Kennedy, W. J. 1977. Upper Cretaceous ammonites from a borehole near Richards Bay, South Africa. S. Afr. Mus. Ann. 72: 69-107.

Klausen, M.B. 2009. The Lebombo monocline and associated feeder dyke swarm: Diagnostic of a successful and highly volcanic rifted margin? Tectonophysics, 468, 42-62.

Leeder, M.R., 1982. Sedimentology (Process and Product). Department of Earth Sciences, University of Leeds. London, George. Allen and Unwin. First published in 1982. 344pp.

Maynard, J. B.; Valloni, R.; Yu, H. S.1982: Composition of modern deep-sea sands from arc related basins. In: Leggett, J. K. ed. Trench forearc geology: Sedimentation and tectonics on modern and ancient plate margins. Geological Society of London special publication 10: 551-561.

McLachlan, I.R. and McMillian, I.K., 1979. Microfaunal biostratigraphy, Chronostratigraphy and history of Mesozoic and Cenozoic deposits on the coastal margin of South Africa. Geological Society of South Africa Special Publication, 6, 161-181.

McLennan, S.M., Hemming, S., McDennial, D.K., Hanson, G.N., 1983. Geochemical approaches to sedimentation, provenance and tectonics. Geol. Soc. Am. Spec. Pap. 284, 21-40.

McMillian, I.K., 2003. Foraminiferally defined biostratigraphic episodes and sedimentation pattern of the Cretaceous drift succession (Early Barremian to Late Masstrichtian) in seven basins on the South African and southern Namibian continental margin. South African Journal of Science, 99, 537-576.

Melluso, L. Cucciniello, C. Petrone, C.M., Lustrino, M., Morra, M.T., Vasconcelos, L., 2008. Petrology of Karoo volcanic rocks in the southern Lebombo monocline, Mozambique. Journal of African Earth Sciences. Elsevier. 139-151.

Monastersky R., 2013. Global carbon dioxide levels near worrisome milestone. News in Focus, Nature, Vol 497, Macmillian Publishers Limited.13-14.

Mining Weekly, 2010. Newly launched atlas identifies viable sites for SA carbon storage. http://www.miningweekly.com/article/newly-launched-atlas-identifies-viable-sites-for-sa-carbon-storage-2010-09-10-1.

Nesbitt, H. W., and Young, G.M., 1984. Prediction of some weathering trends of plutonic and volcanic rocks based on thermodynamic and kinetic considerations. Geochimica et Cosmochimica Acta, v. 48, p. 1523-1534.

North, F. K., 1985, Petroleum Geology. Allen & Unwin, Inc., Winchester, MA., 607pp.

Odin, G.S., Fullagar, P.D. (1988). Geological significance of the glaucony facies. In Green Marine Clays. Elsevier, Amsterdam, the Netherlands. Pp295-332.

Palma, R.M., López-Gómez, J. and Piethé, R.D., 2007. Oxfordian ramp system (La Manga Formation) in the Bardas Blancas area (Mendoza Province) Neuquen Basin, Argentina: facies and depositional sequences. *Sedimentary Geology*, *195*(3), pp.113-134.

Petroleum Agency SA, 2008. Petroleum Exploration: Information and opportunities 2008. Petroleum Agency South Africa, 30 pp.

Pettijohn, F. J., 1975. Sedimentary rocks. Third Edition. Harper & Row, Publishers. New York, Evanston, San Francisco, and London. SBN 06-045191-2. Pp13-425.

Pettijohn, F. J., P.E. Potter and Siever, 1973. *Sand and Sandstone*. Berlin: Springer-Verlag in Greensmith, J.T. 1978. *Petrology of the sedimentary rocks*, London: Allen & Unwin, 6th ed. 17-67.

Prather, J.K., 1905. Glauconite. *The Journal of Geology*, *13*(6), pp.509-513.

Reineck, H.E., Singh, I.B., 1980. Depositional Sedimentary Environments with Reference to Terrigenous Clastics. Springer-Verlag, second, revised and updated Edition. Berlin. Pp130-457.

Roser, B.P., Korsch, R.J., 1986. Determination of tectonic setting of sandstone-mudstone suites using SiO_2 content and K_2O/Na_2O ratio. J. Geol. 94. 635-650.

Rutherford, S., D'hondt, S. and Prell, W., 1999. Environmental controls on the geographic distribution of zooplankton diversity. *Nature*, *400*(6746), pp.749-753.

Scrutton, R.A., Dingle, R.V., 1976. Observations on the process of sedimentary basin formation at the margins of southern Africa. Tectonophysics. 36: 143-156.

Selley, R.C., 1982. An introduction to sedimentology. Academic Press Inc., A Subsidiary of Harcourt Brace Jovanovich, Publishers. Second Edition. London. 7-10.

Sharief, F.A., 1986. Depositional environments of the Triassic system in central Saudi Arabia. *Geological Journal*, *21*(4), pp.403-420.

Shone, R.W., 2006. Onshore post-Karoo Mesozoic deposits, *In*: Johnson, M.R., Anhaeusser, C.R. and Thomas, R.J. (Eds.), The Geology of South Africa. Geological Society of South Africa, Johannesburg/Council for Geoscience, Pretoria, 541 – 552.

Siedner, G., Mitchell, J.G., 1976. Episodic Mesozoic volcanism in Namibia and Brazil: A K-Ar isochron study bearing on the opening of the South Atlantic. Earth Planet. Sci. Lett. 30: 292-303.

Singh, V. and McLachlan, I., 2003. South Africa's east coast frontier offers untested mid to deep water potential. Oil and Gas Journal, 101 (22), 40-45.

Tankard, A.J., Jackson, M.P.A., Eriksson, K.A., Hobday, D.K., Hunter, D.R. and Minter, W.E.L., 1982. *Crustal Evolution of Southern Africa*. Springer-Verlag, New York, 523 pp. By Linstrom, W. (1987). 407-423.

Tucker, M. E., 1991. *Sedimentary petrology: an introduction to the origin of sedimentary rocks*, second edition, Blackwell Scientific, Oxford, 1991, and 1992. 260pp.

Tucker, M.E. ed., 2009. *Sedimentary petrology: an introduction to the origin of sedimentary rocks*. John Wiley & Sons. 261pp.

Van Vuuren, C.J., Broad, D.S. Jungslager, E.H.A., Roux, J and McLachlan, I.R. (1998). Oil and Gas. In: Cloete M., Viljoen J.H.A., and Stapelberg F.D.J. 2010. Technical Report of the Geological Storage of Carbon Dioxide in South Africa. Council for Geosciences. 236pp.

Verdon, J.P., 2010. Microseismic Monitoring and Geomechanical Modeling of CO2 Storage in Subsurface Reservoirs. Doc. Thesis, University of Bristol, Department of Earth Science.1-5.

UNFCCC (The United Nations Frameworks Convention on Climate Change), 2008. http://unfccc.int/essential_background/convention/items/2627.php

Watkeys, M.K. (2002). Development of the Lebombo rifted volcanic margin of SE Africa. In: Menzies, M.A., Baker, J., Ebinger, C. and Klemper, S. Magmatic Rifted Margins. Geological Society of America, Special Paper 362, 27-46.

Weibel, R., Kjoller, C., Bateman, K., Nielsen, L. H., Frykman, P., Springer, N., Laier, T., 2011. Mineral changes in CO2 experiments – Examples from Danish onshore saline aquifers. GHGT-10. Energy Procedia. 4, 4495-4502.

Zaixing, J., Ling, G., Chao, L., Yuan, W. and Min, L., 2013. Lithofacies and sedimentary characteristics of the Silurian Longmaxi Shale in the southeastern Sichuan Basin, China. *Journal of Palaeogeography*, *2*(3), pp.238-251.

10. LIST OF ABSTRACTS DESCENDING FROM THIS THESIS AND PUBLISHED AT CONFERENCES

1. Ndongani, F.L..; Tibane, L.V.; Harris, P; Altermann, W.: Petrography*, Mineralogy and Geochemistry of Rocks in the Borehole ZA, Onshore Zululand Basin: Evaluation for Carbon Dioxide Storage.* University of Pretoria, Department of Geology, Kumba Exxaro Chair in Geodynamics, South African Centre for Carbon Dioxide and Storage, GeoSpectral Imaging. Abstract Presented at International Geological Congress (IGC) Cape Town 2016, Published on American Geosciences Institute. Page 4564. https://www.americangeosciences.org/igc/16172.

Abstract Copy:

Paper Number: 4564

Petrography, Mineralogy and Geochemistry of Rocks in the Borehole ZA, Onshore Zululand Basin: Evaluation for Carbon Dioxide Storage

Luzolo Ndongani, F.[1,2], Tibane, L.V.[1] , Harris, P[3], and Altermann, W.[1]

[1]University of Pretoria, Department of Geology, Kumba Exxaro Chair in Geodynamics

[2]South African Centre for Carbon Dioxide and Storage

[3]GeoSpectral Imaging

The Cretaceous Zululand Basin of South Africa is one of the possible sites proposed for geological CO_2 sequestration [1]. This contribution aims to investigate the suitability of the sedimentary rocks of the onshore Zululand Basin in KwaZulu-Natal, South Africa, for a permanent sequestration of CO_2. Unfortunately, the bottom part of the 1779.96 m deep drill core ZA, drilled by SOEKOR in the 1960s is not preserved and the core starts only at 1602 m depth.

The onshore Zululand Basin covers an area of 7500 km^2, extending from St Lucia northwards into Mozambique. The preserved core from 1602 to 1041 m is characterised by dark grey coloured calcareous siltstone beds, rich in foraminifera and algae fossils, a greyish brown medium to coarse grained glauconitic intercalations, overlain by the succession of siltstone layers with some interbeds of calcareous and glauconitic siltstones (Makatini and Mzinene Formations). The middle part of the sequence (Mzinene Formation) shows brownish sandstone layers interbedded with limestone rich in algae and calcareous sandstone layers. Invertebrate fossils are common throughout the formation. The St Lucia Formation closing-up the Zululand Group, is similar to the Mzinene Formation, except that it is thicker, more fossil rich and contains more glauconite [2]. In the core, above 675m depth, it displays an alternation of siltstone and sandstone layers followed by 245 m thick calcareous siltstone overlain by glauconitic sandstone and algae limestone layers.

The middle sandstone strata between 1035 to 678 m, meet the criteria for a suitable reservoir. It is bounded on top by a 42 m thick siltstone and sandstone layers as a possible cap rocks, covered by 242 m thick calcareous siltstone and sandstone. Petrographically, the middle sandstone rocks are characterised as subarkose, arkosic wackes and calcareous sandstone and they contain mostly quartz, calcite and plagioclase minerals with a respective average of 47, 21 and 15%. Other minerals such as smectite, mica, hematite, zeolite, glauconite and lithic fragments also occur. The geochemical investigation of these sandstones reflects their mineralogical contents and shows the predominance of SiO_2 (55wt%), CaO (11wt%), Al_2O_3

(10wt%) and Fe_2O_3 (7wt%) contents followed by other major oxides such as MgO, Na_2O, K_2O, H_2O, MnO, TiO_2, P_2O_5 and Cr_2O_3 summing up to c. 8%. The porosity and the permeability of the middle sandstone rocks are respectively over 30% and 30mD. The predominance of quartz, calcite and plagioclase minerals are also evident in the possible cap rock layer. However, there is an increase of clay mineral contents, which is supported by the spectral results (mineral and index chemical results) showing the evidence of aforementioned different clay minerals at this depth.

The treatment of the rock samples with CO_2 under supercritical conditions of 100ºC and pressure of 100 bars, during a period of two weeks shows a dissolution reaction on the surface of quartz grains and the calcite cement has reacted creating secondary porosity and changing permeability of the rock.

Therefore, the middle sandstone and the overlying siltstone rocks are unsuitable for injecting carbon dioxide because of the important amount of calcite content and authigenic minerals which may be dissolved during the $scCO_2$ - mineral reaction, creating secondary porosity. The progressive increase of the pore pressure may lead to the disintegration of the entire layers [3].

References:

[1] Cloete M. et al. 2010. Council for Geosciences. 236pp.

[2] Kennedy, W.J., Klinger, H.C. 1972. *Palaeontology*. 15: 539-549

[3] Gaus, I. et al. 2008. *International journal of greenhouse gas control*, pp. 605–625

2. Landman, B.E.[1,2]; Ndongani, F.L.[1,2]; Hugo, D. [1]; Tibane, L.V. [1]; Altermann, W.[1], 2015. Evaluation of Rocks in Boreholes ZA, ZB, ZC and NZA of the Onshore Zululand Basin for Carbon Dioxide Storage.[1]University of Pretoria; [2]South African Centre for Carbon Capture and Storage. 4th South African Carbon Capture and Storage (CCS) Conference, Capital 20 West Hotel Sandton, 2015. Poster presentation.

Abstract copy:

Sedimentary basins and their deep saline aquifers in particular, are being investigated as possible repositories for large volumes of anthropogenic CO_2 to mitigate global warming and related climate changes (Cloete et al., 2010). The Cretaceous Zululand Basin of South Africa is one of the possible sites proposed in the “Atlas on Geological Storage of Carbon Dioxide” for geological CO_2 storage, however little is known on its sedimentary facies, geochemical and mineralogical properties.

Thus, this contribution aims to investigate the suitability of the sedimentary rocks of the onshore Zululand Basin in KwaZulu-Natal, South Africa, for a permanent sequestration of CO_2. Different methods were performed in order to develop a sedimentological and petrographic model for the basin, such as the determination of the lithostratigraphy, petrography, mineralogy and geochemistry, based on the Zululand cores.

The NZA drill core displays strikingly different lithofacies to the other Zululand boreholes and thus cannot be correlated based only on lithological grounds. Biostratigraphy is needed.

The bottom of the NZA sequence is characterised by the pyroclastic rocks of the Fenda Formation. It is overlain by the calcareous sandstones of the Makatini and St Lucia Formations. Dividing the Makatini and St Lucia Formations is a pink terrestrial limestone at ca. 480 m depth. The Mzinene Formation is not identified in the stratigraphy of the NZA drill core.

ZA, ZB and ZC drill cores display similar lithologies from the bottom to the top of the sequences. The reddish paleosol sediment observed at the bottom of the ZC sequence indicates the presence of the weathered Lebombo Basement, it is overlain by alternating sandstone and siltstone beds of the Makatini Formation. A shallow dip angular unconformity

is encountered marking the limit of the Makatini and Mzinene Formations. It is characterised by the occurrence of the sandstone beds across the drill cores. The following Mzinene Formation comprises sandstone and calcareous sandstone beds. The upper angular unconformity indicating the boundary between the Mzinene and St Lucia Formations is located at ca. 680-650m depth. This upper angular unconformity is characterised by the presence of a thin sandstone bed ca. 20-90m thick. It is known from outcrops but invisible in the drill cores. The uppermost St Lucia Formation comprises mostly calcareous sandstone beds with glauconitic siltstones, sandstones beds and bioclastic limestone bed on top. The middle sandstone of the Mzinene Fm and the overlying clastic and calcareous siltstone rocks of the St Lucia Fm are unsuitable for injecting carbon dioxide because of the important amount of calcite content and authigenic minerals which are dissolved during the $scCO_2$ - mineral reaction, creating secondary porosity. The progressive increase of the pore pressure may lead to the disintegration of the entire beds.

Laboratory tests and modelling and geomechanical tests must be performed meticulously to understand whether the reservoir and particularly the cap rock should be investigated. During injection the interaction between minerals and $scCO_2$ must be monitored in order to avoid leakage or even collapse of the reservoir and cap rock.

Andre´, L., Audigane, P., Azaroual, M., Menjoz, A., 2007. Numerical modelling of fluid–rock chemical interactions at the supercritical CO_2 - liquid interface during supercritical CO_2 injection into a carbonate reservoir, the Dogger aquifer (Paris Basin, France). Energy Conversion and Management 48, 1782–1797.

Cloete M., Viljoen J.H.A., and Stapelberg F.D.J. 2010. *Technical Report of the Geological Storage of Carbon Dioxide in South Africa*. Council for Geosciences. 236pp.

Gerrard, I. 1972a. Report on progress on the evaluation of the Zululand Basin. Report. SOEKOR, PSV 1325 (unpubl.) In: Cloete M., Viljoen J.H.A., and Stapelberg F.D.J. 2010. *Technical Report of the Geological Storage of Carbon Dioxide in South Africa*. Council for Geosciences. 236pp.

Gaus, I., Audigane, P., Andre´, L., Lions, J., Jacquemet, N., Durst, P., Czernichowski-Lauriol, L., and Azaroual, M., 2008. Geochemical and solute transport modelling for CO2 storage, what to expect from it? *International journal of greenhouse gas control,* pp. 60 5 – 62 5.

Kennedy, W.J., Klinger, H.C. (1972). Hiatus concretions and hard ground horizons in the Cretaceous of Zululand. *Palaeontology*. 15: 539-549.

Pettijohn, F. J., P.E. Potter and Siever 1973. *Sand and Sandstone*. Berlin: Springer-Verlag in Greensmith, J.T. 1978. *Petrology of the sedimentary rocks*, London: Allen & Unwin, 6th ed. 17-67pp.

Tucker, M. E. 1991. *Sedimentary petrology: an introduction to the origin of sedimentary rocks*, second edition, Blackwell Scientific, Oxford, 1991, 1992. 260pp.

Van Vuuren, CJ., Broad, D.S. Jungslager, E.H.A., Roux, J and McLachlan, I.R. (1998). Oil and Gas. In: Cloete M., Viljoen J.H.A., and Stapelberg F.D.J. 2010. *Technical Report of the Geological Storage of Carbon Dioxide in South Africa*. Council for Geosciences. 236pp.

3. Tibane L.V.[1], Harris, P.[2], Landman, B.[1], Modisha, O.[1], Ndongani, F.[1], Altermann, W.[1], 2013. The suitability of the onshore Zululand basin for geological co_2 storage: sedimentology, mineralogy and borehole correlations. Carbon Capture and Storage Conference, 3-4 October. Cedar Park Hotel, Wood mead in Johannesburg. Oral Presenter.

   Abstract copy:

CALL FOR PAPERS:

CARBON CAPTURE AND STORAGE CONFERENCE 3-4 OCTOBER, 2013
Title:
THE SUITABILITY OF THE ONSHORE ZULULAND BASIN FOR GEOLOGICAL CO_2 STORAGE: SEDIMENTOLOGY, MINERALOGY AND BOREHOLE CORRELATIONS
Name:
Prof W. Altermann
Affiliation:
[1]Department of Geology, University of Pretoria, Kumba-Exxaro Chair in Geodynamics, Pretoria, South Africa [2]GeoSpectral Imaging, Office E6, Block E, Somerset Office Estate, 604 Kudu Street, Allen's Nek, 1737: phil@geospectral.co.za
Email:
wlady.altermann@up.ac.za
Tel:
0124204137
Authors:
Tibane L.V.[1], Harris, P.[2], Landman, B.[1], Modisha, O.[1], Ndongani, F.[1], , Altermann, W.[1]
Abstract (200 words): Carbon capture and storage (CCS) measures in South Africa aim at injection of anthropogenic CO_2 into underground geological formations. One of the possible test sides is the onshore Zululand Basin from which several drill cores from 1960's exists. This study investigates the lithostratigraphic, mineralogical and geochemical compositions for the suitability of the Zululand basin for CO_2 storage. Boreholes BHA (1779.96 m), BHB (1602.33 m), NZA (571.2 m), and ZF1/85 (57.2 m) are investigated. The drill cores were logged and 100 samples were collected. The entire length of the four boreholes was recorded using sisuRock Mobile spectral imaging instrument (sisuMobi) by GeoSpectral Imaging. The recorded images and digital data information is currently under evaluation. Petrography, X-Ray Fluorescence, and X-Ray Diffraction were applied to all samples. Several samples were also made available for direct CO_2 absorption investigations by Prof. Nicola Wagner at Witwatersrand University. The petrography indicated that the Zululand Basin sedimentary rocks consist of siltstones intercalated with argillaceous rocks, sandstones, mudstones, calcareous sandstones, and some carbonate rocks. The clastic rocks consist of quartz, plagioclase, calcite, hematite, mica, and clay minerals. This mineralogy is supported by the XRD and XRF results. The data will be used for borehole correlations, assessments and perform laboratory experiments to investigate the CO_2 Storage conditions of the basin, and study the positive and/or negative impacts on reservoir quality resulting from CO_2 injection.

4. Fillsmith Ndongani[1,2], V. Tibane[1], W. Altermann[1], 2014. Physical, mineralogical, chemical and morphological properties of the Zululand basin based on Borehole BHA. [1]University of Pretoria, Department of Geology, [2]SACCCS. 2014 UP-CCS Working Group Conference. Progress in CO2 Storage projects in Geology and Development Plans. Burgundies Club Hall, University of Pretoria, Main Campus. Pretoria. Oral Presenter.

   Abstract copy:

Physical, mineralogical, chemical and morphological properties of the Zululand basin based on Borehole BHA by Fillsmith Ndongani[1,2], V. Tibane[1], W. Altermann[1] *[1]University of Pretoria, Department of Geology, [2]SACCCS*

Based on the drill cores from the onshore Zululand basin, drilled by Soekor in the 1960'ies the basin is investigated as to its suitability as a test site for geological CO_2 storage. The stratigraphy of the Zululand basin comprises three formations: The Makatini Formation unconformably overlies much older Lebombo Group volcanic rocks. It comprises small pebble conglomerates, sandstone, silts/siltstones and limestones. The thickness of the measured outcropping sections of the Makatini Formation is more than 80 m.
The upward following Mzinene Formation, consists of glauconitic siltstones and crossbedded sandstones which contain a rich invertebrate fauna including bivalves, gastropods, ammonites, nautiloids and echinoids. The combined thickness of Makatini and the overlying Mzinene Formations is up to 722 m as indicated by the borehole data. The top-most St Lucia Formation is lithologically very similar to the Mzinene Formation, but is separated from the latter by a slight angular unconformity not visible in the borehole but interpreted from seismic profiles. The thickness of St Lucia Formation is 900 m, as indicated by the borehole data.
The petrography indicates that the Zululand Basin sedimentary rocks consist of siltstones, sandstones, calcareous sandstones, intercalated with argillaceous rocks and mudstones. The grains consist of quartz, plagioclase, calcite, mica, clay minerals and accessory iron minerals in places. This is supported by the XRD and XRF results.
BHA and BHB contain sandstones at the depth greater than 800 m. The sandstones are of mineralogical compositions that can react with CO_2. The sandstones are bounded at the top and bottom by mudstones intercalating with siltstones. The overlying mudstones contain the suitable mineralogy for trapping of CO_2 after injection.

11. APPENDICES

APPENDIX A: PETROGRAPHIC DESCRIPTION OF ZA SAMPLES

Sample ID (Depth)	Rock name	Rock type	Visual observation	Microscopic observation
A1 (105.5 – 105.3 m)	Limestone	Bioclastic limestone	Light brown coloured, fine grained, weakly indurated, massive rock with strong reaction with HCl (5%). The rock contains about 5mm thick calcitic plates of algae and broken fossils.	The limestone consists mainly of different type algal fragments displaying various shapes including elongated (up to 1mm size), spherical, plate, and carapaces showing polygonal shapes. The elongated shape is the most dominant. The algae fossils are associated with other fossils such as foraminifera, bivalve, gastropods and pellets. These fossils are mostly unbroken and cemented with each other. Clasts of angular quartz and altered plagioclase are present. Clay minerals including smectite associated with a limonite occur in the sediment and fill the pore space and the internal part of the fossils. Calcite and silica are also present supporting the grains (Fig. 22 and Appendix B1).
A2 (189.98 – 188.1 m)	Siltstone	Calcareous siltstone	Light brown coloured, massive rock, weakly to moderately indurated, containing broken fossils and effervescent with HCl.	Consisting of angular monocrystalline quartz (40-55µm), plagioclase (45µm) and flake of muscovite (200 µm) with skeletal fragments supported by a matrix calcite (micrite) associated with smectite, zeolite, hematite and subrounded glauconite. The skeletal fragments include a 30mm thick plate of alga, foraminifera, and unbroken and broken ooids, pellets and plant debris (Appendix B1).
A3 (218.6 – 218.5 m)	Siltstone	Siltstone	Dark brown in colour, massive rock, weakly indurated, containing dark spot of organic matter, not effervescent with HCl.	Compositionally immature (poorly sorted) containing subrounded quartz (50µm) associated with plagioclase (55µm). These grains are embedded in a clayey matrix mainly smectite and some subrounded glauconite associated with calcite. The rock contains also volcanic fragments and calcitic veins (Appendix B1).
A4 (246.6 - 246.5 m)	Sandstone	Glauconitic sandstone	Dark brown to green coloured, weakly indurated and massive with organic matter.	Fine grained, poorly sorted compositionally immature, comprising subrounded green glauconite grains (50%) filling the spaces between grains. Calcitic to hematitic matrix. The grains include subangular quartz (120 µm), plagioclase (150 µm). The calcite cement occurs along the glauconite

				and clasts edges. (Fig.19 and Appendix 1).
A5 (311.3 - 311.2 m)	Sandstone	Arkose	Brown coloured, weakly to moderately indurated and parallel bedded rock. The sample does effervescence with HCl.	Poorly sorted and fine grained rock consisting of subangular monocrystalline quartz (100 µm and 60%), angular plagioclase (90 µm and 25%), with flakes of mica (200 µm and 1%) in the matrix of smectite forming a mixed matrix of chlorite, and rare illite associated with hematite (1 %). These mixed matrix partly replaced by glauconite grains (Appendix B1).
A6 (379.5 - 379.3 m)	Siltstone	Calcareous siltstone	Brown-grey coloured, massive texture and moderately indurated, slightly effervescence with HCl and containing bivalve (5cm) and black spots of organic matter.	Contains monocrystalline subangular quartz (56 µm, 15%), plagioclase (75 µm, 15%), chloritised biotite (2%) with large calcite grains (sparite) and skeletal fragments supported by calcite cement and calcite and clayey matrix. The clay minerals include smectite, limonite and glauconite, representing 15% of the rock. Hematite also occurs associated with clay minerals and displays a red staining visible macroscopically. The fossils consist of bivalve, foraminifera and ooids. There is also evidence of organic matter (Appendix B1)
A7 (426.7 - 426.4 m)	Siltstone	Calcareous siltstone	Dark – brown, massive texture, weakly indurated. Reaction with HCl and broken fossils.	Poorly sorted rock containing subangular quartz (45µm, 3%), altered plagioclase (50 µm, 15%), microcline (1%) and calcite grains within a clayey (37%) and micritic (15%) matrix. Clay minerals include smectite, glauconite and limonite. Skeletal fragments such as foraminifera, bivalve and ooids, and pellets also occur embedded in the matrix and are crudely broken (Appendix B1).
A8 (445.6 - 445.5 m)	Siltstone	Calcareous siltstone	Brown grey coloured, massive and weakly to moderately indurated. Effervescence with HCl (10%) with common plant remains and broken fossils.	Poorly sorted, containing angular quartz (53µm, 35%), plagioclase (40-70 µm, 15%), and flake of biotite (altered) in a micritic matrix (35%) associated with some clay minerals (15%) such as smectite, and chlorite, some glauconite. Hematite is also evident in the matrix and causing a red staining visible macroscopically. Bioclasts occur embedded in the matrix. They include foraminifera, and plant remains, broken bivalve filled by clay and ooids. Some calcite cement occurs between grains and at the edges of skeletal fragments (Appendix B1).
A9 (482.19 - 482.14 m)	Siltstone	Siltstone	Brown, moderately	Consists of subangular quartz (58 µm, 25%) and plagioclase (55 µm,

			indurated and massive texture, with black spot of organic matter.	18%) partly altered flakes of muscovite and fossils of foraminifera, and large calcified fossil stamp filled by quartz and calcite grains, ooids (Appendix B1).
A10 (536.5 - 536.4 m)	Siltstone	Calcareous siltstone	Brown grey coloured, weakly indurated, massive texture, effervescent with HCl. Bivalves (5cm), plant debris and broken fossils.	Poorly sorted, having calcite cement with clayey matrix (25%). The calcite cement shows a poikilotopic texture. The clayey matrix is composed of smectite with subrounded glauconite and hematite. Cements and matrix are supporting clasts of angular quartz (50 µm, 25%), idiomorphic plagioclase (50 µm, 15%), and flakes of muscovite (1%) (Appendix B2).
A11 (562.7 - 562.6 m)	Siltstone	Calcareous siltstone	Dark brown coloured, moderately indurated, massive rock. Plenty of black spots of organic matter.	Immature rock consisting of subangular monocrystalline quartz (45µm, 25%) and plagioclase (55µm, 17%), sparite grains (11µm, 30%), flakes of mica (120 µm) supported by calcite and clayey (28%) matrix. The smectite is the most abundant clay mineral in the rock; it is associated with other clays such as chlorite. Limonite and glauconite are common. The rock is rich in fossils: gastropods, foraminifera. (Appendix B2)
A12 (575.7 - 575.5 m)	Siltstone	Calcareous siltstone	Dark brown, moderately indurated, massive rock, effervescence with HCl and containing plant debris.	Poorly sorted rock containing clasts of subangular quartz (48 µm, 40%), plagioclase (50 µm, 13%), calcite grains (60 µm), and flakes of mica in a calcite cement showing poikilotopic texture with clayey matrix. The clay minerals include smectite, chlorite, glauconite (6%) and limonite. Glauconite tends to replace all clay minerals. Calcitic veinlets are common. Fossils such as ooids and plant debris are also present (Appendix B2).
A13 (613 - 612.8 m)	Siltstone	Glauconitic siltstone	Glauconitic siltstone, dark brown to green coloured, weakly indurated, massive rock. Does not effervescence with HCl.	Immature rock consisting of subrounded glauconite grains (33%) associated with smectite, chlorite and hematite as a matrix supporting subangular monocrystalline quartz (50 µm, 40%), plagioclase (53 µm, 15%), broken shells and plant remains. Calcite veins are present. (Appendix B2).
A14 (625.1 – 625 m)	Siltstone	Siltstone	Dark brown, moderately indurated, massive rock, containing black spots of organic matter and broken fossils.	Poorly sorted (immature rock) comprising angular grains of quartz (58 µm, 37%), plagioclase (52 µm, 23%), flakes of biotite (55 µm, 3%) in clayey matrix associated with calcite and hematite. The clay minerals contain smectite (23%), glauconite (8%) and chlorite (2%). Poikilotopic calcite and elongated calcified

				skeletal fragment are common (Appendix B2).
A15 (632.9 - 632.8 m)	Siltstone	Siltstone	Dark-brown, moderately indurated, massive rock with broken fossils.	Immature texture, containing angular quartz (40 µm, 36%), plagioclase (55 µm, 18%) and mica flakes (200 µm). Some plagioclase grains are altered. Organic matter from plant debris also occurs in the rock. The clasts are supported by clayey matrix made up with smectite, chlorite, and limonite associated with hematite (3%). The rock contains broken fossils including bivalves and the entire rock looks weathered (Appendix B2).
A16 (648.9 - 648.8 m)	Sandstone	Arkosic wacke	Brown coloured, medium to coarse grained, moderately to well indurated and porous.	Poorly to moderately sorted, consisting of subangular and subrounded monocrystalline and polycrystalline quartz and chert grains (600 µm). Some plagioclase grains (500 µm) which look shattered (volcanic?) or altered with angular shapes. Lithic and shell fragments associated with plant debris are also evident in the rock. The shells fragments are macroscopically visible. The grains are supported by clayey matrix dominated by smectite with some chlorite and associated with hematite. Calcite cement is also present and occurs as veinlets in the section (Appendix B2).
A17 (651.9 - 651.7 m)	Siltstone	Siltstone	Brown coloured, weakly indurated, and laminated rock (Fig. 28).	Compositionally immature rock consisting of subangular quartz (25 µm), plagioclase (40 µm) and flakes of muscovite supported by clay minerals, mainly smectite with chlorite. Macroscopic observation reveals bivalves (5-6 cm thick) and abundant black spots of organic matter. In thin section presence of gastropods and broken shells is evident. (Fig. 18 and Appendix B2).
A18 (685.5 - 685.4 m)	Sandstone	Arkosic wacke	Medium grained sandstone, brown coloured, moderately to well indurated, porous rock (Fig. 29).	Moderately sorted (submature rock) consisting of subangular monocrystalline quartz (450 µm) some shattered, plagioclase (350 µm) grains of volcanic tuffs (lithic fragments) and some calcite grains (sparite) supported by smectite and chlorite as a matrix (Fig. 29 and Appendix B2).
A19 (710.5 - 710.4 m)	Sandstone	Subarkose	Dark brown medium grained, moderately indurated and porous. The rock contains black	Immature rock containing angular quart (350 µm), plagioclase (300 µm), biotite, volcanic tuffs and euhedral zircon mineral supported by a matrix of with smectite mostly with some hematite. Organic matters also occur (Appendix B2).

			spots of organic matter.	
A20 (760.9 - 760.7 m)	Sandstone	Arkosic wacke	Fine grained, dark-brown coloured rock, moderately indurated, porous and organic matter.	Poorly sorted rock consisting of subangular monocrystalline quartz (180 µm), plagioclase (200 µm), flakes of mica (200 µm) filled by a matrix of clay minerals, smectite and chlorite associated with calcite and hematite. Organic matter and broken shells are present (Appendix B2).
A21 (788.2 - 788.1 m)	Sandstone	Calcareous sandstone	Brown grey medium to coarse grained, calcareous sandstone, porous with a lot of fossils visible macroscopically: bivalves (1-2cm), gastropods (1-2cm), elongated calcified algae.	The rock is moderately sorted (submature), containing angular monocrystalline quartz (600 µm), plagioclase (450 µm), microcline, flakes of mica, lithic fragments and sparite grains (700 µm) with large shell fragments, elongated calcified algae, bivalves, foraminifera, supported by calcite cement and clayey matrix (Appendix B3).
A22 (855.6 - 855.5 m)	Sandstone	Calcareous sandstone	Fine grained sandstone, brown coloured, moderately to well indurated and massive rock with no apparent sedimentary structures. Various fossils are visible macroscopically such as bivalves, and gastropods.	Poorly sorted (immature) containing subangular monocrystalline quartz (70 µm), plagioclase (95 µm), and flakes of biotite (150 µm), with large shell fragments, foraminifera, bivalves, supported by mixed clay and calcite matrix. Clay minerals comprise smectite, and chlorite with some hematite and glauconite (Appendix B3).
A23 (911.4 - 911.3 m)	Sandstone	Calcareous sandstone	Brown grey fine grained calcareous sandstone, moderately to well indurated and cross bedded rock with irregular lamination, rich in broken shells and 3cm bivalves. The sample reacts with 5% HCl. See Fig. 20).	Immature textured (poorly sorted), calcareous sandstone rich in calcite cement showing poikilotopic texture and calcite matrix supporting clast grains such as monocrystalline angular quartz (130 µm) Fig. 30C and D, plagioclase (180 µm), flakes of mica with skeletal broken shells including gastropods and intact foraminifera. Clay minerals and hematite also are included in the matrix; they comprise smectite, chlorite and glauconite (150 µm). See Fig. 20 and Appendix B3).
A24 (965.9 - 965.8 m)	Sandstone	Arkosic wacke	Fine grained sandstone, dark-brown coloured, weakly to moderately indurated, with visible unbroken and broken fossils of gastropods	Immature rock (poorly sorted) containing subangular monocrystalline quartz (90 µm), plagioclase (100 µm), flake of biotite (130 µm) some of them chloritized. The grains are supported by clayey matrix dominated by smectite (7%), followed by glauconite, chlorite associated with calcite and hematite.

			(5cm), and bivalves.	Very long algae fragments, foraminifera, gastropods, bivalves and plant debris also occur in the section (Appendix B3).
A25 (1035.5 - 1035.4 m)	Limestone	Bioclastic limestone (Packstone)	Moderately to well indurated, showing 2 beds of different colours. The grey layer rich carbonate matter and reacts stronger with HCl than the brown layer. The entire sample is rich in broken shells some of which reach 5cm size.	Packstone rich in algae (elongated fragments) associated with other skeletons including bivalve shells by quartz and calcite grains, foraminifera, other large shell fragment and unbroken bivalve. The large shell is surrounded by calcite cement (poikilotopic) and matrix generations, rich in carbonate matter, fine grained clay minerals and some coarser material and coarse grained matrix. The section also contains clast grains of about 50 µm size including subangular quartz, angular and altered plagioclase and clay minerals associated with hematite in the matrix (Appendix B3).
A26 (1076.9 - 1076.8 m)	Siltstone	Siltstone	Dark brown coloured moderately indurated with shell fragments.	Composed of subangular monocrystalline quartz (53 µm), plagioclase (50 µm), flakes of altered muscovite (60 µm) supported by clayey matrix of smectite and chlorite. Calcite grains look altered. Bivalves, foraminifera, broken shell and plant debris with black organic matter are also present in the rock (Appendix B3).
A27 (1129.9 - 1129.8 m)	Siltstone	Siltstone	Brown coloured siltstone, moderately indurated, and massive.	Compositionally immature, consisting of subangular monocrystalline quartz (51 µm), plagioclase (53 µm) with some fossils such as elongated plant and algae fragments, calcified broken shells, foraminifera, bivalves and ooids, supported by clayey matrix mainly smectite with hematite (Appendix B3).
A28 (1171.1 - 1170.1 m)	Siltstone	Siltstone	Dark brown siltstone, moderately indurated with no sedimentary structures, visible black organic matter, broken fossils and bivalve shells of about 6cm size. The rock reacts with HCl.	Containing angular monocrystalline quartz (50 µm), altered plagioclase (52 µm), microcline, flakes of mica (muscovite) with ooids and foraminifera embedded in clayey matrix associated with hematite. The clay content is led by smectite followed by glauconite and chlorite (Appendix B3).
A29 (1194.2 - 1194.1 m)	Siltstone	Siltstone	Dark brown, moderately indurated, massive rock with plant debris and	Containing subangular quartz (46 µm), subangular plagioclase (60 µm), and flakes of biotite embedded by clayey matrix with hematite. The matrix is dominated by smectite.

			organic matter with weak effervescence to HCl.	Foraminifera, broken shells and plant debris are common (Appendix B3).
A30 (1242.1 – 1242 m)	Siltstone	Siltstone	Dark-brown and moderately indurated, not porous and fossils are not visible macroscopically.	Constituted of angular quartz (45 µm), plagioclase (50 µm), flakes of mica with some foraminifera in a clayey matrix (smectite and chlorite,) associated with hematite and calcite (Appendix B3).
A31 (1294.2 - 1294.1 m)	Siltstone	Siltstone	Dark brown coloured, moderately indurated and massive rock containing 5mm sized of clasts of quartz grains, black thin strings of organic matter and bivalve (5cm).	Consisting of subangular monocrystalline quartz (45 µm), plagioclase (48 µm), and flakes of mica with few skeletal fragments, supported by clayey matrix rich in smectite and associated with hematite (Appendix B4).
A32 (1324.1 – 1324 m)	Siltstone	Glauconitic siltstone	Dark green siltstone, weakly to moderately indurated showing a lot of cracks.	Glauconitic siltstone composed mostly of subrounded glauconite grains as part of the matrix with chlorite and smectite supporting subangular monocrystalline quartz and detrital plagioclase (Appendix B4).
A33 (1369.2 – 1369 m)	Siltstone	Siltstone	Brownish coloured weakly to moderately indurated, massive rock containing fossils such as gastropods (2-3cm), bivalves (2cm) and colonies of small fossils.	Consisting of silt-size subangular quartz (50 µm) and plagioclase (55 µm) grains with a few shell fragments in the matrix of clayey minerals (smectite and chlorite) and calcite filling cracks (Appendix B4).
A34 (1415.8 - 1415.6 m)	Siltstone	Siltstone	Grey coloured, well indurated with small black organic matter and react with 5% HCl.	Containing large calcite cement with poikilotopic texture, surrounding silt-sized subangular monocrystalline quartz, plagioclase, foraminifera and broken shells, subrounded glauconite supported by calcite cement associated with clay minerals and hematite matrix (Appendix B4).
A35 (1445.4 - 1445.2 m)	Siltstone	Siltstone	Greyish brown siltstone, weakly to moderately indurated with fissures containing black organic material, few bivalves, and clast of quartz (2mm).	Consisting of subangular monocrystalline quartz (50 µm), angular and altered plagioclases (55 µm), and flakes of mica with broken shells and organic black matter supported by clayey matrix led by smectite, chlorite, associated with hematite (Appendix B4).

A36 (1484.4 - 1484.3 m)	Siltstone	Siltstone	Grey brown coloured, weakly to moderately indurated rock, with some fossils. The rock effervesces with HCl.	Calcareous siltstone containing monocrystalline subangular quartz (45 µm), angular and altered plagioclases (50 µm), mica flakes, and rare zircon grains. Planktonic foraminifera, sponges, ooids, calcified broken shells and plant debris are supported by a matrix of calcite and clay minerals such as smectite and chlorite, associated with hematite (Appendix B4).
A37 (1507.9 - 1507.8 m)	Siltstone	Siltstone	Dark-brown siltstone, moderately indurated with black spots of organic matter, does not effervescence with HCl.	Consisting of monocrystalline subangular quartz (55 µm), angular and cracked plagioclases (60 µm), and mica flakes in clayey matrix dominated by smectite with small amount of chlorite associated with hematite and some organic matter (Appendix B4).
A38 (1529.5 1529.4 m)	Siltstone	Glauconitic siltstone	Dark green coloured siltstone, moderately to well indurated and of massive texture, with organic matter. The rock does not effervescence with HCl.	Glauconitic siltstone consisting of monocrystalline quartz (45 µm), detrital and shattered plagioclases (50 µm) and flakes of mica with some broken shells embedded in a glauconitic matrix with some smectite, limonite and chlorite (Appendix B4).
A39 (1592.7 - 1592.6 m)	Siltstone	Calcareous siltstone	Dark-grey carbonate rock, well indurated, massive texture and strongly effervescence in contact with 5% of HCl. The rock contains abundant iron mineral, black spots of organic matter occur along the iron mineral.	Calcareous siltstone with calcite matrix, hematite and some clay minerals including smectite and chlorite which support clast grains such as subangular quartz (40 µm), plagioclase (50 µm), flakes of micas (60 µm), calcite grains and abundant broken shells (Appendix B4).
A40 1597.5 - 1597.4 m)	Siltstone	Calcareous siltstone	Dark grey carbonate rock, well indurated, massive texture, strongly effervescence in contact with 5% of HCl with calcite minerals (Fig. 17).	Calcareous siltstone containing plagioclase (25 µm), quartz (30 µm) and light green to brown glauconite, indicating the presence of limonite. Plant debris, large calcite grains (sparite), foraminifera and algae fossils are also present. The grains are embedded in a calcite matrix. (Fig. 17, Appendix B4).

APPENDIX B: PETROGRAPHIC Photographs AND MICROGRAPHS OF ZA SAMPLES

APPENDIX B1: SAMPLES A1 – A10

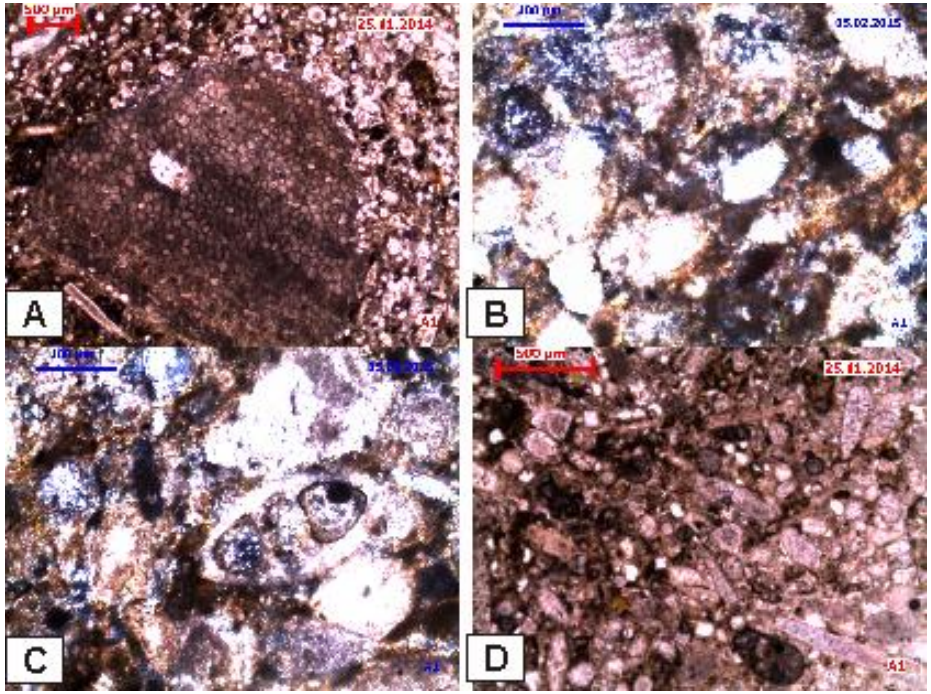

Sample A1 Bioclastic limestone. A: Bioclasts of algae showing polygonal shape. B: Silt-sized plagioclase grain surrounded by calcified algae fragments with specules. C. Well preserved foraminifera. D. Abundant elongated algae fragments.

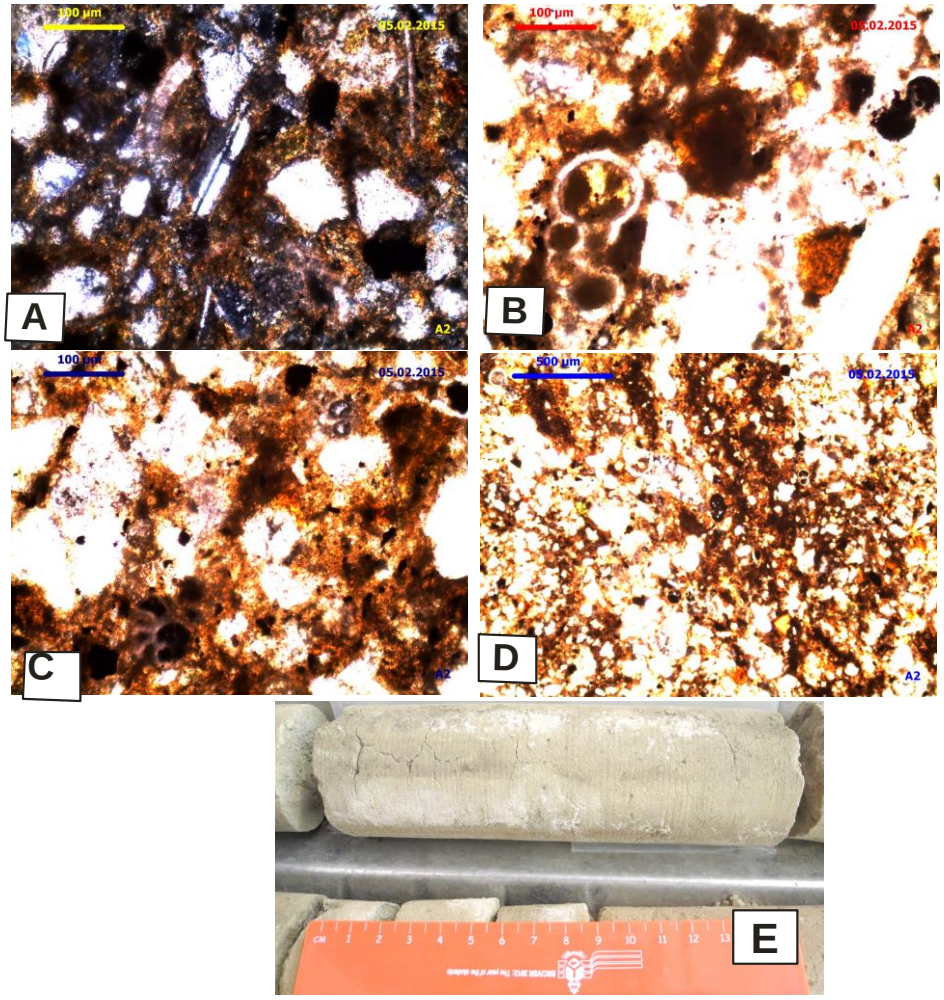

Sample A2. Calcareous siltstone. A and D plagioclase and quartz grains in the calcite and clay matrix. B. Multichambered foraminifera and calcified shells. C. Foraminifera fossil in clay and calcite matrix. E. Light brown to grey massive siltstone with shell fragments.

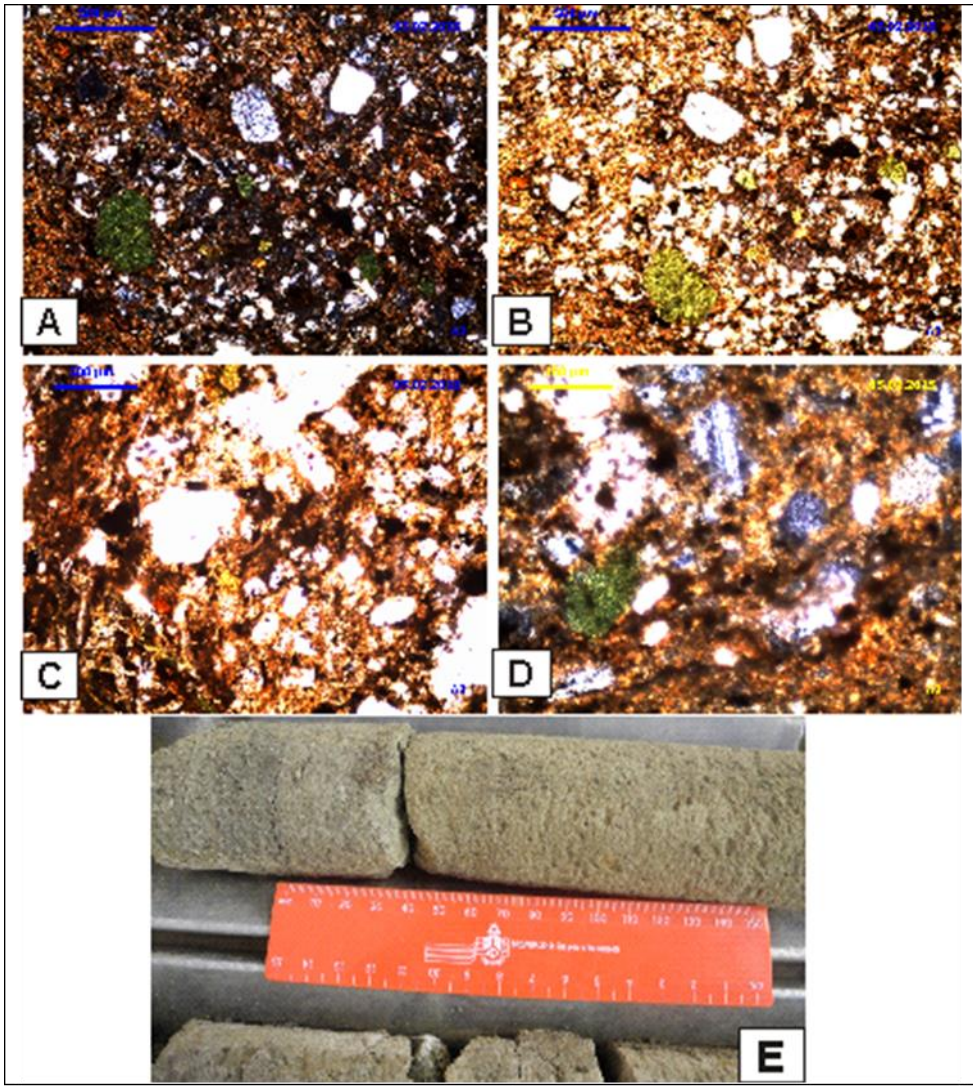

Sample A3. Siltstone. A (XPL) and B (PPL) Photomicrograph shows clast of quartz and plagioclase in clayey matrix associated with glauconite. C (PPL) Lithic fragments and quartz clasts supported in a clayey matrix. D (XPL) Plagioclase grains in the clayey matrix. E: Picture showing a dark brown finely bedded siltstone.

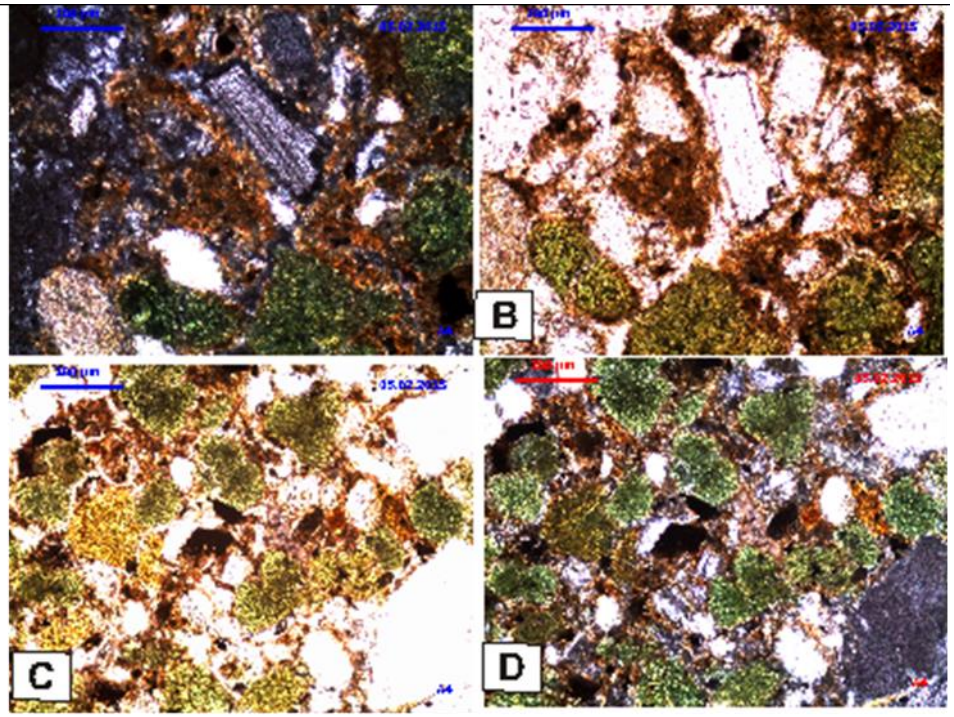

Sample A4. Glauconitic sandstone. A (XPL) and B (PPL) Microphotograph showing euhedral plagioclase grains surrounded by subrounded glauconite grains. C(PPL) and D(XPL): quartz and plagioclase grains associated with green subrounded glauconite grains.

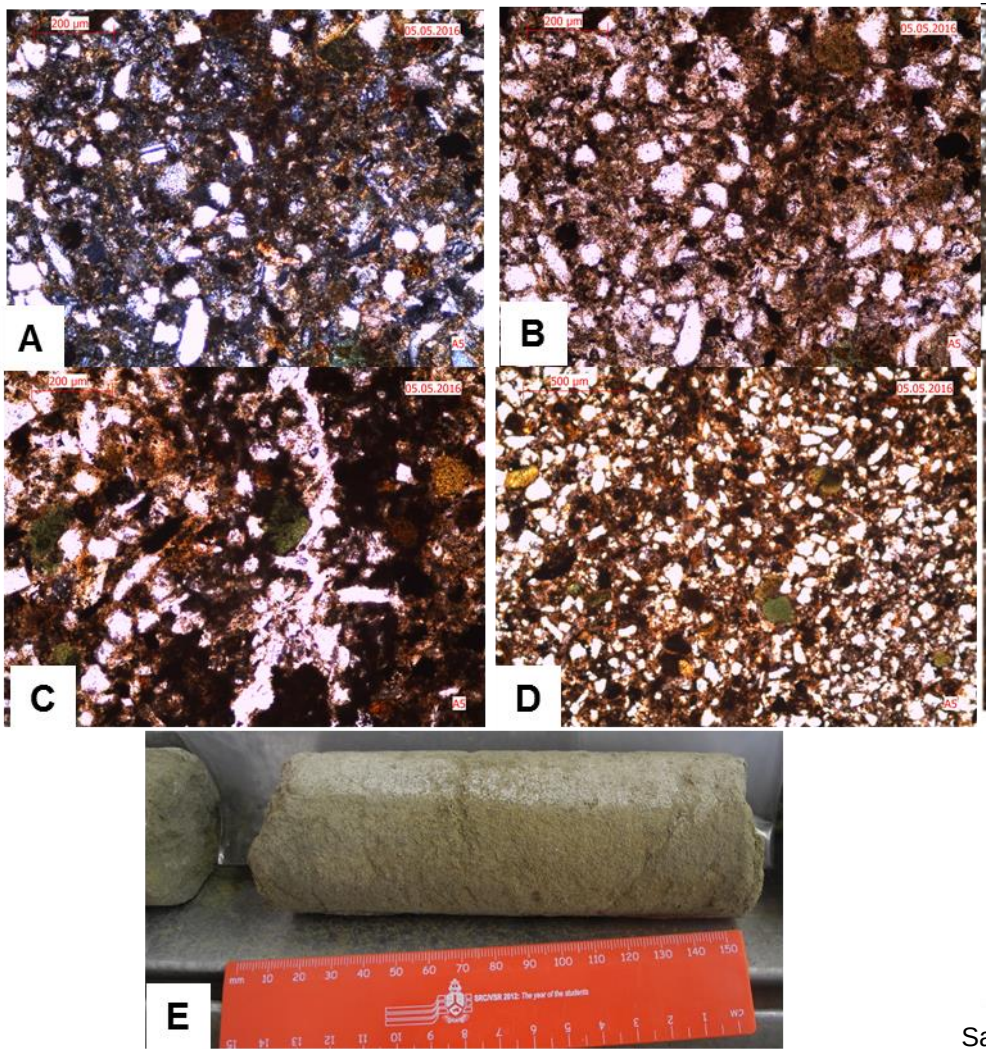

Sample A5. Sandstone: A (PPL) and B (XPL) Microphotograph showing sand-sized angular quartz and plagioclase grains supported by clayey matrix and some glauconite grains. C (PPL): Silica gel filling the crack in the sandstone. D (XPL): plagioclase, quartz and subrounded glauconite in a clayey matrix. E. Picture of a brown and grey coloured fine grained, indistinctly crossbedded sandstone.

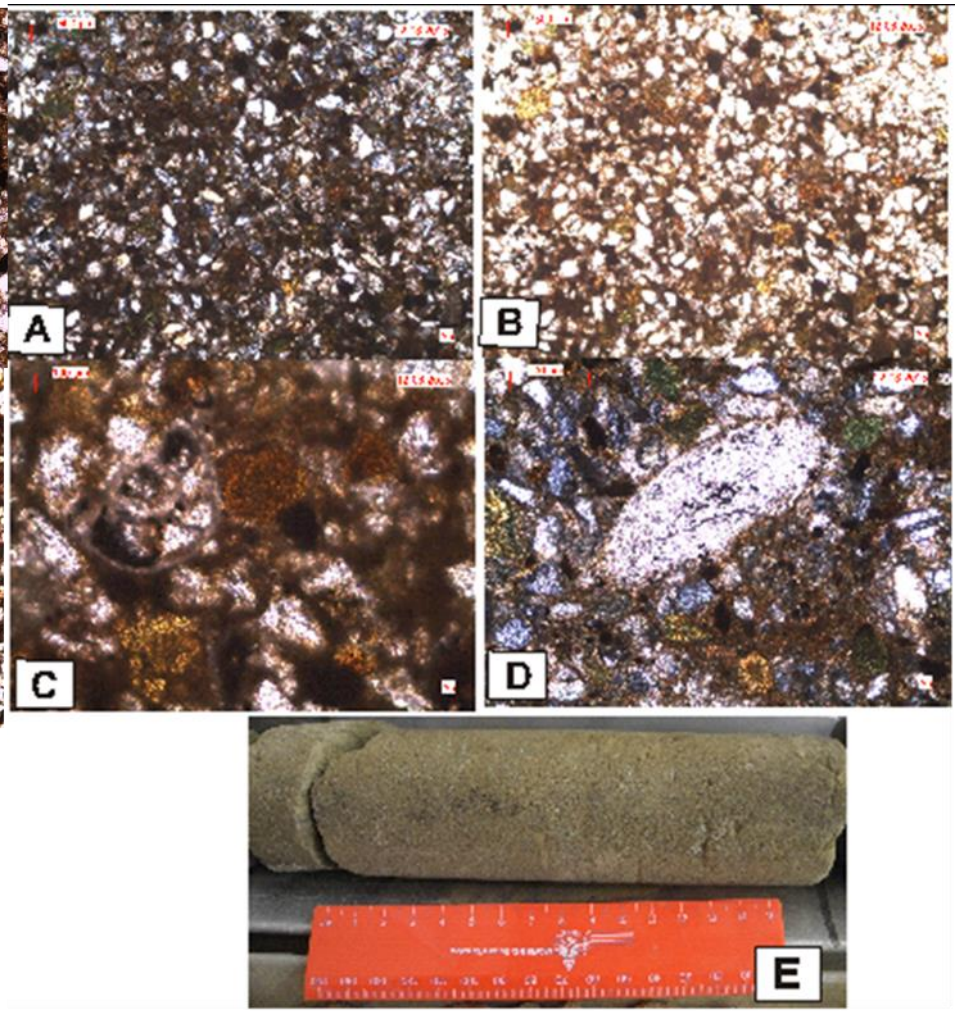

Sample A6. Calcareous silty sandstone A (XPL) and B (PPL) Microphotograph showing silt-sized subangular quartz and plagioclase clasts supported by calcite cement. C (PPL): broken foraminifera, glauconite and calcite grains occurring in the calcareous siltstone. D (XPL): Calcified algae, black organic matter, plagioclase grains. E. Picture showing a brown-grey laminated, lenticular siltstone.

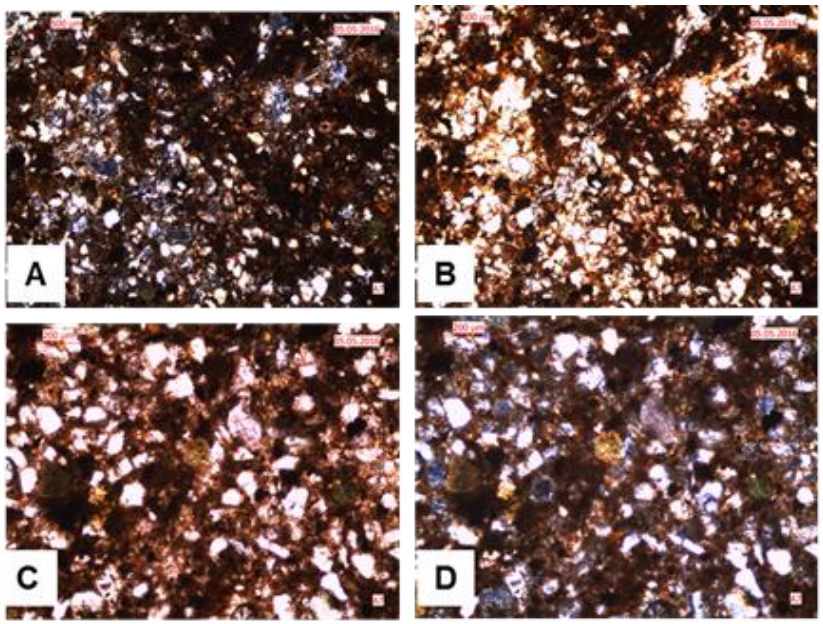

Sample A7. Siltstone. A (XPL), B (PPL), C (PPL) and D (XPL): Microphotograph showing quartz, plagioclase and calcite grains in calcite and clay matrix. E. Picture showing a weakly indurated brownish siltstone.

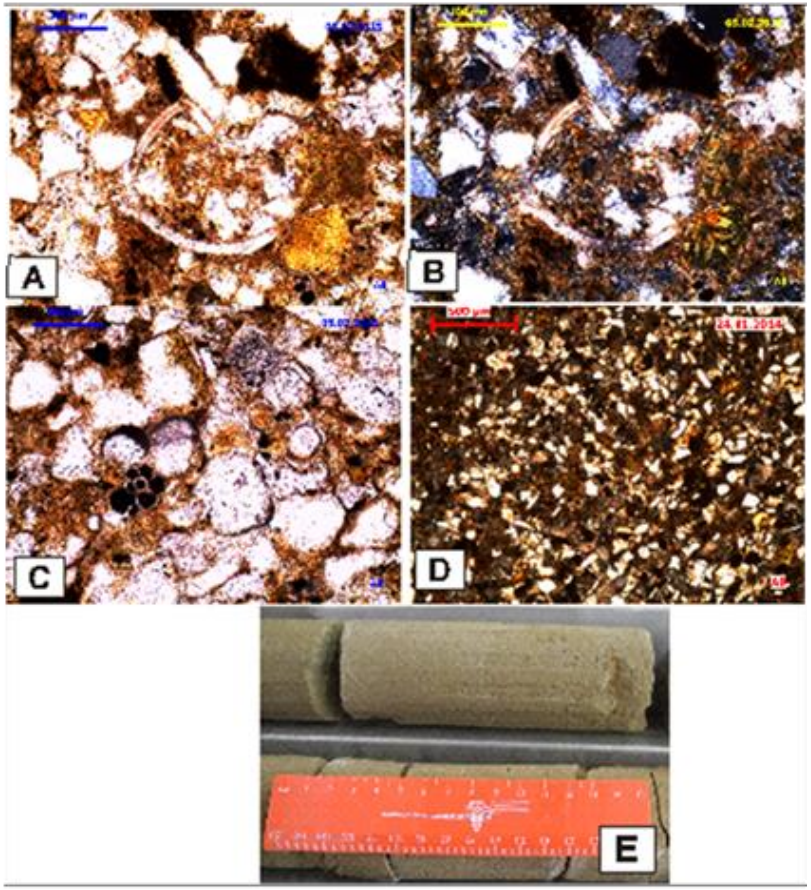

Sample A8. Calcareous siltstone: A (PPL) and B (XPL): Microphotograph showing almost intact bivalve shell filled by quartz and clay detritus. C. Calcareous siltstone containing calcite, quartz grains with a w well preserved foraminifera (globigerina), and some clay minerals coating the grains. D. Microphotograph showing silt-sized grains of quartz, plagioclase and calcite supported by a brownish clayey matrix. E. Brown coloured moderately indurated siltstone displaying no sedimentary structures.

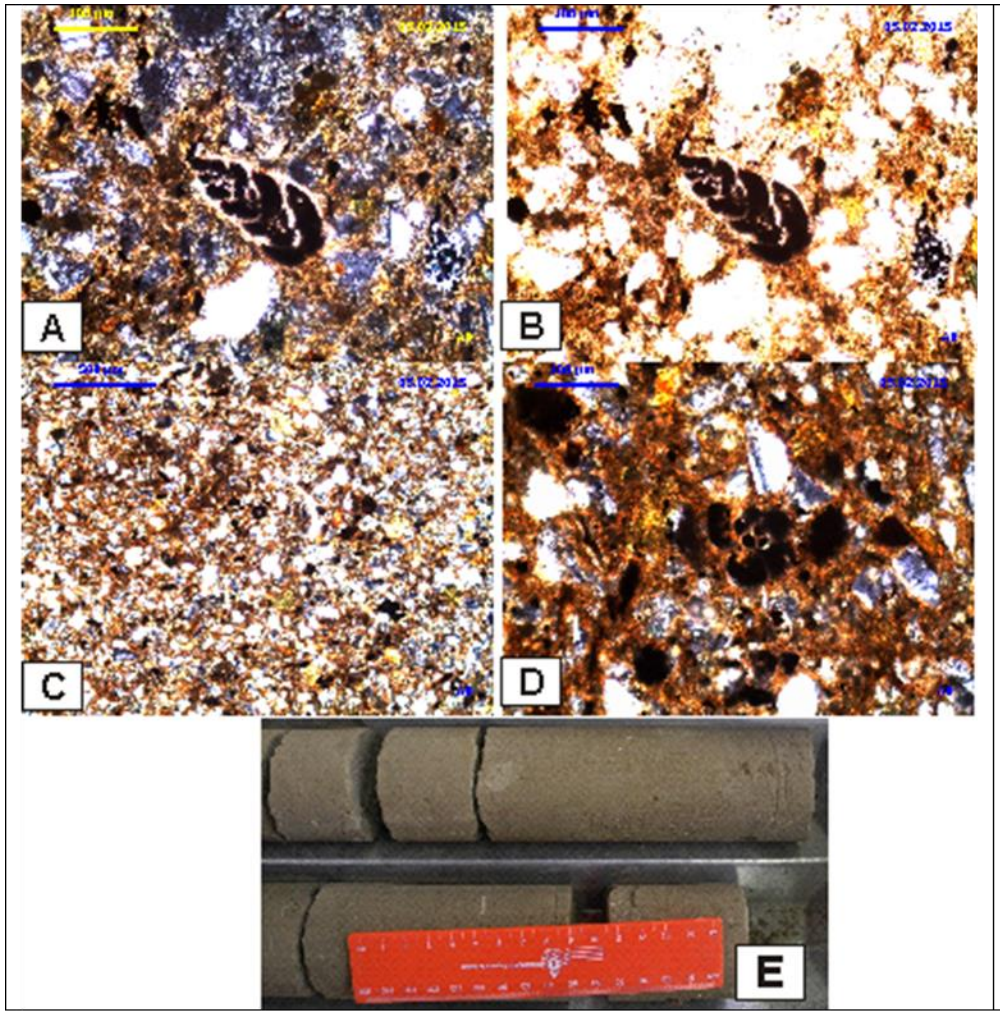

Sample A9. Siltstone: A (XPL) and B (PPL): Microphotograph showing clast of quartz, plagioclase with foraminifera fossils in calcite and clay matrix. C. Silt sized grain of quartz and plagioclase, and calcite grains in calcite and clay matrix. D. Microphotograph picture showing plagioclase, quartz grains and foraminifera supporting by a yellow brown clayey matrix associated with calcite. E. Picture showing a moderately indurated brownish siltstone sediment

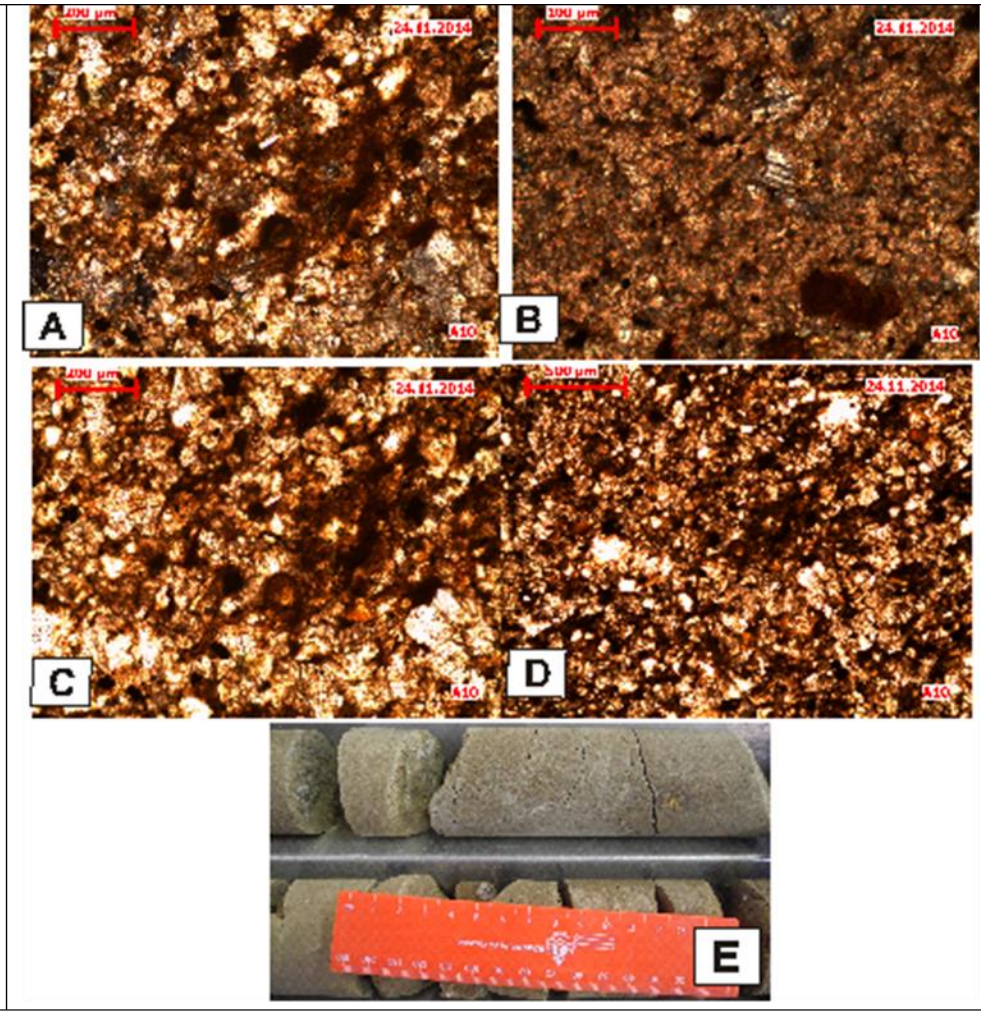

Sample A10. Calcareous siltstone: A (PPL), B (XPL) and C (PPL): Microphotograph showing calcite grain and cement, and some clay minerals in the matrix. D. Microphotograph showing weathering of the calcite grains and filling of clay minerals in the calcite cement. E. Picture showing a moderately indurated brown grey siltstone with irregular lenticular structures, mottled and probably bioturbated.

APPENDIX B2: SAMPLES A11 – A20

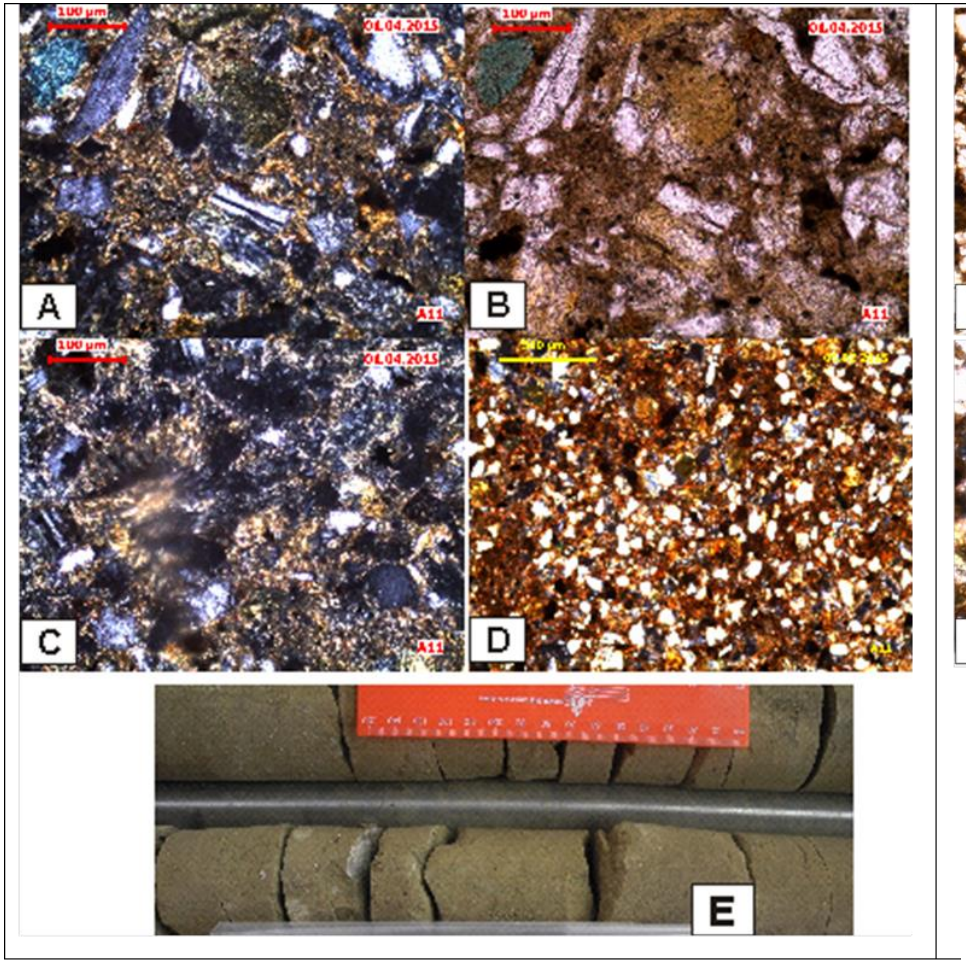

Sample A11. Calcareous siltstone: A (XPL), B (PPL) and C (XPL) Microphotographs showing clast of plagioclase and quartz in calcite and clayey matrix. D (PPL) Silt of quartz and plagioclase clasts supported by yellow brown clay associated with calcite. E: Picture showing a dark brown finely bedded siltstone with large calcareous fossil fragments and streaks and spots rich in organic matter.

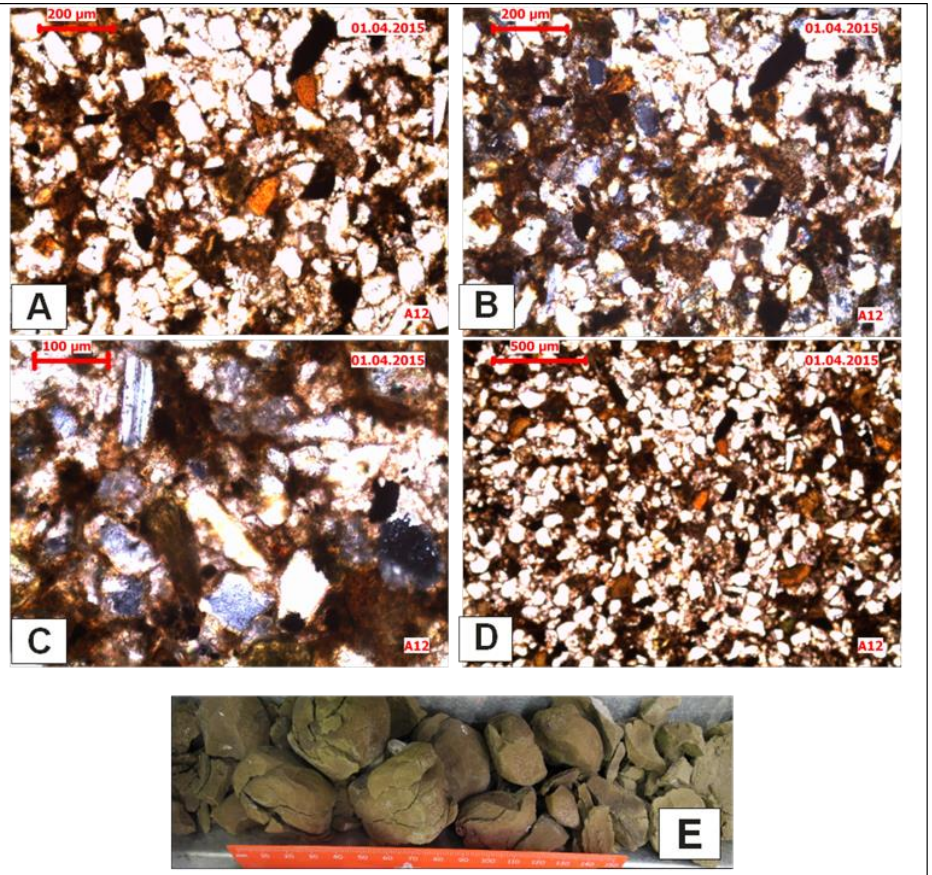

Sample A12. Calcareous siltstone (Microphotographs and picture). A (PPL) and B (XPL) Grains of quartz, plagioclase and calcite in calcite cement. Coating of what by brown clay minerals associated with hematite occurs and clayey matrix. C (XPL) plagioclase and quartz grains coated at the edge by clay minerals. D (PPL). Microphotograph showing silt-sized clasts of quartz and plagioclase with some calcite grains. E: Picture showing dark brown and weathered mottled, lenticular siltstone

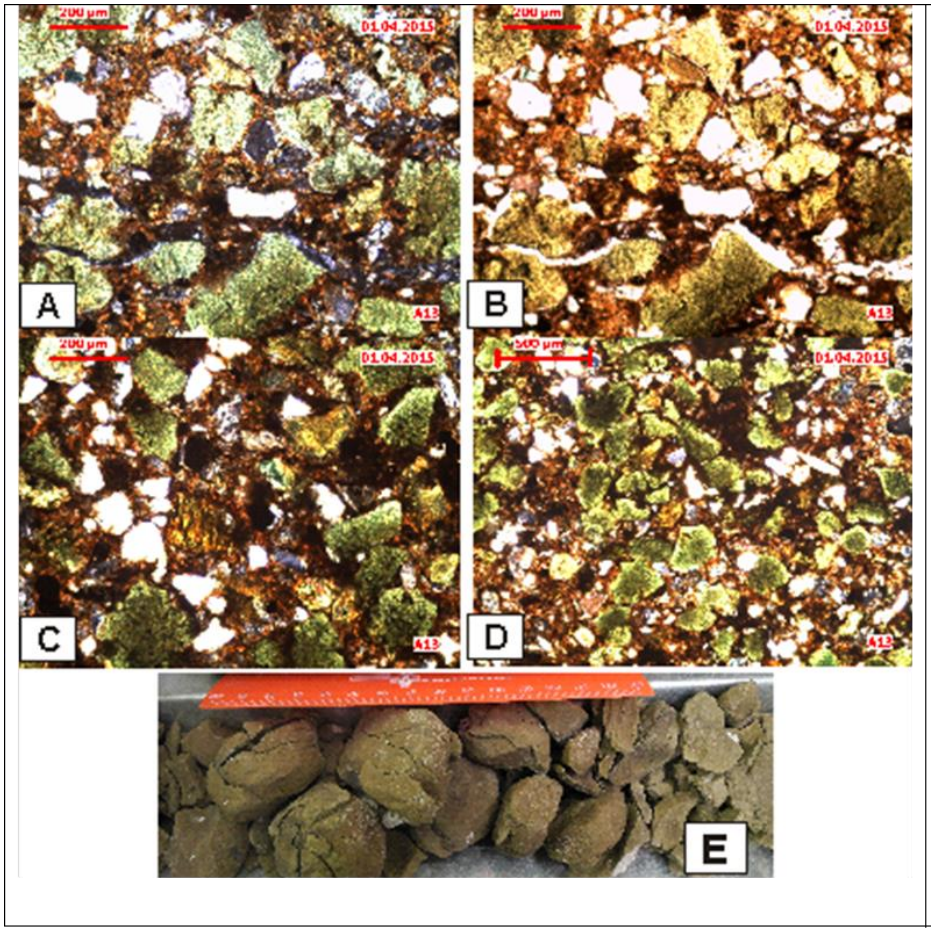

Sample A13. Glauconitic siltstone: A (XPL) and B (PPL) Microphotographs showing subrounded glauconite, clast of quartz and plagioclase, with cracks filled by calcite cement. C (XPL) angular plagioclase and quartz in glauconitic matrix. D (PPL) an overall of silt sized clast of quartz and plagioclase supported by glauconite associated with clays as a matrix. E. Weakly indurated greenish brown bioturbated siltstone with white spots of shell fragments.

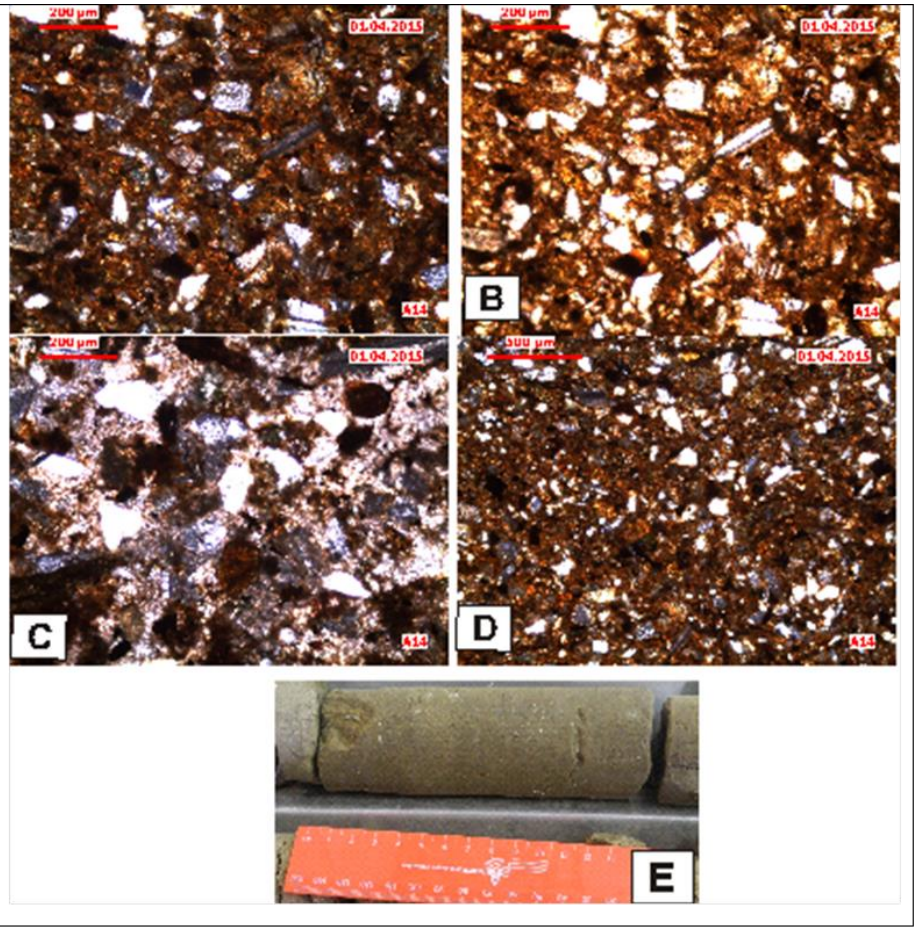

Sample A14. Siltstone: A (XPL) and B (PPL) Microphotographs showing angular shape of quartz, plagioclase grains and mica flakes supported by clay matrix. C (XPL) Calcite cement supported clast of plagioclase and quartz. D (XPL) Silt-sized clast in the matrix. E. Moderately indurated, dark brown indistinctly bedded siltstone containing white spots of shell fragments.

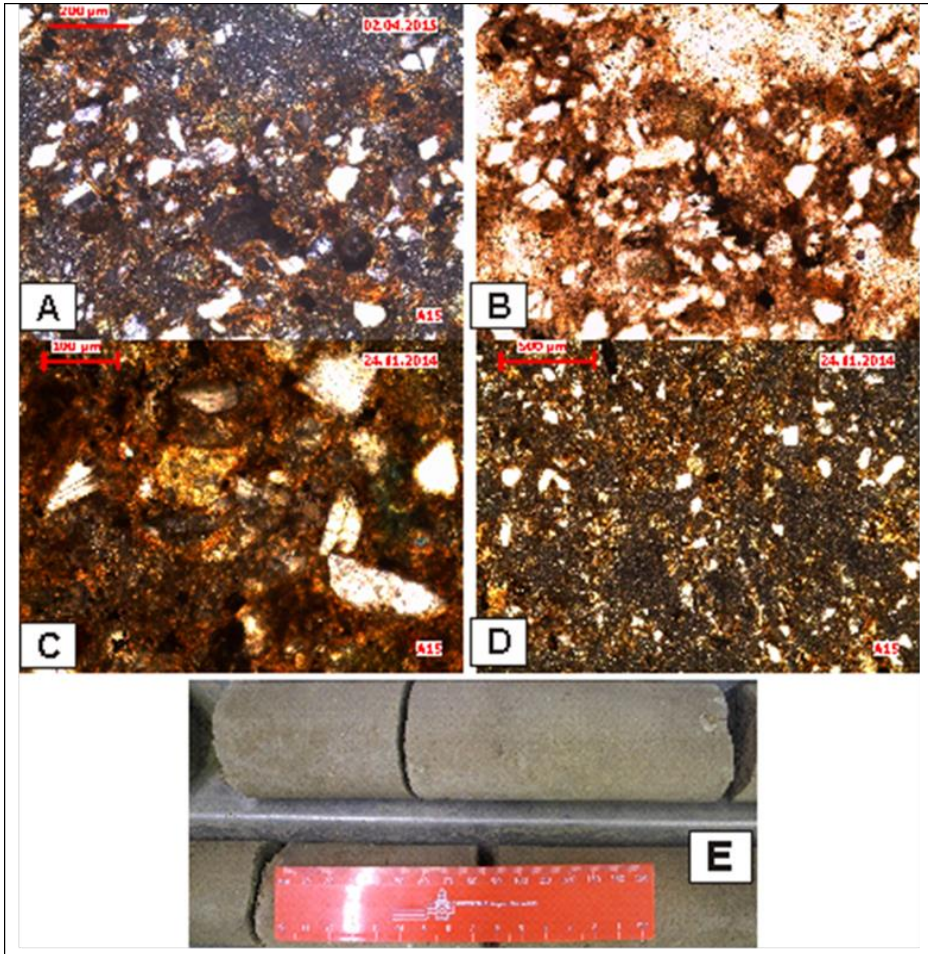

Sample A15. Siltstone: A (XPL) and B (PPL) Microphotographs showing angular quartz and plagioclase in a clayey matrix associated with hematite. C brown clay matrix supporting plagioclase grains. D (XPL) Grains are mainly silt-sized quartz and plagioclase, supported by clayey matrix. E. Dark brown, moderately indurated siltstone lacking clear sedimentary structures.

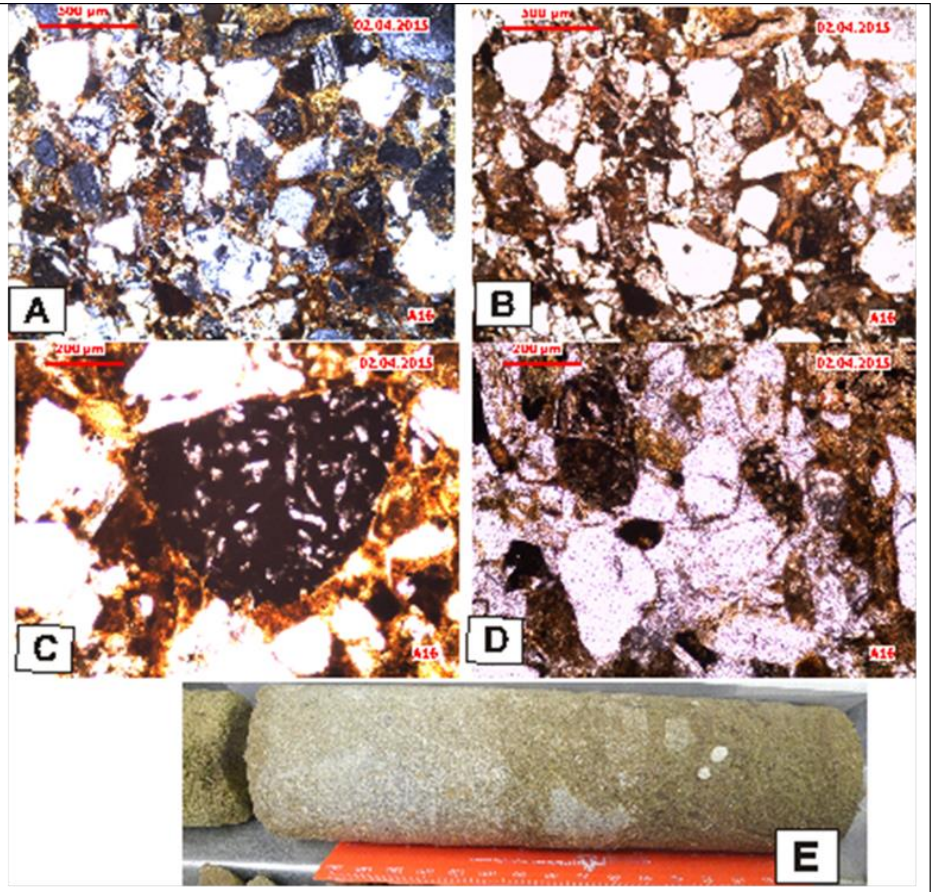

Sample A16. Arkosic wacke: A (XPL) and B (PPL) Microphotographs showing angular quartz and plagioclase grains supported by clayey matrix. C. Large lithic fragment of glassy lava, and smaller plagioclase and quartz grains supported by matrix of clay minerals. D (PPL) Quartz, plagioclase and lithic fragments supported by clay minerals as matrix. E. Brown grey coloured sandstone rich in calcite grains (white in colour) from shell fragments. Irregular bedding and bioturbation are evident from colour variation.

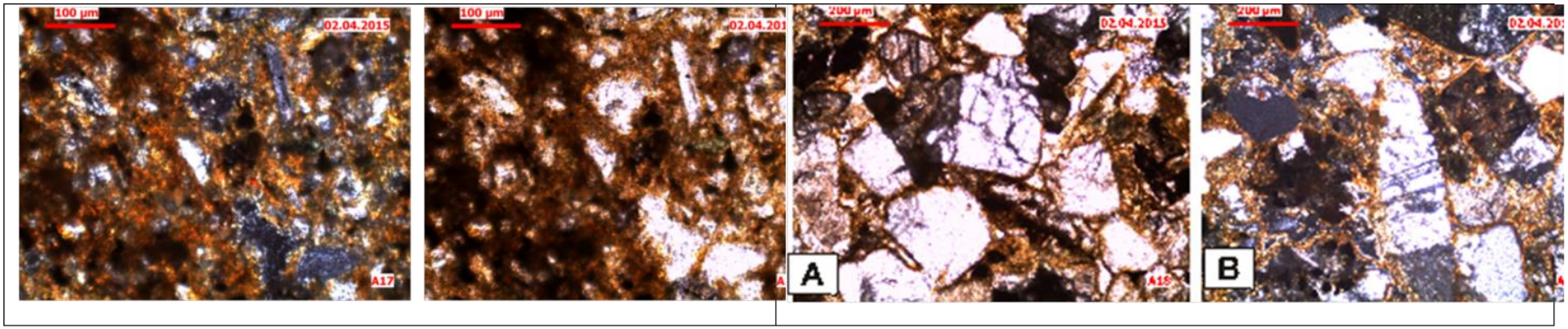

Sample A17. Siltstone: A (XPL) and B (PPL) Microphotographs showing plagioclase, quartz and mica flakes supported by clayey matrix associated with hematite.

Sample A18. Arkosic wacke: A: Microphotograph showing shattered plagioclase grains with coating of clay minerals under crossed polarised light. B. large plagioclase grain and clay minerals in the matrix, under plane polarised light.

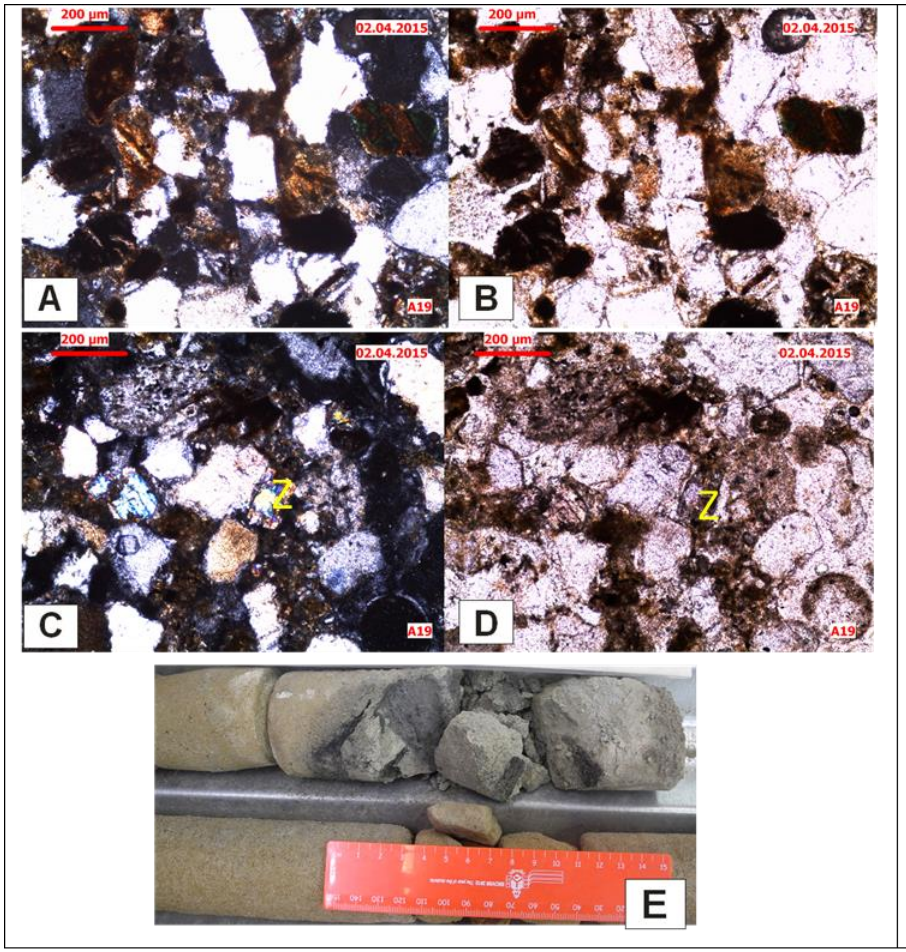

Sample A19. Subarkose: A, B, C and D: Microphotographs. A (XPL) and B (PPL): Detrital angular quartz, plagioclase, and pyroxene grains with lithic fragment. C (XPL) and D (PPL): euhedral zircon (Z), subangular quartz, altered plagioclase and pyroxene grains. E. Dark brown weakly to moderately indurated sandstone with lenses enriched in organic matter (dark grey) and whitish bioturbated spots.

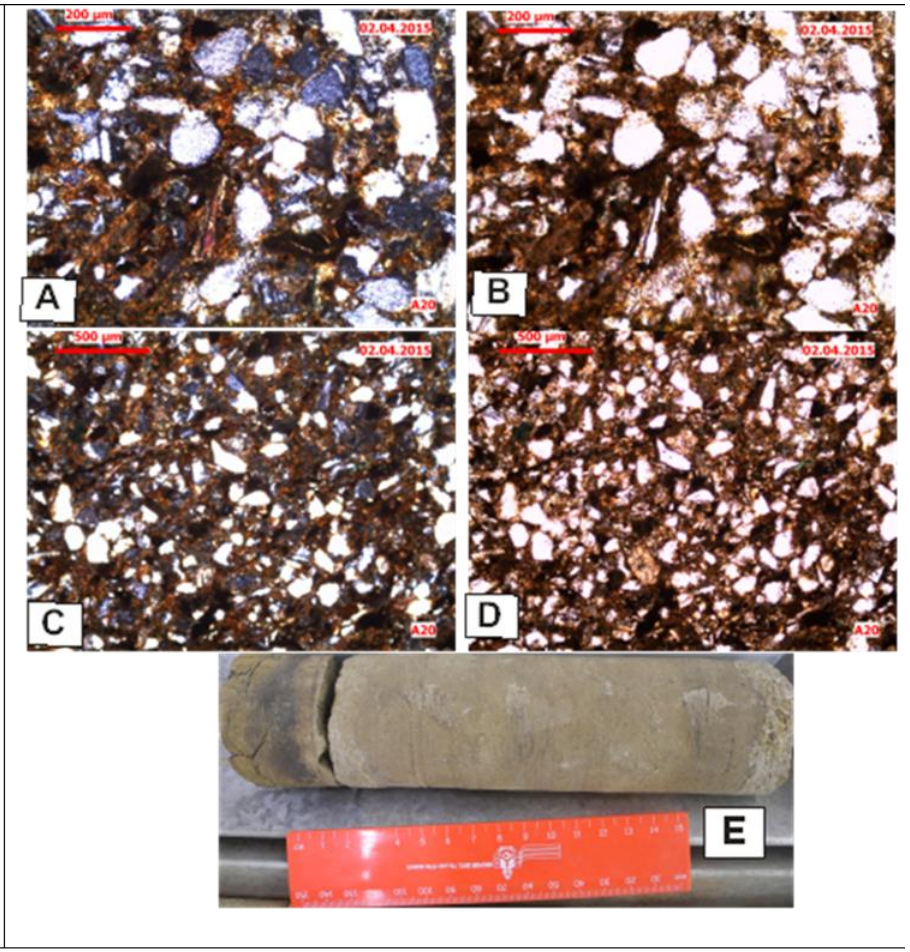

Sample A20. Arkosic wacke: A, B, C and: Microphotographs. A (XPL) and B (PPL): angular plagioclase and quartz grains in clayey matrix. C (XPL) and D (PPL): an overall of sand-sized clasts (plagioclase, quartz and mica flakes) supported by clay minerals as a matrix. E. Arkosic wacke laminae and streaks rich in organic matter and calcareous intercalations.

APPENDIX B3: SAMPLES A21 – A30

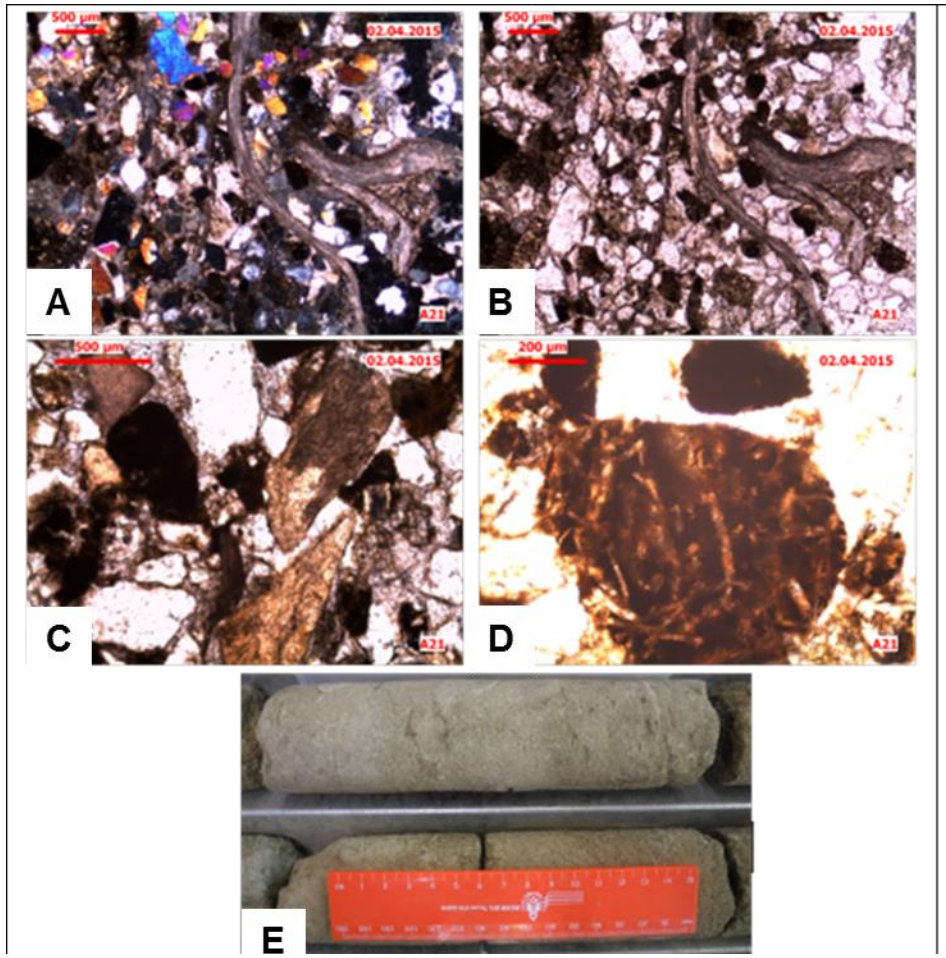

Sample A21. Calcareous sandstone: A, B, C and D: Microphotographs. A (XPL) and B (PPL): quartz, plagioclase and calcite grains associated with elongated shells. C: large calcified fossils surrounded by plagioclase and quartz grains in calcite cement under PPL. D: Lithic fragment (devitrified volcanic glass, well rounded) in calcareous sandstone under PPL. E. Brown grey weakly to moderately indurated, bioturbated calcareous sandstone with indistinct bedding and irregular wavy streaks of organic matter.

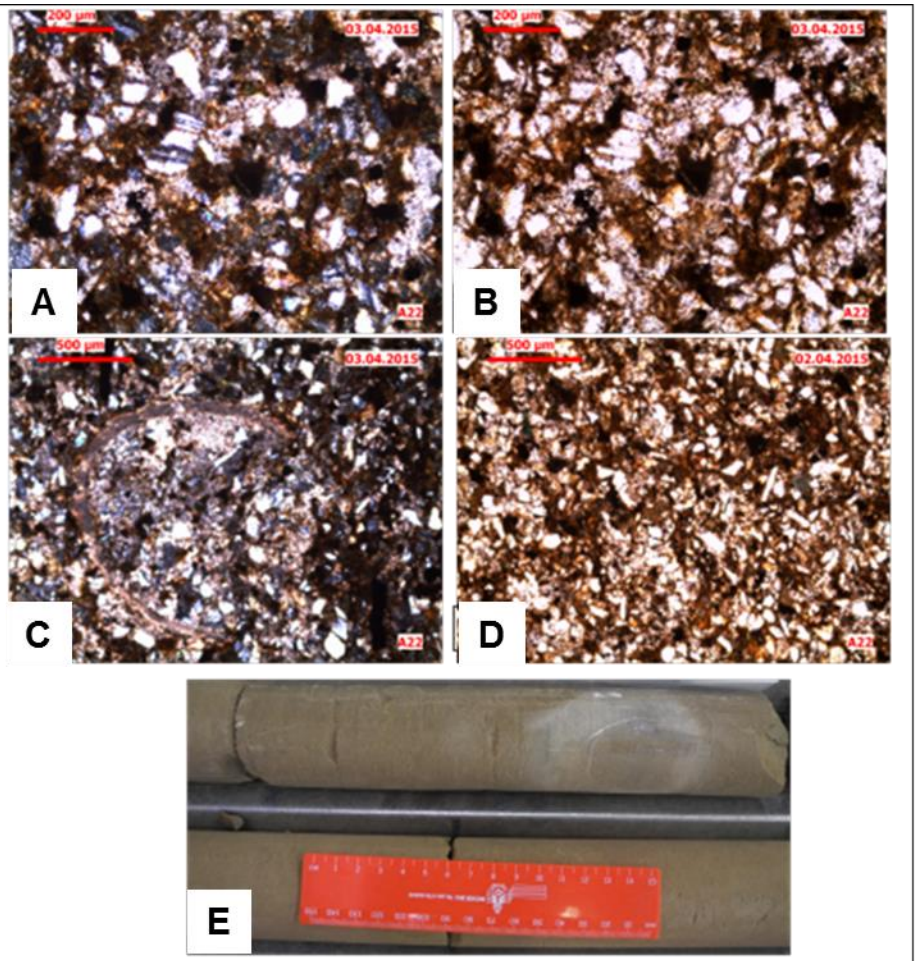

Sample A22. Calcareous sandstone: A, B, C and D: Microphotographs. A (XPL) and B (PPL): Angular plagioclase, quartz grains in clayey and calcite matrix. C (XPL): Bivalve filled by grains and calcite cement. D (PPL) Sand clasts (plagioclase and quartz) with calcite grains in a clayey and calcite matrix. E: Brown coloured moderately indurated and indistinctly bedded and laminated sandstone.

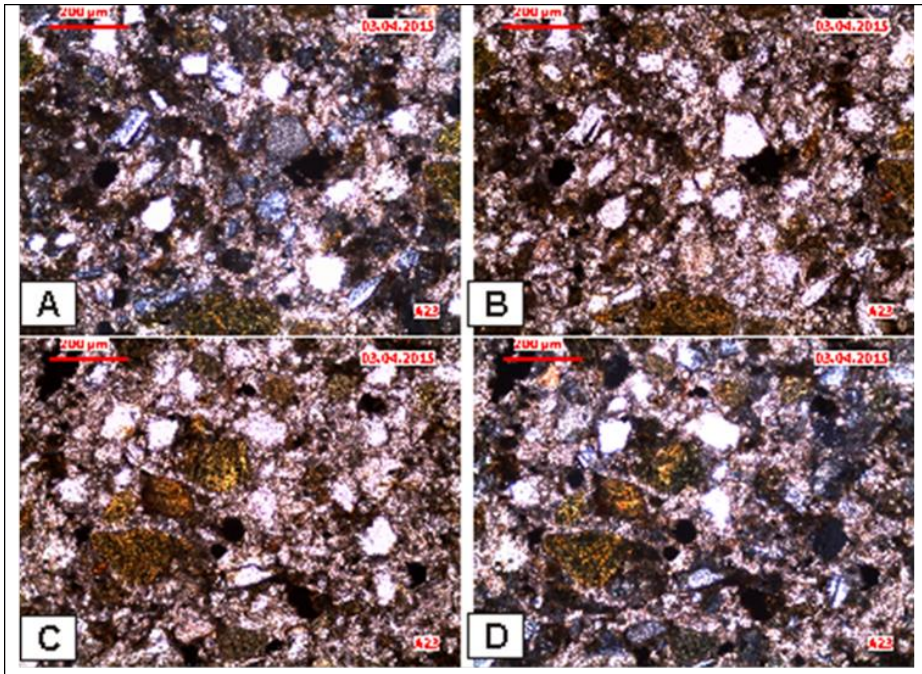

Sample A23. Calcareous sandstone: A, B, C and D: Microphotographs. A (XPL) and B(PPL): angular quartz and plagioclase grains in calcite matrix. C (PPL) and D (XPL): Clay minerals with hematite and glauconite in clayey and calcite matrix.

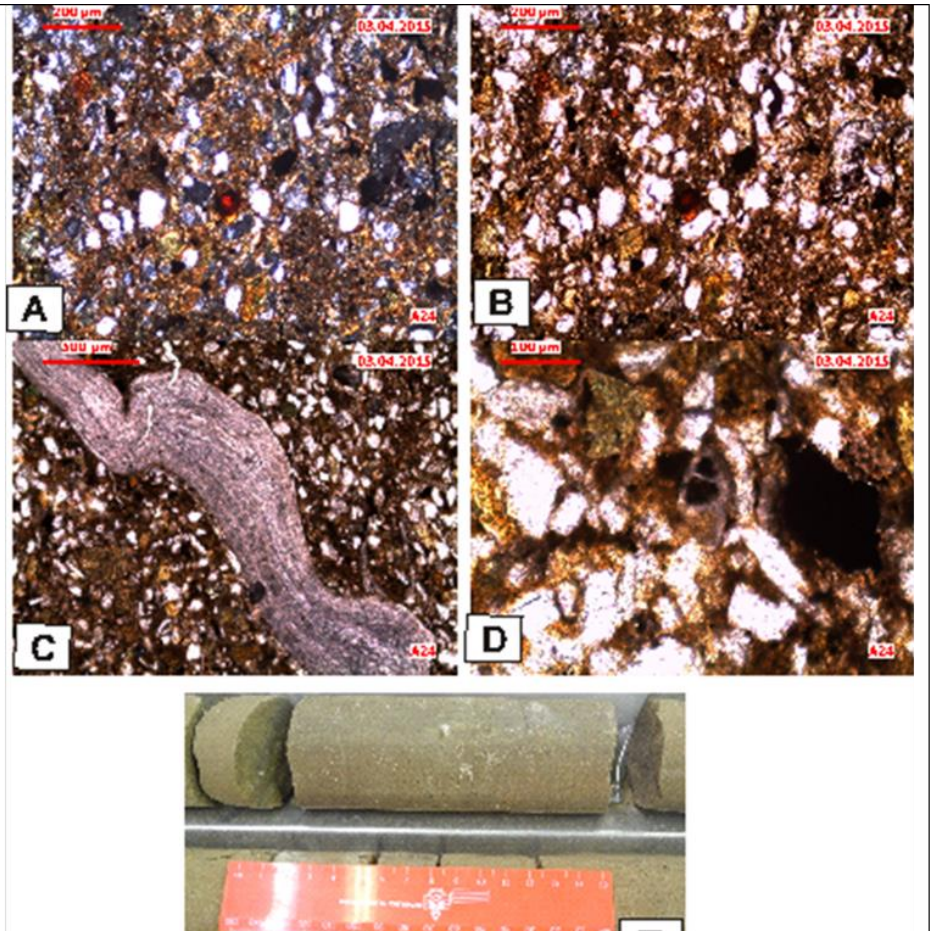

Sample A24. Arkosic wacke: A, B, C and D: Microphotographs. A (XPL) and B (PPL): monocrystalline quartz and plagioclase grains supported by clayey matrix. C (XPL): elongated calcified algae (chlorophyta) in an immature fine grained sandstone. D (PPL): Gastropod fragment surrounded by grains of calcite, quartz and plagioclase, and embedded in clay minerals. E: dark brown coloured, weakly to moderately indurated sandstone with fragmented fossils and indistinct wavy lamination.

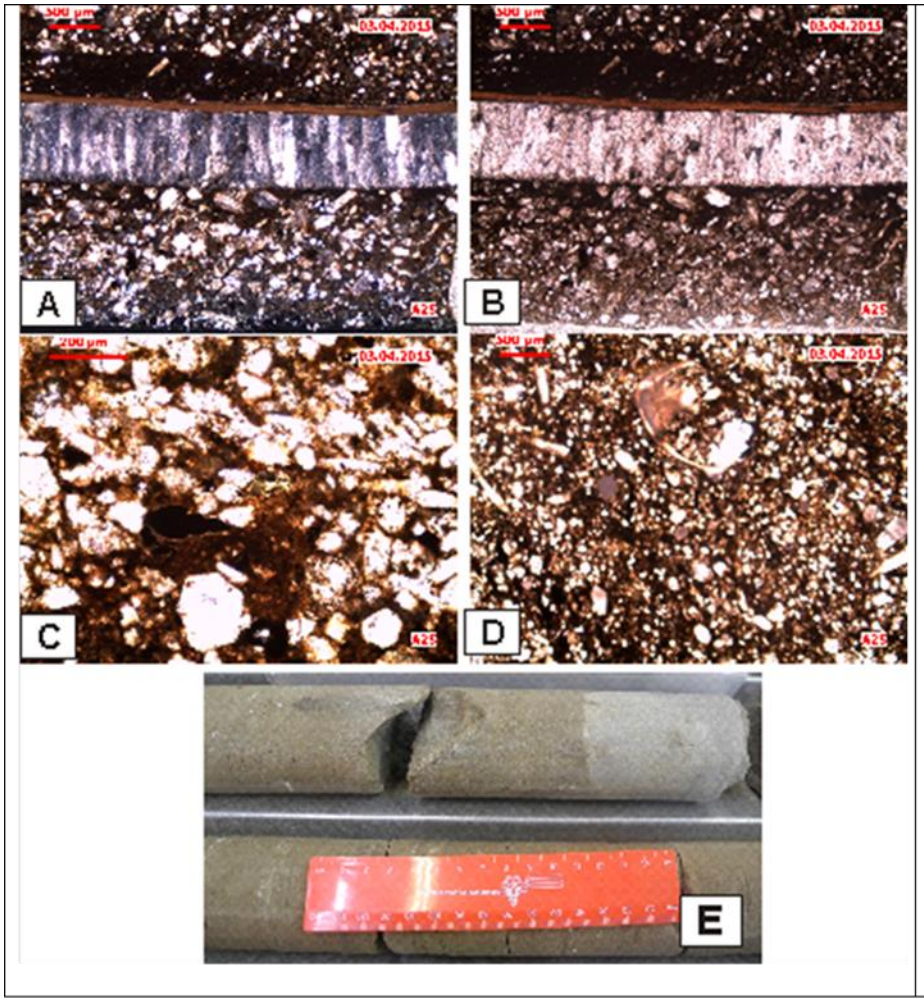

Sample A25. Bioclastic limestone: A, B, C and D: Microphotographs. A (XPL) and B(PPL): elongated shell fragment associated with grains of quartz, plagioclase and calcite in the clayey and micritic matrix. C (PPL) sparite grains supported by clay and micrite matrix. D. Brachiopods with shell fragments associated with quartz and plagioclase grains embedded in a clayey and micritic matrix. E. Bioclastic limestone picture showing two beds of different colour: grey bed is harder than the brown grey and rich in carbonate minerals than the brown grey bed.

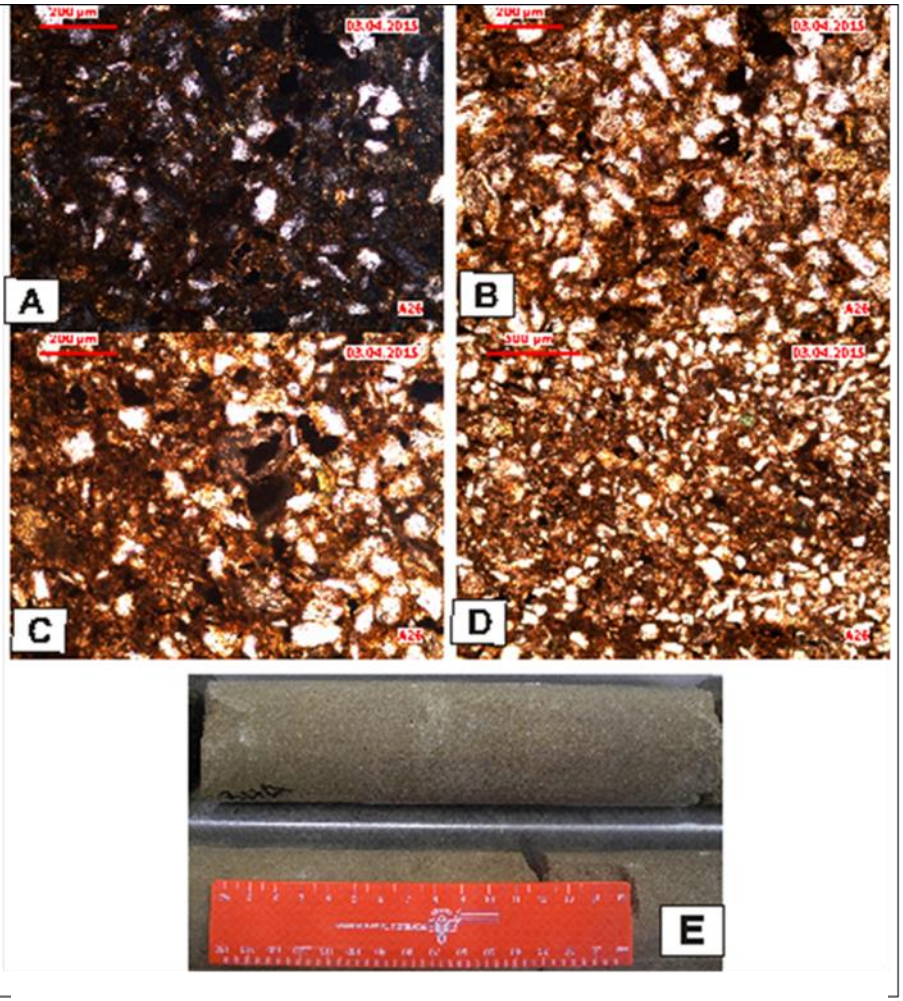

Sample A26. Siltstone. Microphotographs: A (XPL), B(PPL), C(PPL) and D (PPL): Angular clast of quartz and plagioclase in brown clayey matrix. E. dark brown coloured laminated siltstone containing white patches of broken shells.

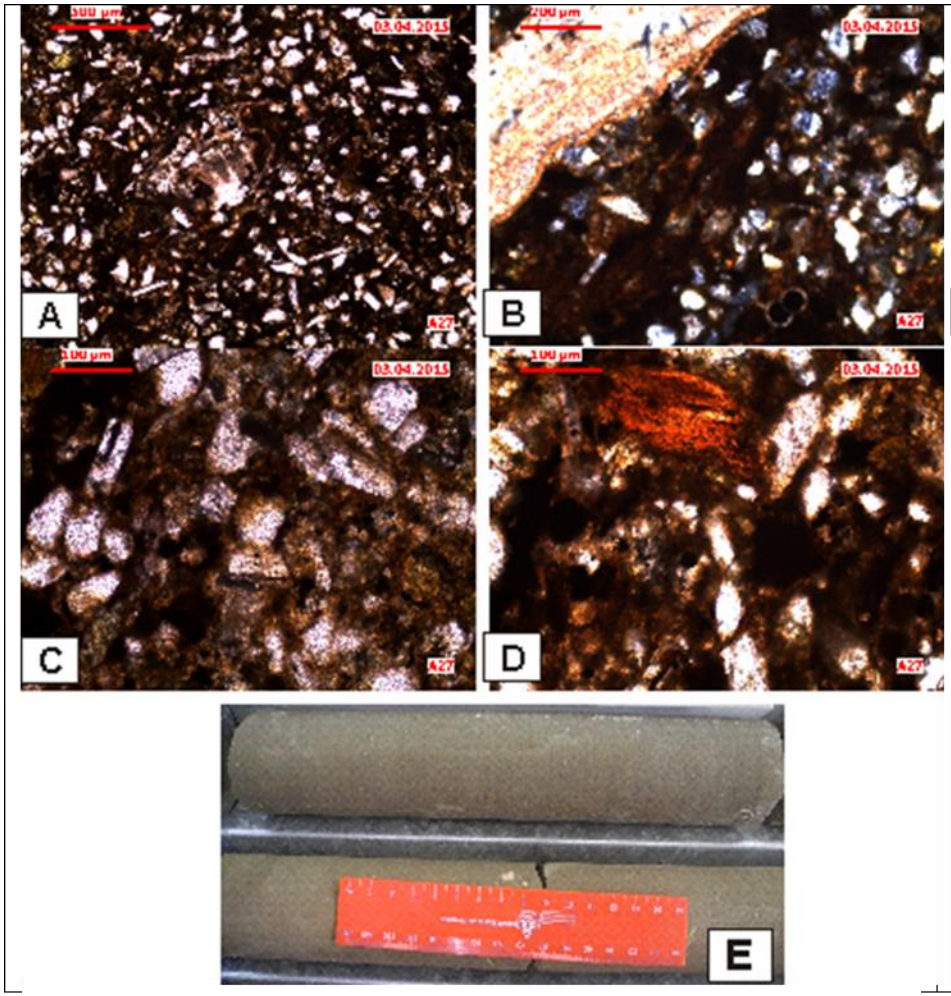

Sample A27. Siltstone. A, B, C and D: Microphotographs. A (PPL) and B (XPL): angular quartz and plagioclase grains associated with shell fragments in clayey matrix. C (PPL): Angular plagioclase and quartz embedded in the matrix. D (PPL): Hematite mineral surrounded by quartz grains supported by clayey matrix. E: Brownish coloured moderately indurated bioturbated laminated siltstone.

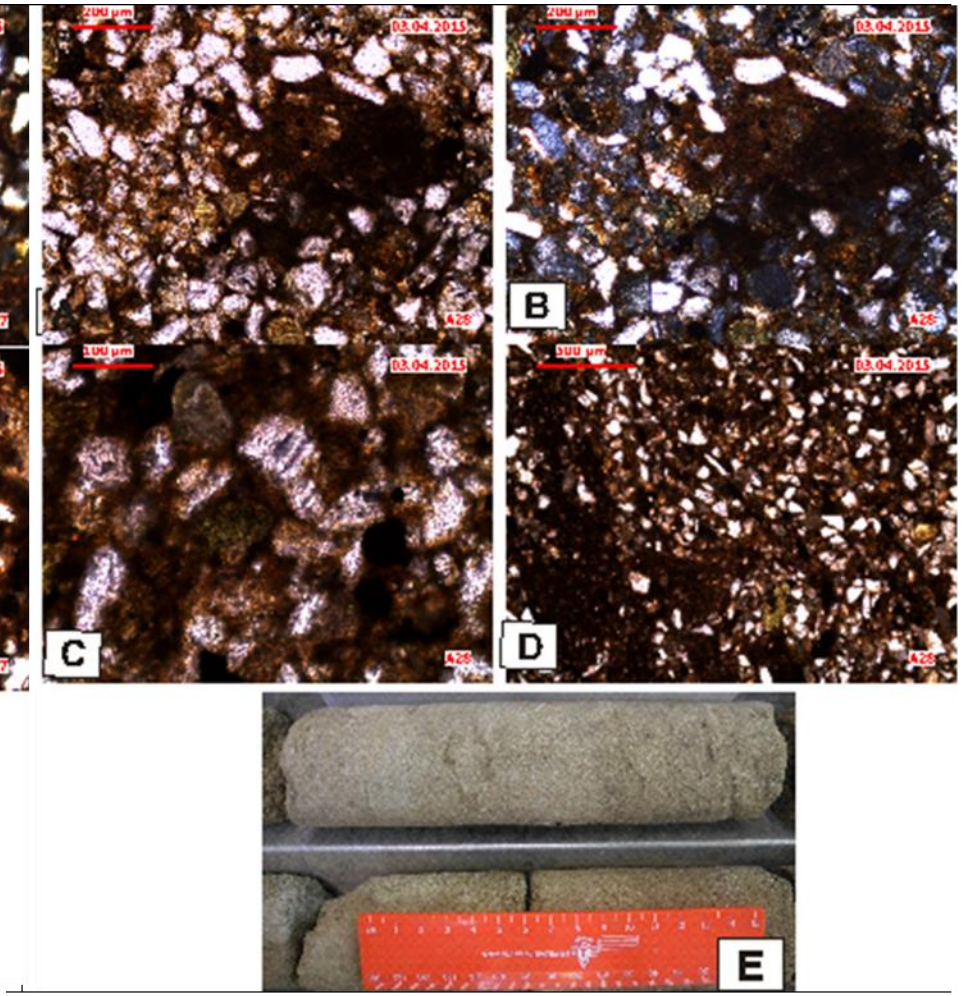

Sample A28. Siltstone. A, B, C and D: Microphotographs. A (PPL) and B (XPL): angular quartz and plagioclase grains in brown clayey matrix with black organic matter. C: plagioclase grains coated by brown clay minerals associated with dark organic matter. D: Overall silt-sized grains of quartz and plagioclase in clayey matrix with black organic matter. E: greyish highly bioturbated wavy laminated siltstone with white patches of broken shells.

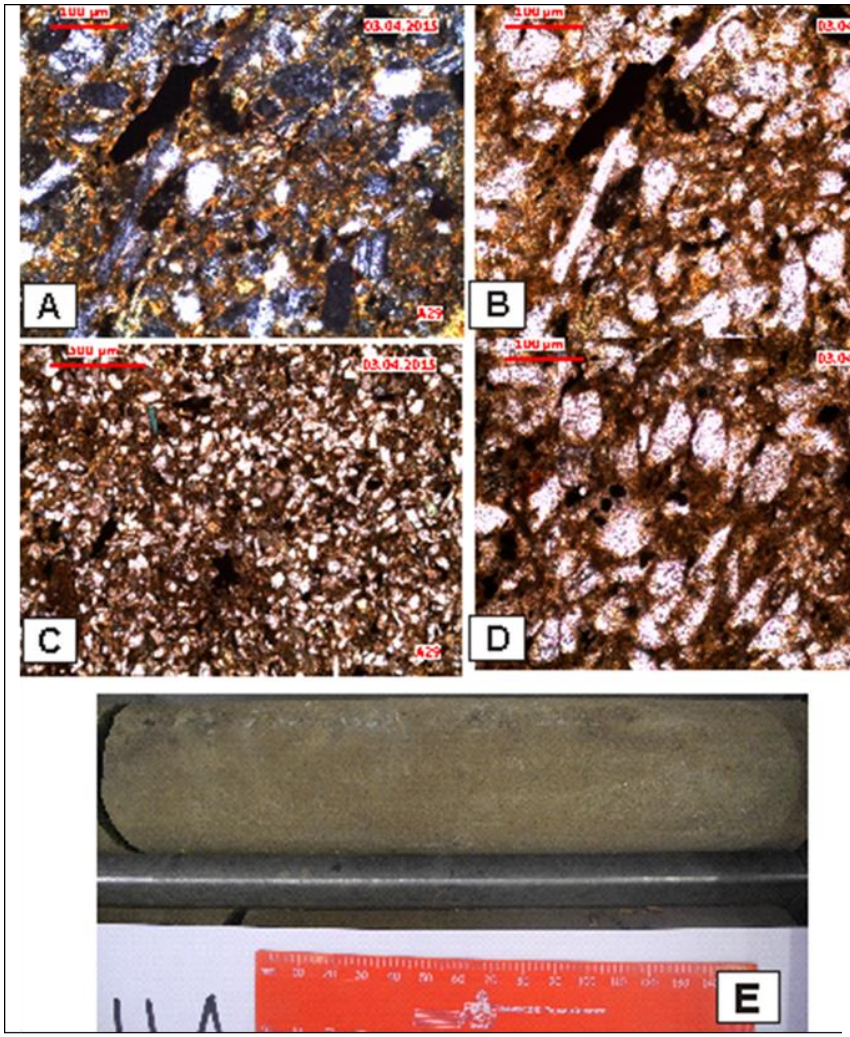

Sample A29. Siltstone: A, B, C and D: Microphotographs. A (XPL) and B (PPL): angular plagioclase and subangular quartz grains with pore spaces filled by black organic matter and brown clay mineral. C (PPL) and D (PPL) a dominance of silt sized grains of quartz and plagioclase supported by clayey matrix. E: dark brown locally bioturbated and laminated siltstone.

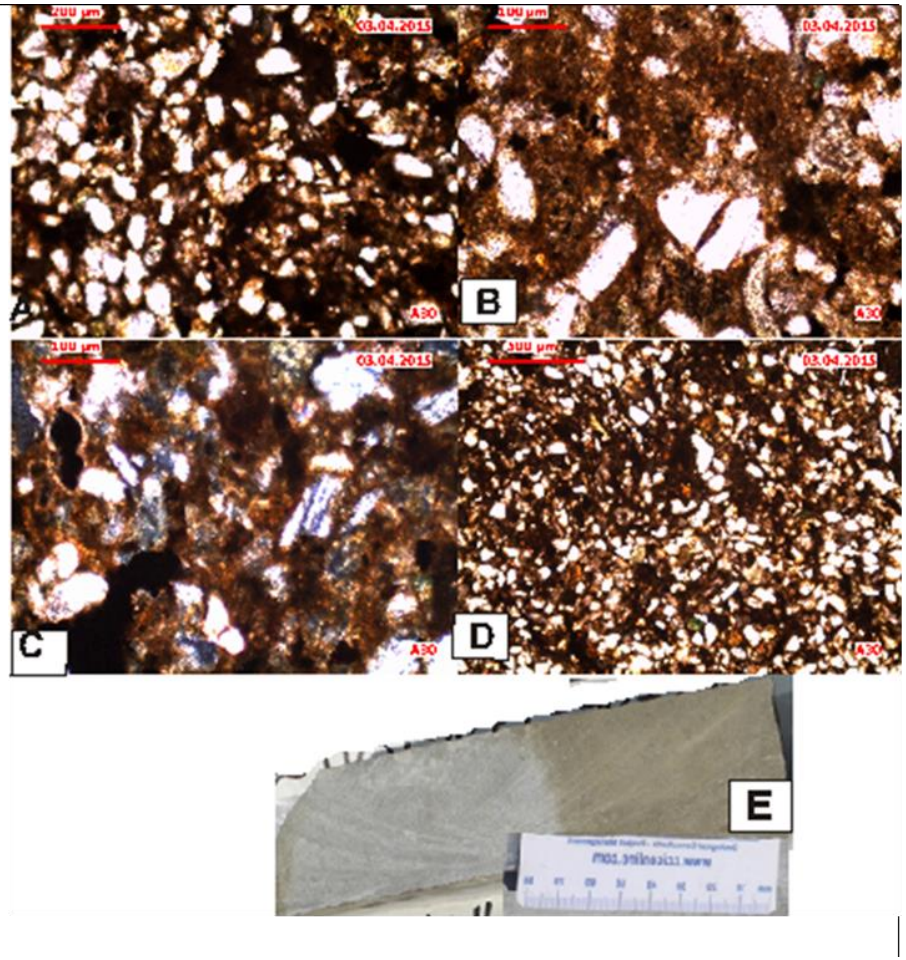

Sample A30. Siltstone: A, B, C and D: Microphotographs. A (PPL): angular grains of quartz and plagioclase in clayey matrix with black organic matter. B. Brown clayey matrix and broken shells under PPL. C: Plagioclase and angular quartz with foraminifera fossil and organic matter. D: sediment dominated by silty sized grains of quartz and plagioclase supported by clayey matrix. E: Grey and brownish coloured bioturbated siltstone.

APPENDIX B4: SAMPLES A31 – A40

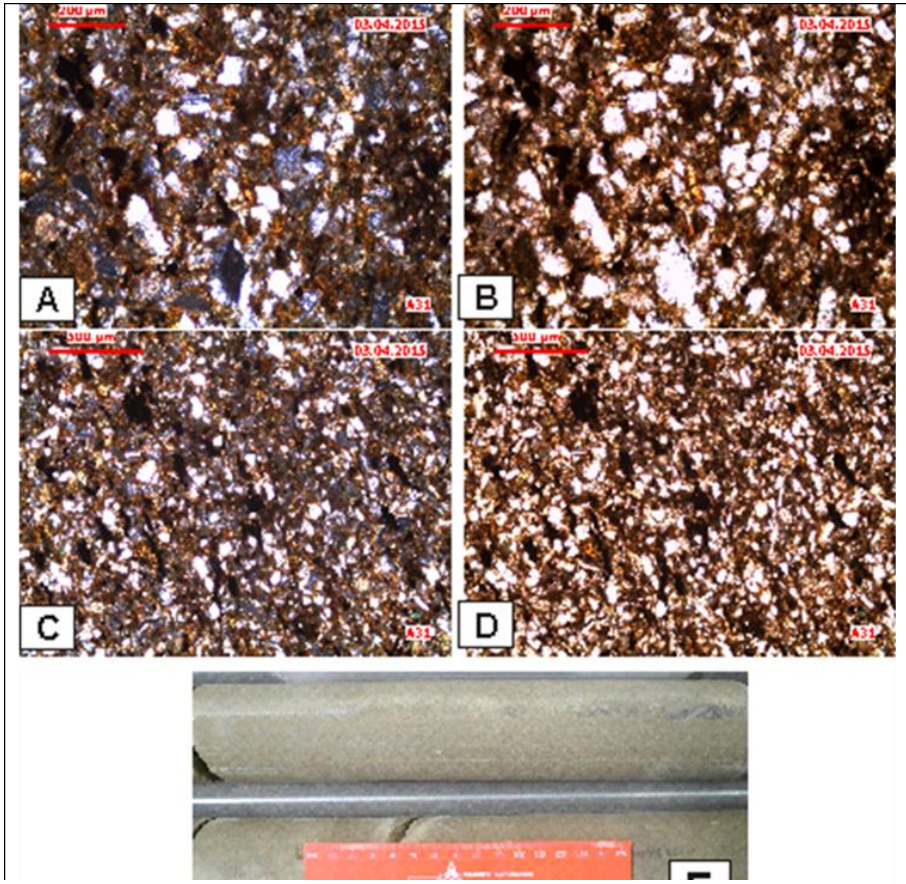

Sample A31. Siltstone. A, B, C and D: Microphotographs. A (XPL) and B (PPL): angular quartz and plagioclase in brown clayey matrix. C (XPL) and D (PPL): overall of silt-sized clasts (quartz and plagioclase) supported by clayey matrix. E: Dark brown coloured siltstone lacking clear sedimentary structures due the bioturbation

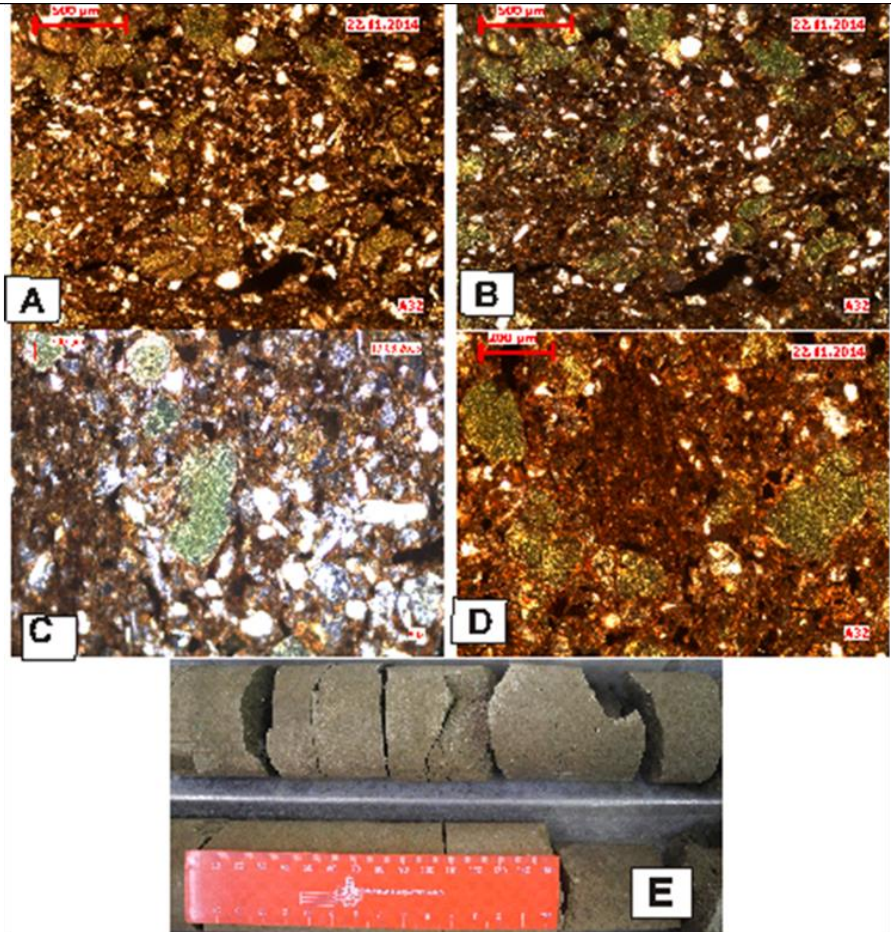

Sample A32. Glauconitic siltstone. A, B, C and D: Microphotographs. A (PPL) and B (XPL): Siltstone rich in glauconite, quartz and plagioclase grains floating in clayey matrix. C (XPL): clast of quartz and plagioclase in the matrix with glauconite and clay minerals associated with organic matter. D (PPL): The silty mudstone is dominated by glauconite grains associated with other clay minerals and organic matter as matrix supporting silt- sized clast of quartz and plagioclase. E: picture showing a dark green coloured siltstone not clear lamination.

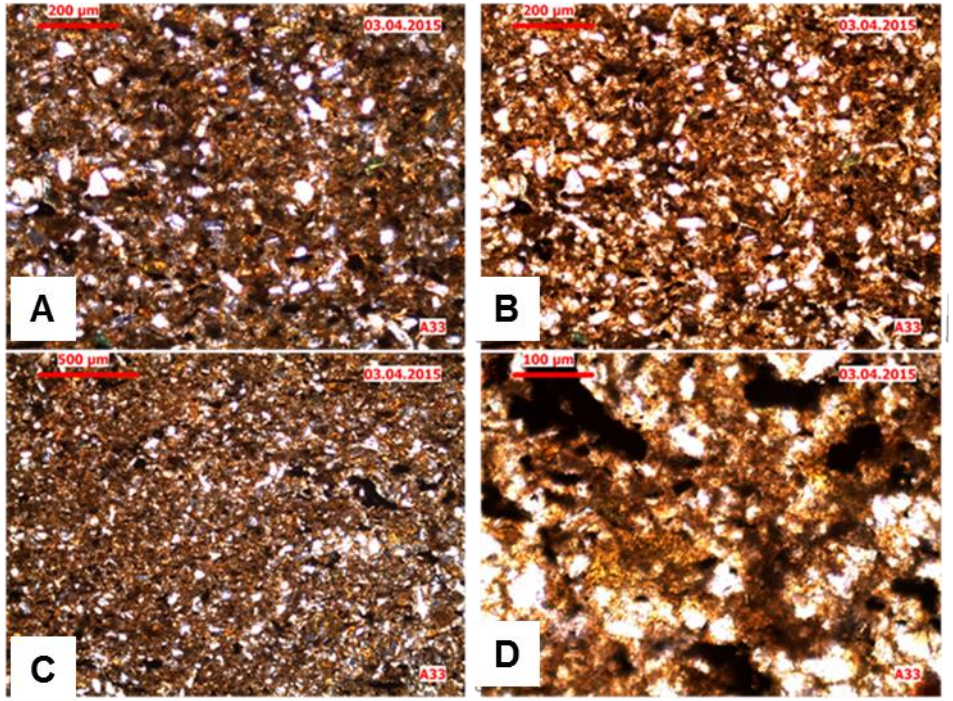

Sample A33. Siltstone: A, B, C and D: Microphotographs. A (XPL) and B (PPL): angular quartz and plagioclase in clayey matrix. C (XPL): silt-sized clasts of quartz and plagioclase supported by clayey matrix. D (PPL): brownish clay minerals as a matrix with black organic matter. E: picture showing brownish coloured, weakly indurated bioturbated siltstone

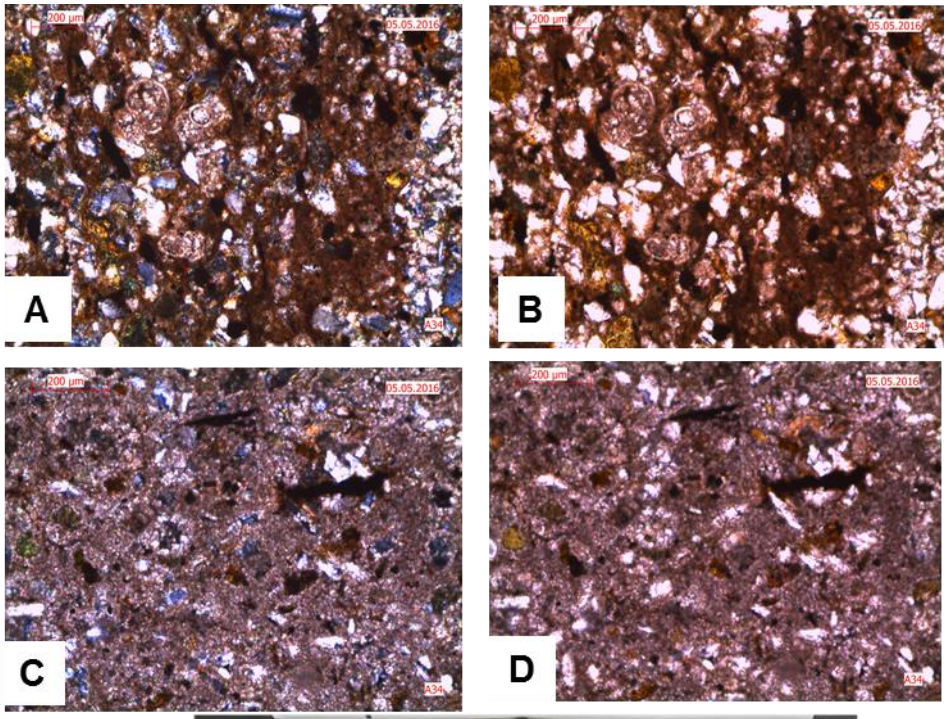

Sample A34. Calcareous siltstone. A, B, C and D: Microphotographs. A (XPL) and B (PPL): angular quartz, plagioclase with foraminifera fossils in micritic and clayey matrix. C (PPL) and D (XPL): Micritic matrix supporting angular grains of quartz and plagioclase with some hematite E: Picture showing grey coloured weakly to moderately indurated wavy bedded and laminated siltstone.

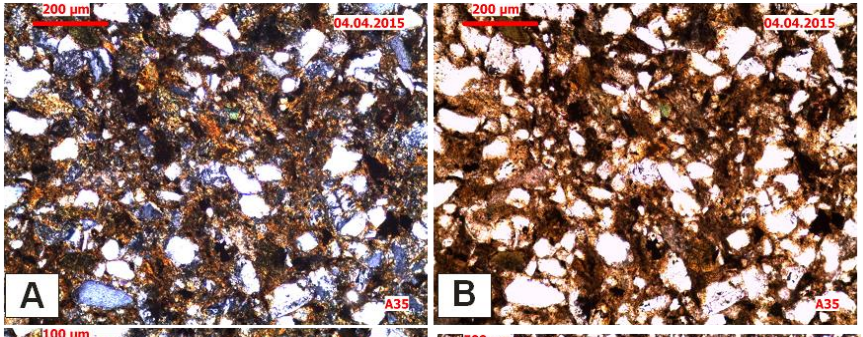

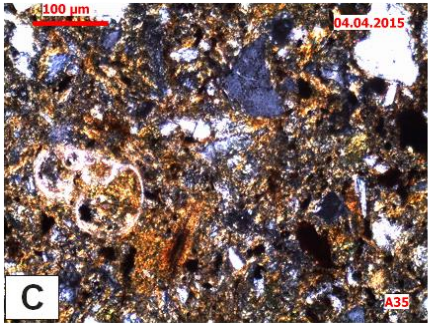

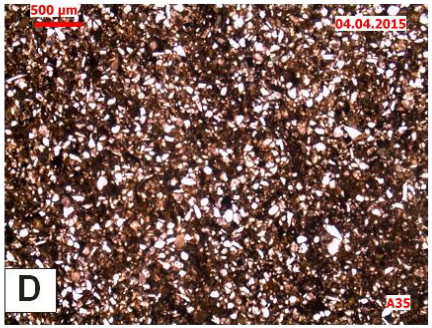

Sample A35. Siltstone: A, B, C and D: Microphotographs. A (XPL) and B (PPL): Angular quartz and plagioclase in clayey matrix. C (XPL): alteration of pyroxene to clay mineral and foraminifera fossil. D: Silt-sized grains of quartz and plagioclase supported by clay matrix. E: Greyish brown highly bioturbated siltstone.

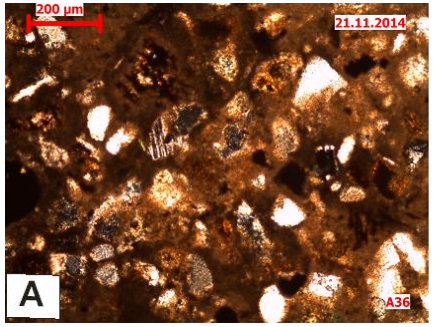

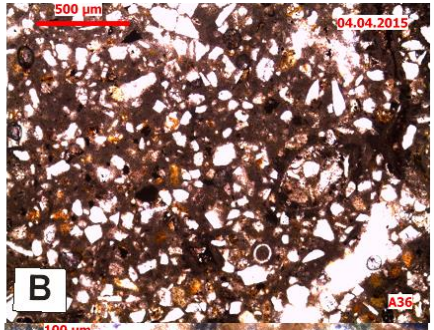

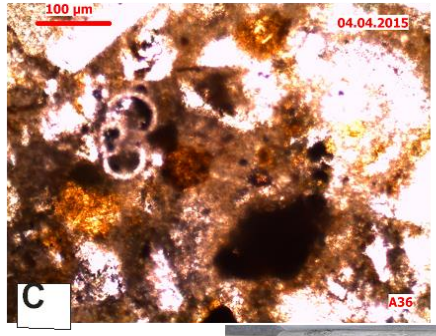

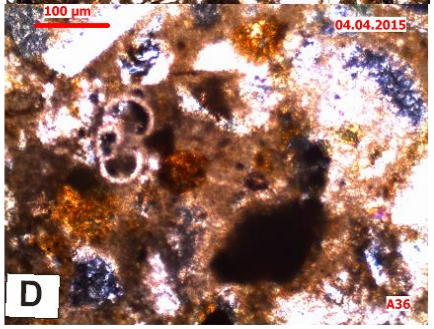

Sample A36. Siltstone: A, B, C and D: Microphotographs. A (PPL): altered plagioclase and quartz grains in clayey matrix associated with hematite. B (XPL): Silt-sized grains of quartz, plagioclase with spicule fossils supported by clayey matrix associated with hematite. C (PPL) and D (XPL): Foraminifera fossil, hematite associated with clay in the matrix. E: grey brown laminated siltstone.

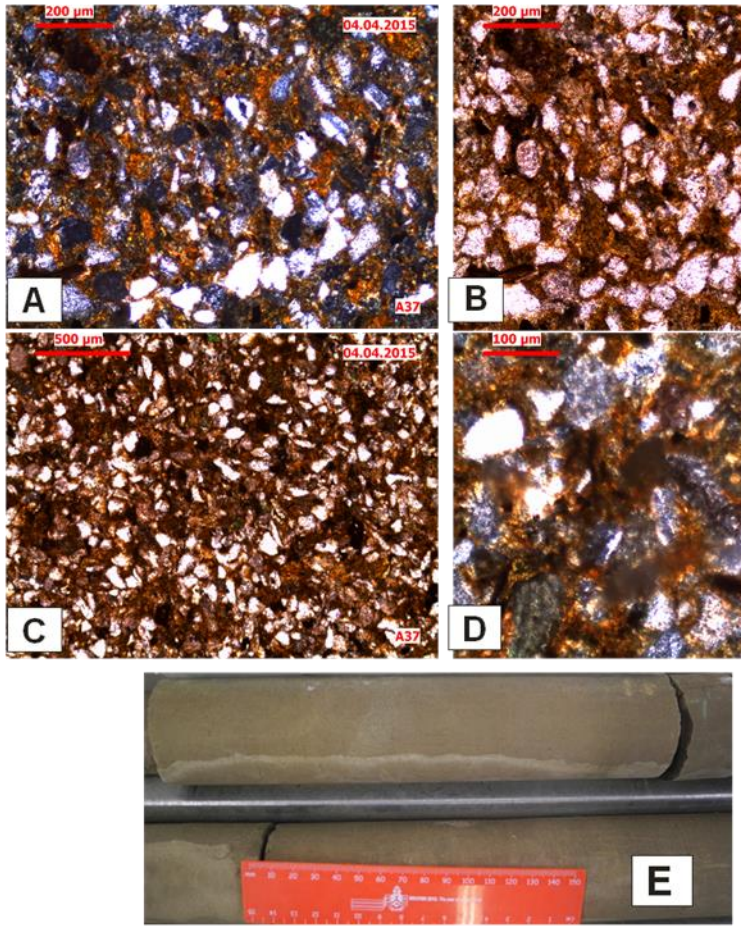

Sample A37. Siltstone: A, B, C and D: Microphotographs. A (XPL) and B (PPL): angular quartz and plagioclase in brown clayey matrix. C (PPL): Silt-sized grains of quartz and plagioclase supported by brown clay minerals. D: Plagioclase and subangular quartz clasts filled by clay minerals. E: Dark brown laminated siltstone.

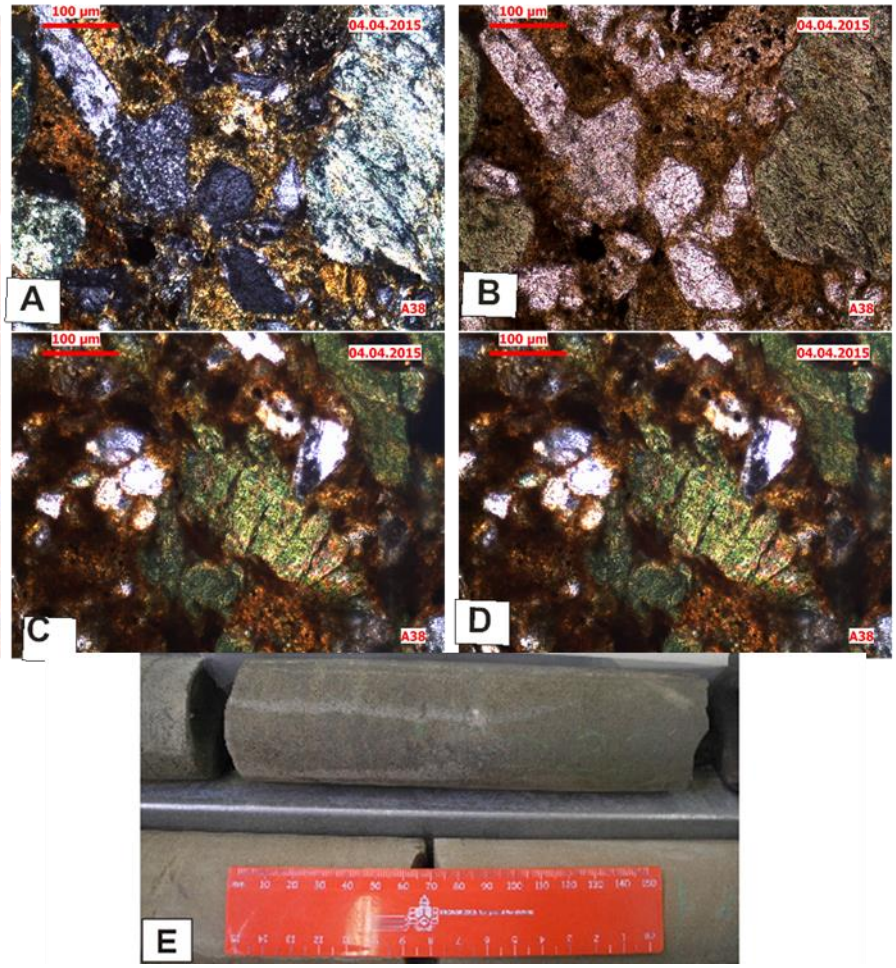

Sample A38. Glauconitic siltstone. A, B, C and D: Microphotographs. A (XPL) and B (PPL): altered plagioclase in clayey matrix. C (XPL and PPL): alteration of pyroxene and glauconitisation of clay minerals. E : Greenish laminated and moderately indurated siltstone with black spots of organic matter.

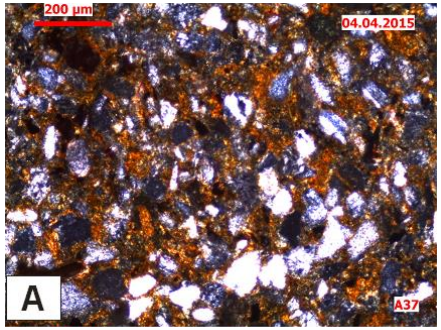
200 µm
04.04.2015
A
A37

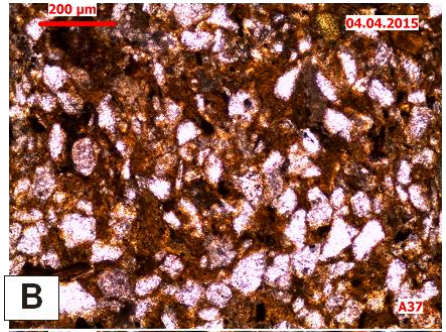
200 µm
04.04.2015
B
A37

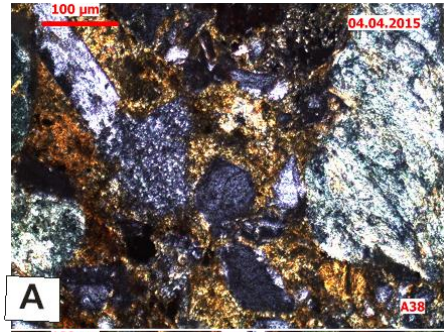
100 µm
04.04.2015
A
A38

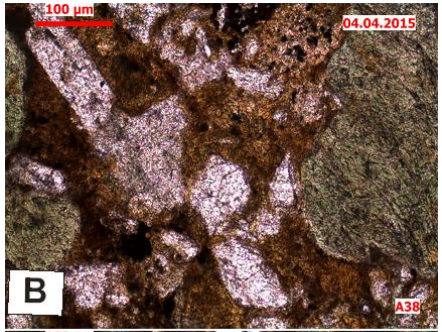
100 µm
04.04.2015
B
A38

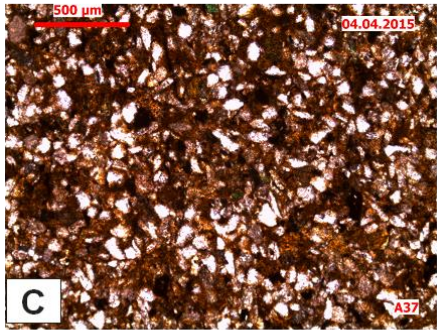
500 µm
04.04.2015
C
A37

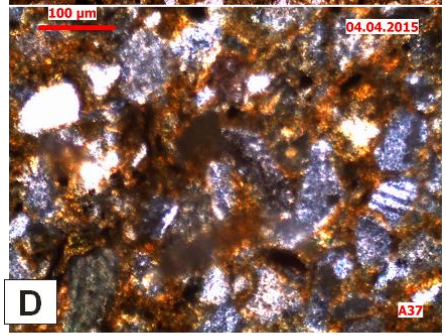
100 µm
04.04.2015
D
A37

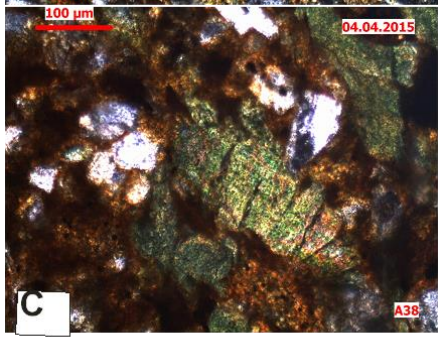
100 µm
04.04.2015
C
A38

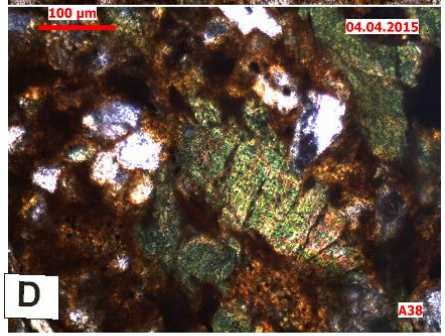
100 µm
04.04.2015
D
A38


E

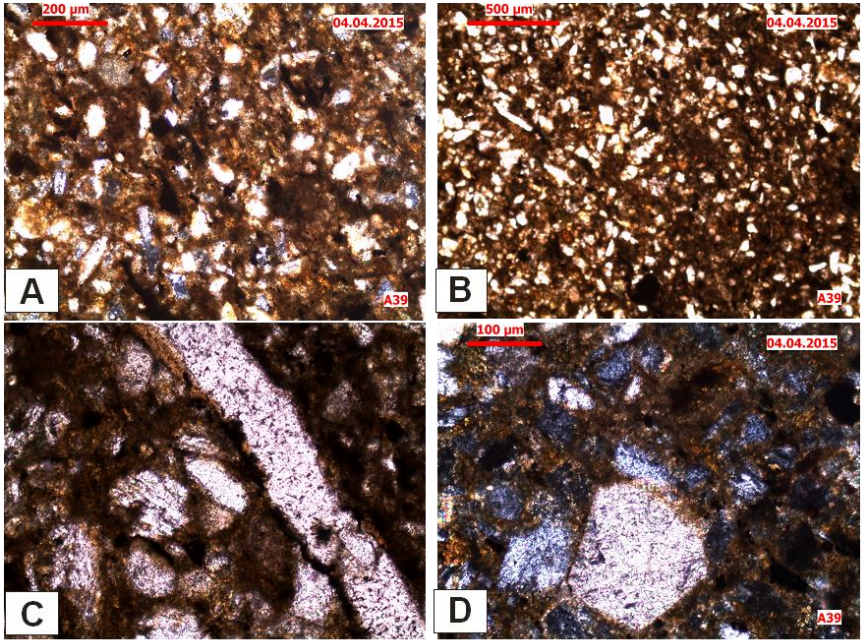

Sample A39. Calcareous siltstone. A, B, C and D: Microphotographs. A (XPL) and B (PPL): Cast of plagioclase and quartz with calcite grain in calcite and clayey matrix. C (PPL): calcite cements filling a crack in the sediment. D: euhedral calcite grains under XPL. E: Dark grey moderately indurated bioturbated calcareous siltstone with indistinct lenses.

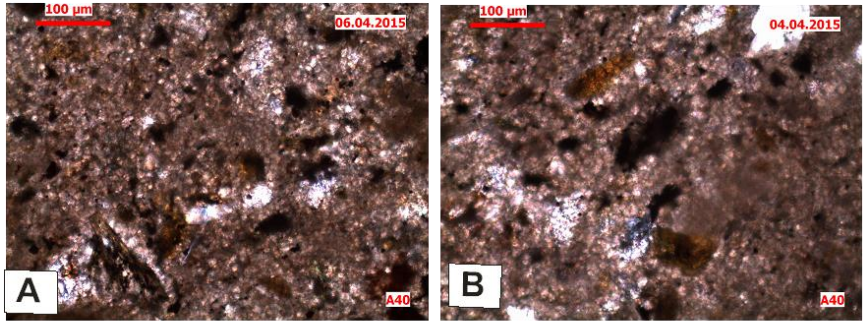

Sample A40. Calcareous siltstone (Microphotographs). A: mica flake and limonite in calcite matrix. B: Black organic matters and limonite supported by calcite matrix.

APPENDIX C: MINERALOGY AND GEOCHEMICAL DATA OF THE ZA CORE

C1: MINERALOGICAL DATA OF THE ZA CORE

Sample ID (Depth)	Rock type	Calcite	Hematite	Gypsum	Microcline	Plagioclase	Quartz	Mica	Chlorite	Zeolite(Clinoptillolite/Healandite)	Smectite	Glauconite	Sum of clays	Lithic	Sum of minerals
A1 (105.5 – 105.3m)	Bioclastic limestone	73.00	1.00	0.00	2.00	10.00	9.00	0.00	1.00	0.00	3.00	1.00	5.00	0.00	100.00
A2 (189.98 – 188.1m)	Calcareous siltstone	17.00	2.00	0.00	4.00	23.00	32.00	1.00	0.00	8.00	10.00	3.00	21.00	9.00	100.00
A3 (218.6 – 218.5m)	Siltstone	13.00	4.00	0.00	0.00	13.00	46.00	0.00	0.00	11.00	6.00	7.00	24.00	11.00	100.00
A4 (246.6 - 246.5m)	Glauconitic arkosic wacke	4.00	2.00	0.00	0.00	18.00	43.00	0.00	1.00	2.00	0.00	30.00	33.00	2.00	100.00
A5 (311.3 - 311.2m)	Arkose	5.00	2.00	0.00	0.00	24.00	57.00	1.00	1.00	0.00	5.00	5.00	11.00	1.00	100.00
A6 (379.5 - 379.3m)	Calcareous siltstone	45.00	2.00	0.00	0.00	16.00	15.00	0.00	0.00	7.00	10.00	5.00	22.00	7.00	100.00
A7 (426.7 - 426.4m)	Siltstone	17.00	3.00	0.00	1.00	19.00	32.00	2.00	2.00	7.00	10.00	7.00	26.00	9.00	100.00
A8(445.6 - 445.5m)	Calcareous siltstone	34.00	2.00	0.00	0.00	15.00	34.00	2.00	0.00	0.00	11.00	2.00	13.00	2.00	100.00
A9 (482.19 - 482.14m)	Siltstone	13.00	3.00	0.00	0.00	21.00	25.00	3.00	0.00	3.00	26.00	6.00	35.00	6.00	100.00
A10 (536.5 - 536.4m)	Calcareous siltstone	33.00	2.00	0.00	0.00	17.00	27.00	0.00	0.00	3.00	14.00	4.00	21.00	3.00	100.00
A11 (562.7 - 562.6m)	Calcareous siltstone	32.00	2.00	0.00	0.00	18.00	27.00	0.00	0.00	2.00	15.00	4.00	21.00	2.00	100.00
A12 (575.7 - 575.5m)	Calcareous siltstone	33.00	1.00	0.00	0.00	13.00	40.00	3.00	0.00	0.00	6.00	5.00	11.00	3.00	101.00
A13 (613 - 612.8m)	Glauconitic siltstone	4.00	3.00	0.00	0.00	15.00	40.00	5.00	0.00	0.00	0.00	33.00	33.00	5.00	100.00
A14 (625.1 – 625m)	Siltstone	2.00	3.00	0.00	0.00	23.00	37.00	3.00	2.00	3.00	20.00	7.00	32.00	6.00	100.00
A15 (632.9 - 632.8m)	Siltstone	2.00	3.00	0.00	0.00	20.00	40.00	3.00	2.00	3.00	23.00	4.00	32.00	6.00	100.00
A16 (648.9 - 648.8m)	Arkosic wacke	10.00	2.00	0.00	0.00	18.00	33.00	0.00	0.00	0.00	30.00	7.00	37.00	0.00	100.00
A17 (651.9 - 651.7m)	Siltstone	10.00	4.00	0.00	0.00	28.00	13.00	2.00	3.00	4.00	30.00	6.00	43.00	6.00	100.00
A18 (685.5 - 685.4m)	Arkosic wacke	0.00	0.00	0.00	0.00	17.00	65.00	0.00	0.00	0.00	12.00	6.00	18.00	0.00	100.00
A19 (710.5 - 710.4m)	Subarkose	0.00	12.00	0.00	0.00	18.00	63.00	2.00	0.00	0.00	4.00	1.00	5.00	2.00	100.00
A20 (760.9 - 760.7m)	Arkosic wacke	2.00	0.00	2.00	0.00	15.00	63.00	0.00	0.00	2.00	12.00	4.00	18.00	2.00	100.00
A21 (788.2 - 788.1m)	Calcareous sandstone	48.00	0.00	0.00	0.00	8.00	41.00	0.00	0.00	0.00	3.00	0.00	3.00	0.00	100.00
A22 (855.6 - 855.5m)	Calcareous sandstone	28.00	2.00	0.00	0.00	17.00	29.00	2.00	0.00	5.00	15.00	2.00	22.00	7.00	100.00
A23 (911.4 - 911.3m)	Calcareous sandstone	60.00	0.00	0.00	0.00	6.00	23.00	2.00	2.00	0.00	4.00	3.00	9.00	2.00	100.00
A24 (965.9 - 965.8m)	Arkosic wacke	6.00	3.00	0.00	0.00	27.00	45.00	3.00	4.00	3.00	6.00	3.00	16.00	6.00	100.00
A25 (1035.5 - 1035.4m)	Bioclastic limestone	79.00	0.00	0.00	0.00	5.00	9.00	0.00	0.00	3.00	4.00	0.00	7.00	3.00	100.00
A26 (1076.9 - 1076.8m)	Siltstone	5.00	2.00	0.00	0.00	24.00	31.00	0.00	3.00	14.00	20.00	1.00	38.00	14.00	100.00
A27 (1129.9 - 1129.8m)	Siltstone	8.00	3.00	0.00	0.00	18.00	36.00	0.00	0.00	3.00	32.00	0.00	35.00	3.00	100.00
A28 (1171.1 - 1170.1m)	Siltstone	6.00	2.00	0.00	0.00	22.00	42.00	3.00	3.00	0.00	20.00	2.00	25.00	3.00	100.00
A29 (1194.2 - 1194.1m)	Siltstone	4.00	2.00	0.00	0.00	30.00	30.00	3.00	2.00	2.00	23.00	4.00	31.00	5.00	100.00
A30 (1242.1 – 1242m)	Siltstone	10.00	2.00	0.00	0.00	20.00	32.00	3.00	3.00	6.00	22.00	2.00	33.00	9.00	100.00
A31 (1294.2 - 1294.1m)	Siltstone	6.00	2.00	0.00	0.00	14.00	35.00	0.00	3.00	4.00	35.00	1.00	43.00	4.00	100.00
A32 (1324.1 – 1324m)	Glauconitic siltstone	3.00	2.00	0.00	0.00	25.00	26.00	3.00	4.00	3.00	9.00	25.00	41.00	6.00	100.00
A33 (1369.2 – 1369m)	Siltstone	8.00	4.00	0.00	0.00	19.00	23.00	0.00	4.00	8.00	32.00	2.00	46.00	8.00	100.00
A34 (1415.8 - 1415.6m)	Calcareous siltstone	57.00	0.00	0.00	0.00	9.00	21.00	2.00	2.00	2.00	2.00	5.00	11.00	4.00	100.00
A35 (1445.4 - 1445.2m)	Siltstone	0.00	2.00	0.00	0.00	15.00	27.00	2.00	3.00	2.00	40.00	9.00	54.00	4.00	100.00
A36 (1484.4 - 1484.3m)	Siltstone	27.00	0.00	0.00	0.00	17.00	31.00	0.00	3.00	2.00	20.00	0.00	25.00	2.00	100.00
A37 (1507.9 - 1507.8m)	Siltstone	0.00	0.00	0.00	0.00	15.00	44.00	0.00	3.00	2.00	36.00	0.00	41.00	2.00	100.00
A38 (1529.5 1529.4m)	Glauconitic siltstone	0.00	2.00	0.00	0.00	13.00	28.00	3.00	10.00	0.00	41.00	3.00	54.00	3.00	100.00
A39 (1592.7 - 1592.6m)	Calcareous siltstone	57.00	0.00	0.00	0.00	4.00	29.00	0.00	0.00	3.00	2.00	3.00	8.00	3.00	98.00
A40 (1597.5 - 1597.4m)	Calcareous siltstone	57.00	4.00	0.00	0.00	11.00	14.00	0.00	0.00	3.00	5.00	6.00	14.00	3.00	100.00

C2: GEOCHEMICAL DATA OF ZA SAMPLES (ZA ROCKS AND CHEMICAL ELEMENTS)

Sample ID (Depth)	Rock type	SiO2	TiO2	Al2O3	Fe2O3	MnO	MgO	CaOt	P2O5	Cr2O3	LOI	H2O-
A1 (105.5 – 105.3 m)	Bioclastic limestone	23.07	0.33	5.29	2.68	0.04	1.54	35.60	0.05	0.01	29.67	2.30
A2 (189.98 – 188.1 m)	Calcareous siltstone	58.65	0.88	10.69	6.15	0.06	3.21	7.87	0.10	0.03	8.12	3.88
A3 (218.6 – 218.5 m)	Siltstone	64.32	0.80	9.69	6.73	0.04	2.84	5.59	0.11	0.03	6.60	4.07
A4 (246.6 - 246.5 m)	Glauconitic arkosic wacke	50.48	1.01	10.95	7.36	0.12	3.57	17.29	0.11	0.03	4.94	3.77
A5 (311.3 - 311.2 m)	Arkose	60.32	0.94	12.18	7.56	0.06	4.18	4.45	0.10	0.03	5.16	3.04
A6 (379.5 - 379.3 m)	Calcareous siltstone	54.82	0.87	11.25	7.03	0.06	3.81	4.13	0.09	0.03	12.59	3.34
A7 (426.7 - 426.4 m)	Siltstone	52.07	0.99	12.40	8.32	0.06	3.38	8.00	0.10	0.03	9.17	3.33
A8 (445.6 - 445.5 m)	Calcareous siltstone	46.81	0.96	10.32	7.42	0.09	3.26	14.77	0.09	0.03	12.27	3.56
A9 (482.19 - 482.14 m)	Siltstone	51.95	1.04	12.90	9.12	0.08	4.25	7.16	0.10	0.03	7.99	4.23
A10 (536.5 - 536.4 m)	Calcareous siltstone	47.31	0.94	11.67	7.57	0.10	3.02	12.46	0.09	0.02	11.99	3.65
A11 (562.7 - 562.6 m)	Calcareous siltstone	53.05	0.93	10.69	7.80	0.08	2.88	10.68	0.09	0.03	9.49	3.65
A12 (575.7 - 575.5 m)	Calcareous siltstone	49.17	0.86	9.33	6.39	0.09	2.25	15.57	0.09	0.03	12.95	2.47
A13 (613 - 612.8 m)	Glauconitic siltstone	53.40	0.93	10.15	6.94	0.10	2.45	16.93	0.10	0.03	5.38	3.31
A14 (625.1 – 625 m)	Siltstone	57.10	0.93	11.31	13.42	0.05	3.42	2.49	0.10	0.03	5.68	4.20
A15 (632.9 - 632.8 m)	Siltstone	58.47	1.06	12.92	9.86	0.06	3.68	3.27	0.11	0.03	5.17	3.84
A16 (648.9 - 648.8 m)	Arkosic wacke	55.74	0.98	9.68	12.33	0.08	4.69	5.54	0.14	0.03	6.32	4.88
A17 (651.9 - 651.7 m)	Siltstone	45.58	1.27	13.89	11.79	0.15	4.40	8.75	0.27	0.03	8.57	4.47
A18 (685.5 - 685.4 m)	Arkosic wacke	67.54	0.91	9.80	7.54	0.09	4.04	3.25	0.13	0.03	2.49	2.73
A19 (710.5 - 710.4 m)	Subarkose	60.45	0.78	9.05	8.84	0.05	1.43	2.92	0.09	0.02	11.44	1.77
A20 (760.9 - 760.7 m)	Arkosic wacke	62.51	0.82	12.25	7.23	0.08	3.02	3.35	0.08	0.02	4.67	3.05
A21 (788.2 - 788.1 m)	Calcareous sandstone	55.05	0.35	5.89	3.01	0.06	1.04	18.15	0.07	0.01	12.77	1.82
A22 (855.6 - 855.5 m)	Calcareous sandstone	49.38	0.95	11.02	7.84	0.10	3.55	12.66	0.10	0.02	10.10	3.88
A23 (911.4 - 911.3 m)	Calcareous sandstone	27.89	0.65	5.75	5.10	0.73	1.81	31.38	0.14	0.02	24.08	1.42
A24 (965.9 - 965.8 m)	Arkosic wacke	58.64	1.08	13.44	9.28	0.06	3.66	4.24	0.12	0.03	5.49	4.30
A25 (1035.5 - 1035.4 m)	Bioclastic limestone	22.64	0.44	5.30	3.13	0.55	1.28	36.50	0.09	0.01	28.79	1.06
A26 (1076.9 - 1076.8 m)	Siltstone	59.58	1.03	12.53	9.06	0.07	3.77	4.45	0.11	0.03	4.93	4.00
A27 (1129.9 - 1129.8 m)	Siltstone	56.92	1.13	12.42	9.64	0.09	4.07	6.04	0.12	0.03	5.15	3.98
A28 (1171.1 - 1170.1 m)	Siltstone	58.83	1.11	12.55	9.62	0.08	4.02	4.93	0.11	0.03	4.77	3.71
A29 (1194.2 - 1194.1 m)	Siltstone	56.79	1.03	13.08	9.32	0.08	3.92	4.70	0.11	0.03	6.36	3.28
A30 (1242.1 – 1242 m)	Siltstone	57.24	0.98	12.57	8.98	0.09	3.75	6.31	0.13	0.03	6.01	3.37
A31 (1294.2 - 1294.1 m)	Siltstone	55.13	1.05	13.45	9.44	0.08	3.82	5.23	0.12	0.03	6.35	3.48
A32 (1324.1 – 1324 m)	Glauconitic siltstone	53.86	1.00	12.69	12.40	0.07	3.82	3.94	0.14	0.03	5.97	4.04
A33 (1369.2 – 1369 m)	Siltstone	49.47	1.17	13.96	10.44	0.09	3.89	6.62	0.14	0.02	8.29	3.73
A34 (1415.8 - 1415.6 m)	Calcareous siltstone	34.98	0.64	8.27	5.04	0.21	1.74	25.42	0.09	0.01	19.68	1.28
A35 (1445.4 - 1445.2 m)	Siltstone	60.41	1.12	13.96	8.95	0.06	3.95	3.06	0.11	0.03	4.80	3.42
A36 (1484.4 - 1484.3 m)	Siltstone	46.69	0.86	10.92	6.58	0.18	2.71	15.25	0.19	0.02	13.40	2.16
A37 (1507.9 - 1507.8 m)	Siltstone	62.88	1.06	13.22	8.58	0.06	3.90	2.76	0.13	0.03	3.96	3.54
A38 (1529.5 1529.4 m)	Glauconitic siltstone	58.07	1.05	11.55	13.84	0.10	4.56	2.85	0.16	0.04	4.32	3.17
A39 (1592.7 - 1592.6 m)	Calcareous siltstone	22.54	0.52	5.74	3.32	0.39	1.29	35.60	0.09	0.01	27.51	0.97
A40 (1597.5 - 1597.4 m)	Calcareous siltstone	21.59	0.48	5.79	4.03	0.80	1.42	35.95	0.13	0.01	28.09	1.07

C3: GEOCHEMICAL DATA (CALCULATIONS)

Sample ID (Depth)	CaOt	CaO (Calcite)	CaO*(Plagioclase)	Al2O3/SiO2	SiO2/Al2O3	K2O/Na2O	Na2O+CaO	Al2O3/Na2O+CaO	Al2O3+CaO+Na2O+K2O	(Al2O3/Al2O	(Al2O3/Al2O3+CaO+Na2O+K2O) x 100	SiO2/Al2O3 vs CaO	SiO2 vs K2O/Na2O	Na2O+K2O	Log (K2O/Na2O)
A1 (105.5 – 105.3m)	35.60	31,31253931	4,289388946	0.23	4.36	1.77	36.14	0.15	42.38	0.12	12.49	0.12	13.04	1.49	0.25
A2 (189.98 – 188.1m)	7.87	3,344371261	4,524737589	0.18	5.49	0.75	10.09	1.06	22.44	0.48	47.63	0.70	78.19	3.88	-0.12
A3 (218.6 – 218.5m)	5.59	2,796237262	2,796237262	0.15	6.64	1.09	7.29	1.33	18.84	0.51	51.43	1.19	59.00	3.56	0.04
A4 (246.6 - 246.5m)	17.29	3,143729537	14,14678292	0.22	4.61	0.76	19.42	0.56	32.00	0.34	34.21	0.27	66.01	3.76	-0.12
A5 (311.3 - 311.2m)	4.45	0,766778393	3,680536286	0.20	4.95	0.77	6.98	1.74	21.11	0.58	57.72	1.11	78.73	4.48	-0.12
A6 (379.5 - 379.3m)	4.13	3,047226072	1,083458159	0.21	4.87	0.79	6.54	1.72	19.68	0.57	57.15	1.18	69.64	4.30	-0.10
A7 (426.7 - 426.4m)	8.00	3,779041033	4,223634096	0.24	4.20	0.94	10.44	1.19	25.14	0.49	49.34	0.52	55.52	4.73	-0.03
A8 (445.6 - 445.5m)	14.77	10,24652598	4,520526166	0.22	4.54	0.73	16.86	0.61	28.71	0.36	35.94	0.31	64.04	3.62	-0.14
A9 (482.19 - 482.14m)	7.16	2,738379041	4,423535374	0.25	4.03	0.79	9.88	1.31	24.91	0.52	51.79	0.56	66.17	4.84	-0.11
A10 (536.5 - 536.4m)	12.46	8,224770269	4,237002866	0.25	4.05	0.82	14.75	0.79	28.30	0.41	41.24	0.33	57.56	4.17	-0.09
A11 (562.7 - 562.6m)	10.68	6,835819625	3,845148539	0.20	4.96	0.89	12.77	0.84	25.32	0.42	42.22	0.46	59.53	3.95	-0.05
A12 (575.7 - 575.5m)	15.57	11,16779144	4,399432992	0.19	5.27	0.95	17.25	0.54	28.18	0.33	33.12	0.34	51.62	3.28	-0.02
A13 (613 - 612.8m)	16.93	3,564450466	13,36668925	0.19	5.26	0.96	18.75	0.54	30.64	0.33	33.13	0.31	55.71	3.56	-0.02
A14 (625.1 – 625m)	2.49	0,198908018	2,287442202	0.20	5.05	2.15	4.15	2.72	19.05	0.59	59.35	2.03	26.50	5.26	0.33
A15 (632.9 - 632.8m)	3.27	0,296852631	2,96852631	0.22	4.52	0.99	5.69	2.27	21.00	0.62	61.54	1.39	59.35	4.81	-0.01
A16 (648.9 - 648.8m)	5.54	1,979608894	3,563296009	0.17	5.76	0.86	7.66	1.26	19.16	0.51	50.51	1.04	64.99	3.94	-0.07
A17 (651.9 - 651.7m)	8.75	2,30257847	6,447219716	0.30	3.28	0.79	11.41	1.22	27.39	0.51	50.69	0.38	58.00	4.76	-0.10
A18 (685.5 - 685.4m)	3.25	0	3,248828809	0.15	6.89	0.56	5.69	1.72	16.86	0.58	58.11	2.12	120.22	3.82	-0.25
A19 (710.5 - 710.4m)	2.92	0	2,917249537	0.15	6.68	0.60	5.59	1.62	16.26	0.56	55.67	2.29	100.04	4.29	-0.22
A20 (760.9 - 760.7m)	3.35	0,393679909	2,952599319	0.20	5.10	0.44	7.01	1.75	20.87	0.59	58.71	1.52	142.85	5.27	-0.36
A21 (788.2 - 788.1m)	18.15	15,55926598	2,593210997	0.11	9.34	0.49	20.01	0.29	26.81	0.22	21.98	0.51	112.27	2.76	-0.31
A22 (855.6 - 855.5m)	12.66	7,875676136	4,781660511	0.22	4.48	0.57	15.04	0.73	27.41	0.40	40.21	0.35	86.88	3.73	-0.25
A23 (911.4 - 911.3m)	31.38	28,52721229	2,852721229	0.21	4.85	1.15	32.28	0.18	39.06	0.15	14.71	0.15	24.24	1.93	0.06
A24 (965.9 - 965.8m)	4.24	0,770678357	3,468052608	0.23	4.36	0.87	6.51	2.06	21.93	0.61	61.32	1.03	67.73	4.24	-0.06
A25 (1035.5 - 1035.4m)	36.50	34,32569754	2,172512502	0.23	4.27	0.69	37.34	0.14	43.22	0.12	12.26	0.12	32.86	1.43	-0.16
A26 (1076.9 - 1076.8m)	4.45	0,766570953	3,679540576	0.21	4.76	0.89	6.77	1.85	21.36	0.59	58.65	1.07	67.24	4.39	-0.05
A27 (1129.9 - 1129.8m)	6.04	1,859756194	4,184451437	0.22	4.58	0.72	8.49	1.46	22.67	0.55	54.77	0.76	78.53	4.21	-0.14
A28 (1171.1 - 1170.1m)	4.93	1,057253779	3,876597191	0.21	4.69	0.81	7.22	1.74	21.63	0.58	58.03	0.95	72.66	4.14	-0.09
A29 (1194.2 - 1194.1m)	4.70	0,552736833	4,145526251	0.23	4.34	0.81	7.19	1.82	22.29	0.59	58.66	0.92	70.02	4.52	-0.09
A30 (1242.1 – 1242m)	6.31	2,102154303	4,204308606	0.22	4.55	0.67	8.73	1.44	22.92	0.55	54.86	0.72	85.97	4.04	-0.18
A31 (1294.2 - 1294.1m)	5.23	1,569550853	3,662285323	0.24	4.10	0.75	7.88	1.71	23.31	0.58	57.67	0.78	73.72	4.64	-0.13
A32 (1324.1 – 1324m)	3.94	0,422031216	3,5169268	0.24	4.24	1.28	6.11	2.08	21.58	0.59	58.82	1.08	42.07	4.95	0.11
A33 (1369.2 – 1369m)	6.62	1,960551102	4,656308867	0.28	3.54	0.87	9.23	1.51	25.48	0.55	54.81	0.54	56.79	4.90	-0.06
A34 (1415.8 - 1415.6m)	25.42	21,95206159	3,466114987	0.24	4.23	1.01	26.90	0.31	36.66	0.23	22.56	0.17	34.64	2.97	0.00
A35 (1445.4 - 1445.2m)	3.06	0	3,058784041	0.23	4.33	1.00	5.05	2.77	20.99	0.67	66.51	1.41	60.46	3.97	0.00
A36 (1484.4 - 1484.3m)	15.25	9,358270201	5,892244201	0.23	4.27	0.86	16.94	0.64	29.31	0.37	37.26	0.28	54.09	3.14	-0.06
A37 (1507.9 - 1507.8m)	2.76	0	2,763139605	0.21	4.75	0.71	5.06	2.61	19.92	0.66	66.37	1.72	88.19	3.94	-0.15
A38 (1529.5 1529.4m)	2.85	0	2,850983708	0.20	5.03	0.97	4.84	2.38	18.32	0.63	63.04	1.76	60.01	3.92	-0.01
A39 (1592.7 - 1592.6m)	35.60	33,26649377	2,334490791	0.25	3.92	0.95	36.54	0.16	43.17	0.13	13.30	0.11	23.78	1.82	-0.02
A40 (1597.5 - 1597.4m)	35.95	30,13557282	5,81563686	0.27	3.73	1.14	36.72	0.16	43.38	0.13	13.36	0.10	18.98	1.64	0.06

APPENDIX D: TABLE SHOWING THE LITHOSTRATIGRAPHIC SEQUENCE OF ZA CORE

BHID	From (m)	To (m)	Sedimentary facies	Sample ID	Lithological description	Formation	Depositional environments
ZA	0	89	Missing		Missing	Missing	Missing
ZA	89	129.84	Bioclastic limestone (grainstone)	A1	Light brown weakly indurated bioclastic limestone containing numerous fossils algaes, mainly echinoderms, bivalves preserved and broken apart, elongated, calcified, plant remains and lenses of crystallised calcite (0.5 cm thick, 1-2 cm length), effervescence reaction with HCl	Saint Lucia	Carbonate shelf
ZA	129.84	153.31	Bioturbated siltstone		Brownish weakly to moderately indurated structureless siltstone with carbonate matter, compacted, and with few fossils.	Saint Lucia	Inner to middle shelf
ZA	153.31	196.19	Bioturbated calcareous siltstone	A2	Light brown bioturbated, moderately indurated siltstone with carbonate material (effervescence with HCl) containing very fine shell fragments (mm size)	Saint Lucia	Inner to middle shelf
ZA	196.19	240.61	Laminated siltstone	A3	Brown grey moderately indurated finely bedded muddy siltstone with a few fossils (gastropods, 2mm size) and carbonate material (effervescence with HCl)	Saint Lucia	Inner to middle shelf
ZA	240.61	256.03	Structureless glauconitic arkosic wacke	A4	Dark green porous and weakly to moderately indurated, structureless fine grained sandstone with no sedimentary structure containing organic matter (plant remains) making rock porous with few fossils.	Saint Lucia	Inner shelf
ZA	256.03	360	Cross-bedded arkose	A5	Brownish moderately indurated fine grained sandstone with indistinctly cross bedding containing organic matter and few broken shells.	Saint Lucia	Inner shelf
ZA	360	415	Bioturbated calcareous siltstone	A6	Brownish grey moderately indurated calcareous siltstone with bivalves (3-5 mm), gastropods, foraminifera and dark spots of organic matter.	Saint Lucia	Inner to middle shelf
ZA	415	426.72	Bioturbated calcareous siltstone	A7	Brown and dark brown weakly to moderately indurated siltstone with gastropod, bivalves (about 5mm), broken shells, black spots of organic matter, plant remains.	Saint Lucia	Inner to middle shelf
ZA	426.72	482.14	Bioturbated calcareous siltstone	A8	Brown and grey weakly to moderately indurated siltstone with gastropods, bivalves (about 5mm), and broken shells, black spots of organic matter and plant remains.	Saint Lucia	Inner to middle shelf
ZA	482.14	536.24	Bioturbated calcareous siltstone	A9	Brown and dark brown weakly to moderately indurated with irregular lenticular structured destroyed by bioturbation siltstone with gastropods, bivalves (about 5mm), broken shells, and black spots of organic matter from plant remains.	Saint Lucia	Inner to middle shelf
ZA	536.24	562.66	Bioturbated calcareous siltstone	A10	Brown and grey weakly to moderately indurated irregular lenticular structures, mottled and bioturbated siltstone with gastropod, bivalves (about 5mm), broken shells, black spot of organic matter from plant remains.	Saint Lucia	Inner to middle shelf with tidal currents
ZA	562.66	575.51	Bioturbated calcareous siltstone	A11	Brown and grey weakly to moderately indurated finely bedded siltstone with gastropod, bivalves (about 5mm), broken shells, ooids, black spots organic matter from plant remains.	Saint Lucia	Inner to middle shelf
ZA	575.51	612.8	Bioturbated calcareous siltstone	A12	Grey brown weakly to moderately indurated mottled, lenticular structures, siltstone with gastropod, bivalves (about 5mm), broken shells, and black spots of organic.	Saint Lucia	Inner to middle shelf
ZA	612.8	625.09	Bioturbated glauconitic siltstone	A13	Green and dark brown very weakly indurated bioturbated siltstone with fossils such as gastropods, bivalves and carbonate matter (effervesce with HCl)	Saint Lucia	Inner to middle shelf
ZA	625.09	628.9	Bioturbated bedded siltstone	A14	Dark brown moderately indurated siltstone with carbonate material (effervesce with HCl) and fossils such as bivalves and gastropods (3-5mm)	Saint Lucia	Inner to middle shelf
ZA	628.9	635.43	Bioturbated siltstone	A15	Dark brown well indurated indistinctly bedded siltstone (fine grained) containing gastropod fossils	Saint Lucia	Inner to middle shelf

ZA	635.43	649.3	Bioturbated arkosic wacke	A16	Grey-brown well indurated Irregular bedding and bioturbated fine to medium grained sandstone with fossils (gastropods shells) and carbonate material (react with HCl)	Saint Lucia	Inner shelf
ZA	649.3	654	Laminated siltstone	A17	Brownish weakly indurated laminated siltstone with black spot of organic matter from plant remains and bivalves (5-6 cm large)	Saint Lucia	Inner to middle shelf
ZA	654	675.31	Laminated siltstone		Brownish and grey weakly indurated laminated siltstone with clast material (about 1mm), no fossils, no carbonate matter (no reaction with HCl)	Saint Lucia	Inner to middle shelf
ZA	675.31	678.92	Parallel bedded arkosic wacke	A18	Greyish moderately indurated mud to fine grained and parallel bedded sandstone with a few fossils	Mzinene	Inner shelf
ZA	678.92	710.41	Parallel bedded arkosic wacke		Brownish moderately to well indurated medium to coarse grained and parallel bedded sandstone, no visible fossils, no carbonate material (no reaction to HCl)	Mzinene	Inner shelf
ZA	710.41	731.95	Bioturbated structure subarkose	A19	Brown grey moderately to well indurated Bioturbated lenticular structure subarkose fine grained sandstone supported by mud matter, no reaction with, no carbonate material only black spot of organic matter (plant remains)	Mzinene	Inner shelf with tidal currents
ZA	731.95	748.44	Bioturbated subarkose		Brownish moderately indurated fine to medium grained sandstone, some fossils (shells), a little bit porous, no reaction to HCl, no carbonate matter	Mzinene	Inner shelf with tidal currents
ZA	748.44	749.66	Bioturbated subarkose		Brown grey moderately indurated silt to fine grained sandstone with fossils, and carbonate material (reaction with HCl)	Mzinene	Inner shelf with tidal currents
ZA	749.66	761.49	Laminae structures arkosic wacke	A20	Brown grey moderately indurated silt to fine grained sandstone, displaying lamination structures with irregular wavy bedding between a calcareous layer (10-15 cm thick) which reacts with HCl.	Mzinene	Inner shelf
ZA	761.49	763.93	Laminae structures arkosic wacke		Greyish dark moderately to well indurated silt to fine grained sandstone, laminae and streaks rich in organic matter and calcareous intercalations, dark spot of organic material (from plant remains).	Mzinene	Inner shelf
ZA	763.93	771.96	Laminae structures arkosic wacke		Greyish brown moderately to well indurated silt to fine grained sandstone, no carbonate matter (no reaction with HCl,), no fossils	Mzinene	Inner shelf
ZA	771.96	773.48	Laminae structures arkosic wacke		Brownish well indurated rock, medium to coarse grained sandstone, no reaction, no fossils	Mzinene	Inner shelf
ZA	773.48	787.6	Laminae structures arkosic wacke		Greyish moderately indurated fine grained sandstone, no reaction with HCl, no fossils,	Mzinene	Inner shelf
ZA	787.6	795.76	Bioturbated calcareous sandstone	A21	Greyish-brown well indurated rock, coarse grained calcareous sandstone with clast (quartz and calcite), fossils (bivalves: 1-3cm and gastropods: 1-2cm) and elongated calcified skeletal matter (about 5cm), very porous and react with HCl	Mzinene	Inner shelf
ZA	795.76	840.33	Parallel bedded arkosic wacke		Brown well indurated rock, irregular bedded fine to medium sandstone, porous and does not effervescence with HCl	Mzinene	Inner shelf
ZA	840.33	866.14	Irregular laminae calcareous sandstone	A22	Brown grey moderately indurated rock, indistinctly bedded and laminated fine grained sandstone with gastropods, bivalves, and does not effervescence with HCl	Mzinene	Inner shelf
ZA	866.14	965	Irregular laminae calcareous sandstone	A23	Brown grey well indurated rock silt to fine grained sandstone with few fossils (bivalves: 4mm large), and carbonate layers (effervesce with HCl): 5cm (3035'8"-3036') and 10cm (2997'4"-2998')	Mzinene	Inner shelf
ZA	965	1035.7	Wavy bedded arkosic wacke	A24	Brownish grey well indurated rock, indistinct wavy bedded fine grained sandstone containing gastropod fossils (5cm), and calcareous layers reacting with HCl: 20cm (3397'-3397'8"),	Mzinene	Inner shelf with tidal currents
ZA	1035.7	1041.3	Bioclastic limestone: packstone	A25	Greyish brown well indurated rock, bioturbated calcareous rock containing gastropod fossils (5cm), and calcareous layers reacting with HCl: 20cm (3397'-3397'8"),	Mzinene	Inner shelf
ZA	1041.3	1099.4	Wavy laminated siltstone	A26	Brownish well indurated laminated mud to siltstone with few fossils (gastropods), visible black matter (from plants), and calcareous layers (packstones): 8cm thick (3867'5"-3867'8"), 10 cm thick (3810'4"-3810'8"), 20cm (3766'-3766'8"), 23cm (3587'-3587'9"), 15cm (3558'3"-3559'), 15cm (3456'2"-3456'8") between which reacts with HCl	Mzinene	Inner to middle shelf with tidal currents
ZA	1099.4	1170.9	Laminated siltstone	A27	Brownish well indurated mud to siltstone with carbonate matter, visible black matter from plant remains and few fossils (gastropods)	Mzinene	Inner to middle shelf
ZA	1170.9	1192.1	Wavy laminated siltstone	A28	Brownish well indurated Highly bioturbated irregular wavy laminated mud to siltstone with carbonate matter, visible black matter from plant remains and few fossils (gastropods)	Mzinene	Inner to middle shelf with tidal currents
ZA	1192.1	1242.1	Wavy laminated siltstone	A29	Dark brown moderately indurated mud, siltstone, fossils (bivalves about 1mm), plant remains and reacts with HCl	Mzinene	Inner to middle shelf with tidal currents
ZA	1242.1	1263.4	Wavy laminated siltstone	A30	Dark brown moderately indurated locally bioturbated mud, siltstone, fossils (bivalves about 1mm), plant remains and reacts with HCl	Mzinene	Inner to middle shelf with tidal currents
ZA	1263.4	1315.5	Wavy laminated siltstone	A31	Greyish moderately indurated mud to siltstone with some clast (fine grained), thin shells including bivalves(about 1mm), dark spot of organic matter from plant material	Mzinene	Inner to middle shelf with tidal currents
ZA	1315.5	1323.5	Wavy laminated siltstone		Brown moderately indurated siltstone with some clasts, bivalve shells, and black organic matter (from plant remains)	Mzinene	Inner to middle shelf
ZA	1323.5	1326.6	Laminated glauconitic siltstone	A32	Dark brown and green weakly indurated siltstone with no clear lamination large clast of quartz mineral (2mm), few fossils. Does react with HCl where contains fossils	Mzinene	Inner to middle shelf

ZA	1326.6	1386.8	Bioturbated siltstone	A33	Brown moderately indurated bioturbated siltstone, few fossils (gastropods: 2-3cm), bivalves: 2cm), intercalate with fine grained and carbonate layer of about 30 cm thick that effervescence with HCl	Mzinene	Inner to middle shelf
ZA	1386.8	1445.2	Wavy laminated calcareous siltstone	A34	Brown grey wavy bedded and laminated siltstone, few animal fossils, intercalate with fine grained, mud material of about 5 feet and softer contain also fine grained grey sandstone of about 2-3 feet that carbonate	Mzinene	Inner to middle shelf with tidal currents
ZA	1445.2	1481.3	Wavy laminated calcareous siltstone	A35	Brownish grey weakly indurated, highly bioturbated siltstone, few animal fossils, intercalated with mud material of about 5 feet which is softer.	Mzinene	Inner to middle shelf with tidal currents
ZA	1481.3	1507.8	Bioturbated siltstone	A36	Brownish grey mixture of mud and siltstone, highly bioturbated and laminated reacts to HCl, few fossils	Mzinene	Inner to middle shelf
ZA	1507.8	1512.1	Bioturbated siltstone	A37	Brownish grey mixture of mud and siltstone, laminated reacts to HCl, few fossils	Mzinene	Inner to middle shelf
ZA	1512.1	1577.3	Laminated glauconitic siltstone	A38	Dark grey well indurated mudstone and siltstone, effervescence with HCl (carbonate), contains dark spots of organic matter and red mineral (hematite)	Mzinene	Inner to middle shelf
ZA	1577.3	1595.6	Bioturbated calcareous siltstone	A39	Grey moderately indurated, bioturbated calcareous mud to siltstone with indistinct lenses, few fossils, effervescence with HCl, and dark spots of organic matter (plan remains)	Mzinene	Inner to middle shelf
ZA	1595.6	1602.7	Bioturbated calcareous siltstone	A40	Grey moderately indurated, bioturbated calcareous mud to siltstone with indistinct lenses, few fossils, effervescence with HCl, and dark spots of organic matter (plan remains)	Makatini	Inner to middle shelf
ZA	1602.7	1780	Missing		Missing	Makatini	Missing

APPENDIX E: COMPILED RESULTS OF THE ZA CORE